PALEOSEISMOLOGY OF UTAH, VOLUME 27

GEOLOGIC MAPPING AND PALEOSEISMIC INVESTIGATIONS OF THE WASHINGTON FAULT ZONE, WASHINGTON COUNTY, UTAH, AND MOHAVE COUNTY, ARIZONA

edited by William R. Lund

MISCELLANEOUS PUBLICATION 15-6
UTAH GEOLOGICAL SURVEY
a division of
UTAH DEPARTMENT OF NATURAL RESOURCES
2015

PALEOSEISMOLOGY OF UTAH, VOLUME 27

GEOLOGIC MAPPING AND PALEOSEISMIC INVESTIGATIONS OF THE WASHINGTON FAULT ZONE, WASHINGTON COUNTY, UTAH, AND MOHAVE COUNTY, ARIZONA

edited by William R. Lund

Cover photo: *Southeast-directed 2011 Google Earth™ image of the Washington fault just north of the Utah-Arizona border. The fault separates white and red "bacon stripes" of the Triassic Moenkopi Formation from late Quaternary reddish-brown alluvial and colluvial deposits.*

ISBN 978-1-55791-918-2

MISCELLANEOUS PUBLICATION 15-6
UTAH GEOLOGICAL SURVEY
a division of
UTAH DEPARTMENT OF NATURAL RESOURCES
2015

STATE OF UTAH
Gary R. Herbert, Governor

DEPARTMENT OF NATURAL RESOURCES
Michael Styler, Executive Director

UTAH GEOLOGICAL SURVEY
Richard G. Allis, Director

PUBLICATIONS
contact
Natural Resources Map & Bookstore
1594 W. North Temple
Salt Lake City, UT 84114
telephone: 801-537-3320
toll-free: 1-888-UTAH MAP
website: mapstore.utah.gov
email: geostore@utah.gov

UTAH GEOLOGICAL SURVEY
contact
1594 W. North Temple, Suite 3110
Salt Lake City, UT 84114
telephone: 801-537-3300
website: geology.utah.gov

Research supported by the Utah Geological Survey and the U.S. Geological Survey (USGS), Department of the Interior, under USGS National Earthquake Hazards Reduction Program award number G11AP20061 The views and conclusions contained in this document are those of the authors and should not be interpreted as necessarily representing the official policies, either expressed or implied, of the U.S. Government.

The Miscellaneous Publication series provides non-UGS authors with a high-quality format for documents concerning Utah geology. Although review comments have been incorporated, this document does not necessarily conform to UGS technical, editorial, or policy standards. The Utah Department of Natural Resources, Utah Geological Survey, makes no warranty, expressed or implied, regarding the suitability of this product for a particular use. The Utah Department of Natural Resources, Utah Geological Survey, shall not be liable under any circumstances for any direct, indirect, special, incidental, or consequential damages with respect to claims by users of this product.

The Utah Geological Survey does not endorse any products or manufacturers. Reference to any specific commercial product, process, service, or company by trade name, trademark, or otherwise, does not constitute endorsement or recommendation by the Utah Geological Survey.

FOREWORD

The Paleoseismology of Utah series makes the results of paleoseismic investigations in Utah available to geoscientists, engineers, planners, public officials, and the general public. These studies provide critical information regarding paleoearthquake parameters such as earthquake timing, recurrence, displacement, slip rate, fault geometry, and segmentation, which can be used to characterize potential seismic sources and evaluate the long-term seismic hazard of Utah's Quaternary faults.

This Miscellaneous Publication presents the results of four individual investigations undertaken to acquire new geologic and paleoseismic data on the Washington fault zone in Utah and northernmost Arizona. (1) New 1:24,000-scale geologic mapping provides improved information on the location and length of young surface ruptures and the relative ages of displaced surficial deposits along the Washington fault zone. A principal result of this new mapping is that the former Northern section of the Washington fault zone has been subdivided into the newly defined Fort Pearce and Washington Hollow sections. (2) A detailed paleoseismic trenching investigation of a scarp formed on a latest Quaternary alluvial fan near Dutchman Draw in Arizona provides new information on paleoearthquake timing, displacement, and recurrence necessary for evaluating the seismic hazard presented by the Fort Pearce section to the St. George metropolitan area. (3) Trace element and major oxide geochemical correlation and radiometric dating ($^{40}Ar/^{39}Ar$) of mafic volcanic flows displaced across the fault zone in Arizona provide long-term (early to middle Quaternary) vertical slip-rate estimates for the Fort Pearce and Sullivan Draw sections of the fault. (4) A geotechnical consultant's surface-fault-rupture-hazard investigation conducted for the Utah Department of Transportation provides new information on fault locations, number of earthquakes, and displacement per earthquake on the central part of the Fort Pearce section. Based on the results of this investigation, the Utah Department of Transportation relocated two proposed elevated interchange structures and several hundred meters of roadway to avoid risk from future surface rupture.

Determining the paleoseismic parameters of the Washington fault zone is critical to understanding the segmentation of the northern, urbanized part of the fault zone; for refining probabilistic earthquake-hazard assessments; and improving earthquake-hazard evaluations for the St. George metropolitan area, all of which help reduce earthquake-related risks to the region's residents.

William Lund, Editor

Paleoseismology of Utah Series

PALEOSEISMOLOGY OF UTAH SERIES PUBLICATIONS

UGS publications produced as part of the Paleoseismology of Utah series may be found online at http://geology.utah.gov/ghp/consultants/paleoseismic_series.htm and can be accessed directly using the links provided below.

1. Fault behavior and earthquake recurrence on the Provo segment of the Wasatch fault zone at Mapleton, Utah County, Utah—Paleoseismology of Utah, Volume 1, 1991, by Lund, W.R., Schwartz, D.P., Mulvey, W.E., Budding, K.E., and Black, B.D.: Utah Geological Survey Special Study 75, 41 p., online, http://ugspub.nr.utah.gov/publications/special_studies/SS-75.pdf.

2. Paleoseismic analysis of the Wasatch fault zone at the Brigham City trench site, Brigham City, Utah, and the Pole Patch trench site, Pleasant View, Utah—Paleoseismology of Utah, Volume 2, 1991, by Personius, S.F.: Utah Geological Survey Special Study 76, 39 p., online, http://ugspub.nr.utah.gov/publications/special_studies/SS-76.pdf.

3. The number and timing of paleoseismic events on the Nephi and Levan segments, Wasatch fault zone, Utah—Paleoseismology of Utah, Volume 3, 1991, by Jackson, M.: Utah Geological Survey Special Study 78, 23 p., 3 plates, online, http://ugspub.nr.utah.gov/publications/special_studies/SS-78.pdf.

4. Seismotectonics of north-central Utah and southwestern Wyoming—Paleoseismology of Utah, Volume 4, 1994, by West, M.W.: Utah Geological Survey Special Study 82, 93 p., 5 plates, scale 1:100,000, online, http://ugspub.nr.utah.gov/publications/special_studies/SS-82.pdf.

5. Neotectonic deformation along the East Cache fault zone, Cache County, Utah—Paleoseismology of Utah, Volume 5, 1994, by McCalpin, J.P.: Utah Geological Survey Special Study 83, 37 p., online, http://ugspub.nr.utah.gov/publications/special_studies/ss-83.pdf.

6. The Oquirrh fault zone, Tooele County, Utah—surficial geology and paleoseismicity—Paleoseismology of Utah, Volume 6, 1996, by Lund, W.R., editor: Utah Geological Survey Special Study 88, 64 p., 2 plates, scale 1:24,000, online, http://ugspub.nr.utah.gov/publications/special_studies/SS-88.pdf.

7. Paleoseismic investigation on the Salt Lake City segment of the Wasatch fault zone at the South Fork Dry Creek and Dry Gulch sites, Salt Lake County, Utah—Paleoseismology of Utah, Volume 7, 1996, by Black, B.D., Lund, W.R., Schwartz, D.P., Gill, H.E., and Mayes, B.H.: Utah Geological Survey Special Study 92, 22 p., 1 plate, online, http://ugspub.nr.utah.gov/publications/special_studies/SS-92.pdf.

8. Paleoseismic investigation at Rock Canyon, Provo segment, Wasatch fault zone, Utah County, Utah—Paleoseismology of Utah, Volume 8, 1998, by Lund, W.R., and Black, B.D.: Utah Geological Survey Special Study 93, 21 p., 2 plates, online, http://ugspub.nr.utah.gov/publications/special_studies/SS-93.pdf.

9. Paleoseismic investigation of the Clarkston, Junction Hills, and Wellsville faults, West Cache fault zone, Cache County, Utah—Paleoseismology of Utah, Volume 9, 2000, by Black, B.D., Giraud, R.E., and Mayes, B.H.: Utah Geological Survey Special Study 98, 23 p., 1 plate, online, http://ugspub.nr.utah.gov/publications/special_studies/SS-98.pdf.

10. Post-Bonneville paleoearthquake chronology of the Salt Lake City segment, Wasatch fault zone, from the 1999 "megatrench" site—Paleoseismology of Utah, Volume 10, 2002, by McCalpin, J.P.: Utah Geological Survey Miscellaneous Publication 02-7, 38 p., online, http://ugspub.nr.utah.gov/publications/misc_pubs/MP-02-7WFZ-SLC.pdf.

11. Post-Provo paleoearthquake chronology of the Brigham City segment, Wasatch fault zone, Utah—Paleoseismology of Utah, Volume 11, 2002, by McCalpin, J.P., and Forman, S.L.: Utah Geological Survey Miscellaneous Publication 02-9, 46 p., online, http://ugspub.nr.utah.gov/publications/misc_pubs/MP-02-9WFZ-BrigCity.pdf.

12. Neotectonics of Bear Lake Valley, Utah and Idaho; a preliminary assessment—Paleoseismology of Utah, Volume 12, 2003, by McCalpin, J.P.: Utah Geological Survey Miscellaneous Publication 03-4, 43 p., online, http://ugspub.nr.utah.gov/publications/misc_pubs/MP-03-4.pdf.

13. Holocene earthquake history of the northern Weber segment of the Wasatch fault zone, Utah—Paleoseismology of Utah, Volume 13, 2006, by Nelson, A.R., Lowe, M., Personius, S., Bradley, L., Forman, S.L., Klauk, R., and Garr, J.: Utah Geological Survey Miscellaneous Publication 05-8, 39 p., 2 plates, online, http://ugspub.nr.utah.gov/publications/misc_pubs/MP-05-8.pdf.

14. Paleoseismic investigation and long-term slip history of the Hurricane fault in southwestern Utah—Paleoseismology of Utah, Volume 14, 2007, by Lund, W.R., Hozik, M.J., and Hatfield, S.C.: Utah Geological Survey Special Study 119, 81 p., CD, online, http://ugspub.nr.utah.gov/publications/special_studies/SS-119.pdf.

15. Surficial-geologic reconnaissance and scarp profiling on the Collinston and Clarkston Mountain segments of the Wasatch fault zone, Box Elder County, Utah—paleoseismic inferences, implications for adjacent segments and issues for diffusion-equation scarp-age modeling—Paleoseismology of Utah, Volume 15, 2007, by Hylland, M.D.: Utah Geological Survey Special Study 121, 18 p., CD, online, http://ugspub.nr.utah.gov/publications/special_studies/SS-121.pdf.

16. Paleoseismic reconnaissance of the Sevier fault, Kane and Garfield Counties, Utah—Paleoseismology of Utah, Volume 16, 2008, by Lund, W.R, Knudsen, T.R., and Vice, G.S.: Utah Geological Survey Special Study 122, 31 p., CD, online, http://ugspub.nr.utah.gov/publications/special_studies/SS-122.pdf.

17. Paleoseismic investigation of the northern strand of the Nephi segment of the Wasatch fault zone at Santaquin, Utah—Paleoseismology of Utah, Volume 17, 2008, by DuRoss, C.B., McDonald, G.N., and Lund, W.R.: Utah Geological Survey Special Study 124, 33 p., 1 plate, online, http://geology.utah.gov/online/ss/ss-124.pdf.

18. Paleoseismic investigation of the northern Weber segment of the Wasatch fault zone at Rice Creek trench site, North Ogden, Utah—Paleoseismology of Utah, Volume 18, 2009, by DuRoss, C.B., Personius, S.F., Crone, A.J., McDonald, G.N., and Lidke, D.J.: Utah Geological Survey Special Study 130, 37 p., 2 plates, CD, online, http://geology.utah.gov/online/ss/ss-130.pdf.

19. Late Quaternary faulting in East Canyon Valley, Northern Utah—Paleoseismology of Utah, Volume 19, 2010, by Piety, L.A., Anderson, L.W., and Ostenaa, D.A.: Utah Geological Survey Miscellaneous Publication 10-5, 40 p., CD, online, http://geology.utah.gov/online/mp/mp10-05/mp10-05.pdf.

20. Compilation of U.S. Bureau of Reclamation Seismotectonic Studies in Utah, 1982–1999—Paleoseismology of Utah, Volume 20, 2011, compiled by Lund, W.R., Bowman, S.D., and Piety, L.A.: Utah Geological Survey Miscellaneous Publication 11-2, variously paginated, CD, online, http://geology.utah.gov/online/mp/mp11-02/mp11-2.pdf.

21. Compilation of 1982–83 seismic safety investigation reports of eight SCS dams in southwestern Utah (Hurricane and Washington fault zones) and low-sun-angle aerial photography, Washington and Iron Counties, Utah, and Mohave County, Arizona—Paleoseismology of Utah, Volume 21, 2011, by Bowman, S.D., Young, B.W., and Unger, C.D.: Utah Geological Survey Open-File Report 583, 4 p., 2 plates, 6 DVD set, online, http://geology.utah.gov/online/ofr/ofr-583/ofr-583.pdf.

22. Late Holocene earthquake history of the Brigham City segment of the Wasatch fault zone at the Hansen Canyon, Kotter Canyon, and Pearsons Canyon trench sites, Box Elder County, Utah —Paleoseismology of Utah, Volume 22, 2012, by DuRoss, C.B., Personius, S.F., Crone, A.J., McDonald, G.N., and Briggs, R.: Utah Geological Survey Special Study 142, 28 p., 3 plates, 5 appendices, online, http://geology.utah.gov/online/ss/ss-142/ss-142.pdf.

23. Compilation of U.S. Geological Survey National Earthquake Hazards Reduction Program Final Technical Reports for Utah—Paleoseismology of Utah, Volume 23, 2013, by Bowman, S.D., and Lund, W.R.: Utah Geological Survey Miscellaneous Publication 13-3, 9 p. + 56 reports, online, http://geology.utah.gov/online/mp/mp13-03/mp13-03.pdf.

24. Evaluating surface fault chronologies of graben-bounding faults in Salt Lake Valley, Utah—new paleoseismic data from the Salt Lake City segment of the Wasatch fault zone and the West Valley fault zone—Paleoseismology of Utah, Volume 24, 2014, by DuRoss, C.B., and Hylland, M.D.: Utah Geological Survey Special Study 149, 76 p., 2 plates, 14 appendices, online, http://geology.utah.gov/online/ss/ss-149.pdf.

25. History of late Holocene earthquakes at the Willow Creek site on the Nephi segment, Wasatch fault zone, Utah—Paleoseismology of Utah, Volume 25, 2014, by Crone, A.J., Personius, S.F., DuRoss, C.B., Machette, M.N., and Mahan, S.A.: Utah Geological Survey Special Study 151, 43 p., 3 appendices, online, http://geology.utah.gov/online/ss/ss-151.pdf.

26. Compilation of 1970s Woodward-Lundgren & Associates Wasatch fault investigation reports and low-sun-angle aerial photography, Wasatch Front and Cache Valley, Utah and Idaho—Paleoseismology of Utah, Volume 26, 2015, compiled by Bowman, S.D., Hiscock, A.I., and Unger, C.D., Utah Geological Survey Open-File Report 632, (8 p., 6 pl., 9 DVD set, online, http://geology.utah.gov/online/ofr/ofr-632.

CONTENTS

INTRODUCTION TO THE WASHINGTON FAULT ZONE
by William R. Lund 1

GEOLOGY OF THE FORT PEARCE AND WASHINGTON HOLLOW SECTIONS OF THE WASHINGTON FAULT ZONE, WASHINGTON COUNTY, UTAH, AND MOHAVE COUNTY, ARIZONA
by Tyler R. Knudsen 9

UTAH GEOLOGICAL SURVEY DUTCHMAN DRAW PALEOSEISMIC INVESTIGATION, FORT PEARCE SECTION, WASHINGTON FAULT ZONE, MOHAVE COUNTY, ARIZONA
by William R. Lund, Tyler R. Knudsen, Christopher B. DuRoss, and Greg N. McDonald 43

LONG-TERM VERTICAL SLIP-RATE ESTIMATES FROM DISPLACED MAFIC VOLCANIC FLOWS, FORT PEARCE AND SULLIVAN DRAW SECTIONS, WASHINGTON FAULT ZONE, MOHAVE COUNTY, ARIZONA
by William R. Lund and Tyler R. Knudsen 87

SURFACE-FAULT-RUPTURE-HAZARD INVESTIGATION FOR A PORTION OF THE SOUTHERN PARKWAY NORTHERN EXTENSION (STATE ROUTE 7), FORT PEARCE SECTION, WASHINGTON FAULT ZONE, WASHINGTON COUNTY, UTAH
by David B. Simon, David R. Black, Jonathan R. Hanson, and Peter D. Rowley 107

INTRODUCTION TO THE WASHINGTON FAULT ZONE

by

William R. Lund

This report is part of Utah Geological Survey Miscellaneous Publication 15-6, *Surficial Geologic Mapping and Paleoseismic Investigations of the Washington Fault Zone, Washington County, Utah, and Mohave County, Arizona*—Paleoseismology of Utah, Volume 27.

Bibliographic citation for this report: Lund, W.R., 2015, Introduction to the Washington fault zone, *in* Lund, W.R., editor, 2015, Surficial geologic mapping and paleoseismic investigations of the Washington fault zone, Washington County, Utah, and Mohave County, Arizona—Paleoseismology of Utah, Volume 27: Utah Geological Survey Miscellaneous Publication 15-6, p. 1–8, CD.

CONTENTS

ABSTRACT 1
INTRODUCTION 1
Background 1
Purpose and Scope of Work 3
Setting 4
WASHINGTON FAULT ZONE 4
Overview 4
Evidence of Quaternary Surface Faulting 6
Previous Paleoseismic Investigations 6
REDUCING EARTHQUAKE LOSSES 6
REFERENCES 7

FIGURES

Figure 1. Location of the Washington fault zone and other major Quaternary normal faults in southwestern Utah 2
Figure 2. Washington fault zone study area showing fault sections as proposed by Pearthree (1998), and as modified for this study 3
Figure 3. Intermountain Seismic Belt and significant Utah historical earthquakes 5

INTRODUCTION TO THE WASHINGTON FAULT ZONE

by William R. Lund

ABSTRACT

The Washington fault zone is a 97-km-long (straight line), down-to-the-west normal fault that extends from northern Arizona into southwestern Utah. The Washington fault zone is one of several large Quaternary normal faults that define a transitional boundary between the Colorado Plateau and Basin and Range physiographic provinces in northern Arizona and southwestern Utah. In Utah, the fault zone trends through the rapidly urbanizing St. George metropolitan area in Washington County. Scarps formed on unconsolidated Quaternary deposits and soft bedrock along the Washington fault zone in Utah and northernmost Arizona provide evidence of late Quaternary surface faulting. Therefore, the Washington fault zone is considered active and capable of producing future large earthquakes that represent a significant seismic hazard to the St. George metropolitan area.

Based on structural and geomorphic evidence, previous workers divided the Washington fault zone into three fault sections from south to north: Sullivan Draw, Mokaac, and Northern. New geologic mapping (Knudsen, this volume) identified the Washington Hollow fault, which is along strike with and north of the Washington fault zone, as a fourth section of the Washington fault zone distinct from the Northern section to the south. Because the previously defined Northern section is no longer the northernmost section of the Washington fault zone, to avoid future confusion, Knudsen (this volume) has renamed the Northern section the Fort Pearce section. Additionally, the new geologic mapping shows that the previously defined Mokaac section and the Dutchman Draw fault, previously mapped as independent structures, are most likely strands of the larger Fort Pearce section, and Knudsen (this volume) redefined them as such.

The papers in this volume present the results of four investigations undertaken to acquire new geologic and paleoseismic data on the Washington fault zone in Utah and northernmost Arizona. (1) New geologic mapping provides better information on the location and length of young surface ruptures and the relative ages of displaced surficial deposits along the Fort Pearce and Washington Hollow sections. (2) A paleoseismic trenching investigation of a scarp formed on a latest Quaternary alluvial fan near Dutchman Draw in Arizona provides new information on paleoearthquake timing, displacement, and recurrence necessary for evaluating the seismic hazard presented by the Fort Pearce section to the St. George metropolitan area. (3) Trace element and major oxide geochemical correlation and radiometric dating ($^{40}Ar/^{39}Ar$) of mafic volcanic flows displaced across the fault zone in Arizona provide long-term (early to middle Quaternary) vertical-slip-rate estimates for the Fort Pearce and Sullivan Draw sections. (4) A geotechnical consultant's surface-fault-rupture-hazard investigation conducted for the Utah Department of Transportation provides additional information on fault locations, number of earthquakes, and displacement per earthquake on the Fort Pearce section.

INTRODUCTION

Background

The Washington fault zone is one of several large Quaternary normal faults that define a transitional boundary between the Colorado Plateau and Basin and Range physiographic provinces in northern Arizona and southwestern Utah (figure 1). In Utah, the fault zone trends through the rapidly urbanizing St. George metropolitan area in Washington County. Scarps formed on unconsolidated Quaternary deposits and soft bedrock along the Washington fault zone in Utah and northernmost Arizona provide evidence of late Quaternary surface faulting. Therefore, the Washington fault zone is considered active and capable of producing future large earthquakes that represent a significant seismic hazard to the St. George metropolitan area.

Based on structural and geomorphic evidence, previous workers divided the Washington fault zone into three fault sections from south to north: the Sullivan Draw, Mokaac, and Northern sections (Pearthree, 1998) (figure 2). New geologic mapping (Knudsen, this volume) identified the Washington Hollow fault, which is along strike with and north of the Washington fault zone, as part of the Washington fault zone and distinct from the Northern section to the south. Because the previously defined Northern section is no longer the northernmost section of the Washington fault zone, to avoid future confusion, Knudsen (this volume) has renamed it the Fort Pearce section (figure 2). Additionally, the new geologic mapping shows that the Mokaac section and the Dutchman Draw fault, previously mapped as independent structures, are most likely strands of the larger Fort Pearce section, and Knudsen (this volume) redefines them as such.

In Utah, the Fort Pearce section trends through the St. George metropolitan area, which experienced a nearly 53% population increase between 2000 and 2010 (U.S. Census Bureau, 2011). Despite an economic downturn beginning in 2008, the area's rapid growth is expected to resume once the region's

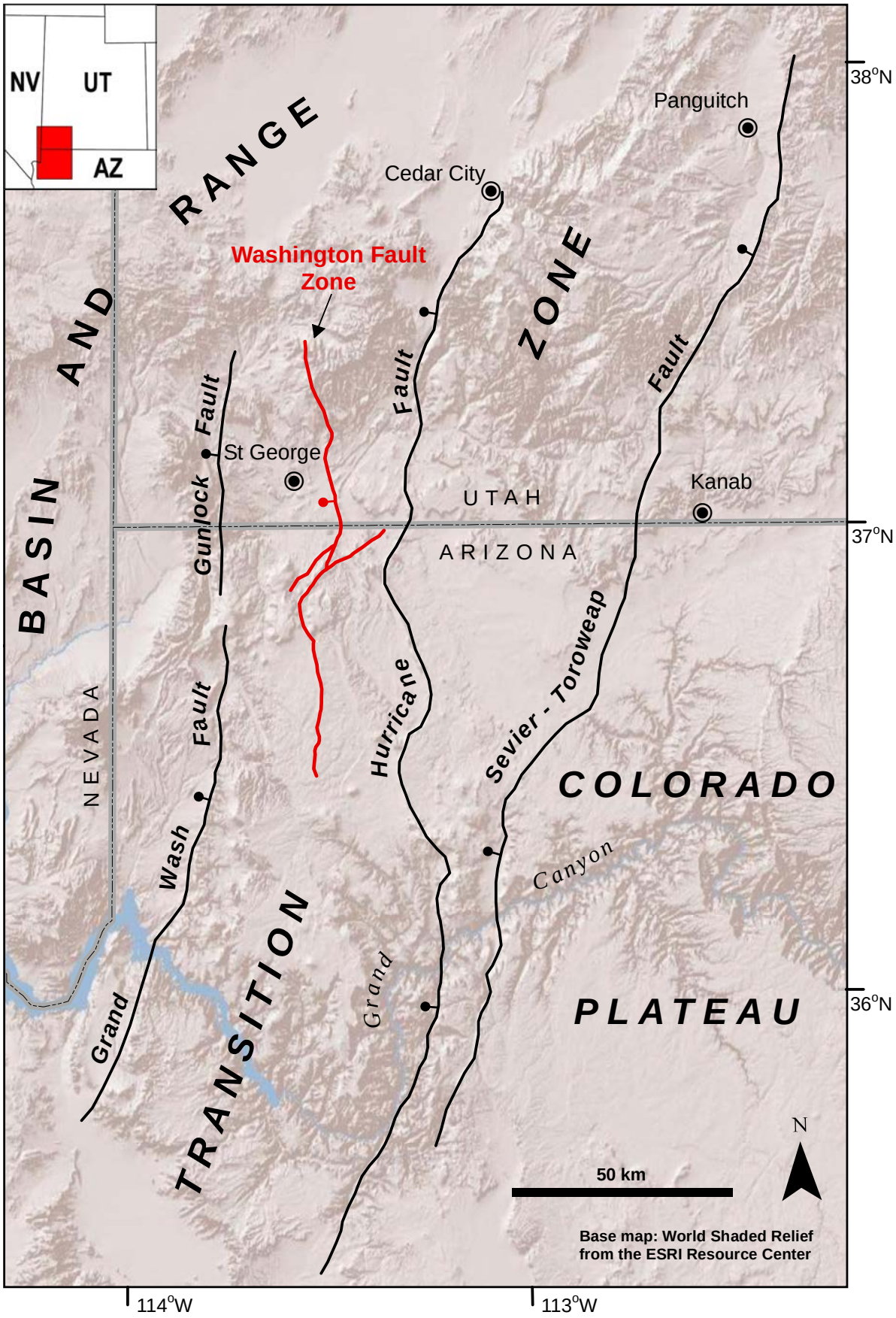

Figure 1. *Location of Washington fault zone (red lines) and other major Quaternary normal faults (black lines) in southwestern Utah. Ball and bar on downthrown side of fault.*

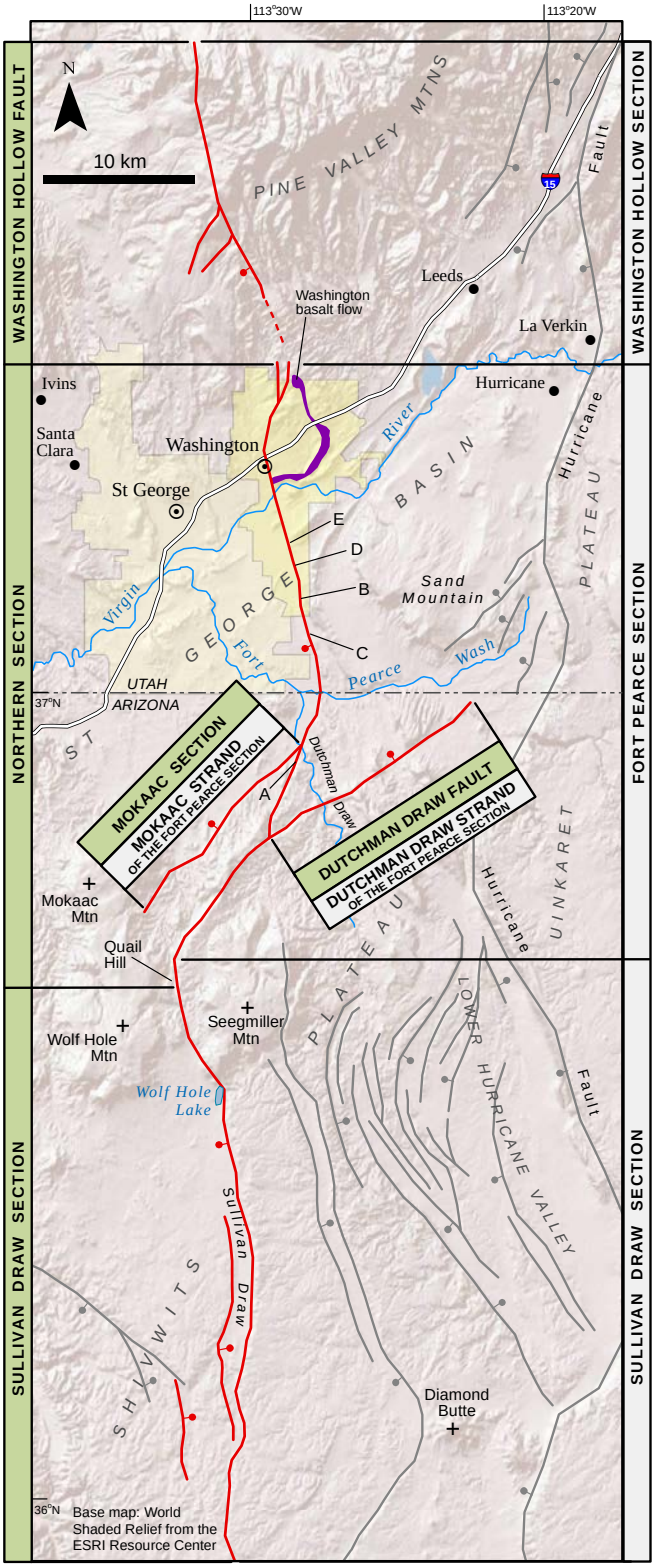

Figure 2. *Washington fault zone study area showing fault sections as proposed by Pearthree (1998; green column on left side of figure), and as modified by Knudsen (this volume; gray column on right side of figure). Yellow shading indicates St. George and Washington City boundaries. Additional Quaternary normal faults are shown as gray lines. A = faulted alluvial fan near Dutchman Draw, B = SBI (this volume) surface-fault-rupture-hazard investigation, C = Anderson and Christenson (1989) fault-scarp investigation, D = ESA (1982) dam site seismic-safety evaluation, E = AGEC surface-fault-rupture-hazard investigation.*

economy recovers. The 2010 U.S. Census placed the population of the St. George metropolitan area at 138,115 (U.S. Census Bureau, 2011), and estimates of future growth predict that the area's population will exceed 700,000 by 2050 (Utah Governor's Office of Planning and Budget, 2008). The communities of St. George (pop. 72,897), Santa Clara (pop. 6033), Ivins (pop. 6753), Hurricane (pop. 13,748), and La Verkin (pop. 4060) (U.S. Census Bureau, 2011) are all within 20 km of the Fort Pearce section (figure 2) and will experience strong ground shaking in the event of a large earthquake on that section of the Washington fault zone. Washington City (pop. 18,761) (U.S. Census Bureau, 2011) lies directly on the trace of the Fort Pearce section, and can expect surface-fault rupture, in addition to strong ground shaking during a large Fort Pearce-section earthquake.

Recognizing the earthquake hazard presented by the Washington fault zone to the St. George metropolitan area, the Utah Quaternary Fault Parameters Working Group (UQFPWG), which is convened annually by the Utah Geological Survey (UGS) to help set Quaternary fault research priorities for Utah, identified the Fort Pearce (then Northern) section as one of its top five research priorities in 2008 (http://geology.utah.gov/ghp/workgroups/pdf/uqfpwg/UQFPWG-2008_Summary.pdf). In response to the UQFPWG priority ranking, the UGS undertook three investigations (geologic mapping, paleoseismic trenching, and correlation and dating of displaced lava flows) to better define the earthquake hazard presented by the Washington fault zone to the St. George metropolitan area. Results of those investigations are presented in the papers in this volume. This volume also includes the results of a surface-fault-rupture-hazard investigation conducted by Simon Bymaster, Inc. (SBI) for the Utah Department of Transportation (UDOT) Southern Parkway (State Route [SR] 7) northern extension. The SBI investigation provides additional information on the number of earthquakes and displacement per earthquake on the Fort Pearce section in Utah.

Purpose and Scope of Work

The purpose of the investigations presented in this volume was to develop new geologic and paleoseismic information for the Washington fault zone in Utah, and in particular for the part of the fault zone which trends through the St. George metropolitan area (figure 2). The scope of work included:

1. 1:24,000-scale geologic mapping of the Washington fault zone in Utah and northernmost Arizona (Knudsen, this volume). This included a review of geologic literature, maps, aerial photographs, and other imagery available for the Washington fault zone, and particularly data related to previous paleoseismic investigations and geologic mapping of the fault.

2. Paleoseismic trenching of a faulted alluvial fan near Dutchman Draw in Arizona (point A on figure 2) to

develop new information on paleoearthquake timing, displacement, and recurrence for the Fort Pearce section (Lund and others, this volume). This task included preparation of site topographic and geologic maps, scarp profiling, trenching, and radiocarbon and optically stimulated luminescence dating of carbon and sediment samples from trenches.

3. Geochemical correlation and radiometric dating ($^{40}Ar/^{39}Ar$) of displaced mafic volcanic flows in Arizona to determine long-term (early to middle Quaternary) vertical-slip-rate estimates for the southern part of the Fort Pearce section and northern end of the Sullivan Draw section (Lund and Knudsen, this volume).

4. Synthesis of results from a surface-fault-rupture-hazard investigation conducted on the Fort Pearce section by SBI for the UDOT (Simon and others, this volume). The SBI investigation evaluates the surface-fault-rupture hazard to a portion of a proposed freeway alignment and three elevated freeway interchanges that are part of a northern extension to the Southern Parkway in the St. George metropolitan area (point B on figure 2).

This new information, along with earthquake recurrence and vertical slip-rate estimates derived from the paleoseismic data, help characterize the earthquake hazard presented by the Washington fault zone to the urbanizing St. George, Utah, metropolitan area.

Setting

In Utah, most earthquakes are associated with the Intermountain Seismic Belt (ISB) (Smith and Sbar, 1974; Smith and Arabasz, 1991), an approximately 150-km-wide, north-south trending zone of earthquake activity that extends from northern Montana to northwestern Arizona (figure 3). Since 1850, there have been at least 15 earthquakes of magnitude (M) 5.5 or greater within the ISB (University of Utah Seismograph Stations [UUSS], 2012). Included among those events are Utah's two largest historical earthquakes, the estimated M 6.5 1902 Richfield earthquake, and the M 6.6 1934 Hansel Valley earthquake, which produced Utah's only historical surface faulting (figure 3). In an average year, Utah experiences more than 700 earthquakes, but most are too small to be felt (UUSS, 2012). Moderate-magnitude earthquakes (M 5.5–6.5) happen in Utah on average every seven years (UUSS, 2012), the most recent being the M_L 5.8 St. George earthquake on September 2, 1992 (Christenson, 1995; figure 3). Large-magnitude earthquakes (M 6.5–7.5) occur much less frequently in Utah, but geologic evidence shows that most areas of the state within the ISB, including the St. George metropolitan area, have experienced large surface-faulting earthquakes in the Holocene (Lund and others, 2007, 2008b).

Historical surface faulting has not occurred in southwestern Utah, but the area has a pronounced record of seismicity. At least 20 earthquakes equal to or greater than M 4 have occurred in southwestern Utah over the past century (Christenson and Nava, 1992; UUSS, 2012), the largest being the estimated M 6 1902 Pine Valley earthquake (Williams and Tapper, 1953) and the M_L 5.8 1992 St. George earthquake. The Pine Valley earthquake is pre-instrumental and poorly located, and therefore, cannot be unequivocally attributed to a recognized fault. However, the epicenter is west of the surface trace of the west-dipping Hurricane fault, so the earthquake may have occurred on that structure. Based chiefly on its epicentral location and focal mechanism, Pechmann and others (1995) concluded that the St. George earthquake could have resulted from slip on the Hurricane fault.

Despite a lack of historical surface faulting, geologic data for faults in southwestern Utah indicate a moderate rate of long-term Quaternary activity. Mid-Quaternary basalt flows are displaced more than 300 m in several locations and latest Quaternary and Holocene alluvial and colluvial deposits are displaced meters to tens of meters (Anderson and Christenson, 1989; Lund and others, 2007, 2008b). Prominent among the Quaternary faults in southwestern Utah are the Hurricane (Lund and others, 2007), Sevier (Lund and others, 2008a), and Washington fault zones.

WASHINGTON FAULT ZONE

Overview

The Washington fault zone is a 97-km-long (straight line end-to-end), down-to-the-west, normal fault that trends from northern Arizona into the St. George, Utah, metropolitan area (figure 2; Biek and others, 2009). The Washington fault zone lies west of the longer, late Quaternary-active Hurricane fault (Lund and others, 2007; figure 1), and crosses much of the St. George metropolitan area before dying out north of Washington City. In Utah, displacement on the Washington fault zone decreases northward, in a sense opposite to the northward-increasing displacement of the Hurricane fault. According to Peterson (1983), the fault reaches its maximum displacement (about 670 m) 10 km south of the Utah-Arizona state line. Billingsley (1993) reported about 500 m of displacement at the state line, and Hayden (2005) estimated about 185 m of displacement south of Washington City in Utah.

Figure 2 shows the boundaries and section names as defined by Pearthree (1998). Based on the paleoseismic information available prior to this investigation, Black and others (2003) assigned an age category of <15,000 years for the timing of the most recent surface-faulting paleoearthquake on the Fort Pearce (then Northern) section.

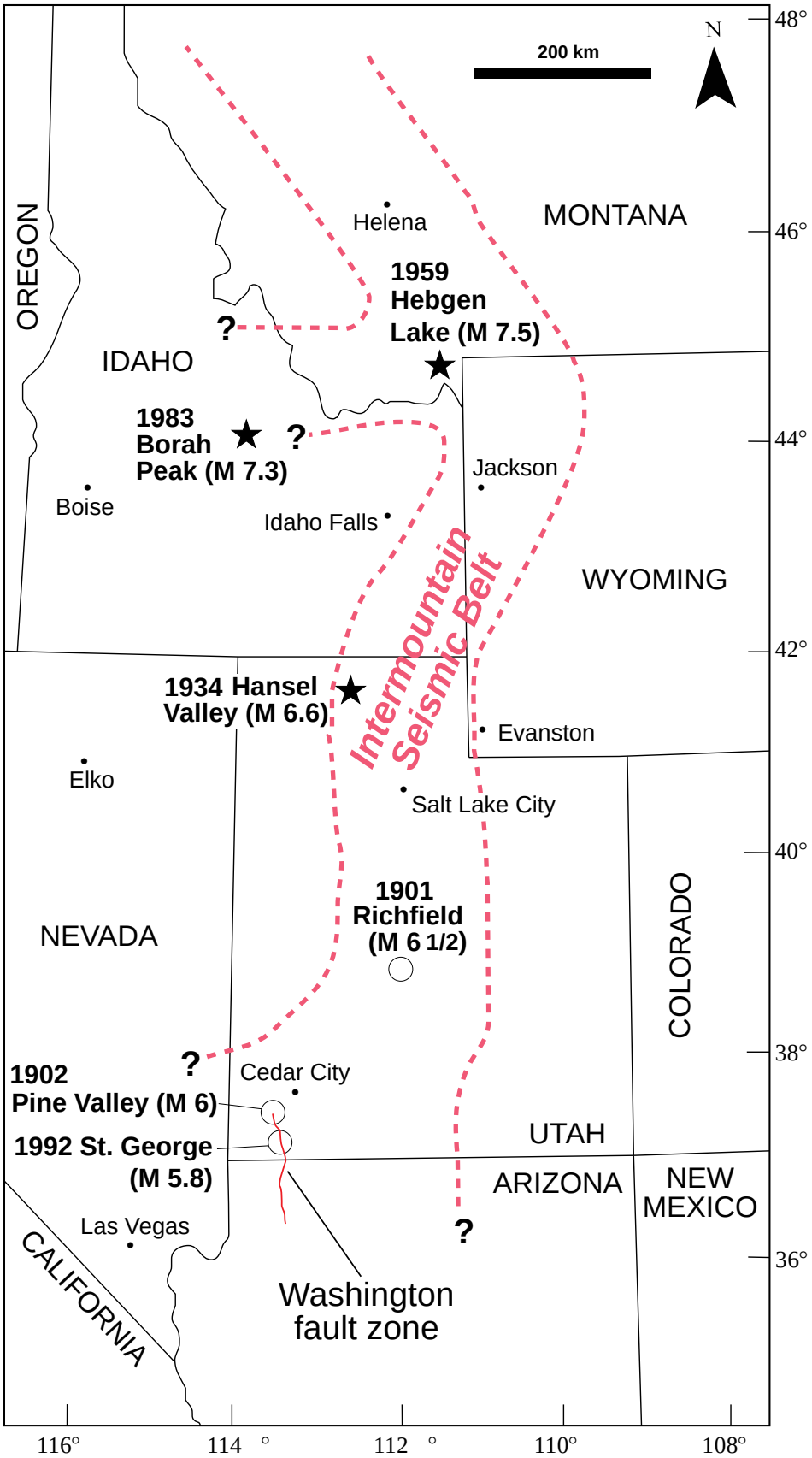

Figure 3. *Intermountain Seismic Belt and significant Utah historical earthquakes. Stars denote earthquakes that caused surface rupture; open circles denote earthquakes without surface rupture. Note that the Washington fault zone is a west-dipping normal fault; therefore, the hypocenters of the 1902 Pine Valley and 1992 St. George earthquakes are most likely on the also west-dipping fault plane of the Hurricane fault, the surface trace of which lies several kilometers east of the Washington fault zone (see figure 1).*

Evidence of Quaternary Surface Faulting

Although long suspected of being active in recent geologic time, prior to this investigation, little was known about the surface-faulting history of the Washington fault zone. Situated in the transition zone between the Colorado Plateau and Basin and Range physiographic provinces, the geomorphology of the St. George basin is dominated by erosion driven by the rapid incision of the Virgin River and its tributaries (figure 2). Consequently, fault scarps are chiefly preserved on bedrock along the fault zone in Utah and Arizona. In areas where the bedrock is resistant, a prominent linear escarpment marks the position of the fault, but in areas of soft bedrock, escarpments are deeply embayed or almost completely eroded. In the latter areas, the main fault trace is often buried by loose eolian sand. Because it is farther away from the large, actively incising drainages in Utah and has not been subject to urban development, the part of the Fort Pearce section that lies in Arizona preserves isolated fault scarps on latest Quaternary alluvial-fan deposits.

In Utah, a short subsidiary splay of the Fort Pearce section displaces the Washington basalt flow (figure 2) about 4.6 m. Potassium-argon (K-Ar) dating by Best and others (1980) places the age of the flow at 1.7 ± 0.1 Ma. More recent argon-argon ($^{40}Ar/^{39}Ar$) dating of the flow yielded ages of 0.87 ± 0.04 and 0.98 ± 0.02 Ma (Biek, 2003). Timing of the earthquake(s) that displaced the basalt flow is unknown other than being younger than the age of the flow. Based on geomorphic relations observed elsewhere on what Pearthree (1998) defined as the Northern section, he assigned a time of <130 ka for the most recent surface faulting. Anderson and Christenson (1989) profiled a 3.5-m-high fault scarp in Utah, preserved on mixed colluvial and alluvial deposits near the Utah-Arizona border (point C of figure 2), and based on diffusion modeling, estimated a late Quaternary age of about 15 ka for the scarp.

Previous Paleoseismic Investigations

In addition to the Anderson and Christenson (1989) scarp profile, Earth Sciences Associates, Inc. (ESA) trenched the Northern (Fort Pearce) section of the Washington fault zone as part of a U.S. Soil Conservation Service (SCS; now Natural Resources Conservation Service) seismic-safety investigation of flood-retention structures in Utah (ESA, 1982, 1983; compiled by Bowman and others, 2015) (point D on figure 2). ESA reported a few inches of vertical displacement in "younger" deposits, but was unsure if this small displacement was fault related or the result of differential compaction of loose eolian sediments across the fault. However, ESA identified "older" deposits that were displaced about a meter and represent at least one and possibly more surface-faulting earthquakes (ESA, 1982). The absence of organic carbon or other datable material in their trenches prevented ESA from refining their relative age assessments beyond "younger" and "older" categories, which they estimated to be 5 to 10 ka and 10 to 25 ka, respectively.

In 2007, Applied Geotechnical Engineering Consultants, Inc. (AGEC) excavated five trenches to locate the buried trace of the Washington fault zone where it crosses a proposed subdivision in Washington City (Payton, 2007; point E on figure 2). One trench produced an excellent exposure of the fault, and AGEC allowed the UGS to make a reconnaissance log of one trench wall, and collect samples for optically stimulated luminescence (OSL) dating. Results of the logging and dating indicated that the fault zone has likely experienced at least three surface-faulting earthquakes in the past 76 kyr, the most recent possibly in Holocene time (Lund and others, 2008b). However, the UGS had less than two days to spend in the trench, and significant questions remained regarding both the number and timing of paleoearthquakes. In particular, the rupture from the most recent surface-faulting earthquake extended to within 25 cm of the ground surface through loose eolian sand. The rupture displaced a moderately developed soil Bk horizon, indicating that the event could be as young as Holocene. The trench was later reoccupied and logged in detail by SBI for a surface-fault-rupture-hazard investigation conducted on a portion of the Fort Pearce section for UDOT (Simon and others, this volume).

REDUCING EARTHQUAKE LOSSES

Results of the new geologic mapping and paleoseismic investigations presented in this volume will help reduce losses from future earthquakes by permitting more accurate earthquake-hazard evaluations for hazard mitigation in the rapidly urbanizing St. George, Utah, metropolitan area. Results of these investigations better define the location, length, rates of activity, and earthquake magnitudes for the Washington fault zone in Utah. These data are critical for improving deterministic seismic-source characterization models and probabilistic earthquake-hazard analyses for the St. George metropolitan area. Study results will also be used to update the U.S. Geological Survey's (USGS) *Quaternary Fault and Fold Database of the United States*, the UGS *Quaternary Fault and Fold Database of Utah*, and the USGS *National Seismic Hazards Maps* for Utah and Arizona, which are incorporated into the International Building Code and International Residential Code, which are adopted statewide in Utah. Additionally, the geologic map of the Fort Pearce and newly defined Washington Hollow sections better defines the fault's location, and will help planners, geologists, and engineers reduce surface-fault-rupture hazard to future development.

REFERENCES

Anderson, R.E., and Christenson, G.E., 1989, Quaternary faults, folds, and selected volcanic features in the Cedar City 1° x 2° quadrangle, Utah: Utah Geological and Mineral Survey Miscellaneous Publication 89-6, 29 p., 1 plate, scale 1:250,000.

Best, M.G., McKee, E.H., and Damon, P.E., 1980, Space-time-composition patterns of late Cenozoic mafic volcanism, southwestern Utah and adjoining areas: American Journal of Science, v. 280, p. 1035–1050.

Biek, R.F., 2003, Geologic map of the Harrisburg Junction quadrangle, Washington County, Utah: Utah Geological Survey Map 191, 42 p., 2 plates, scale 1:24,000.

Biek, R.F., Rowley, P.D., Hayden, J.M., Hacker, D.B., Willis, G.C., Hintze, L.F., Anderson, R.E., and Brown, K.D., 2009, Geologic map of the St. George and east part of the Clover Mountains 30′ x 60′ quadrangles, Washington and Iron Counties, Utah: Utah Geological Survey Map 242, 101 p., 2 plates, scale 1:100,000.

Billingsley, G.H., 1993, Geologic map of the Wolf Hole Mountain and vicinity, Mohave County, northwestern Arizona: U.S. Geological Survey Miscellaneous Investigation Series Map I-2296, scale 1:31,680.

Black, B.D., Hecker, S., Hylland, M.D., Christenson, G.E., and McDonald, G.N., 2003, Quaternary fault and fold database and map of Utah: Utah Geological Survey Map 193DM, scale 1:50,000, CD.

Bowman, S.D., Hiscock, A.I., and Unger, C.D., 2015, Compilation of 1970s Woodward-Lundgren & Associates Wasatch fault investigation reports and low-sun-angle aerial photography, Wasatch Front and Cache Valley, Utah and Idaho—Paleoseismology of Utah, Volume 26: Utah Geological Survey Open-File Report 632, 8 p., 6 plates, 9 DVD set.

Bowman, S.D., and Lund, W.R., 2013, Compilation of U.S. Geological Survey National Earthquake Hazards Reduction Program final technical reports for Utah—Paleoseismology of Utah, Volume 23: Utah Geological Survey Miscellaneous Publication 13-3, 20 reports, variously paginated.

Bowman, S.D., Young, B.W., and Unger, C.D., 2011, Compilation of 1982–83 seismic safety investigation reports of eight SCS dams in southwestern Utah (Hurricane and Washington fault zones) and low-sun-angle aerial photography, Washington and Iron Counties, Utah, and Mohave County, Arizona—Paleoseismology of Utah, Volume 21: Utah Geological Survey Open-File Report 583, 4 p., 2 plates.

Christenson, G.E., editor, 1995, The September 2, 1992 M_L 5.8 St. George earthquake: Utah Geological Survey Circular 88, 41 p.

Christenson, G.E., and Nava, S.J., 1992, Earthquake hazards in southwestern Utah, *in* Harty, K.M., editor, Engineering and environmental geology of southwestern Utah: Utah Geological Association Publication 21, p. 123–137.

Earth Sciences Associates, 1982, Phase I report, seismic safety investigation of eight SCS dams in southwestern Utah: Unpublished consultant's report for the U.S. Soil Conservation Service, Portland, Oregon, dated December 1982, ESA project no. D118, variously paginated.

Earth Sciences Associates, 1983, Phase II report, seismic safety investigation of eight SCS dams in southwestern Utah: Unpublished consultant's report for the U.S. Soil Conservation Service, Portland, Oregon, dated February 1983, ESA project no. D118, variously paginated.

Governor's Office of Planning and Budget, 2008, Population area and component of change: Demographic and Economic Analysis Section, online, http://www.governor.utah.gov/dea/projections.html, accessed September 30, 2011.

Hayden, J.M., 2005, Geologic map of the Washington Dome quadrangle, Washington County, Utah: Utah Geological Survey Map 209, 29 p., 2 pl., scale 1:24,000.

Lund, W.R., Bowman, S.D., and Piety, L.A., 2011, Compilation of U.S. Bureau of Reclamation seismotectonic studies in Utah, 1982–1999—Paleoseismology of Utah, Volume 20: Utah Geological Survey Miscellaneous Publication 11-2, eight reports, variously paginated.

Lund, W.R., Hozik, M.J., and Hatfield, S.C., 2007, Paleoseismic investigation and long-term slip history of the Hurricane fault in southwestern Utah—Paleoseismology of Utah, Volume 14: Utah Geological Survey Special Study 119, 81 p.

Lund, W.R., Knudsen, T.R., and Vice, G.S., 2008a, Paleoseismic reconnaissance of the Sevier fault, Kane and Garfield Counties, Utah—Paleoseismology of Utah, Volume 16: Utah Geological Survey Special Study 122, 37 p.

Lund, W.R., Knudsen, T.R., Vice, G.S., and Shaw, L., 2008b, Geologic hazards and adverse construction conditions, St. George–Hurricane metropolitan area, Washington County, Utah: Utah Geological Survey Special Study 127, 105 p.

Payton, C.C., 2007, Surface fault rupture hazard study, proposed Zippy LLC, 47-acre site, Washington Fields, Washington City, Utah: Unpublished consultant's report for Zippy, LLC by Applied Geotechnical Engineering Consultants, Inc., Project Number 2070301, 15 p., 22 figures.

Pearthree, P.A., compiler, 1998, Quaternary fault data and map for Arizona: Arizona Geological Survey Open-File Report 98-24, 122 p., 1 plate in pocket, scale 1:750,000.

Pechmann, J.C., Arabasz, W.J., and Nava, S.J., 1995, Seismology, *in* Christenson, G.E., editor, The September 2, 1992 M_L 5.8 St. George earthquake, Washington County, Utah: Utah Geological Survey Circular 88, p. 1.

Peterson, S.M., 1983, The tectonics of the Washington fault zone, northern Mohave County, Arizona: Brigham Young University Geology Studies, v. 30, part 1, p. 83–94.

Smith, R.B., and Arabasz, W.J., 1991, Seismicity of the Intermountain seismic belt, *in* Slemmons, D.B., Engdahl, E.R., Zoback, M.D., and Blackwell, D.D., editors, Neotectonics of North America: Boulder, Colorado, Geological Society of America, Decade Map Volume, p. 185–228.

Smith, R.B., and Sbar, M.L., 1974, Contemporary seismicity in the Intermountain Seismic Belt: Geological Society of America Bulletin, v. 85, p. 1205–1218.

University of Utah Seismograph Stations, 2012, Regional earthquake information: Online, http://www.quake.utah.edu/REGIONAL/eqfaq.htm, accessed July 7, 2012.

U.S. Census Bureau, 2011, State and county quickfacts: Online, http://quickfacts.census.gov/qfd/states/49/4965330.html, accessed November 3, 2011.

Williams, J.S., and Tapper, M.L., 1953, Earthquake history of Utah: Bulletin of the Seismological Society of America, v. 43, p. 191–218.

GEOLOGY OF THE FORT PEARCE AND WASHINGTON HOLLOW SECTIONS OF THE WASHINGTON FAULT ZONE, WASHINGTON COUNTY, UTAH, AND MOHAVE COUNTY, ARIZONA

by

Tyler R. Knudsen

Utah Geological Survey
Cedar City, Utah

This report is part of Utah Geological Survey Miscellaneous Publication 15-6, *Geologic Mapping and Paleoseismic Investigations of the Washington Fault Zone, Washington County, Utah, and Mohave County, Arizona*—Paleoseismology of Utah, Volume 27.

Bibliographic citation for this report: Knudsen, T.R., 2015, Geology of the Fort Pearce and Washington Hollow sections of the Washington fault zone, Washington County, Utah, and Mohave County, Arizona, *in* Lund, W.R., editor, 2015, Surficial geologic mapping and paleoseismic investigations of the Washington fault zone, Washington County, Utah, and Mohave County, Arizona—Paleoseismology of Utah, Volume 27: Utah Geological Survey Miscellaneous Publication 15-6, p. 11–42, 2 plates, CD.

CONTENTS

ABSTRACT 11
INTRODUCTION 11
PREVIOUS WORK 14
METHODS 15
GEOLOGY OF THE FORT PEARCE AND WASHINGTON HOLLOW SECTIONS OF THE WASHINGTON FAULT ZONE 15
Fort Pearce Section 15
Quail Hill to Fort Pearce Wash 15
Fort Pearce Wash to Washington City 18
Mokaac Strand 23
Dutchman Draw Strand 24
Washington Hollow Section 25
RELATION BETWEEN THE WASHINGTON FAULT ZONE AND OTHER TRANSITION ZONE FAULTS 28
SUMMARY AND CONCLUSIONS 30
ACKNOWLEDGMENTS 31
REFERENCES 31
APPENDIX A Description of Map Units 35

FIGURES

Figure 1. Washington fault zone and fault sections in southwestern Utah and northwestern Arizona as defined in this study. 12
Figure 2. Lithologic column of geologic units that crop out in the map area 13
Figure 3. Geologic quadrangle map coverage of the Fort Pearce and Washington Hollow sections of the Washington fault zone 16
Figure 4. The Washington fault zone places Fossil Mountain Member over the younger Harrisburg Member 17
Figure 5. Obsequent fault scarp formed along the Washington fault zone 19
Figure 6. A splay of the Washington fault zone exposed in a stream cut 19
Figure 7. Oblique aerial view of a scarp formed in Triassic bedrock and Quaternary unconsolidated deposits 20
Figure 8. Oblique aerial view of fault scarp formed on the Washington lava flow 22
Figure 9. Splay of the Washington fault zone exposed in a stream cut north of Washington City 22
Figure 10. Major splay of the Washington fault zone within the Navajo Sandstone 23
Figure 11. Dutchman Draw fault exposed on the southwest flank of an unnamed mesa in Arizona 25
Figure 12. Summary of geologic mapping of the Washington fault zone and Washington Hollow fault between Interstate 15 and the Pine Valley Mountains 26
Figure 13. Joints of probable Cretaceous age near Washington Hollow that are unaffected by the Washington fault zone 27
Figure 14. Displacement map of faults in the Colorado Plateau–Basin and Range transition zone in southwestern Utah and northwestern Arizona 29
Figure 15. Schematic block diagram of the Colorado Plateau–Basin and Range transition zone in southwestern Utah and northwestern Arizona 30

PLATES

Plate 1. Geologic map of the northern part of the Fort Pearce section and the Washington Hollow sections of the Washington fault zone, Washington County, Utah, and Mohave County, Arizona ..... on CD
Plate 2. Geologic map of the southern part of the Fort Pearce section of the Washington fault zone, Washington County, Utah, and Mohave County, Arizona ..... on CD

GEOLOGY OF THE FORT PEARCE AND WASHINGTON HOLLOW SECTIONS OF THE WASHINGTON FAULT ZONE, WASHINGTON COUNTY, UTAH, AND MOHAVE COUNTY, ARIZONA

by Tyler R. Knudsen

ABSTRACT

The 97-km-long Washington fault zone is one of several west-dipping normal faults in the structural and seismic transition between the Colorado Plateau and Basin and Range physiographic provinces. As defined by previous workers, the Northern section of the Washington fault zone extends from the southern margin of the St. George basin in northwestern Arizona northward into southwestern Utah and terminates near Washington City. New geologic mapping reveals minor structures linking the Northern section of the Washington fault zone with the west-dipping Washington Hollow fault that extends north of Washington City and across the southwestern shoulder of the Pine Valley Mountains, indicating the two faults are part of the same tectonic structure. However, minimal displacement, structural complexity, and a 45° change in fault strike between the Washington Hollow fault and Washington fault zone indicate the Washington Hollow fault should be considered a separate section of the Washington fault zone which I herein name the Washington Hollow section. Because the previously defined Northern section is no longer the northernmost section of the Washington fault zone, I rename the Northern section, the Fort Pearce section. Geologic-map relations indicate the boundary of the Fort Pearce section with the Sullivan Draw section to the south is best placed near the head of Quail Canyon, where a 50° change in strike is accompanied by a significant change in vertical displacement along the fault. The lengths (straight line) of the newly defined Fort Pearce and Washington Hollow sections are 37 and 22 km, respectively.

The west-dipping Mokaac and Dutchman Draw faults, each about 16 km long, branch from the Fort Pearce section in Arizona, and have been discussed as separate faults or sections (Mokaac section) of the Washington fault zone in previous paleoseismic studies. Because the Dutchman Draw and Mokaac faults have the greatest displacement near their junction with the Fort Pearce section, and because they appear to have similar slip rates, I redefine the Dutchman Draw and Mokaac faults as strands of the Fort Pearce section of the Washington fault zone, rather than individual faults or fault sections capable of independent earthquake rupture.

The surface expression of the Fort Pearce section is dominated by prominent bedrock escarpments up to 250 m high. The scarps are likely enhanced by erosional retreat of softer bedrock exposed in the fault hanging wall. Because the geomorphology of the St. George basin is dominated by erosion, fault scarps on unconsolidated deposits are rare and isolated. Detailed surficial mapping identified two previously unknown fault scarps formed on late Pleistocene to Holocene alluvial deposits in Arizona. One site is on the main strand of the Fort Pearce section and the other is on a subsidiary fault of the Mokaac splay of the Fort Pearce section. The remaining known scarps on unconsolidated deposits along the Fort Pearce section in Utah and Arizona appear to be bedrock cored. The Washington Hollow section has two scarps up to 8 m high on Pleistocene alluvial deposits; Holocene alluvial deposits are not displaced. The Washington Hollow section displaces a 1.2 Ma basalt flow 12 m, yielding a Pleistocene-Holocene vertical slip rate of 0.01 mm/yr.

Geologic-map patterns, slip budgets, and structural similarities among the Washington fault zone, Hurricane fault zone and Main Street, Grand Wash, and other lesser faults indicate that most or all transition-zone normal faults in the study area may be structurally linked and part of the same tectonic system. Several lines of evidence support a model where the Colorado Plateau–Basin and Range boundary in this area initially developed along the Grand Wash fault in the early to middle Miocene. Beginning in the Pliocene, the locus of tensional stress migrated eastward eventually initiating movement on the Hurricane fault zone. Internal strain within the intervening block became great enough by the Pleistocene to create the Washington fault zone and Main Street and other lesser faults. The nature of structural linkage among the transition zone faults and whether the faults sole into a regional master detachment remain unknown.

INTRODUCTION

The Washington fault zone is one of several north- to northeast-striking, west-dipping normal faults within the structural transition zone between the Colorado Plateau and Basin and Range physiographic provinces (figure 1). In terms of displacement and length, the Washington fault zone is a relatively minor structure compared to larger faults in the transition zone, namely the Hurricane and Sevier-Toroweap faults to the east, and the Grand Wash/Gunlock fault to the west.

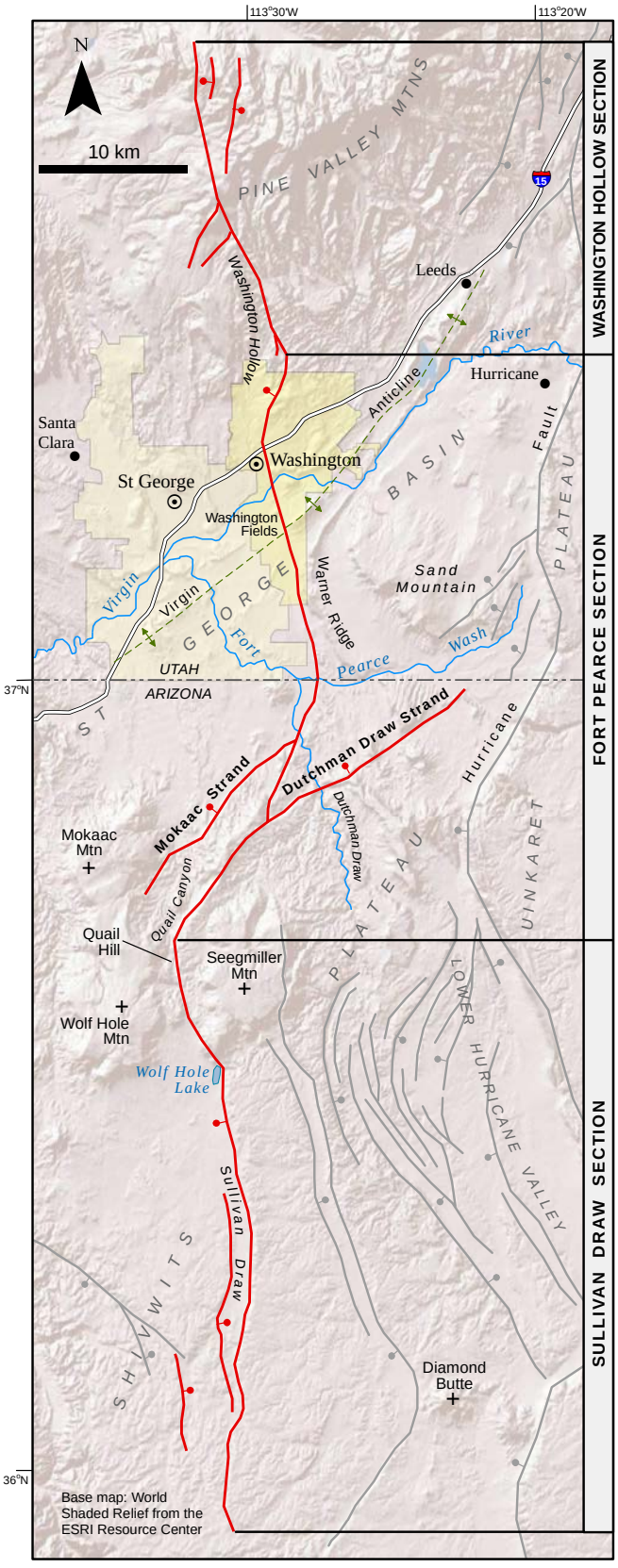

Figure 1. *Washington fault zone (red lines) showing fault sections in southwestern Utah and northwestern Arizona as defined in this study. Yellow shading indicates St. George and Washington City boundaries. Additional Quaternary faults are shown as gray lines. Fault section boundaries are based on results of this study; see Lund (this volume) for section boundaries as defined by earlier workers.*

The Washington fault zone bisects the St. George structural block, which is bounded by these larger faults. The Washington fault zone extends for 97 km (straight line) from the southwest flank of the Pine Valley Mountains in southern Utah southward through the St. George basin and into the Shivwits Plateau of northern Arizona (figure 1). In Utah, the fault trends directly through downtown Washington City and the urbanizing Washington Fields area, where the fault crosses the Virgin River and truncates the southwest part of the Sevier-age Virgin anticline. South of Washington City, the Washington fault zone parallels Warner Ridge until crossing Fort Pearce Wash near the Utah-Arizona border (figure 1). The fault continues into Arizona where it forms high bedrock escarpments traversing the southern part of the St. George basin. Farther south, the fault forms a conspicuous graben within the Shivwits Plateau.

Bedrock exposed along the Washington fault zone ranges in age from the Permian Queantoweap Sandstone to Quaternary basalt flows (figure 2; see appendix A for unit descriptions). The rock units represent an over 4000-m-thick section of chiefly marine and continental rock types that include limestone, mudstone, claystone, shale, sandstone, conglomerate, evaporite, and basalt. Previous workers reported maximum displacements on the Washington fault zone ranging from 500 m (Billingsley, 1992a) to 750 m (Anderson and Christenson, 1989) at, or just south of, the Utah-Arizona border. Displacement decreases northward to an estimated 455 m about 5 km north of the border (Hayden, 2005), and to about 210 m near Washington City (Willis and Higgins, 1995), before the fault bifurcates and becomes obscured within the thick Jurassic Navajo Sandstone. South of the displacement maximum, displacement decreases to about 400 m in the Quail Canyon area (Billingsley, 1990b), and to about 76 m near Wolf Hole Lake (Billingsley, 1990b) (figure 1). The fault displays minor offset (<50 m) for another 30 km southward before dying out at the head of Sullivan Draw on the Shivwitz Plateau (Billingsley and Workman, 2000; Billingsley and Wellmeyer, 2003).

Previous workers have subdivided the Washington fault zone in Arizona into three sections based on amount of displacement and scarp morphology. Menges and Pearthree (1983) defined the Seegmuller Mountain section as extending from Quail Hill to the Utah-Arizona border (figure 1) (the spelling of Seegmiller Mountain varies from Seegmuller, Segmiller, to Seegmiller, depending on publication or U.S. Geological Survey [USGS] quadrangle map; I use Seegmiller hereafter because it appears on the most recent USGS 7.5-minute quadrangle map). They defined the Sullivan Draw section extending south from Quail Hill to the fault's southern terminus near the head of Sullivan Draw on the Shivwitz Plateau. In Arizona, Menges and Pearthree (1983) defined a prominent fault, subparallel to the Washington fault zone to the east, as the Mokaac Wash section. The Mokaac Wash section has a maximum displacement of about 400 m near its junction with the main Washington fault zone about 5 km south of the Utah border. Pearthree (1998) renamed the Seegmuller segment, the

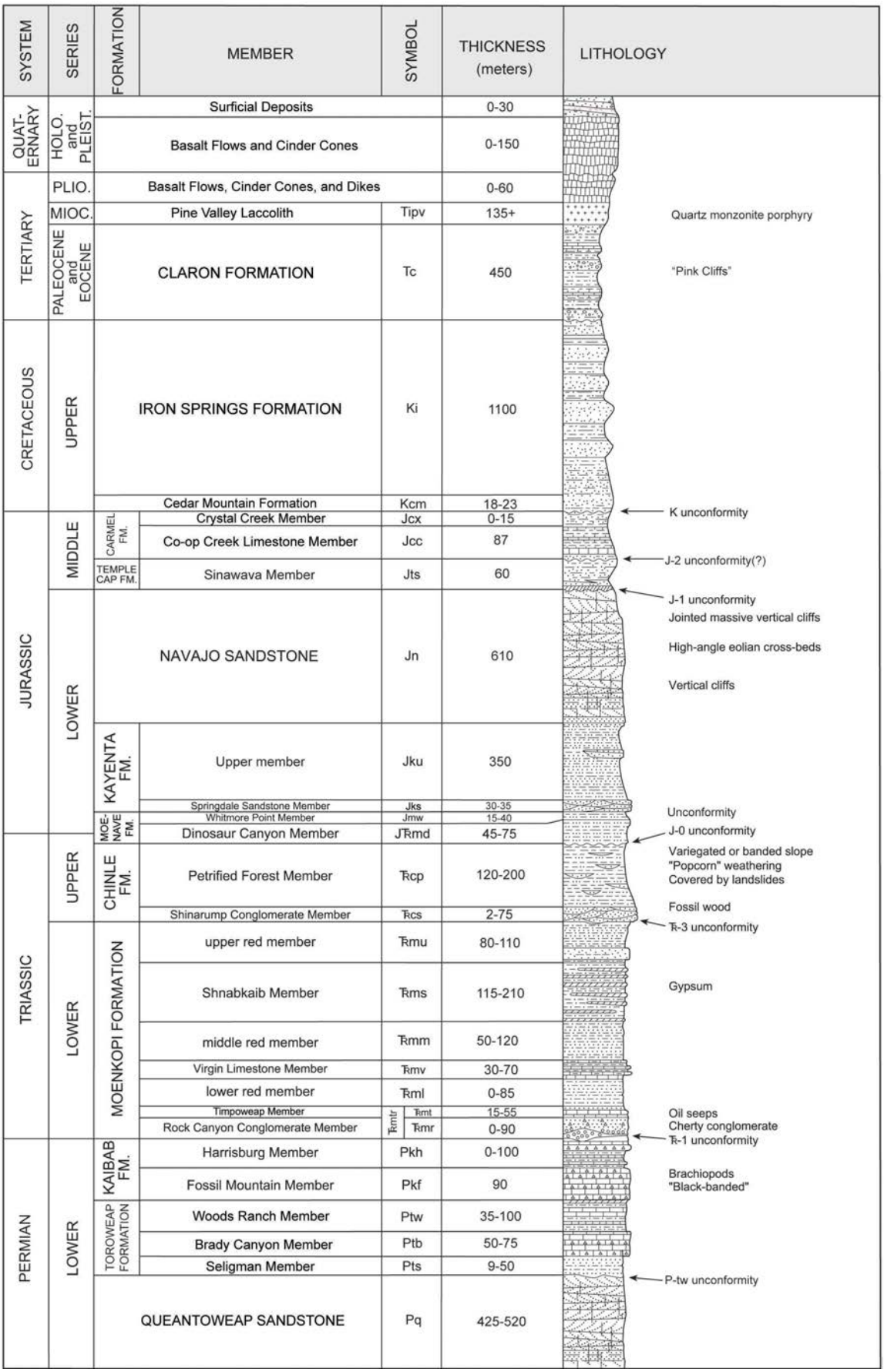

Figure 2. *Lithologic column of geologic units that crop out in the map area. Modified from Biek and others (2009).*

Northern section, and the Mokaac Wash segment, the Mokaac section. He left the Sullivan Draw section name unchanged. Since we discovered no likely section boundaries along the Washington fault zone from the Utah border north into Washington City (figure 1), we expand the definition of the Northern section to include that part of the fault in Utah. Additionally, since I define a new northernmost section of the Washington fault zone (Washington Hollow section) in this study (see below), I rename the Northern section, the Fort Pearce section.

About 6 km south of the Mokaac/Fort Pearce section intersection, a second prominent fault branches from the Fort Pearce section and extends 16 km to the northeast (figure 1). Hamblin and Best (1970) first mapped the fault, which Menges and Pearthree (1983) later named the Yellowhorse Flat fault zone. Billingsley (1992a, 1992b) mapped the splay in greater detail and renamed it the Dutchman Draw fault. The fault has a maximum displacement of about 115 m near its intersection with the Fort Pearce section (Billingsley, 1992a). Displacement decreases to about 15 m at the Utah border shortly before being obscured by Quaternary surficial deposits. The structural relation between the Fort Pearce section and the Dutchman Draw fault is analogous to the relation between the Fort Pearce section and Mokaac strand (see above); I therefore redefine the Dutchman Draw fault as the Dutchman Draw strand of the Fort Pearce section.

North of Washington City, Willis and Higgins (1995) and Hacker (in preparation [a]) mapped the northwest-trending, west-dipping Washington Hollow fault traversing the southwest shoulder of the Pine Valley Mountains (figure 1). Willis and Higgins (1995) estimated the fault has about 150 m of displacement, and they discussed the possibility that the fault may connect to the Washington fault zone through a wide breccia zone in Washington Hollow (figure 1). Results of this mapping show the Washington Hollow and Washington fault zones are parts of the same fault zone, and I herein define the Washington Hollow fault as the northernmost section of the Washington fault zone.

The accompanying 1:24,000-scale geologic map (plates 1 and 2) provide new information on the location and length of young surface ruptures and the relative ages of displaced surficial deposits along the Fort Pearce and Washington Hollow sections of the Washington fault zone. This report and map can be used to better define the location of the Fort Pearce and Washington Hollow sections, their major strands, and their section boundaries, which will be useful to planners, geologists, and engineers involved in reducing surface-fault-rupture hazard to future development.

PREVIOUS WORK

Dobbin (1939) named and mapped the Utah portion of the Washington fault zone as part of a structural-geologic study of the St. George area. He recognized three key fault characteristics: (1) the fault displaces the Cretaceous Virgin anticline, (2) fault displacement in Utah increases southward into Arizona, and (3) the fault, in places, consists of multiple splays. Cook (1960) included the Washington fault zone on his geologic map of Washington County, and reported an estimated 2500 feet (760 m) of throw at the state line. The Washington fault zone appears on Hintze's (1963) *Geologic Map of Southwestern Utah* and Stokes and Heylmun's (1963) tectonic map of southwestern Utah. A regional gravity survey and Bouguer gravity anomaly map by Cook and Hardman (1967) shows only a minor deflection of gravity contours across the fault, consistent with a mostly bedrock-against-bedrock fault with thin surficial cover on the downthrown block. Hamblin (1970a) described the Washington fault zone as a "small-scale version" of the Hurricane fault, noting that the two faults have parallel surface traces with salients and reentrants at roughly the same latitudes. He also noted that the fault zone cuts a Tertiary basalt flow (newly acquired $^{40}Ar/^{39}Ar$ radiometric ages indicate an early Quaternary age for this basalt flow; see Lund and Knudsen, this volume) on the south side of Seegmiller Mountain, and inferred that most of the relief across the fault is due to differential erosion of strata of differing erosional resistance that are juxtaposed by the fault. Hamblin and Best's (1970) photogeologic map accompanying their field-trip road log of the St. George basin–Shivwits Plateau region, provides the earliest detailed mapping of the Washington fault zone in Arizona. Hamblin (1963, 1970b), Best and Brimhall (1970), and Best and Hamblin (1970) distinguished and described basalt flows in the western Grand Canyon region based on relative age and geochemistry, providing a framework for developing relative timing relations for the Washington fault zone and nearby faults. Best and others (1980) and Wenrich and others (1995) refined relative basalt ages in the western Grand Canyon region with K-Ar radiometric dating. Cordova (1978) and Hurlow (1998) mapped a portion of the Washington fault zone near Washington City as part of a groundwater investigation of the Navajo Sandstone in Utah.

As part of a seismic-safety investigation of several U.S. Soil Conservation Service (now Natural Resources Conservation Service) dams in southwestern Utah, Earth Sciences Associates, Inc. (ESA, 1982, 1983; compiled by Bowman and others, 2011) excavated several trenches across Washington-fault-zone-related lineaments at Gypsum Wash Dam east of Washington Fields in Utah (plate 1). Based on soil development and stratigraphy, ESA estimated relative ages of faulted Quaternary deposits and concluded that the Washington fault zone at Gypsum Wash has had late Pleistocene movement and likely Holocene movement.

Peterson (1983) produced the only previous study that focused solely on the Washington fault zone. His detailed structural analysis and accompanying map cover the fault zone in Arizona from the state line southward to Wolf Hole Lake. Major conclusions of his report include: (1) basalts of at least two

different ages are displaced by the fault zone (Stage I and II flows of Hamblin, 1963), (2) south of the state line, several splays comprise a 4-km-wide fault zone where "maximum displacement commonly shifts from one fault plane to another," (3) the fault planes, where exposed, are steeply west dipping, (4) slickensides show nearly pure dip-slip movement, (5) differential erosion caused by juxtaposition of units with differing mechanical properties is the main factor controlling scarp development, (6) both normal and reverse drag are common along the fault, but reverse drag is more extensive, and (7) in more brittle rocks, reverse drag is expressed as antithetic faulting and graben formation.

Christenson and Deen (1983) mapped parts of the Washington fault zone near St. George and Washington City for their report on the engineering geology of that area. They recognized that subsidiary faults displace the Washington basalt flow on the west end of Washington Black Ridge.

Menges and Pearthree (1983) prepared a neotectonic map for Arizona that includes the Washington fault zone. Based on multiple scarp profiles, landform analysis of bedrock scarps, and the estimated ages of faulted and unfaulted geologic units, they concluded that the most recent faulting from near the Utah-Arizona border to the intersection with the Dutchman Draw fault is late Pleistocene or younger. South of the fault intersection, they estimated the most recent faulting to be middle Pleistocene or younger. Their inset map of the fault zone implies that several scarps are developed on "alluvial piedmonts" including one about 2 km north of the Utah border. Analysis of scarp profiles from these sites yielded scarp ages ranging from late Pleistocene to early Holocene.

As part of an inventory of Quaternary structures in the Cedar City 1° x 2° quadrangle, Anderson and Christenson (1989) made a reconnaissance study of the Washington fault zone in Utah. They reported rake angles of striations ranging from pure dip slip to 50° south, indicating possible sinistral (left lateral) movement, and identified parts of the fault that are east dipping, indicating a local reverse sense of movement. They concluded that a prominent fault scarp north of Interstate 15 in Washington City is due largely to differential erosion rather than to tectonic movement, which indicates that little displacement has occurred on that part of the fault in late Quaternary time. South of Washington City, they profiled a scarp developed on a thin mixed alluvial-colluvial deposit, and by comparing the profile to Lake Bonneville shoreline scarps having similar morphologies, estimated the scarp age as late Pleistocene.

The Washington fault zone and major splays have been mapped at 1:24,000 scale in Arizona by Billingsley (1990a, 1990b, 1991a, 1991b, 1992a, 1992b). Recent 1:24,000-scale geologic mapping by the Utah Geological Survey (UGS) of the Washington Dome (Hayden, 2005), St. George (Hayden and Willis, 2011), Harrisburg Junction (Biek, 2003), and Washington (Willis and Higgins, 1995) quadrangles includes portions of the trace of the Washington fault zone in Utah. Biek and others' (2009) 1:100,000-scale geologic map of the St. George 30′ x 60′ quadrangle includes the Washington fault zone in Utah and was derived from published 1:24,000-scale geologic maps and previously unpublished field data.

METHODS

The geologic map of the Fort Pearce and Washington Hollow sections of the Washington fault zone that accompanies this report (plates 1 and 2) combines new geologic mapping accomplished for this study and bedrock and surficial geology compiled from existing geologic quadrangle maps (figure 3). Because the pre-existing geologic mapping did not focus primarily on late Cenozoic surface faulting, our new map emphasizes late Cenozoic unconsolidated deposits and volcanic rocks, and their relation to displacement on the Fort Pearce and Washington Hollow sections of the Washington fault zone. The primary aerial photography sets used for mapping were 1981 Project 810941 1:24,000-scale morning and afternoon low-sun-angle photos (ESA, 1982, compiled by Bowman and others, 2011), 1983 Project 3214 1:24,000-scale color photos (IntraSearch, 1983), and 2002 Bureau of Land Management Project AZ-02-AC 1:24,000-scale color photos (Bureau of Land Management, 2002).

GEOLOGY OF THE FORT PEARCE AND WASHINGTON HOLLOW SECTIONS OF THE WASHINGTON FAULT ZONE

Fort Pearce Section

Quail Hill to Fort Pearce Wash

Previous workers placed the Sullivan Draw–Fort Pearce section boundary at Quail Hill (Menges and Pearthree, 1983; Pearthree, 1998) (figure 1), where there is a significant change in the Washington fault zone's surface expression. South of Quail Hill, the fault zone is near the base of the east-facing slope of Wolf Hole Mountain. North of Quail Hill, the fault defines an increasingly higher, west-facing escarpment formed on Permian Kaibab Formation limestone. The significant change in morphology at Quail Hill is likely enhanced by differential erosion of rocks with varying resistance to erosion on opposite sides of the fault. South of Quail Hill, the easily eroded Harrisburg Member of the Permian Kaibab Formation is in fault contact with the equally weak and easily eroded Shnabkaib Member of the Triassic Moenkopi Formation, resulting in little relief across the fault. Escarpment formation in that area is controlled by differential erosion of the resistant Pliocene Wolf Hole lava flow which caps Wolf Hole Mountain to the west (plate 2). North of Quail Hill, the Washington fault zone juxtaposes resistant limestone of the Fossil

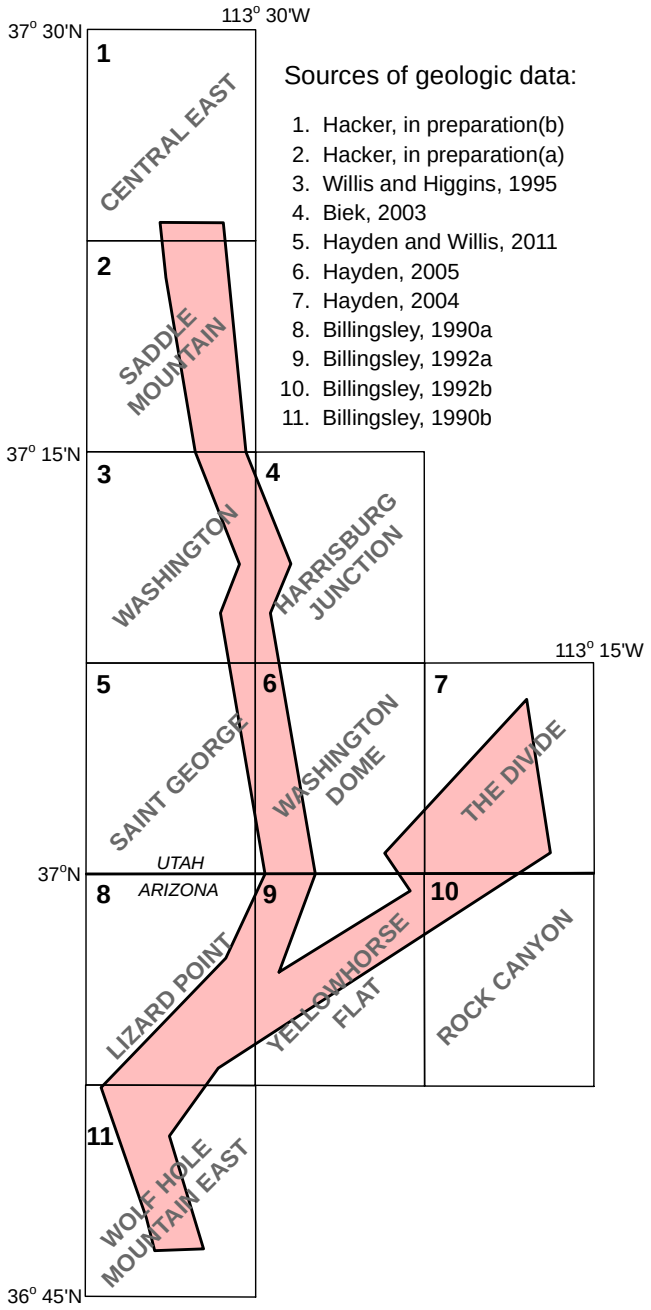

Figure 3. *Geologic quadrangle (7.5-minute) map coverage of the Fort Pearce and Washington Hollow sections of the Washington fault zone.*

Mountain Member of the Kaibab Formation in the footwall against colluvium- and alluvium-mantled, easily eroded shale of the Harrisburg Member and Moenkopi Formation in the hanging wall. Differential erosion along the fault has formed a west-facing escarpment that rises from no relief at Quail Hill to 250 m high at a prominent bend in the fault less than 3 km to the north. The fault's 50° change in strike from north-northwest to north-northeast at the bend is accompanied by a rhombic pattern of secondary faults in the footwall.

Since the change in scarp morphology at Quail Hill is due chiefly to differential erosion, and has no apparent tectonic implications, I propose that the Fort Pearce–Sullivan Draw section boundary be placed at the prominent fault bend 3 km to the north. The fault bend is also coincident with where Billingsley (1990b) showed a north-to-south decrease in fault displacement from 167 m at a point about 0.8 km north of the bend to 122 m about 1 km south of the bend.

North of the fault bend, escarpment height increases to about 300 m. The main fault trace is positioned about midway up the cliff face and is poorly exposed due to partial cover by colluvium and slope-wash deposits. Where exposed, the fault plane is nearly vertical and, in some places, dips steeply to the east (Billingsley, 1993). About 4.5 km northeast of the bend, a short section (~170 m long) of the fault appears to have vertically displaced alluvial and colluvial deposits (Qca) up to 1.5 m (station 1, plate 2). The deposits appear to be only a few meters thick and the scarp is likely bedrock cored at shallow depth.

About 5 km northeast of the fault bend, a 5-km-long by 0.5-km-wide lava flow remnant ($Tbqd_1$) in the fault hanging wall is in fault contact with the Harrisburg Member in the fault footwall (plate 2). The hanging-wall basalt acts as a protective cap rock that preserves a nearly complete section of Moenkopi Formation above the otherwise stripped Kaibab Formation surface below. There, the large topographic escarpment along the fault (~300 m high) is shifted to the western edge of the flow remnant with essentially no scarp development along the fault itself (Peterson, 1983). The flow has been interpreted by previous workers (e.g., Billingsley and Workman, 2000; Downing and others, 2001) to be a displaced remnant of the 2.4 Ma (see Lund and Knudsen, this volume) Seegmiller Mountain flow, which caps Seegmiller Mountain on the fault footwall to the south. However, a new $^{40}Ar/^{39}Ar$ age of 2.9 Ma obtained for the flow as part of this investigation (sample QD1 on plate 2; Lund and Knudsen, this volume) indicates the elevated flow remnant is significantly older and therefore cannot be part of the Seegmiller Mountain flow. Additionally, Billingsley's (1990a, 1993) mapping and plate 2 show a vent area ($Tbqdc_1$ on plate 2) within the flow remnant indicating a local source for the flow.

Near the north end of the remnant flow, the Dutchman Draw fault branches to the northeast from the Washington fault zone that continues to the north-northeast. Since results of this mapping indicate the Dutchman Draw fault is better defined as a strand of the Fort Pearce section rather than as an independent fault (see Dutchman Draw discussion below), hereafter, it is called the Dutchman Draw strand.

North of the intersection with the Dutchman Draw strand, the Fort Pearce section consists of one to three closely spaced splays that have formed steep cliffs on the Kaibab Formation. Starting about 2 km north of the intersection with the Dutchman Draw strand, one of the westernmost splays forms a nearly continuous 1- to 2-m-high bedrock fault scarp formed on the Kaibab Formation extending to the north for about 3 km. The scarp appears sharp and relatively young on aerial

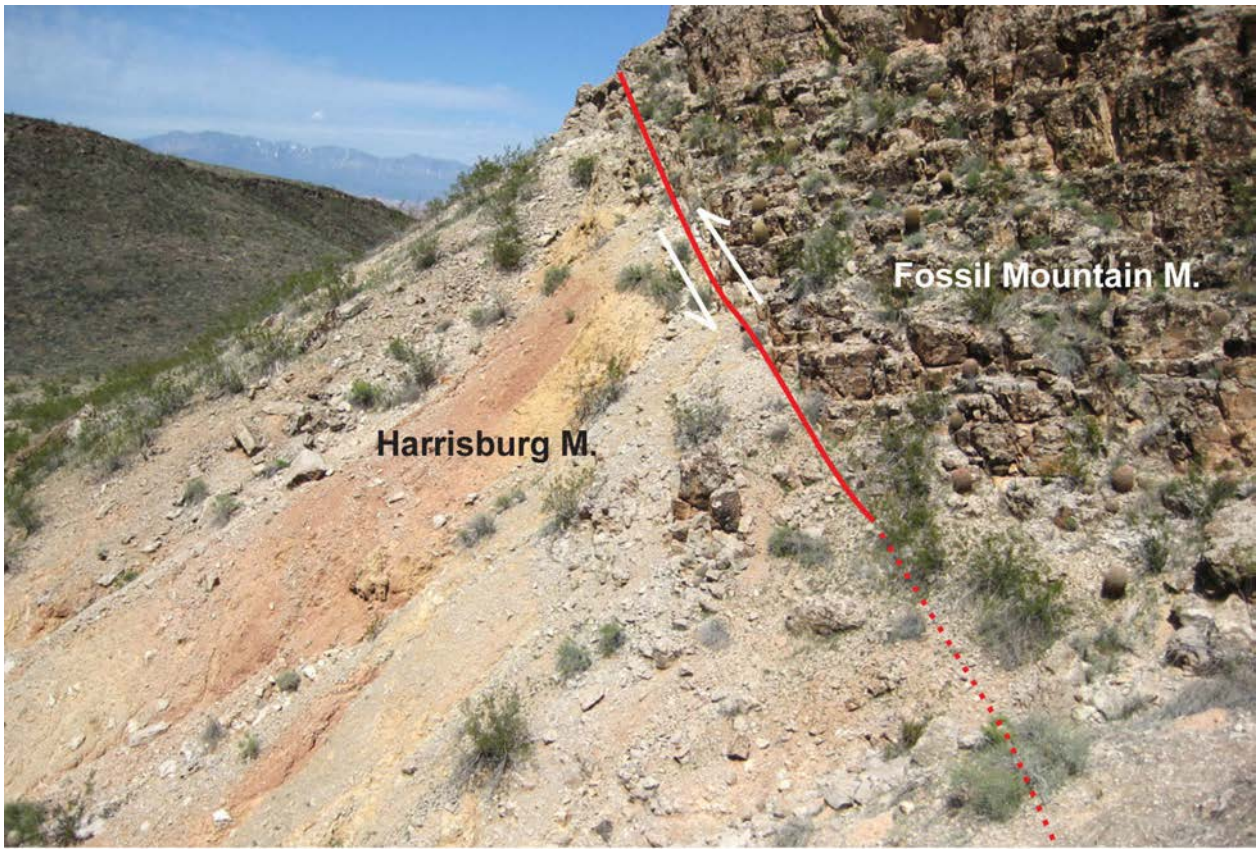

Figure 4. *A splay of the Washington fault zone places Fossil Mountain Member of the Kaibab Formation over the younger Harrisburg Member (reverse faulting) about 9 km south of the Utah-Arizona state line. View is to the north.*

photography, but is less well expressed in the field due to partial cover by colluvium and slope-wash deposits. The fault zone is well exposed in several drainages, revealing steeply dipping fault planes that locally dip to the east (figure 4). One possibility for the apparent reverse sense of faulting is that the steeply west-dipping fault at depth may take advantage of pre-existing east-dipping fracture sets within resistant Kaibab Formation limestone as the fault projects to the surface. Several slickenlines exposed in the fault zone indicate nearly pure dip-slip movement. This area exhibits the greatest stratigraphic displacement documented anywhere along the Fort Pearce section, with the Fossil Mountain Member of the Kaibab Formation juxtaposed with the upper red member of the Moenkopi Formation, implying a maximum throw of about 660 m (Peterson, 1983).

Near Dutchman Draw (figure 1), the Fort Pearce section consists of two sub-parallel splays that have produced moderately high bedrock escarpments about 300 m apart. The eastern splay juxtaposes various members of the Kaibab and Moenkopi Formations. Short sections (<300 m) of the eastern splay are overlain by unfaulted, mid-Pleistocene to Holocene pediment deposits (Qap).

The western splay generally defines a bedrock-alluvium contact between a moderately high bedrock escarpment to the east and a broad alluvial plain to the west. About 0.6 km south of Dutchman Draw, the western splay displaces a late Pleistocene to Holocene alluvial fan (Qaf_2) for a distance of approximately 100 m (plate 2). The scarp is up to 4 m high and is the location of a detailed UGS paleoseismic trenching investigation (Lund and others, this volume).

The Mokaac fault joins the Fort Pearce section from the southwest near Dutchman Draw (plate 2). Since results of this mapping show that the Mokaac section (Pearthree, 1998) is better defined as a strand of the Fort Pearce section rather than as an independent fault section (see Mokaac Fault discussion below), hereafter, it is called the Mokaac strand.

Several mafic lava flow remnants ($Qbdd_1$ and $Qbdd_2$) cap low mesas (12–60 m high) west of the Fort Pearce section near Dutchman Wash. The flow remnants overlie upper members of the Moenkopi Formation and the Triassic Chinle Formation. Although the flow remnants have not been dated, new geochemical analyses (Lund and Knudsen, this volume) indicate likely correlations between the flow remnants west of Dutchman Draw and flows to the south and southeast on the footwall of the Fort Pearce section. The remnants northwest of the Mokaac strand ($Qbdd_1$) appear to be correlative with either the 1.75 Ma ($^{40}Ar/^{39}Ar$) West Mesa or the 1.28 Ma ($^{40}Ar/^{39}Ar$) East Mesa (Qbe) lava flows about 5–8 km to the southeast (Lund and Knudsen, this volume). The flow remnant bounded by the Mokaac strand and Fort Pearce section

($Qbdd_2$ on plate 2) appears to be correlative with the 2.4 Ma ($^{40}Ar/^{39}Ar$) Seegmiller Mountain flow (Qbs), more than 9 km to the south (plate 2; Lund and Knudsen, this volume). These correlations allow calculation of long-term vertical-slip-rate estimates across all three strands (main, Mokaac, Dutchman Draw) of the Fort Pearce section; slip rate calculations are discussed by Lund and Knudsen (this volume).

Near the displaced alluvial fan, a significant change in escarpment morphology and near-fault bedrock deformation coincides with a change in the dominant geologic unit exposed in the fault footwall. South of the displaced fan, the main fault escarpment exposes the resistant Fossil Mountain Member of the Kaibab Formation and is over 100 m high. A narrow zone of footwall normal drag is expressed as closely spaced, down-to-the-west subsidiary faults in rhombic to anastomosing patterns. North of the displaced fan, the main escarpment consists of easily eroded, gypsiferous mudstone and siltstone of the Harrisburg Member of the Kaibab Formation and the lower red member of the Moenkopi Formation, resulting in a more subdued escarpment typically less than 30 m high. A narrow zone of footwall fault drag is expressed in generally unfaulted bedrock that exhibits sharp monoclinal folding and near-vertical bedding in exposures close to the fault zone.

North of the displaced fan, the main trace of the Fort Pearce section is typically buried beneath alluvial deposits, except for a short section about 400 m north of Dutchman Wash where the fault places Moenkopi bedrock (TRml) and upper Pleistocene fan alluvium (Qaf_3) in the hanging wall against the Harrisburg Member of the Kaibab Formation in the footwall (plate 2). Displaced unconsolidated deposits are not mapped again for several kilometers into Utah.

Fort Pearce Wash to Washington City

Just north of Fort Pearce Wash near the Utah-Arizona border (figure 1), the Fort Pearce section makes a 35° bend to the west and trends N. 14° W. Hayden (2005) estimated normal separation at the border to be 500 m. The regional dip of strata north of Fort Pearce Wash is generally to the east as part of the eastern limb of the Cretaceous Virgin anticline. Normal down-to-the-west drag in the fault footwall superimposed on the regional east-dipping Moenkopi Formation strata has produced a narrow anticline that parallels the fault. In a number of places, anticlinal closure has been attained east of the fault zone (Hayden, 2005) (Punchbowl and Beehive Domes, plate 1).

Near the fault bend about 1 km north of the Utah-Arizona border, a 1- to 2-m-high and 240-m-long, east-facing obsequent fault scarp formed where soft mudstones of the middle red member of the Moenkopi Formation in the fault footwall have eroded faster than mixed alluvial and eolian deposits (unit Qae) in the hanging wall to the west (figure 5; station 2, plate 1).

North of the obsequent scarp, the fault zone resumes a west-facing scarp configuration. The scarp maintains a 2- to 14-m-high and steep (30–45°) geometry for about 4 km where footwall Shnabkaib Member of the Moenkopi Formation is faulted against easily eroded mudstone of the Moenave Formation with a relatively thin cover of mixed alluvial and eolian deposits (Qae, Qac, and Qcao) in the hanging wall. The upper few to several feet of Holocene mixed deposits (units Qae and Qac) appear to overlie the fault and are unbroken; thus the fault is mapped as concealed in those areas. However, the fault is mapped as well defined farther north where late Pleistocene colluvial-alluvial deposits (unit Qcao) appear to be faulted against Shnabkaib bedrock at the surface. The prominent 4-km-long scarp formed on the Shnabkaib Member is likely a result of surface faulting although differential erosion of contrasting lithologies across the scarp has greatly altered scarp heights.

At a point about 3 km north of the Utah-Arizona border, the Fort Pearce section bifurcates into several splays for a distance of less than 350 m (station 3, plate 1). A stream cut exposes a splay that places vertical upper red member Moenkopi Formation strata in fault contact with highly deformed alluvial and eolian deposits (figure 6). The unconsolidated deposits are deformed in a 3-m-wide zone that includes shears, antithetic faulting, and rotated clasts. The faulted unconsolidated deposits have weak carbonate soil morphology and are estimated to be late Pleistocene to early Holocene in age. The faulted units have been beveled and covered by unfaulted stream deposits that are estimated to be middle to late Holocene in age. No scarp is present at the surface.

A bouldery mixed colluvial and alluvial deposit (map unit Qcao) is vertically displaced 3.5 m by the fault about 1.5 km south of the Washington Fields–Warner Valley Road junction (Anderson and Christenson, 1989; Hayden, 2005; station 4, plate 1; figure 7). The scarp is less than 30 m long where formed on Quaternary sediments, but continues to the north and south where it is developed on the Shnabkaib Member of the Moenkopi Formation. Stream cuts across the scarp reveal that it is bedrock cored, and that the overlying mixed colluvial and alluvial deposit is generally less than 1 m thick. Anderson and Christenson (1989) profiled the scarp and found the slope angle and height comparable to those of a 13,000-year-old Lake Bonneville shoreline, and therefore estimated that the scarp formed in the late Pleistocene.

Near Warner Valley Road, the Fort Pearce section consists of several west-dipping splays. Low bedrock scarps indicate the presence of the splays, but I observed no definitive displacement of Quaternary deposits at the surface. In 2009, Simon Bymaster, Inc. (SBI) excavated 13 trenches to evaluate the surface-fault-rupture hazard to part of the proposed Utah Department of Transportation (UDOT) Southern Parkway (State Route [SR] 7) northern extension freeway alignment and three elevated interchanges that were either astride or near surface traces of the Fort Pearce section (see plate 1 for

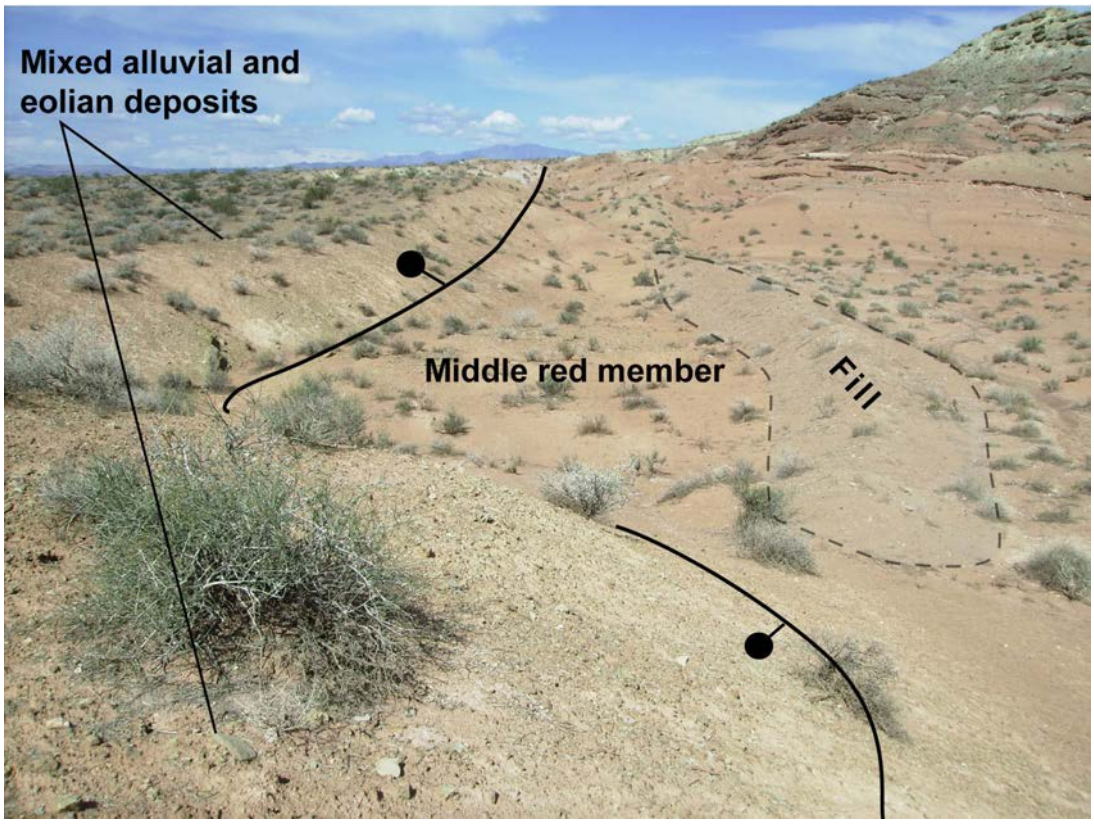

Figure 5. *Obsequent fault scarp formed along the Washington fault zone between unconsolidated basin-fill deposits and the middle red member of the Moenkopi Formation north of Fort Pearce Wash. Bar and ball on downthrown side of fault. View is to the north.*

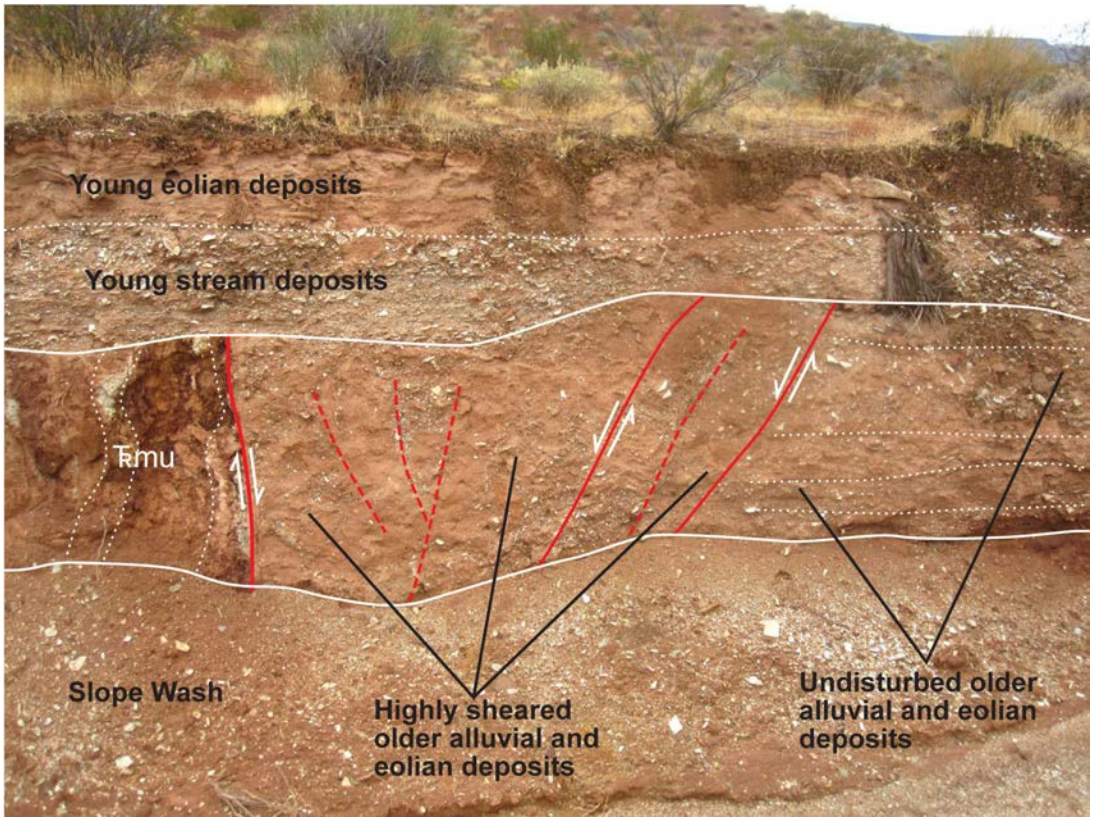

Figure 6. *A splay (red lines) of the Washington fault zone exposed in a stream cut about 1 km north of the Utah state line. TRmu, Triassic upper red member of the Moenkopi Formation. Note the beveled surface formed by erosion on the Moenkopi bedrock. View is to the south.*

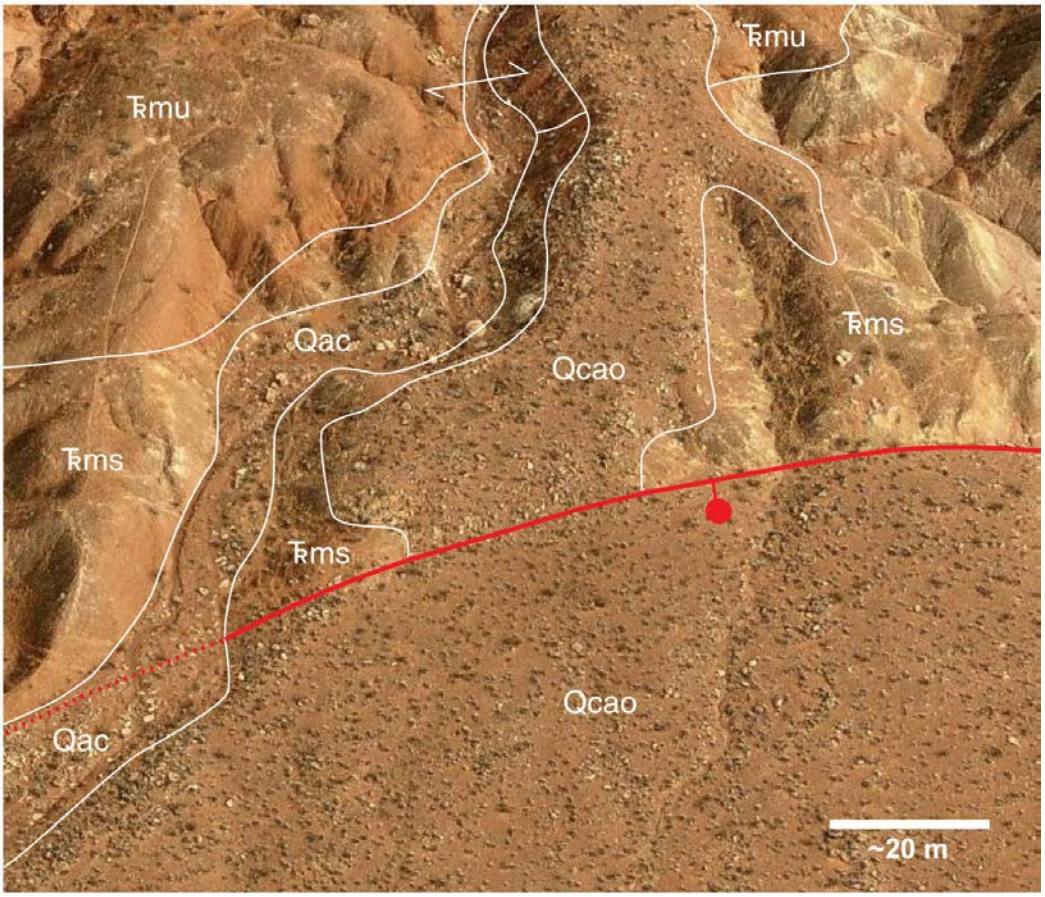

Figure 7. *Oblique aerial view to the east of a scarp formed in Triassic bedrock and Quaternary unconsolidated deposits 1.5 km south of the Washington Fields-Warner Valley Road junction. Undated photo acquired by Pictometry International and viewed using Microsoft Bing Maps (http://www.bing.com/maps/). Qac, Quaternary mixed alluvium and colluvium; Qcao, Quaternary older mixed colluvium and alluvium; TRmu, Triassic upper red member of the Moenkopi Formation; TRms, Triassic Shnabkaib Member of the Moenkopi Formation. Bar and ball on downthrown side of fault.*

trench locations). SBI excavated 11 trenches along the westernmost splays near Warner Valley Road, and two additional trenches to the north near the Gypsum Wash flood-control dam (plate 1). Trenching results indicate Holocene fan deposits are displaced to within less than 1 m of the ground surface by the Fort Pearce section in this area. See Simon and others (this volume) for details of their surface-fault-hazard investigation.

North of Warner Valley Road and in the vicinity of the Gypsum Wash dam, the expression of the Fort Pearce section becomes more subdued and is mapped as a concealed fault (plate 1). Aside from a few short (<125 m long) bedrock scarps, any fault scarps formed on Quaternary deposits that may have existed in this area are now obscured by dam construction. As part of a seismic-safety investigation of the Gypsum Wash dam, ESA (1982) excavated several trenches (see plate 1 for trench locations) across photolineaments near the dam's foundation. ESA excavated two trenches across what they considered a "major trace" of the fault zone and exposed a near-vertical shear plane displacing gypsiferous shale bedrock, an "older alluvial-fan" deposit, and an overlying "younger alluvial-fan" deposit. The absence of datable material in the trenches prevented ESA from refining their relative age assessments (which were based on soil development) beyond their "younger" and "older" categories, which they estimated to be 5000-10,000 years old and 10,000–25,000 years old, respectively. The bedrock was displaced below the floor of the trench in the fault hanging wall, indicating a minimum displacement of 1.2 m. The fault displaced young alluvium above the bedrock about 5 cm before dying out within 0.6 m of the ground surface. ESA stated that the 5 cm of displacement in the young alluvium could be either tectonic or due to differential compaction across the fault plane. Trenches excavated farther west revealed several east- and west-dipping faults that offset stratified late Pleistocene "older alluvium" up to several feet. Overlying "young alluvium" estimated to be Holocene in age was unfaulted. ESA (1982) found no datable material to constrain rupture timing, but concluded that the Washington fault zone at Gypsum Wash has had late Pleistocene and likely Holocene movement.

North of Gypsum Wash dam, the Fort Pearce section intersects and truncates the southern nose of the Washington Dome portion of the Virgin anticline. At this intersection, a heavily dissected bedrock escarpment formed on the Harris-

burg Member of the Kaibab Formation and lower Moenkopi Formation strata is about 450 m long. The exact position of the fault in this area was unknown until Applied Geotechnical and Engineering Consultants (AGEC) excavated five trenches across the concealed trace of the fault zone near the bedrock escarpment as part of a surface-fault-rupture-hazard investigation for a proposed residential development (see plate 1 for trench locations). Trench T-1 exposed the main trace of the fault zone. The UGS made a brief reconnaissance investigation of the exposed fault and collected several samples of colluvial/eolian sand from within, above, and below what were interpreted to be faulting-related colluvial wedge deposits and submitted them to the Utah State University Luminescence Laboratory for optically stimulated luminescence (OSL) age analysis. Results of reconnaissance logging and OSL analysis indicated that the Fort Pearce section has likely experienced at least three surface-faulting earthquakes at this site since 76 ka, the most recent possibly in latest Pleistocene time (Lund and others, 2008). The trench, which remained open for several years, was later logged in detail by SBI, as part of their surface-fault-rupture-hazard investigation for UDOT (Simon and others, this volume).

North of Washington Dome, the Fort Pearce section traverses the eastern margin of Washington Fields—a relatively flat, low-lying agricultural area south of the Virgin River that is rapidly being converted to residential development. Any surficial expression of the fault that may have existed in this area has been destroyed, and the main fault is mapped as concealed beneath Quaternary deposits (Qae) (plate 1).

A 1.5-km-long, west-dipping, subsidiary fault splay exposed in Moenkopi Formation strata parallels the main Fort Pearce section less than 0.5 km east of Washington Fields. The subsidiary splay forms a well-defined, linear bedrock scarp where the middle red member of the Moenkopi Formation is in fault contact with the Virgin Limestone Member to the east. The escarpment is clearly visible on 1983 color aerial photos (ESA, 1983; compiled by Bowman and others, 2011), but has been destroyed by residential development in recent years. Additionally, the 1983 aerial photos show a 25-m-long section of the scarp developed in mixed alluvial and eolian deposits (Qae; station 5, plate 1). Because the subsidiary splay is buried by the same map unit immediately to the north, it is possible that the Quaternary sediments forming the scarp are unfaulted and draped over a preexisting bedrock scarp rather than displaced by surface faulting.

North of the Virgin River, the Fort Pearce section is mapped as concealed where it parallels the linear western end of Washington Black Ridge. Highly deformed mudstones and sandstones of the Chinle Formation exposed in road cuts along Washington Fields Road indicate that the main fault is likely coincident with the roadway at the base of the ridge.

Washington Black Ridge is capped by the Washington lava flow, which has $^{40}Ar/^{39}Ar$ radiometric ages of 0.87 and 0.98 Ma (Biek and others, 2009). The flow erupted from a cinder cone 5 km north of Washington City, flowed south along the ancestral Grapevine Wash, and then flowed west along the ancestral Virgin River (plate 1). The downstream termination of the flow coincides with the main trace of the Fort Pearce section, and is within 500 m of the north-to-south-flowing Mill Creek drainage. Anderson and Christenson (1989) proposed three possible explanations for the Washington flow's termination: (1) the distal end of the flow has been displaced down to the west by the Washington fault zone and subsequently buried by alluvium, (2) the western continuation of the flow has been eroded away by Mill Creek, and (3) the flow terminated at its present location and never extended across the fault. I researched the Utah Division of Water Right's water-well database (Utah Division of Water Rights, 2011) for wells drilled along the projected downthrown continuation of the Washington flow near Mill Creek. Drillers' logs for two water wells immediately west of Mill Creek in the SW1/4NW1/4 section 23, T. 42 S., R. 15 W. and the NW1/4SW1/4 section 23, T. 42 S., R. 15 W., Salt Lake Base Line and Meridian (see plate 1 for approximate locations) show unconsolidated alluvium to a depth of 30 m. If the Washington flow is present beyond Mill Creek, it is more than 30 m below the surface, which would result in more than 90 m of displacement when compared to the flow capping Washington Black Ridge, which stands an additional 60 m above stream level. I consider the evidence inconclusive for any of the three flow termination scenarios proposed by Anderson and Christenson (1989).

Four subsidiary fault splays 0.5 km east of the main Fort Pearce section displace the Washington flow by as much as 4.5 m (Anderson and Christenson, 1989; Biek, 2003; Hayden, 2005; figure 8). Two of the smaller scarps have been destroyed by residential development in recent years.

The Fort Pearce section is obscured by development where it traverses through Washington City; however, late 1930s-era aerial photos (Utah Automated Geographic Reference Center, 2012a) show that the main trace defines the western edge of a low, poorly defined, mostly bedrock escarpment through the town.

Near Interstate 15, the Fort Pearce section consists of three parallel, northwest-trending splays that form prominent, but discontinuous west-facing scarps. The western splay is considered the main fault because it juxtaposes Kayenta Formation and Navajo Sandstone indicating about 200 m of stratigraphic separation, and because that splay has substantial footwall and hanging-wall deformation associated with it. In contrast, the middle and eastern splays are wholly contained within the Kayenta Formation, and appear to have only a few tens of meters of displacement.

Despite sharp, up to 8-m-high west-facing scarps formed on all three splays near Interstate 15, I consider scarp formation there to primarily result from differential erosion rather than

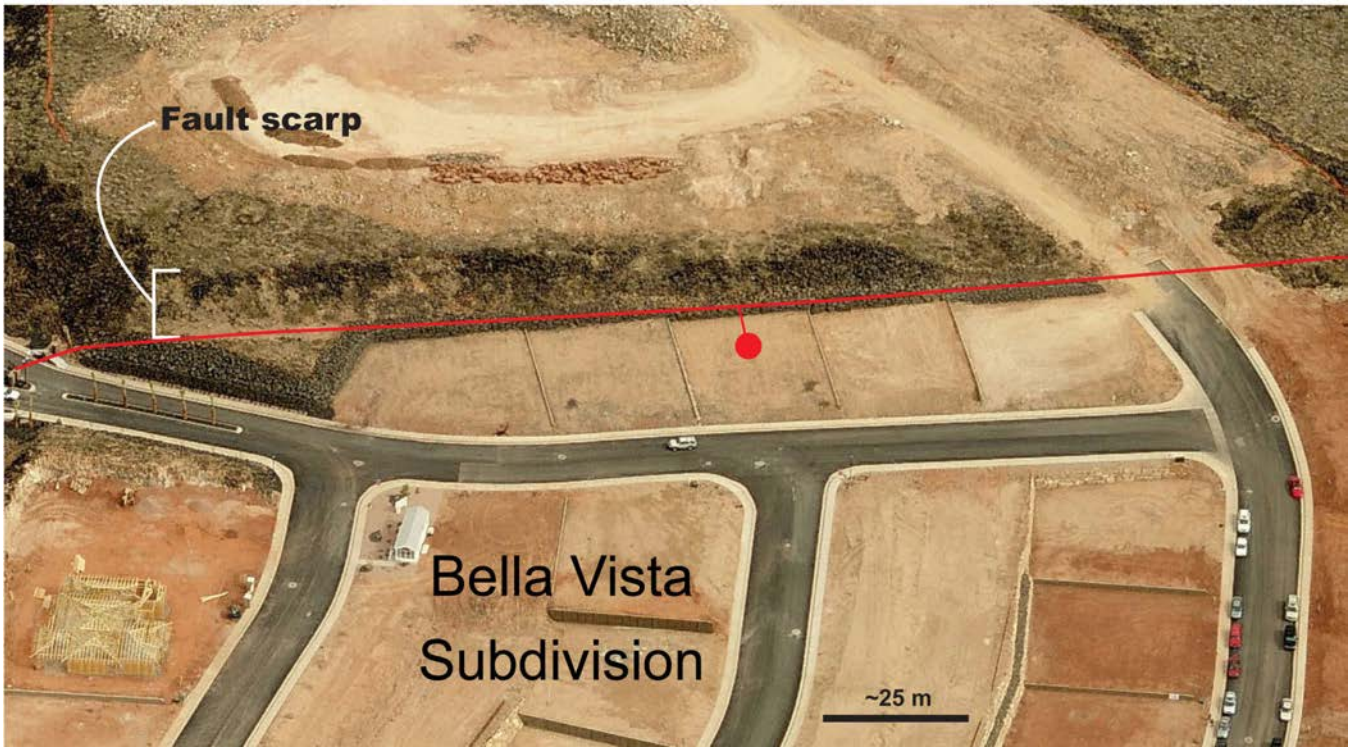

Figure 8. *Oblique aerial view to the east of fault scarp formed on the Washington lava flow. Bar and ball on downthrown side. Scarp is 4.5 m high. Undated photo acquired by Pictometry International and viewed using Microsoft Bing Maps (http://www.bing.com/maps/).*

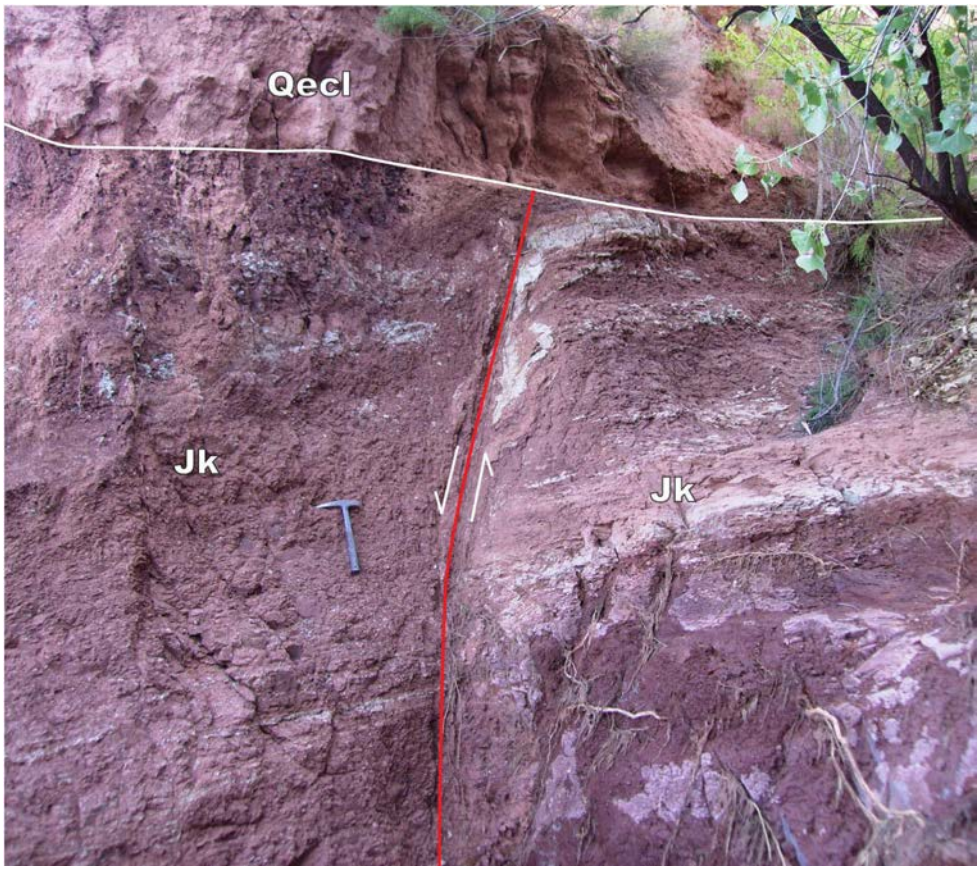

Figure 9. *Splay of the Washington fault zone (red line) exposed in a stream cut north of Washington City. Note the minor fault drag in the Kayenta Formation (Jk), and the unbroken Pleistocene carbonate-cemented sand (Qecl) covering the fault. View to the northwest.*

surface fault rupture. For example, the 6-m-high scarp developed on the main body of the Kayenta Formation (Jk) along the northern part of the eastern splay is obsequent since map patterns of the displaced Kayenta main body-Springdale (Jk-Jks) contact across the fault indicate the fault is east dipping.

Just north of a residential development, an ephemeral stream incises a scarp formed on the middle splay and exposes the fault, which dips 65° southwest and juxtaposes middle parts of the Kayenta Formation (figure 9; station 6, plate 1). The faulted bedrock has been beveled by erosion, and is covered with about 0.5 m of moderately indurated sand with a strongly-developed pedogenic carbonate soil horizon (Qecl) estimated to be middle to late Pleistocene in age (Anderson and Christenson, 1989; Willis and Higgins, 1995). The calcic sand unit is unbroken, indicating that this part of the fault zone has likely not ruptured since at least the late Pleistocene. Anderson and Christenson (1989) investigated the middle splay and concluded that the scarp is the result of accelerated erosion of hanging-wall bedrock that has been weakened by groundwater seepage from springs and intense fracturing rather than surface faulting. I agree with their assessment, which explains the anomalously short length (~400 m) of the 8-m-high scarp.

North of Washington City, the Fort Pearce section continues to bifurcate as it enters an area of densely jointed Navajo Sandstone. Beyond the Washington City water tanks (plate 1), fault displacement is contained entirely within the homogeneous Navajo Sandstone and becomes difficult to map. Closely spaced joint sets that parallel the fault splays are difficult to differentiate from faults on aerial photos and on the ground (figure 10). Large sheets of eolian sand that bury the fault exposures also complicate mapping in this area. The Fort Pearce section can be traced with some confidence to near the cinder cone that produced the Washington flow (unit Qbwc on plate 1) before it becomes obscured in a zone of northwest-trending fractures.

Mokaac Strand

The 16-km-long Mokaac strand lies to the west of and is subparallel with the Fort Pearce section of the Washington fault zone. Similar to the Fort Pearce section, the Mokaac strand dips to the west and creates a prominent escarpment capped by Kaibab Formation limestone. The escarpment height reaches about 180 m near the midpoint of the fault. Stratigraphic separation on the fault increases from about 60 m near its southern end where it is partially obscured by landslides on the eastern flank of Mokaac Mountain, to 390 m before merging with the Fort Pearce section to the north (Billingsley, 1990a).

Starting near the Quail Hill Road intersection with the Mokaac strand (plate 2), a 5-km-long, fairly continuous fault scarp formed on resistant Permian bedrock runs northeast

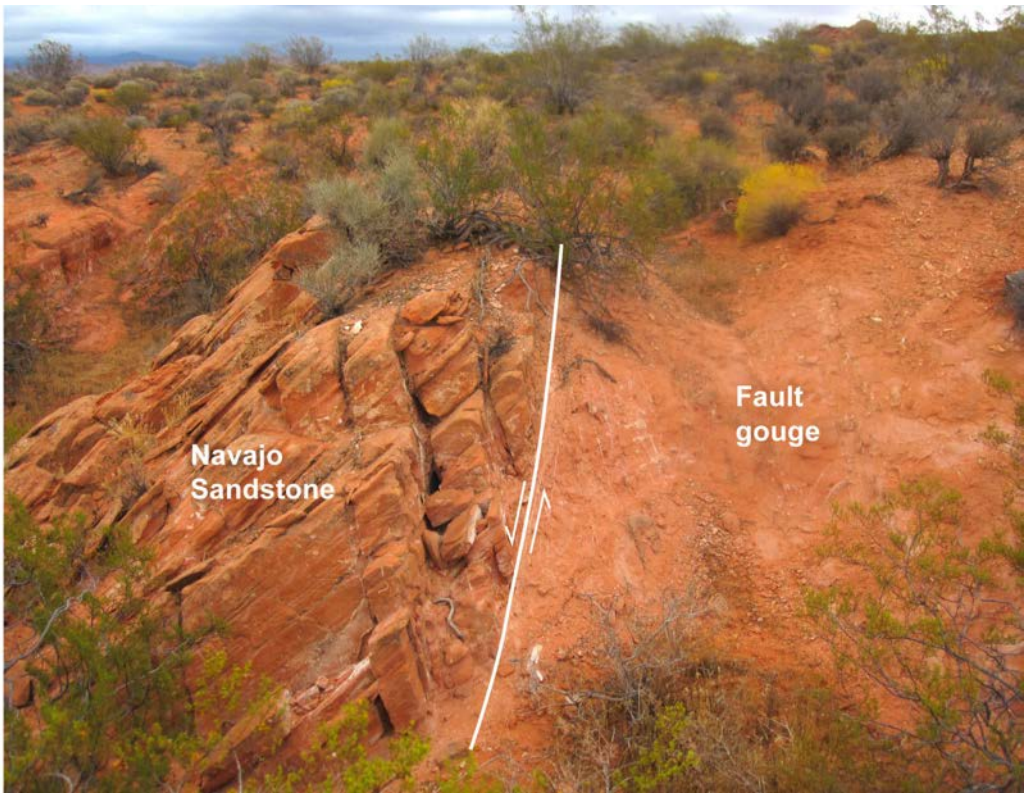

Figure 10. *Major splay (white line) of the Washington fault zone within the Navajo Sandstone north of Washington City. This structure appears similar to many nearby sub-parallel joints visible on aerial photos. Only after a field visit and documentation of fault-related features (fault drag on hanging wall and wide zone of fault gouge in footwall) was this structure identified as a fault. View to the north.*

along the base of the escarpment and defines a bedrock-alluvium/colluvium contact. The fault scarp is up to 4 m high and is commonly covered with a thin mantle of colluvium. Billingsley (1990a, 1993) indicated two locations along the scarp where Holocene alluvium and talus are displaced by as much as 3.7 m. I could not find any scarps developed on unconsolidated deposits that are not bedrock cored along the central and southern Mokaac strand.

At its northern end, the Mokaac strand juxtaposes various non-resistant members of the Moenkopi and Chinle Formations, and has a subdued to nonexistent surface expression. The fault appears to displace and possibly tilt lava flows near Dutchman Draw (plate 2; see Lund and Knudsen, this volume, for a discussion of displaced lava flows) before merging with the Fort Pearce section. A subsidiary, sub-parallel fault splay south of the main Mokaac strand produced a 3- to 5-m-high scarp on the Shnabkaib Member of the Moenkopi Formation, and the scarp continues to the north on late Pleistocene to early Holocene mixed alluvial and eolian deposits (Qae; station 9, plate 2). The part of the scarp developed on unconsolidated deposits is about 0.5 km long and has a maximum height of about 3 m. A stream cut through the scarp exposes a footwall composed of Shnabkaib Member bedrock covered with 2 to 3 m of alluvium; the site appears amenable to paleoseismic trenching. The subsidiary splay continues into a low mesa capped by a mafic volcanic flow, and appears to displace the flow a few meters, before dying out.

There is no obvious indication of a rupture barrier between the Mokaac strand and Fort Pearce section. With maximum displacement on the Mokaac strand near its junction with the Fort Pearce section, the two faults have most likely shared earthquake ruptures in the past. The fault's relatively short length (16 km) supports the inference that the Mokaac strand is accommodating slip originating on the Fort Pearce section rather than generating its own earthquakes. Based on the branching geometry of the Mokaac strand with the Fort Pearce section, it is possible that the Mokaac strand only ruptures during southward-propagating fault rupture on the Fort Pearce section. Additionally, the two faults have similar scarp morphologies, and both have displaced late Pleistocene-Holocene alluvial-fan deposits, thus indicating similar rates of activity. For these reasons, I consider the Mokaac strand to be part of the Fort Pearce section, rather than a separate fault section capable of independent earthquake rupture as proposed by Pearthree (1998). My interpretation is based on the distribution of maximum fault displacements and apparent similar rates of activity. Detailed paleoseismic trench data are necessary to definitively show that the two faults have or have not ruptured synchronously in the past.

Dutchman Draw Strand

From its junction with the Fort Pearce section (plate 2), the Dutchman Draw strand trends northeast and has formed a 120-m-high escarpment in resistant limestone of the Permian Kaibab Formation. Stratigraphic separation near the fault junction is about 115 m and decreases to the north (Billingsley, 1992a). Like other high escarpments along the Washington fault zone, prominent escarpments along the Dutchman Draw strand are likely enhanced by differential erosion because the fault juxtaposes strata of differing resistance.

The Dutchman Draw strand consists of two splays near Joe Blake Hill (plate 2). The southern splay vertically displaces the 1.28 Ma ($^{40}Ar/^{39}Ar$; Lund and Knudsen, this volume) East Mesa lava flow (Qbe) about 45 m. The underlying Kaibab-Moenkopi contact appears to be displaced roughly the same amount, indicating that faulting on the southern splay likely initiated after flow emplacement (Billingsley, 1992a).

Northeast of Joe Blake Hill, the Dutchman Draw strand is partially obscured by landslide and alluvial deposits. The fault is again well displayed on the south flank of an unnamed lava-flow-capped mesa where the Shnabkaib Member of the Moenkopi Formation is downthrown against the middle red member (plate 2, figure 11). The basalt capping the mesa is in the fault hanging wall and could be the downthrown distal remnant of an unnamed volcanic flow on the fault footwall that issued from a volcanic center 2.5 km to the east (Lund and Knudsen, this volume). If the two outcrops are correlative, the flow has been displaced as much as 80 m vertically across the Dutchman Draw strand. Although the age of the unnamed flow has not been determined, cross-cutting relations exposed on the west flank of the mesa indicate the flow postdates at least some movement on the Dutchman Draw strand. Normal drag in the hanging wall has folded the Shnabkaib and upper red members up to 20° to the north. The flat-lying basalt truncates the underlying folded strata indicating that folding and faulting initiated prior to lava deposition (figure 11).

Northeast of the unnamed mesa, there is no apparent relief across the Dutchman Draw strand for several kilometers. However, the fault is well expressed on aerial photos, where the red and white "bacon stripes" of the Shnabkaib Member of the Moenkopi Formation in the footwall are in fault contact with the middle red member.

Stratigraphic separation on the Dutchman Draw strand decreases significantly near Fort Pearce Wash, where the Shinarump Conglomerate Member of the Chinle Formation is displaced about 15 m. In the northern bank of the wash, the Petrified Forest Member of the Chinle Formation is in fault contact with the Shinarump Conglomerate. This is the northernmost definitive exposure of the Dutchman Draw strand that I could find. Billingsley and Graham (2003) mapped a 250-m-long fault scarp on a veneer of late Pleistocene alluvium (Qat_3) north of Fort Pearce Wash. Although the scarp is subdued and nearly imperceptible in the field, I agree with Billingsley and Graham (2003) that the alluvial deposits are likely faulted. Although Billingsley and Graham (2003) extended the Dutchman Draw strand as a concealed fault to the Utah border, Hayden (2004) did not map a fault in the adjoining 7.5-minute quadrangle (The Divide) in Utah. I found

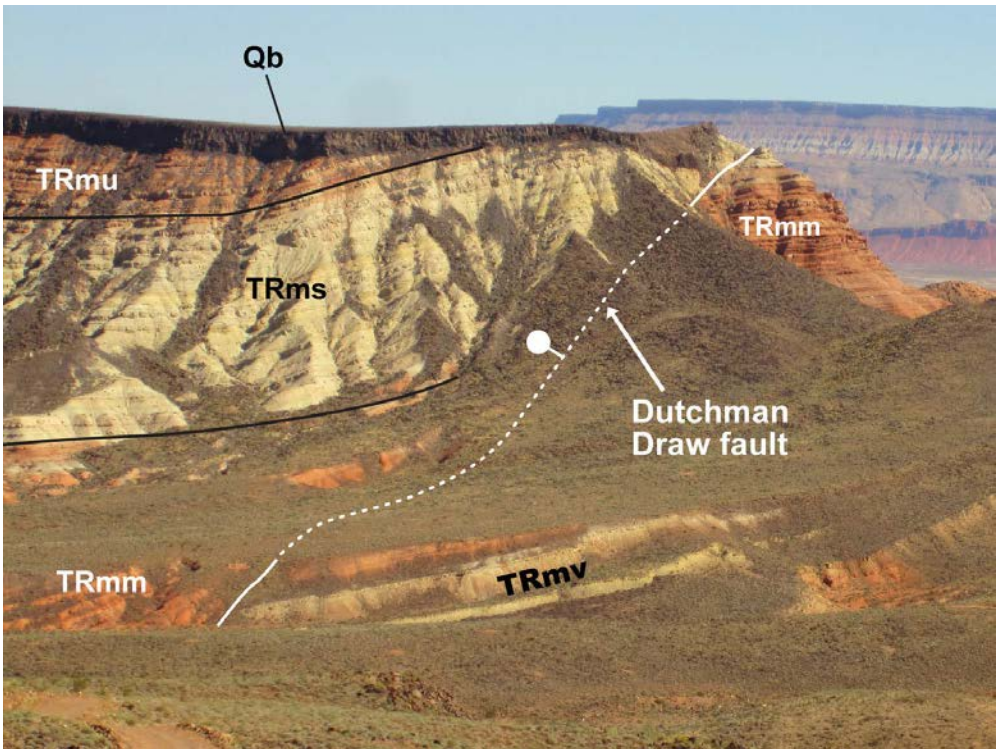

Figure 11. *Dutchman Draw fault exposed on the southwest flank of an unnamed mesa in Arizona. Truncation of fault-drag folding by Quaternary lava flow (Qb) indicates faulting initiated prior to deposition of the flow. View is to the northeast. TRmu, Triassic upper red member of the Moenkopi Formation; TRmm, Triassic middle red member of the Moenkopi Formation; TRms, Triassic Shnabkaib Member of the Moenkopi Formation; TRmv, Triassic Virgin Limestone Member of the Moenkopi Formation. Bar and ball on downthrown side of fault.*

no evidence for continuing the Dutchman Draw strand into Utah, although there is substantial alluvial/eolian cover in the area that may obscure the fault trace. Both west- and east-dipping faults are present along the projection of the Dutchman Draw strand 3.5 km north of the Utah border at Sand Mountain (plate 2). Although not exposed in the intervening interval, it is possible the Dutchman Draw strand connects with the faults at Sand Mountain. At least two of the larger Sand Mountain faults displace the approximately 1 Ma (Biek and others, 2009) Grass Valley flow by as much as 76 m before merging with the nearby Hurricane fault.

Less than 3 km east of where the Dutchman Draw strand approaches the Utah-Arizona border, Hayden (2004) mapped the down-to-the-west Warner Valley fault between Sand Mountain and the Hurricane Cliffs (plate 2). She reported a maximum stratigraphic separation of 550 m on the approximately 5-km-long fault, and stated that the fault quickly dies out in northern Arizona. Geologic maps of this area in Arizona (Billingsley, 1992b; Billingsley and Workman, 2000; this study) show no southern continuation of the Warner Valley fault, indicating that the fault likely does die out abruptly just after entering Arizona. The apparent en echelon right step between the Warner Valley fault and Dutchman Draw strand may indicate that these faults are part of the same fault system (Lund and others, 2008). This is supported by Hamblin and Best (1970) who mapped the two faults in an en echelon relation near the state line. Although obscured by alluvial fans emanating from the Hurricane Cliffs, the Warner Valley fault likely merges with the Hurricane fault.

Although the Dutchman Draw strand has been mapped and discussed separately from the Washington fault zone in previous studies, I consider the Dutchman Draw strand to be part of the Fort Pearce section of the Washington fault zone. Much like the Mokaac strand, total vertical displacement on the Dutchman Draw strand increases toward its junction with the Fort Pearce section, indicating the Dutchman Draw strand most likely accommodates slip from the Fort Pearce section, rather than being independently active. This inference is supported by the relatively short length (16 km) of the Dutchman Draw strand, and similar rates of Quaternary activity as indicated by similar scarp morphologies among the two faults. Based on the branching geometry of the Dutchman Draw strand with the Fort Pearce section, it is possible that the Dutchman Draw strand only ruptures during northward-propagating fault rupture on the Fort Pearce section.

Washington Hollow Section

A 5-km-long zone of fractures and joints extends to the northwest from the Washington flow cinder cone near the end of the Fort Pearce section of the Washington fault zone. This fracture zone trends into the Washington Hollow fault—a west-dipping normal fault with about 150 m of stratigraphic separation (Willis and Higgins, 1995). Some previous work-

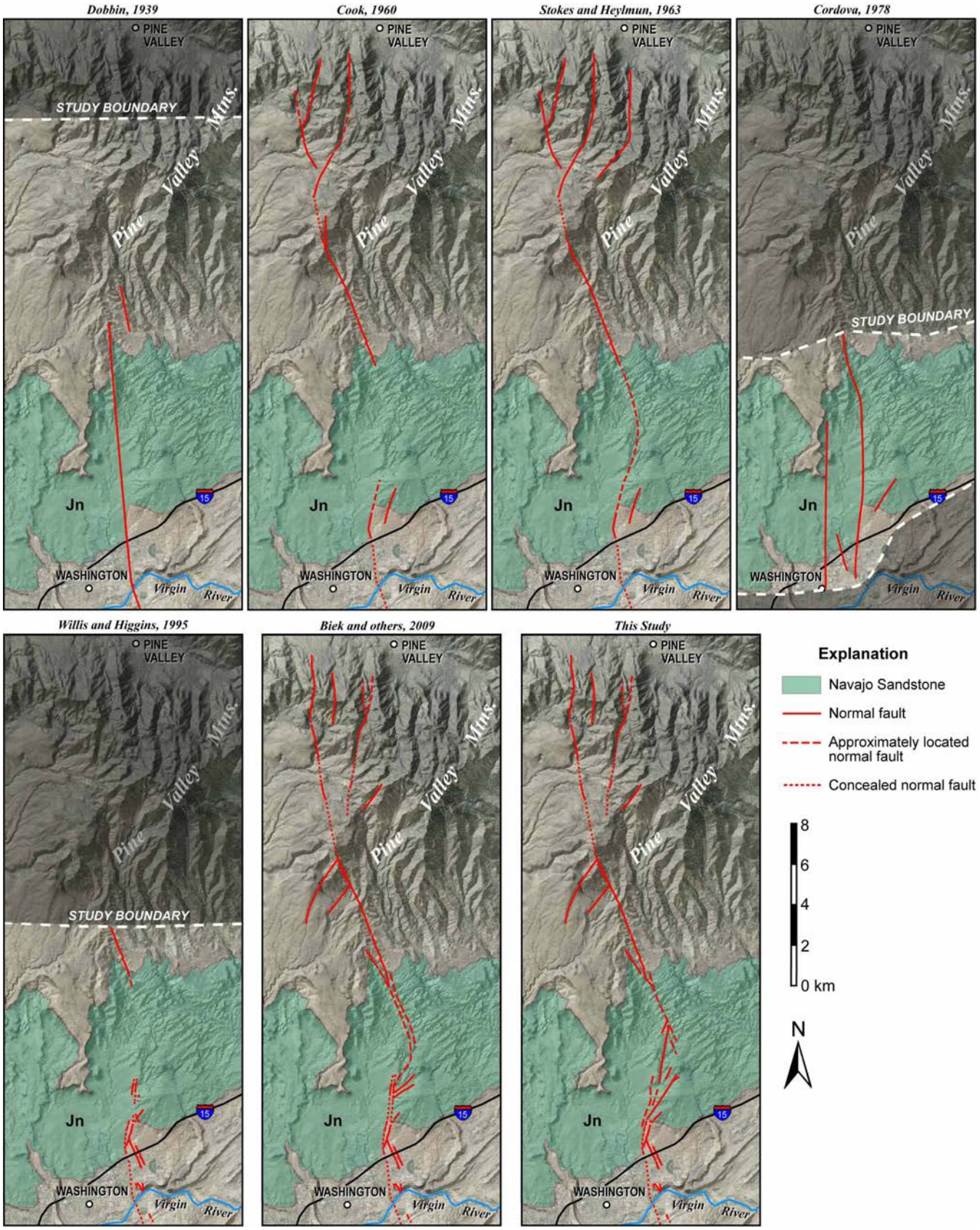

Figure 12. *Summary of geologic mapping of the Washington fault zone and Washington Hollow fault between Interstate 15 and the Pine Valley Mountains. See References section for complete citations.*

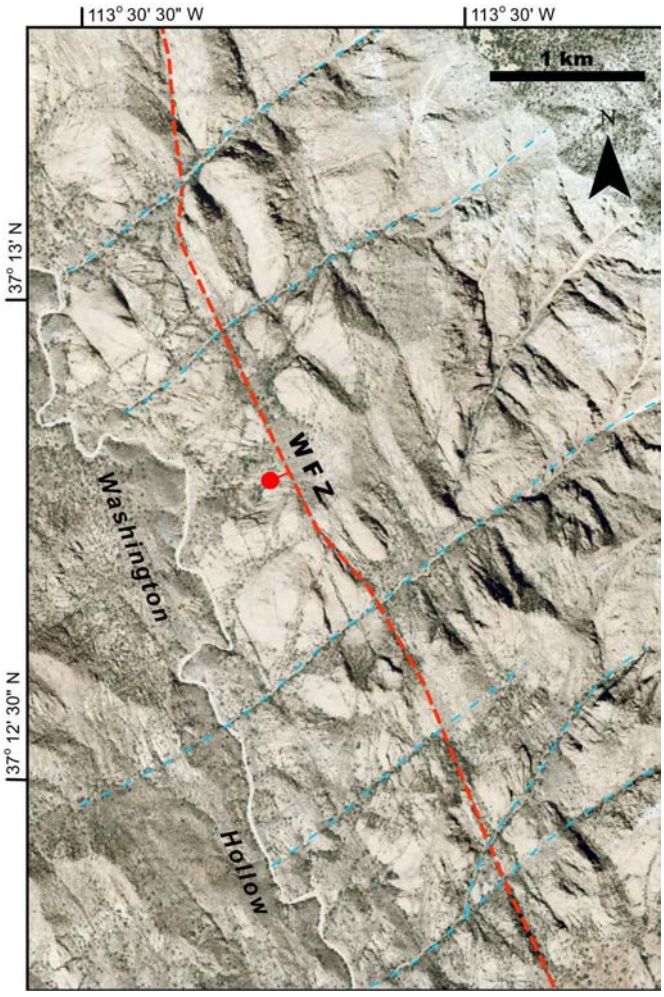

Figure 13. *Joints of probable Cretaceous age (dashed blue lines) near Washington Hollow that show no apparent offset in map view across by the Washington fault zone (WFZ, red line). Bar and ball on downthrown side of fault. Base map is 2006 National Agriculture Imagery Program (NAIP) orthophotography (Utah Automated Geographic Reference Center, 2012b).*

ers have mapped a continuous fault through Washington Hollow connecting the Washington and Washington Hollow faults, while others have mapped them as separate faults (figure 12). A prominent northeast-trending joint set at approximately right angles to the proposed connector fault through Washington Hollow parallels the Cretaceous Virgin anticline and other Sevier-age compressional structures, indicating a likely Sevier age for the joints. The joint set is therefore likely older than the more recent normal faulting, and is clearly visible on aerial photos where it persists with little or no displacement across the proposed connecting fault in Washington Hollow (figure 13), indicating that if a connecting fault does exist, it either has minimal offset or has pure dip-slip movement, in which case the displaced vertical joints would appear continuous across the fault in map view.

I mapped an approximately located, small-displacement fault in Washington Hollow (plate 1) since there is evidence for structural deformation there including brecciation, 1.5–3-m-wide crushed zones, and minor-displacement faulting (Willis and Higgins, 1995) along lineaments that have geometries similar to the two larger faults. Although I placed the fault along one of the more prominent fracture zones, strain has likely been distributed over a relatively wide zone rather than on a single master fault. This zone links the Fort Pearce section of the Washington fault zone and Washington Hollow fault, and I consider this zone of diffuse and low displacement a boundary between two separate fault sections, and therefore map the Washington Hollow fault as a section (Washington Hollow section) of the Washington fault zone, and I refer to it as the Washington Hollow section hereafter.

The following lines of evidence indicate a probable section boundary between the Washington Hollow and Fort Pearce sections near the Washington flow vent: (1) the fault exhibits increased structural complexity where it bifurcates into several smaller splays; such structural complexities are often associated with seismogenic segment boundaries, (2) net displacement across the Fort Pearce section appears to decrease significantly near the Washington flow vent with no single fault or shear zone accommodating more than a few tens of meters of displacement, and (3) the fault displays a 45° change in strike near the vent. The Washington Hollow section from the Washington flow cinder cone to the fault's terminus west of Pine Valley is 22 km long (straight-line).

The Washington Hollow section is clearly expressed at the head of Washington Hollow where it displaces varicolored strata of the Jurassic Temple Cap and Carmel Formations. Farther north, the fault juxtaposes red Tertiary Claron Formation against the pale yellow and brown Cretaceous Iron Springs Formation.

The Washington Hollow section displaces Quaternary unconsolidated deposits in at least two places. The fault forms a scarp (station 7, plate 1) on a linear, relatively thin Pleistocene alluvial-fan deposit (Qafo; Biek and others, 2009; Hacker, in preparation [a]) that caps a high ridge dividing Spring Hollow from Cottonwood Creek. The scarp is 3 to 4 m high and less than 50 m long. North of Grass Knoll, where the fault consists of three to four splays, an east-dipping splay forms a 6- to 8-m-high, 600-m-long scarp on a similar Pleistocene alluvial-fan deposit (Qafo) 0.8 km west of Quaking Aspen Spring (station 8, plate 1; Hacker, in preparation [a]; Biek and others, 2009).

From Cedar Bench to Truman Bench, the Washington Hollow section and subsidiary splays have displaced five different lava flows that range in age from about 450 ka to 1.2 Ma (plate 1; Biek and others, 2009), indicating middle Pleistocene or younger fault movement. I observed the greatest displacement on the fault at Cedar Bench just beyond the western map boundary, where a northeast-trending subsidiary fault displaces the 1.2 Ma ($^{40}Ar/^{39}Ar$ plateau age [UGS unpublished data]) Cedar Bench lava flow by as much as 12 m, yielding an early Pleistocene-Holocene vertical slip rate of 0.01 mm/yr.

The Washington Hollow section dies out on the northern flank of Saddle Mountain where it cannot be traced into the 0.6 Ma ($^{40}Ar/^{39}Ar$ plateau age [UGS unpublished data]) Lark Canyon flow to the north (plate 1; Biek and others, 2009; Hacker, in preparation [b]).

RELATION BETWEEN THE WASHINGTON FAULT ZONE AND OTHER TRANSITION ZONE FAULTS

Although my mapping focused on the northernmost two sections of the Washington fault zone (the revised Fort Pearce and herein defined Washington Hollow sections), the fault's branching pattern and close spatial relation with other nearby transition zone faults prompts questions about how these faults formed and how they interact. A regional view of the various faults and fault zones comprising the transition zone in southwestern Utah and northwestern Arizona reveals a pattern where many of the faults are en echelon, intersect, form rhombic patterns, and have salients and reentrants at similar latitudes (figure 14). Geologic mapping also shows that all major and many minor faults within the transition zone displace Quaternary alluvial deposits (Billingsley and Workman, 2000). Structural patterns and similar relative rates of activity indicate many or all normal-displacement transition zone faults may be structurally linked and part of the same extensional system.

The 87-km-long, west-dipping Main Street fault zone maintains a closely spaced (~5 km) en echelon relation with the Sullivan Draw section of the Washington fault zone for nearly 40 km (figure 14). Hamblin (1970a) and Peterson (1983) considered the Washington and Main Street faults to be part of the same fault system. Billingsley's geologic map of the Littlefield 30′ x 60′ quadrangle shows a southwest-dipping, northwest-trending fault splay with 70 m of vertical displacement and associated monocline branching from the Sullivan Draw section of the Washington fault zone and intersecting the Grand Wash fault (figure 14). Therefore, it appears the Washington fault zone and Grand Wash faults are structurally linked at the surface. Other significant but lesser faults (in terms of displacement and length) in the transition zone at this latitude include the Gyp Pocket, Sunshine Trail, and Sunshine fault zones (Pearthree, 1998; Billingsley and Workman, 2000) that occupy a large reentrant of the Hurricane fault (Hurricane Valley) (figure 14) and are considered subsidiary to the Hurricane fault (Pearthree, 1998). Hamblin (1970a) noted that these lesser faults are concave toward the Hurricane fault and suggested that they are the result of complex hanging-wall deformation being translated over a curved Hurricane fault plane. The easternmost strand of the Sunshine fault zone is parallel to, and lies within 1 km of the Main Street fault and defines the eastern edge of the Main Street horst (figure 14); these closely spaced structures are likely linked at depth. Additionally, results of this mapping (see previous section) indicate that the Washington, Dutchman Draw, Warner Valley, Hurricane, and additional minor faults may all be linked or nearly linked at the surface.

Schramm (1994) proposed a regional fault system linking the Grand Wash, Washington, and Hurricane faults. She used the following lines of evidence to support a displacement transfer zone or regional scale relay ramp bounded by the Hurricane and Grand Wash faults (figure 15) that may be linked at depth with a subhorizontal detachment:

1. The faults have similar geometries.
2. Displacement on the Grand Wash and Hurricane faults increases in opposite directions along strike, consistent with transfer of slip between the two faults (figure 15).
3. Quaternary unconsolidated deposits and basalt flows are displaced by the Hurricane, Washington, and Gunlock-Grand Wash faults, indicating that they all have been active in the Quaternary.
4. Although the earthquake record in this area of the transition zone is incomplete, scattered seismic activity across the region has been attributed to all three faults, indicating all are seismically active.

Whereas Schramm (1994) viewed the Hurricane, Washington, and Grand Wash faults as being contemporaneously active, timing data from subsequent studies indicate that these faults have been active sequentially with some overlap. Movement on the Grand Wash fault initiated in the early or middle Miocene (Bohannon and others, 1993; Billingsley and Workman, 2000), and the fault attained nearly all of its stratigraphic separation by the end of the Miocene (Lucchitta, 1987; Wenrich and others, 1995; Pearthree, 1998). Pleistocene displacement appears to be only a few meters, and Holocene deposits are unfaulted (Pearthree, 1998). Conversely, equal displacement of a 3.6 Ma basalt flow and underlying bedrock near Mt. Trumbull (figure 14) indicates movement on the Hurricane fault initiated in the Pliocene or later at that latitude (Billingsley and Workman, 2000). Similar relations between basalt flows of various ages and other structures in the transition zone led Billingsley and Dyer (2003) to conclude that the Washington and Main Street fault zones and lesser faults between the Main Street and Hurricane faults (Gyp Pocket, Sunshine, and Sunshine Trail faults) became active during the Pleistocene. All major faults and most minor structures east of the Grand Wash fault have been active in the Holocene, since Holocene alluvium has been displaced along parts of the Hurricane fault zone (e.g., Billingsley and Dyer, 2003; Amoroso and others, 2004; Lund and others, 2007), the Washington fault zone (this study), and most lesser structures (Main Street, Sunshine, Sunshine Trail, and Gyp Pocket faults) occupying the Shivwitz Plateau east of the Washington fault zone (Billingsley and Dyer, 2003).

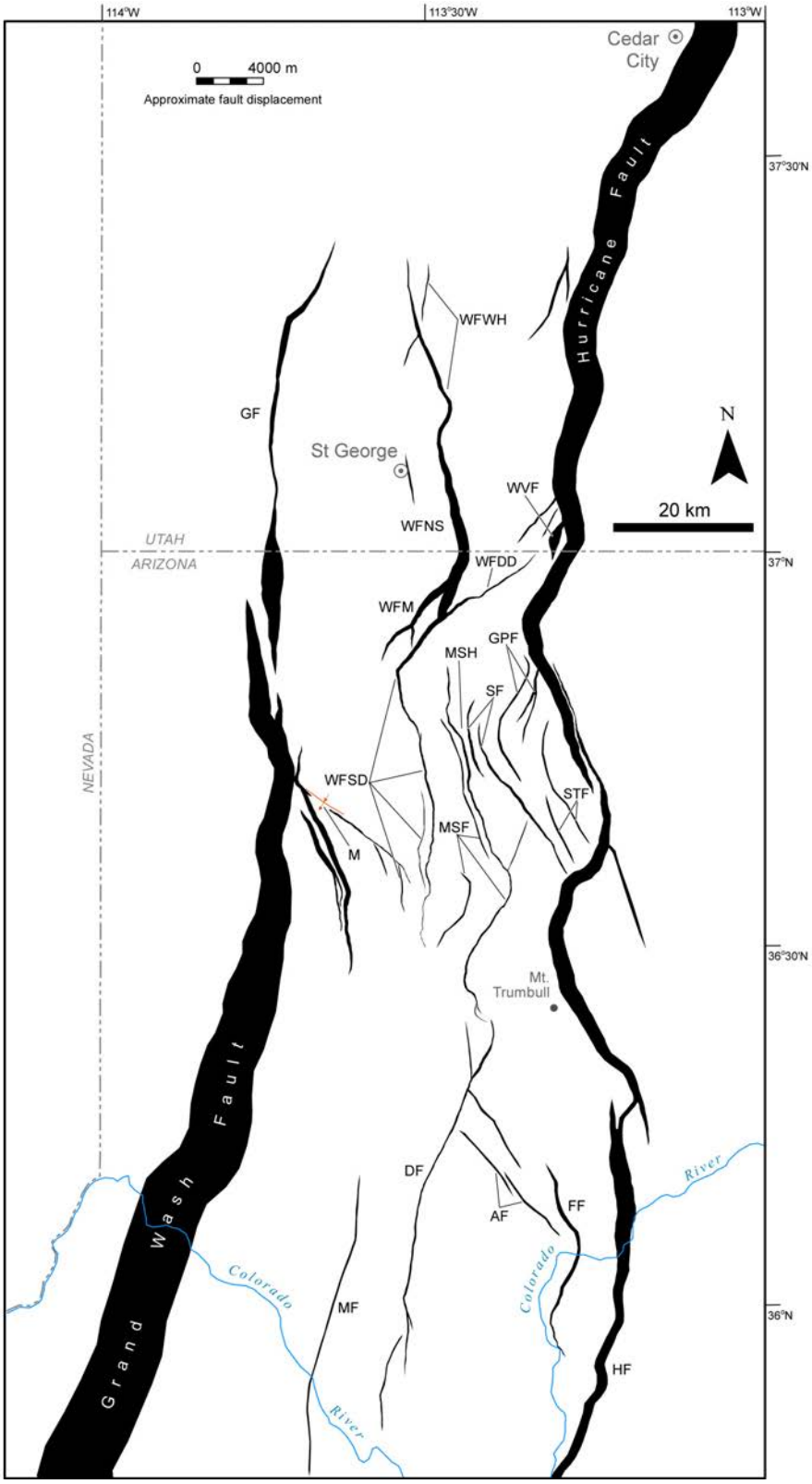

Figure 14. *Displacement map of faults in the Colorado Plateau–Basin and Range transition zone in southwestern Utah and northwestern Arizona. Fault widths are proportional to vertical fault displacement as indicated by alternating scale. AF, Andrus fault; DF, Dellenbaugh fault; FF, Froggy fault; GF, Gunlock fault; GPF, Gyp Pocket fault zone; HF, Hurricane fault; M, southwest-dipping monocline; MF, Merriwhitica fault; MSF, Main Street fault; MSH, Main Street horst; SF, Sunshine fault zone; STF, Sunshine Trail fault zone; WFDD, Dutchman Draw strand of the Fort Pearce section of the Washington fault zone; WFFP, Fort Pearce section of the Washington fault zone; WFM, Mokaac strand of the Fort Pearce section of the Washington fault zone; WFSD, Sullivan Draw section of the Washington fault zone; WFWH, Washington Hollow section of the Washington fault zone; WVF, Warner Valley fault.*

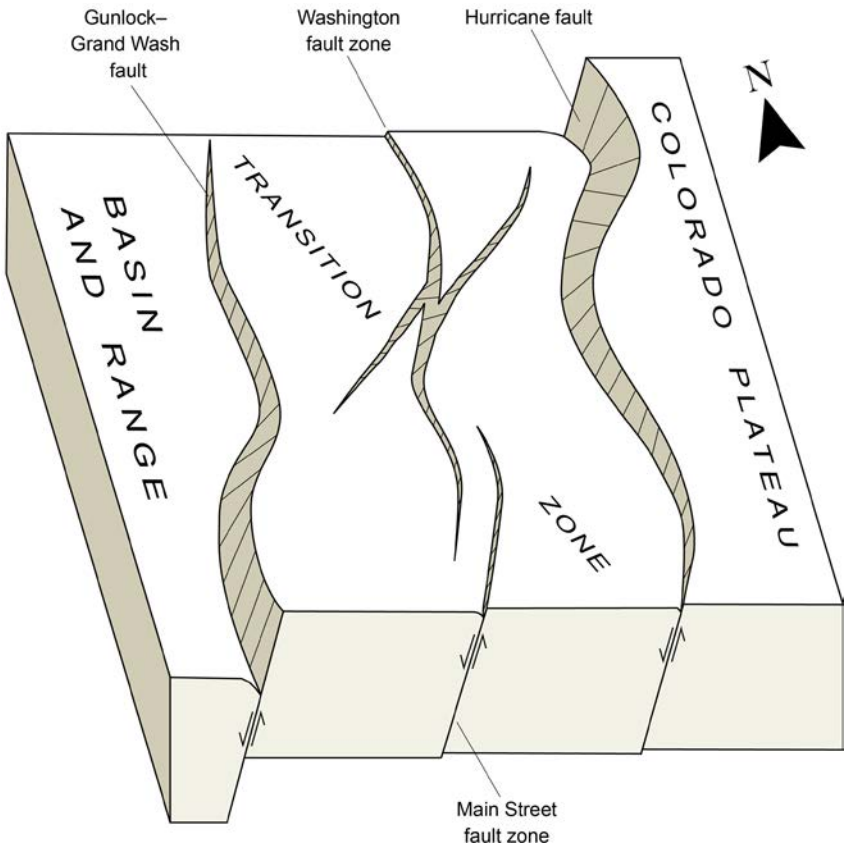

Figure 15. *Schematic block diagram of the Colorado Plateau–Basin and Range transition zone in southwestern Utah and northwestern Arizona. Displacement decreases on the Gunlock–Grand Wash fault as displacement increases on the Hurricane fault, indicating strain may have transferred from the west side of the transition zone to the east side through time. Modified from Schramm (1994). Not to scale.*

I favor a model whereby a narrow Colorado Plateau–Basin and Range transition zone initiated along the Grand Wash fault in early to middle Miocene time. By the Pliocene, the generally east-west tensional stress field had migrated eastward and movement on the Grand Wash fault nearly ceased as the Hurricane fault zone began to develop, possibly along older pre-existing structures (Huntoon, 1990; Billingsley and Wellmeyer, 2003). By Pleistocene time, the internal strain of the intervening block between the Hurricane and Grand Wash faults (the St. George-Shivwitz block) was great enough to form the Washington, Main Street, and other minor fault zones. A west-to-east transfer of strain is also consistent with the fact that basalt flows generally young from west to east, with basalt flows in the Grand Wash trough ranging from 4–6 Ma and flows in the Uinkaret volcanic field typically being less than 850 ka (Wenrich and others, 1995; Billingsley and Workman, 2000).

Whereas geologic-map relations are permissive of structural linkage between many faults in the transition zone in southwestern Utah and northwestern Arizona, it remains unclear if the faults sole into a master detachment at depth, which might permit simultaneous sympathetic rupture of several faults. As an alternative, Schramm (1994) suggested that transition zone faults may simply die out at depth and that mechanical and geometric continuity is accomplished by internal strain of intervening fault blocks. Additional data and analyses are needed to further evaluate the existence of a regional strain transfer zone involving the Grand Wash, Hurricane, and Washington faults.

SUMMARY AND CONCLUSIONS

New geologic mapping of the Fort Pearce and Washington Hollow sections of the Washington fault zone determined or confirmed the following:

1. Similar geometries and amounts of displacement among the Fort Pearce section of the Washington fault zone and the Washington Hollow fault, as well as minor structures bridging the distance between the two sections, indicate that they are both part of the same fault zone. However, minimal displacement and structural complexity north of Washington City, near the Washington flow cinder cone, indicate the Washington Hollow fault is likely a separate section of the Washington fault zone, and I therefore redefine the Washington Hollow fault as the Washington Hollow section of the Washington fault zone.

2. Since the Northern section, as defined by previous workers (Pearthree, 1998), is no longer the northernmost section of the Washington fault zone, I herein rename it the Fort Pearce section of the Washington fault zone.

3. Since displacement on both the Mokaac section (Pearthree, 1998) and Dutchman Draw faults increases toward their junctures with the Fort Pearce section, and because all three faults have similar scarp morphologies indicating similar rates of activity, I believe that the three faults may rupture contemporaneously. It is possible that the Mokaac strand is more likely to rupture during southward-propagating fault rupture on the Fort Pearce section, and the Dutchman Draw strand is more likely to rupture during northward-propagating fault rupture. I consider the Mokaac and Dutchman Draw faults to be major strands of the Fort Pearce section, and herein define them as such.

4. The Fort Pearce–Sullivan Draw section boundary is best placed near the head of Quail Canyon where a 50° change in strike is accompanied by an abrupt change in vertical displacement along the fault.

5. The lengths (straight line) of the newly defined Fort Pearce and Washington Hollow sections are 37 and 22 km, respectively.

6. Due to high rates of erosion in the St. George basin, fault scarps developed on unconsolidated deposits are uncommon and isolated. Only two discontinuous scarps formed on unconsolidated alluvium suitable for paleoseismic trenching were discovered on the Fort Pearce section; both are in Arizona. One site is on the main strand of the Fort Pearce section near Dutchman Draw and was subsequently trenched (see Lund and others, this volume). The second scarp is formed on a subsidiary splay of the Mokaac strand of the Fort Pearce section.

7. Several other scarps formed on unconsolidated deposits along the Fort Pearce section described in previous studies are bedrock cored and likely not suitable for paleoseismic trenching investigations.

8. Prominent bedrock escarpments up to 250 m high along the Fort Pearce section are enhanced by differential erosion of geologic units of differing resistance juxtaposed across the fault.

9. Normal faults comprising the Colorado Plateau–Basin and Range transition zone in southwestern Utah and northwestern Arizona may be structurally linked. Similar geometries, structural styles, rates of activity, as well as evidence for transfer of strain among the Hurricane and Washington fault zones and the Grand Wash, Main Street, and other faults indicate all of the faults may be part of a single regional transfer fault system. Several lines of evidence support a model where the Colorado Plateau–Basin and Range boundary in this area developed along the Grand Wash fault in Miocene time, then beginning in the Pliocene, the locus of strain migrated eastward, initiating development of the southern part of the Hurricane fault zone. Internal strain within the intervening block became great enough by the Pleistocene to create the Washington, Main Street, and other lesser faults.

10. Although surficial geologic mapping indicates that transition zone faults in southwestern Utah and northwestern Arizona are likely linked or nearly linked at the surface, additional data and analyses are necessary to evaluate the possibility that the faults sole into a single regional detachment.

In conclusion, several fault scarps formed on unconsolidated Quaternary deposits and soft bedrock along the Washington fault zone show that the fault is active and poses a significant seismic hazard to the St. George metropolitan area. Well-defined locations of the Fort Pearce and newly defined Washington Hollow sections and their major strands will help planners, geologists, and engineers reduce the surface-fault-rupture hazard to future development in Washington City. Redefining the fault section model for the Washington fault zone, including the addition of the Washington Hollow section, and the redefinition of the Dutchman Draw and Mokaac faults as major strands of the Fort Pearce section, will have a significant impact on future seismic-hazard assessments in the St. George area.

ACKNOWLEDGMENTS

I am grateful to William Lund, Robert Biek, and Grant Willis with the UGS, and Peter Rowley of Geologic Mapping, Inc., for advice, discussions, and information concerning this geologic map. Careful reviews by Christopher DuRoss, Steve Bowman, and Michael Hylland all of the UGS, and Phil Pearthree of the Arizona Geological Survey greatly improved this map and text. Corey Unger, with assistance from Jay Hill, both with the UGS, performed the map cartography.

REFERENCES

Amoroso, L., Pearthree, P.A., and Arrowsmith, J.R., 2004, Paleoseismology and neotectonics of the Shivwits section of the Hurricane fault, northwestern Arizona: Bulletin of the Seismological Society of America, v. 94, no. 5, p. 1919–1942.

Anderson, R.E., and Christenson, G.E., 1989, Quaternary faults, folds, and selected volcanic features in the Cedar City 1° x 2° quadrangle, Utah: Utah Geological and Mineral Survey Miscellaneous Publication 89-6, 29 p., 1 plate, scale 1:250,000.

Best, M.G., and Brimhall, W.H., 1970, Late Cenozoic basalt types in the western Grand Canyon region, *in* Hamblin, W.K., and Best, M.G., editors, The western Grand Canyon region: Utah Geological Society Guidebook to the Geology of Utah, no. 23, p. 57–74.

Best, M.G., and Hamblin, W.K., 1970, Implications of tectonism and volcanism in the western Grand Canyon, *in* Hamblin, W.K., and Best, M.G., editors, The western Grand Canyon region: Utah Geological Society Guidebook to the Geology of Utah, no. 23, p. 75–79.

Best, M.G., McKee, E.H., and Damon, P.E., 1980, Space-time composition patterns of late Cenozoic mafic volcanism, southwestern Utah and adjoining areas: American Journal of Science, v. 280, p. 1035–1050.

Biek, R.F., 2003, Geologic map of the Harrisburg Junction quadrangle, Washington County Utah: Utah Geological Survey Map 191, 42 p., 2 plates, scale 1:24,000.

Biek, R.F., Rowley, P.D., Hayden, J.M., Hacker, D.B., Willis, G.C., Hintze, L.F., Anderson, R.E., and Brown, K.D., 2009, Geologic map of the St. George and east part of the Clover Mountains 30′ x 60′ quadrangles, Washington and Iron Counties, Utah: Utah Geological Survey Map 242, 101 p., 2 plates, scale 1:100,000.

Billingsley, G.H., 1990a, Geologic map of the Lizard Point quadrangle, northern Mohave County, Arizona: U.S. Geological Survey Open-File Report 90-643, scale 1:24,000.

Billingsley, G.H., 1990b, Geologic map of the Wolf Hole Mountain East quadrangle, northern Mohave County, Arizona: U.S. Geological Survey Open-File Report 90-644, scale 1:24,000.

Billingsley, G.H., 1991a, Geologic map of the Sullivan Draw South quadrangle, northern Mohave County, Arizona: U.S. Geological Survey Open-File Report 91-559, scale 1:24,000.

Billingsley, G.H., 1991b, Geologic map of the Sullivan Draw North quadrangle, northern Mohave County, Arizona: U.S. Geological Survey Open-File Report 91-558, scale 1:24,000.

Billingsley, G.H., 1992a, Geologic map of the Yellowhorse Flat quadrangle, northern Mohave County, Arizona: U.S. Geological Survey Open-File Report 92-442, scale 1:24,000.

Billingsley, G.H., 1992b, Geologic map of the Rock Canyon quadrangle, northern Mohave County, Arizona: U.S. Geological Survey Open-File Report 92-449, scale 1:24,000.

Billingsley, G.H., 1993, Geologic map of the Wolf Hole Mountain and vicinity, Mohave County, northwestern Arizona: U.S. Geological Survey Miscellaneous Investigations Series Map I-2296, scale 1:31,680.

Billingsley, G.H., and Dyer, H.C., 2003, Geologic map of the upper Hurricane Wash and vicinity, Mohave County, northwestern Arizona: U.S. Geological Survey Miscellaneous Field Studies Map MF-2410, 23 p., scale 1:31,680.

Billingsley, G.H., and Graham, S.E., 2003, Geologic map of the lower Hurricane Wash and vicinity, Mohave County, northwestern Arizona: U.S. Geological Survey Miscellaneous Field Studies Map MF-2396, 27 p., scale 1:31,680.

Billingsley, G.H., and Wellmeyer, J.L., 2003, Geologic map of the Mount Trumbull 30′ x 60′ quadrangle, Mohave and Coconino Counties, northwestern Arizona: U.S. Geological Survey Geologic Investigations Series Map I-2766, scale 1:100,000.

Billingsley, G.H., and Workman, J.B., 2000, Geologic map of the Littlefield 30′ x 60′ quadrangle, Mohave County, northwestern Arizona: U.S. Geological Survey Geologic Investigations Series Map I-2628, 25 p., 2 plates, scale 1:100,000.

Bohannon, R.G., Grow, J.A., Miller, J.J., and Blank, R.H., Jr., 1993, Seismic stratigraphy and tectonic development of Virgin River depression and associated basins, southeastern Nevada and northwestern Arizona: Geological Society of America Bulletin, v. 105, no. 4, p. 501–520.

Bowman, S.D, Young, B.W., and Unger, C.D., 2011, Compilation of 1982-83 seismic safety investigation reports of eight SCS dams in southwestern Utah (Hurricane and Washington fault zones) and low-sun-angle aerial photography, Washington and Iron Counties, Utah, and Mohave County, Arizona—Paleoseismology of Utah, Volume 21: Utah Geological Survey Open-File Report 583, 4 p., 6 DVD set.

Bureau of Land Management, 2002, Stereoscopic color aerial photographs, project AZ-02-AC, scale 1:24,000.

Christenson, G.E., and Deen, R.D., 1983, Engineering geology of the St. George area, Washington County, Utah: Utah Geological and Mineral Survey Special Studies 58, 32 p., 2 plates.

Cook, E.F., 1960, Geologic atlas of Utah, Washington County: Utah Geological and Mineralogical Survey Bulletin 70, 119 p.

Cook, K.L., and Hardman, E., 1967, Regional gravity survey of the Hurricane fault area and Iron Springs District, Utah: Geological Society of America Bulletin, v. 78, p. 1063–1076.

Cordova, R.M., 1978, Ground-water conditions in the Navajo Sandstone in the central Virgin River basin, Utah: Utah Division of Water Rights Technical Publication 61, 66 p., 1 plate, scale 1:250,000.

Dobbin, C.E., 1939, Geologic structure of St. George district, Washington County, Utah: American Association of Petroleum Geologists Bulletin, v. 23, no. 2, p. 121–144.

Downing, R.F., Smith, E.I., Orndorff, R.L., Spell, T.L., and Zanetti, K.A., 2001, Imaging the Colorado Plateau–Basin and Range transition zone using basalt geochemistry, geochronology, and geographic information systems, *in* Erskine, M.C., Faulds, J.E., Bartley, J.M., and Rowley, P.D., editors, The geologic transition, High Plateaus to Great Basin—a symposium and field guide (The Mackin Volume): Utah Geological Association and Pacific Section of the American Association of Petroleum Geologists, Utah Geological Association Publication 30, p. 127–154.

Earth Sciences Associates, 1982, Phase I report, seismic safety investigation of eight SCS dams in southwestern Utah: Unpublished consultant's report for the U.S. Soil Conservation Service, Portland, Oregon, dated December 1982, ESA project no. D118, variously paginated.

Earth Sciences Associates, 1983, Phase II report, seismic safety investigation of eight SCS dams in southwestern Utah: Unpublished consultant's report for the U.S. Soil Conservation Service, Portland, Oregon, dated February 1983, ESA project no. D118, variously paginated.

Hacker, D.B., in preparation (a), Geologic map of the Saddle Mountain quadrangle, Washington County, Utah: Utah Geological Survey Map, scale 1:24,000.

Hacker, D.B., in preparation (b), Geologic map of the Central East quadrangle, Washington County, Utah: Utah Geological Survey Map, scale 1:24,000.

Hamblin, W.K., 1963, Late Cenozoic basalts of the St. George basin, Utah, *in* Heylmun, E.B., editor, Geology of the southwestern transition between the Basin-Range and Colorado Plateau, Utah: Intermountain Association of Petroleum Geologists, Guidebook to the Geology of Southwestern Utah, p. 84–89.

Hamblin, W.K., 1970a, Structure of the western Grand Canyon region, *in* Hamblin, W.K., and Best, M.G., editors, The western Grand Canyon region: Utah Geological Society Guidebook to the Geology of Utah, no. 23, p. 3–20.

Hamblin, W.K., 1970b, Late Cenozoic basalt flows of the western Grand Canyon, *in* Hamblin, W.K., and Best, M.G., editors, The western Grand Canyon region: Utah Geological Society Guidebook to the Geology of Utah, no. 23, p. 21–37.

Hamblin, W.K., and Best, M.G., 1970, Road log, *in* Hamblin, W.K., and Best, M.G., editors, The western Grand Canyon region: Utah Geological Society Guidebook to the Geology of Utah, no. 23, p. 93–153.

Hayden, J.M., 2004, Geologic map of The Divide quadrangle, Washington County, Utah: Utah Geological Survey Map 197, 31 p., 2 pl., scale 1:24,000.

Hayden, J.M., 2005, Geologic map of the Washington Dome quadrangle, Washington County, Utah: Utah Geological Survey Map 209, 29 p., 2 pl., scale 1:24,000.

Hayden, J.M., and Willis, G.C., 2011, Geologic map of the St. George 7.5′ quadrangle, Washington County, Utah: Utah Geological Survey Map 251, 19 p., 2 plates, scale 1:24,000.

Hintze, L.F., 1963, Geologic map of southwestern Utah, *in* Intermountain Association of Petroleum Geologists Guidebook, 12th Annual Field Conference: Utah Geological and Mineralogical Survey, 1 sheet, scale 1:250,000.

Huntoon, P.W., 1990, Phanerozoic structural geology of the Grand Canyon, *in* Beus, S.S., and Morales, M., editors, Grand Canyon geology: Oxford, New York, Oxford University Press, and Flagstaff, Arizona, Museum of Northern Arizona Press, p. 261–310.

Hurlow, H.A., 1998, The geology of the central Virgin River basin, southwestern Utah, and its relation to ground-water conditions: Utah Geological Survey Bulletin 26, 53 p., 6 plates.

IntraSearch, 1983, Stereoscopic color aerial photographs, project no. 3214, frames 95–126, scale 1:24,000.

Lucchitta, I., 1987, The mouth of the Grand Canyon and edge of the Colorado Plateau in the upper Lake Mead area, Arizona, *in* Beus, S.S., editor, Geological Society of America Centennial Field Guide—Rocky Mountain Section, v. 2, p. 365–370.

Lund, W.R., Hozik, M.J., and Hatfield, S.C., 2007, Paleoseismic investigation and long-term slip history of the Hurricane fault in southwestern Utah—Paleoseismology of Utah, Volume 14: Utah Geological Survey Special Study 119, 81 p.

Lund, W.R., Knudsen, T.R., Vice, G.S., and Shaw, L., 2008, Geologic hazards and adverse construction conditions, St. George–Hurricane metropolitan area, Washington County, Utah: Utah Geological Survey Special Study 127, 105 p.

Lund, W.R., Pearthree, P.A., Amoroso, L., Hozik, M.J., and Hatfield, S.C., 2001, Paleoseismic investigation of earthquake hazard and long-term movement history of the Hurricane fault, southwestern Utah and northwestern Arizona—final technical report: National Earthquake Hazards Reduction Program, unpublished report for U.S. Geological Survey, award no. 99HQGR0026, 120 p.

McKee, E.H., Blank, H.R., and Rowley, P.D., 1997, Potassium-argon ages of Tertiary igneous rocks in the eastern Bull Valley Mountains and Pine Valley Mountains, southwestern Utah, *in* Maldonado, F., and Nealey, L.D., editors, Geologic studies in the Basin and Range–Colorado Plateau transition zone in southeastern Nevada, southwestern Utah, and northwestern Arizona, 1995: U.S. Geological Survey Bulletin 2153, p. 243–252.

Menges, C.M., and Pearthree, P.A., 1983, Map of neotectonic (latest Pliocene-Quaternary) deformation in Arizona: Arizona Geological Survey Open-File Report 83-22, 48 p., 4 plates, scale 1:500,000.

Pearthree, P.A., compiler, 1998, Quaternary fault data and map for Arizona: Arizona Geological Survey Open-File Report 98-24, 122 p., 1 plate, scale 1:750,000.

Peterson, S.M., 1983, The tectonics of the Washington fault zone, northern Mohave County, Arizona: Brigham Young University Geology Studies, v. 30, part 1, p. 83–94.

Reynolds, S.J., Florence, F.P., Welty, J.W., Roddy, M.S., Currier, D.A., Anderson, A.V., and Keith, S.B., 1986, Compilation of radiometric age determinations in Arizona: Arizona Bureau of Geology and Mineral Technology, Geological Survey Branch, Bulletin 197, 258 p.

Rowley, P.D., Williams, V.S., Vice, G.S., Maxwell, D.J., Hacker, D.B., Snee, L.W., and Mackin, J.H., 2006, Interim geologic map of the Cedar City 30′ x 60′ quadrangle, Iron and Washington Counties, Utah: Utah Geological Survey Open-File Report 476DM, scale 1:100,000.

Schramm, M.E., 1994, Structural analysis of the Hurricane fault in the transition zone between the Basin and Range Province and the Colorado Plateau, Washington County, Utah: University of Nevada, Las Vegas, M.S. thesis, 90 p.

Stokes, W.L., and Heylmun, E.B., 1963, Tectonic history of southwestern Utah, *in* Heylmun, E.B., editor, Guidebook to the geology of southwestern Utah: Intermountain Association of Petroleum Geologists Guidebook 12, p. 19–25.

Utah Automated Geographic Reference Center, 2012a, Black and white Soil Conservation Service (SCS) historical aerial imagery acquired in the late 1930s, viewed using AGRC's SGID Image Server for ArcMap: Online, http://gis.utah.gov/data/utah-sgid-image-server/, accessed October 2012.

Utah Automated Geographic Reference Center, 2012b, 2006 National Agriculture Imagery Program (NAIP) 1 meter orthophotography: Online, http://gis.utah.gov/data/aerial-photography/2006-naip-1-meter-color-orthophotography, accessed November 2012.

Utah Division of Water Rights, 2011, Well information program: Online, http://www.waterrights.utah.gov/cgi-bin/wellview.exe?Startup, accessed November 2011.

Utah Geological Survey and New Mexico Geochronology Research Laboratory, 2007, $^{40}Ar/^{39}Ar$ geochronology results from the Antelope Peak, Central East, Goldstrike, Page Ranch, and Saddle Mountain quadrangles, Utah: Utah Geological Survey Open-File Report 508, variously paginated.

Wenrich, K.J., Billingsley, G.H., and Blackerby, B.A., 1995, Spatial migration and compositional changes of Miocene-Quaternary magmatism in the Western Grand Canyon: Journal of Geophysical Research, v. 100, p. 10,417–10,440.

Willis, G.C., and Biek, R.F., 2001, Quaternary incision rates of the Colorado River and major tributaries in the Colorado Plateau, Utah, *in* Young, R.A., and Spamer, E.E., editors, Colorado River origin and evolution—proceedings of the symposium held at Grand Canyon National Park in June 2000: Grand Canyon Association Monograph 12, p. 119–123.

Willis, G.C., and Higgins, J.M., 1995, Interim geologic map of the Washington quadrangle, Washington County, Utah: Utah Geological Survey Open-File Report 324, 90 p., scale 1:24,000.

APPENDIX A

DESCRIPTION OF MAP UNITS

Quaternary Deposits

Human-derived deposits

Qh Artificial fill (Historical) – Borrow material and fill used to construct flood-control dams, retaining ponds, and roadbeds.

Alluvial deposits

Qal_1 Stream deposits (Holocene) – Stratified, moderately to well-sorted gravel, sand, silt, and clay deposited in larger active drainages; includes small alluvial-fan and colluvial deposits, and minor terraces less than 3 m above modern base level; 0 to 10 m thick.

Qat_{2-5} Stream-terrace deposits (Holocene to middle Pleistocene) – Stratified, moderately to well-sorted gravel, sand, silt, and clay that forms level to gently sloping terraces above modern drainages; subscripts denote relative heights above the current drainage (and approximate ages); level 2 deposits are about 3 to 9 m, level 3 deposits are about 9 to 15 m, level 4 deposits are 15 to 25 m, and level 5 deposits are about 25 to 32 m above adjacent drainages; 0 to 20 m thick.

Qatb Boulder-terrace deposits (upper to middle Pleistocene) – Poorly to moderately sorted sand- to boulder-sized material forming poorly developed terraces; clasts are mostly basalt; terraces are at several levels from 6 to 60 m above Mill Creek and Washington Hollow drainages; 0 to 6 m thick.

Qato Older alluvial-terrace deposits (upper to middle Pleistocene) – Moderately sorted sand to boulder deposits that form isolated, gently north-sloping surfaces within the uplifted structural block east of the Mokaac fault; clasts are chiefly from an adjacent remnant of the Seegmiller Mountain flow; found about 25 to 45 m above adjacent drainages; 0 to 10 m thick.

Qap Pediment alluvium (Holocene to middle Pleistocene) – Poorly sorted, subangular to rounded, silt- to boulder-sized alluvial deposits that form a locally resistant cap over eroded bedrock surfaces; 0 to 24 m thick.

Qaf_1 Level-1 fan alluvium (Holocene) – Poorly to moderately sorted, subangular to rounded, boulder- to clay-sized sediment deposited at the mouth of Dutchman Draw and other nearby active washes that have cut through the Washington fault escarpment; deposited principally by debris flows and debris floods on active depositional surfaces; about 3 to 9 m thick.

Qaf_2 Level-2 fan alluvium (Holocene to upper Pleistocene) – Poorly to moderately sorted, subangular to rounded, boulder- to clay-sized sediment deposited at the mouth of Dutchman Draw and other nearby washes that have cut through the Washington fault escarpment; deposited principally by debris flows and debris floods, and typically forms inactive surfaces incised by active drainages; about 3 to 12 m thick.

Qaf_3 Level-3 fan alluvium (upper Pleistocene) – Similar to level-2 fan alluvium, but clasts have more pronounced desert varnish coating; forms inactive surfaces 3 to 10 m above younger alluvial-fan deposits; about 3 to 15 m thick.

Qafy Younger fan alluvium (Holocene to upper Pleistocene) – Poorly to moderately sorted, non-stratified, subangular to subrounded, boulder- to clay-sized sediment deposited at the mouths of streams and washes; forms both active depositional surfaces (Qaf_1 equivalent) and low-level inactive surfaces incised by small streams (Qaf_2 equivalent) undivided here; deposited principally by debris flows and debris floods, but colluvium locally constitutes a significant part of the deposits; about 3 to 20 m thick.

Qafo Older fan alluvium (Pleistocene) – Poorly to moderately sorted, non-stratified, subangular to subrounded, boulder- to clay-sized sediment with moderately developed calcic soils (hardpan or caliche); forms broad, gently sloping, deeply dissected surfaces about 5 to 20 m above adjacent active drainages; deposited principally by debris flows and debris floods; about 3 to 20 m thick.

Colluvial deposits

Qc Colluvium (Holocene to upper Pleistocene) – Poorly sorted, angular, clay- to boulder-size, locally derived sediment deposited principally by slope wash and soil creep; locally includes talus, alluvium, and eolian sand too small to map separately; gradational with talus; includes older colluvium now incised by adjacent drainages; generally less than 6 m thick.

Eolian deposits

Qes Eolian sand (Holocene to upper Pleistocene) – Well-sorted, fine- to medium-grained, well-rounded, frosted quartz sand; sand is recycled principally from the Navajo Sandstone and Kayenta Formation; locally forms small dunes; locally capped by thick calcic soils (hardpan or caliche); typically less than 6 m thick.

Qecl Eolian calcic soils and sand (upper to middle Pleistocene) – Thick pedogenic carbonate (hardpan or caliche) mixed with minor to moderate amounts of eolian sand (Qes); mapped in areas where most eolian sands have been stripped off, leaving calcic-soil caps covering bedrock; 0 to 6 m thick.

Mass-movement deposits

Qmt Talus (Holocene to upper Pleistocene) – Poorly sorted, angular boulders and finer grained interstitial sediment deposited principally by rock fall on and at the base of steep slopes; typically grades downslope into colluvium where impractical to differentiate the two; also includes alluvium in the bottom of washes; generally less than 9 m thick.

Qms Landslides (Holocene to middle [?] Pleistocene) – Very poorly sorted, clay- to boulder-size, locally derived material deposited principally by rotational slump processes; commonly characterized by hummocky topography, numerous subdued internal scarps, and chaotic bedding attitudes; thickness highly variable.

Mixed-environment deposits

Qac, Qaco

Alluvium and colluvium (Holocene to upper Pleistocene) – Poorly to moderately sorted, clay- to boulder-size, locally derived sediments deposited in swales and small drainages; gradational with alluvial and colluvial deposits; older deposits (Qaco) form incised, inactive surfaces up to about 6 meters above modern drainages; generally less than 6 m thick.

Qea Eolian sand and alluvium (Holocene to upper Pleistocene) – Well-sorted, fine- to medium-grained eolian sand reworked by alluvial processes, and poorly to moderately sorted gravel, sand, and silt deposited in small channels; generally less than 6 m thick.

Qae, Qaeo

Alluvium and eolian sand (Holocene to upper Pleistocene) – Moderately sorted gravel, sand, and silt deposited in small channels and on alluvial fans, and well-sorted, fine- to medium-grained eolian sand locally reworked by alluvial processes; younger deposits (Qae) form active depositional surfaces, whereas older deposits (Qaeo) typically form incised, inactive surfaces; generally less than 9 m thick.

Qca, Qcao

Colluvium and alluvium (Holocene to upper Pleistocene) – Poorly sorted, angular to rounded, fine-grained to boulder-sized material deposited on broad, moderate slopes; deposited by slope wash, debris flow, and slope creep processes and lack well-defined drainage patterns; locally include talus, eolian, or alluvial deposits; younger deposits (Qca) form active depositional surfaces whereas older deposits (Qcao) are inactive and deeply incised; 0 to 10 m thick.

Basaltic lava flows

Qbd Divide lava flow (middle Pleistocene) – Dark-gray, fine-grained basalt to basanite with small olivine phenocrysts; forms lava cascade over Hurricane Cliffs; yielded an $^{40}Ar/^{39}Ar$ age of 0.41 ± 0.08 Ma (Hayden, 2004); lava flow is generally 5 to 12 m thick.

Qbla, Qblac

Lark Canyon lava flow and cinder cone (middle Pleistocene) – Dark-gray basalt (Qbla) with small olivine phenocrysts; erupted from a vent at a cinder cone (Qblac) about 3 km southwest of Pine Valley; yielded an $^{40}Ar/^{39}Ar$ plateau age of 0.61 ± 0.04 Ma (0.64 ± 0.04 Ma isochron) (UGS and New Mexico Geochronology Research Laboratory [NMGRL], 2007) and a K-Ar age of 0.56 ± 0.06 Ma (Best and others, 1980); lava flow is generally 6 to 12 m thick.

Qbmk, Qbmkc

Mahogany Knoll lava flow and cinder cone (middle [?] Pleistocene) – Dark-gray basalt (Qbmk) with small olivine phenocrysts; erupted from vents at cinder cones (Qbmkc) on the southwest flank of the Pine Valley Mountains; yielded a K-Ar age of 1.2 ± 0.1 Ma (Best and others, 1980), but based on geomorphic expression, is believed to be younger and of comparable age to nearby lava flows that are about 600 ka (Biek and others, 2009); lava flow is generally 6 to 12 m thick.

Qbrk, Qbrkc

Red Knoll lava flow and cinder cone (middle [?] Pleistocene) – Gray andesite to trachyandesite (Qbrk) that erupted from a vent at a cinder cone (Qbrkc) on the southwest flank of the Pine Valley Mountains; yielded a low-confidence $^{40}Ar/^{39}Ar$ integrated age of 0.45 ± 0.86 Ma (1.12 ± 0.50 Ma isochron) (UGS and NMGRL, 2007), but based on geomorphic expression is probably about 450 to 700 ka (Biek and others, 2009); lava flow is generally 9–18 m thick.

Qbtb, Qbtbc

Truman Bench lava flow and cinder cone (middle [?] Pleistocene) – Dark-gray basalt to trachybasalt (Qbtb) with small olivine phenocrysts; erupted from a vent at a cinder cone (Qbtbc) on the southwest flank of the Pine Valley Mountains; probably about 450 to 700 ka based on comparison with nearby flows (Biek and others, 2009); lava flow is generally 6 to 12 m thick.

Qbpv, Qbpvc

Pine Valley lava flow and cinder cone (middle Pleistocene) – Dark-gray basaltic lava flows (Qbpv) with small olivine phenocrysts; erupted from a number of vents at cinder cones (Qbpvc) west of Pine Valley; yielded an $^{40}Ar/^{39}Ar$ plateau age of 0.67 ± 0.07 Ma (0.67 ± 0.08 Ma isochron) (UGS and NMGRL, 2007); lava flow is generally 6 to 12 m thick.

Qbgk, Qbgkc

Grass Knoll lava flow and cinder cone (middle to lower Pleistocene) – Dark-gray basalt to trachybasalt (Qbgk) with small olivine phenocrysts; erupted from a vent at the Grass Knoll cinder cone (Qbgkc) on the southwest flank of the Pine Valley Mountains; yielded an $^{40}Ar/^{39}Ar$ integrated age of 1.02 ± 0.36 Ma (1.20 ± 0.17 Ma isochron) (UGS and NMGRL, 2007); lava flow is generally 6 to 12 m thick.

Qbw, Qbwc

Washington lava flow and cinder cone (lower Pleistocene) – Medium- to dark-gray to dark-greenish-gray, fine-grained basanite to picrobasalt (Qbw) with abundant clinopyroxine and olivine phenocrysts; erupted from a vent at a cinder cone (Qbwc) about 5 km northeast of Washington; yielded $^{40}Ar/^{39}Ar$ ages of 0.87 ± 0.04 and 0.98 ± 0.02 Ma (Biek, 2003), which fit well with regional incision rates (Willis and Biek, 2001), but Best and others (1980) reported an anomalously old K-Ar age of 1.7 ± 0.1 Ma for this flow; lava flow is 8 to 11 m thick, except near its source, where it is as much as 30 m thick.

Qbgv, Qbgvc

Grass Valley lava flow and cinder cone (lower Pleistocene) – Dark-gray, fine- to medium-grained trachybasalt to basalt (Qbgv) with small olivine phenocrysts; erupted from a vent at a deeply eroded cinder cone (Qbgvc) about 11 km south of Hurricane; yielded an $^{40}Ar/^{39}Ar$ plateau age of 1.09 ± 0.09 Ma (0.966 ± 0.030 Ma preliminary isochron) (UGS unpublished data); lava flow is several meters thick.

Qbr Remnants lava flow (lower Pleistocene) – Dark-brownish-black to dark-gray, medium-grained basanite with small olivine phenocrysts; vertically displaced by the Hurricane fault about 440 m; yielded preferred $^{40}Ar/^{39}Ar$ plateau ages of 1.06 ± 0.03 Ma (1.07 ± 0.08 Ma isochron) and 0.94 ± 0.04 Ma (0.94 ± 0.05 Ma isochron) (Hayden, 2004) and an anomalous $^{40}Ar/^{39}Ar$ plateau age of 1.47 ± 0.34 Ma (1.12 ± 0.50 Ma isochron) (Lund and others, 2001, 2007); typically about 12 m thick.

Qbcb, Qbcbc

Cedar Bench lava flow and cinder cones (lower Pleistocene) – Dark-greenish-gray to brownish-black trachybasalt (Qbcb) with small phenocrysts of clinopyroxine and olivine; yielded an $^{40}Ar/^{39}Ar$ plateau age of 1.23 ± 0.01 Ma (UGS unpublished data); erupted from vents at two overlapping cinder cones (Qbcbc) about 19 km north of St. George; flow is displaced by minor splays of the Washington Hollow fault; lava flow is typically 3 to 9 m thick, but as much as about 30 m thick where it fills paleotopography.

Qbe East Mesa lava flow (lower Pleistocene) – Dark-gray, fine-grained trachybasalt with small olivine phenocrysts; yielded an $^{40}Ar/^{39}Ar$ plateau age of 1.28 ± 0.01 Ma (Lund and Knudsen, this volume) and a K-Ar age of 1.4 ± 0.25 Ma (Wenrich and others, 1995); vertically displaced about 45 m by a splay of the Dutchman Draw fault; thickness varies from about 9 to 55 m.

$Qbdd_1$ Dutchman Draw-1 lava flow (lower Pleistocene?) – Dark-gray, fine-grained trachybasalt with small olivine phenocrysts; caps a series of low hills north of the Mokaac strand of the Washington fault and west of Dutchman Draw; geochemical analyses indicate a possible correlation with either the East Mesa or West Mesa lava flow (Lund and Knudsen, this volume); less than 12 m thick.

Qb Unnamed lava flow (lower Pleistocene?) – Dark-gray, fine-grained basalt with small olivine phenocrysts; likely similar in age to the East Mesa flow based on flow morphology; up to 45 m thick.

Qblbm Little Black Mountain lava flow (lower Pleistocene) – Dark-gray, fine-grained olivine basalt; only a small remnant caps Little Black Mountain; yielded a K-Ar age of 1.7 ± 0.4 Ma (Wenrich and others, 1995); less than 12 m thick.

Qbs Seegmiller Mountain lava flow (lower Pleistocene) – Dark-gray, fine-grained basalt with small olivine and augite phenocrysts; vertically displaced by the Sullivan Draw section of the Washington fault zone as much as 85 m; erupted from a number of probable source areas east of the map area (Billingsley, 1993); yielded an $^{40}Ar/39Ar$ plateau age of 2.3 ± 0.02 Ma (Lund and Knudsen, this volume), an anomalous $^{40}Ar/^{39}Ar$ total gas age of 4.17 ± 0.18 Ma (Downing and others 2001), and K-Ar ages of 2.35 ± 0.31 Ma and 2.44 ± 0.51 Ma (Reynolds and others, 1986); thickness varies from 10 to 60 m.

$Qbdd_2$ Dutchman Draw-2 lava flow (lower Pleistocene?) – Dark-gray, fine-grained basalt with small olivine phenocrysts; caps a series of low ridges and hills west of the Washington fault and south of Dutchman Wash; geochemical analyses indicate a possible correlation with the Seegmiller Mountain flow (Lund and Knudsen, this volume); lava flow is 3 to 12 m thick.

Qbt Twin Peaks lava flow (lower Pleistocene) – Dark-gray to dark-brownish-gray basaltic trachyandesite with large plagioclase and quartz, and small olivine and clinopyroxene phenocrysts; yielded an $^{40}Ar/^{39}Ar$ plateau age of 2.43 ± 0.02 Ma (UGS unpublished data); lava flow is generally about 6 to 24 m thick.

Tertiary

$Tbqd_1$, $Tbqdc_1$

Quail Draw-1 lava flow and cinder cone (Pliocene) – Dark-gray, fine-grained hawaiite basalt with small olivine crystals; caps mesa west of Quail Draw near the intersection of the main and Dutchman Draw strands of the Fort Pearce section of the Washington fault zone; erupted from a vent at a cinder cone (Tbqdc1) marked by light-red basaltic cinder and scoria (Billingsley, 1993); yielded an $^{40}Ar/^{39}Ar$ plateau age of 2.8 ± 0.01 Ma (Lund and Knudsen, this volume) and an $^{40}Ar/^{39}Ar$ plateau age of 3.32 ± 0.04 Ma (Downing and others, 2001); generally less than 20 m thick.

Tbw Wolf Hole Mountain lava flow (Pliocene) – Dark-gray to brownish-black olivine basalt capping Wolf Hole Mountain; erupted from several vents on Wolf Hole Mountain just west of the map area (Billingsley, 1993); yielded a K-Ar age of 3.1 ± 0.4 Ma (Wenrich and others, 1995); between 25 and 50 m thick in the map area.

$Tbqd_2$ Quail Draw-2 lava flow (Pliocene?) – Dark-gray, fine-grained basalt with small olivine crystals; caps small, isolated mesa west of Quail Draw; map relations indicate a possible correlation with the Wolf Hole Mountain lava flow; lava flow is about 8 m thick.

Tipv Pine Valley laccolith (lower Miocene) – Locally flow layered, medium-gray quartz monzonite porphyry with medium- to coarse-grained phenocrysts of plagioclase, pyroxene, biotite, and sanadine; groundmass is fine-grained to microscopic plagioclase, quartz, and pyroxene; yielded a K-Ar age on biotite of 20.9 ± 0.6 Ma (McKee and others, 1997), and $^{40}Ar/^{39}Ar$ ages of 20.47 ± 0.04 and 20.63 ± 0.12 Ma from a sample collected from the base of the laccolith, and 20.32 ± 0.12 and 20.46 ± 0.05 Ma from a sample collected 150 m above the base (Rowley and others, 2006).

Tc Claron Formation (Paleocene to Eocene) – Interbedded mudstone, siltstone, sandstone, conglomerate, and limestone; mudstone is orangish red to reddish brown; sandstone is light-brown, medium- to coarse-grained, cross-bedded to structureless litharenite; about 450 m thick in the southwestern Pine Valley Mountains.

unconformity

Cretaceous

Ki Iron Springs Formation (Upper Cretaceous) – Interbedded, ledge-forming, calcareous, cross-bedded, fine- to medium-grained sandstone, siltstone, and mudstone; contains a few coquina beds, minor carbonaceous shale, and uncommon pebbly sandstone; about 1100 m thick in the Pine Valley Mountains.

Kcm Cedar Mountain Formation (Cretaceous) – Pale-gray to pinkish-gray, bentonitic clay and minor siltstone and fine-grained sandstone; nonresistant and poorly exposed; 18–23 m thick.

unconformity

Jurassic

Jcx Crystal Creek Member of the Carmel Formation (Middle Jurassic) – Reddish-brown, thin-bedded, poorly exposed sandstone and mudstone; 0 to 15 m thick.

Jcc Co-op Creek Member of the Carmel Formation (Middle Jurassic) – Pale-gray, pale-greenish-gray, or pale-yellowish-gray, interbedded limestone, sandstone, and mudstone; fossiliferous; thin uniform bedding; about 87 m thick.

Jtm Manganese Wash Member of the Temple Cap Formation (Middle to Lower Jurassic) – Dark-reddish-brown to pale-gray, slope-forming mudstone, claystone, and gypsum; contains several white, gray, and pink alabaster gypsum beds as much as 3 m thick; about 60 m thick.

unconformity

Jn Navajo Sandstone (Lower Jurassic) – Pale-yellowish-gray to moderate-grayish-red, well-sorted, fine- to medium-

grained quartz sandstone; grains are well rounded and frosted; prominent eolian cross-beds; strongly jointed; about 610 m thick.

Jk Kayenta Formation (Lower Jurassic) – Moderate- to dark-reddish-brown, thin- to thick-bedded siltstone, fine-grained sandstone, and mudstone with planar, low-angle, and ripple cross-stratification; cross-cutting gypsum veinlets are common; about 350 m thick.

Jks Springdale Sandstone Member of the Kayenta Formation (Lower Jurassic) – Pale-reddish-brown to grayish-yellow, fine- to medium-grained, cross-bedded sandstone with interbedded light-purplish-gray siltstone near the middle; weathers to rounded ledges; typically 30 to 35 m thick.

unconformity

Jmw Whitmore Point Member of the Moenave Formation (Lower Jurassic) – Greenish-gray claystone interbedded with pale-brown to pale-red, thin-bedded siltstone with several 8- to 120-cm-thick beds of light-greenish-gray dolomitic limestone containing algal structures and fossil fish scales; nonresistant and poorly exposed; ranges from about 15 to 40 m thick.

JTRmd

Dinosaur Canyon Member of the Moenave Formation (Lower Jurassic to Upper Triassic) – Interbedded moderate-reddish-brown siltstone and pale-reddish-brown to grayish-red, fine-grained, thin-bedded sandstone with laminated cross-beds; forms ledgy slopes; 45 to 75 m thick.

unconformity

Triassic

TRcp Petrified Forest Member of the Chinle Formation (Upper Triassic) – Varicolored, typically gray to purple mudstone, claystone, and siltstone, lesser white to yellow-brown sandstone and pebbly sandstone, and minor chert and nodular limestone; petrified wood is common; commonly forms landslides; about 120 to 200 m thick.

TRcs Shinarump Conglomerate Member of the Chinle Formation (Upper Triassic) – Grayish-orange to moderate-yellowish brown, medium- to coarse-grained sandstone, pebbly sandstone, and lesser pebbly conglomerate; forms prominent cliffs, hogbacks, and mesas; ranges from 2 to 75 m thick.

unconformity

TRmu Upper red member of the Moenkopi Formation (Lower Triassic) – Moderate-reddish-orange to moderate-reddish-brown, mostly thin- to medium-bedded siltstone, mudstone, and fine-grained sandstone with planar, low-angle, and ripple cross-stratification; typically 80 to 110 m thick.

TRms Shnabkaib Member of the Moenkopi Formation (Lower Triassic) – Forms "bacon-striped," ledgy slopes of laminated to thin-bedded, gypsiferous, pale-red to moderate-reddish-brown mudstone and siltstone, resistant, white to greenish-gray gypsum, and minor thin, laminated, light-gray dolomite beds; thickens northwesterly across the map area from 115 to 210 m.

TRmm Middle red member of the Moenkopi Formation (Lower Triassic) – Interbedded, slope-forming, laminated to thin-bedded, moderate-reddish-brown to moderate-reddish-orange siltstone, mudstone, and fine-grained sandstone with thin interbeds and veinlets of greenish-gray to white gypsum; thickens northeasterly across map area from about 50 to 120 m.

TRmv Virgin Limestone Member of the Moenkopi Formation (Lower Triassic) – Light-gray, light-olive-gray, and yellowish-brown limestone and silty limestone that typically forms three to four thin, resistant ledges that are separated by slopes of white to pale-yellow, red, and blue-gray, thin-bedded gypsum and gypsiferous siltstone; generally thickens northward across map area from about 30 to 70 m.

TRml Lower red member of the Moenkopi Formation (Lower Triassic) – Interbedded, slope-forming, laminated to thin-bedded, moderate-reddish-brown mudstone, siltstone, and fine-grained sandstone with local, thin, laminated light-olive-gray gypsum beds and veinlets; thickness ranges from 0 to 85 m.

TRmt Timpoweap Member of the Moenkopi Formation (Lower Triassic) – Lower part consists of light-brown-weathering, light-gray to grayish-orange, thin- to thick-bedded limestone and cherty limestone; upper part consists of grayish-orange, thin- to thick-bedded, slightly calcareous, fine-grained sandstone, siltstone, and mudstone; varies from 0 to 55 m thick.

TRmr Rock Canyon Conglomerate Member of the Moenkopi Formation (Lower Triassic) – Pebble to cobble, clast-supported conglomerate that contains subrounded to rounded chert clasts set in a pinkish-gray to very pale orange, calcareous, medium- to coarse-grained sandstone matrix; also includes a widespread, but thin, well-cemented breccia; conglomerate and breccia clasts are predominantly chert and limestone derived from underlying Kaibab Formation; fills paleovalleys; thickness ranges from 0 to about 90 m.

TRm Moenkopi Formation, undivided (Lower Triassic) – West-dipping, fault-bounded blocks of lower, middle, or upper red strata along the Hurricane fault.

TRmtr Timpoweap and Rock Canyon Conglomerate Members, undivided (Lower Triassic) – Mapped undivided in Arizona.

unconformity

Permian

Pkh Harrisburg Member of the Kaibab Formation (Lower Permian) – Upper part consists mainly of slope-forming, red and gray, gypsiferous siltstone, sandstone, gray gypsum, and thin-bedded gray limestone; medial part consists of an upper dark-brown-weathering cherty limestone bed and a lower light-gray, thick-bedded, sandy limestone bed separated by thin-bedded gypsiferous sandstone; lower part consists of slope-forming, light-red, fine- to medium-grained gypsiferous siltstone and sandstone, interbedded with gray, medium-grained, thin-bedded limestone and gray to white, thick-bedded gypsum. Thickness varies from 0 to 100 m.

Pkf Fossil Mountain Member of the Kaibab Formation (Lower Permian) – Lithologically uniform, light-gray, thick-bedded, fossiliferous limestone and cherty limestone; "black-banded" due to abundant reddish-brown to black ribbon chert and irregular chert nodules; maintains uniform thickness of about 90 m.

unconformity

Ptw Woods Ranch Member of the Toroweap Formation (Lower Permian) – Laterally variable, interbedded, yellowish-gray to light-gray, laminated to thin-bedded dolomite and similarly bedded black chert, massive gypsum, yellowish-orange gypsiferous mudstone and siltstone, and limestone; thickness varies from 35 to 100 m due to dissolution of gypsum.

Ptb Brady Canyon Member of the Toroweap Formation (Lower Permian) – Light- to medium-gray, medium- to coarse-grained, thick-bedded, fossiliferous limestone and cherty limestone; ribbon chert and irregular chert nodules locally make up 30 to 40% of the rock; 50 to 75 m thick.

Pts Seligman Member of the Toroweap Formation (Lower Permian) – Forms slopes of yellowish-brown to grayish-orange, thin-bedded, planar-bedded, fine- to medium-grained sandstone and minor siltstone with brown-weathering nodular chert; thickness ranges from 9 to 50 m.

unconformity

Pq Queantoweap Sandstone (Lower Permian) – Yellowish-brown, pale-orange, and grayish-orange, thick-bedded, cross-bedded, fine- to medium-grained sandstone that weathers to a conspicuous stair-step topography; about 425 to 520 m thick.

UTAH GEOLOGICAL SURVEY DUTCHMAN DRAW PALEOSEISMIC INVESTIGATION, FORT PEARCE SECTION, WASHINGTON FAULT ZONE, MOHAVE COUNTY, ARIZONA

by

William R. Lund[1], Tyler R. Knudsen[1], Christopher B. DuRoss[2], and Greg N. McDonald[3]

[1]Utah Geological Survey, Cedar City, Utah
[2]U.S. Geological Survey, Denver, Colorado
(formerly Utah Geological Survey, Salt Lake City, Utah)
[3]Utah Geological Survey, Salt Lake City, Utah

This report is part of Utah Geological Survey Miscellaneous Publication 15-6, *Surficial Geologic Mapping and Paleoseismic Investigations of the Washington Fault Zone, Washington County, Utah, and Mohave County, Arizona*—Paleoseismology of Utah, Volume 27.

Bibliographic citation for this report: Lund, W.R., Knudsen, T.R., DuRoss, C.B., and McDonald, G.N., 2015, Utah Geological Survey Dutchman Draw paleoseismic investigation, Fort Pearce section, Washington fault zone, Mohave County, Arizona, *in* Lund, W.R., editor, 2015, Surficial geologic mapping and paleoseismic investigations of the Washington fault zone, Washington County, Utah, and Mohave County, Arizona—Paleoseismology of Utah, Volume 27: Utah Geological Survey Miscellaneous Publication 15-6, p. 47–89, 1 plate, CD.

CONTENTS

ABSTRACT 47
INTRODUCTION 47
GEOLOGIC SETTING 48
TRENCHING 51
North Trench 51
Stratigraphy 51
Structure 51
South Trench 52
Stratigraphy 52
Structure 52
Numerical Ages 53
Radiocarbon Ages 53
Optically Stimulated Luminescence Ages 53
PALEOSEISMOLOGY 54
Number of Earthquakes 54
Earthquake Timing and Recurrence 56
Earthquake Timing 56
Earthquake Recurrence 56
Vertical Displacement 57
Scarp Profiles 57
Displaced Trench Stratigraphy 57
Colluvial-Wedge Thickness 58
Vertical Slip Rate 59
Paleoearthquake Magnitude Estimates 59
Paleomagnitude Scaling Relations 59
Regression Parameters 59
Paleomagnitude Estimates 60
Hanks and Kanamori (1979) – seismic moment for all fault types 60
Wells and Coppersmith (1994) – SRL all fault types 60
Stirling and others (2002) – censored instrumental SRL relation 60
Wesnousky (2008) – SRL all fault types 60
Summary 61
SUMMARY AND CONCLUSIONS 61
ACKNOWLEDGMEMTS 61
REFERENCES 62
APPENDICES 63
Appendix A Dutchman Draw site trench geologic unit descriptions 64
Appendix B Examination of bulk soil and AMS radiocarbon analysis of carbon from the Dutchman Draw trenches, Washington fault zone, Arizona 65
Appendix C Utah State University Luminescence Laboratory OSL ages, Dutchman Draw trench site, Washington fault zone, Arizona 79
Appendix D Dutchman Draw trench site OxCal model 85

FIGURES

Figure 1. Dutchman Draw trench site on the main strand of the Fort Pearce section of the Washington fault zone. 48
Figure 2. Dutchman Draw trench site area geologic map showing the location of paleoseismic trenches and scarp profiles... 49
Figure 3. Fault scarp formed on a late Quaternary alluvial fan at the Dutchman Draw trench site. 50
Figure 4. Dutchman Draw trench site geologic and topographic map 50
Figure 5. Dutchman Draw trench site scarp profile #2 58
Figure 6. Dutchman Draw trench site scarp profile #3 58

TABLES

Table 1. AMS radiocarbon age results for carbon samples from the Dutchman Draw site trenches, Arizona 54
Table 2. OSL age results for sediment samples from the Dutchman Draw site trenches, Arizona..... 54
Table 3. Radiocarbon and OSL ages used in OxCal v. 4.1.7 to model earthquake timing at the Dutchman Draw site, Arizona 56
Table 4. Earthquake timing and recurrence (one seismic cycle) at the Dutchman Draw site, Arizona 57

PLATE

Plate 1. Stratigraphic and structural relations exposed in trenches at the Dutchman Draw trench site, Fort Pearce section, Washington fault zone, Arizona .....on CD

UTAH GEOLOGICAL SURVEY DUTCHMAN DRAW PALEOSEISMIC INVESTIGATION, FORT PEARCE SECTION, WASHINGTON FAULT ZONE, MOHAVE COUNTY, ARIZONA

by William R. Lund, Tyler R. Knudsen, Christopher B. DuRoss, and Greg N. McDonald

ABSTRACT

The Utah Geological Survey conducted a paleoseismic trenching investigation to develop new information on paleoearthquake timing and displacement for the Fort Pearce section of the late-Quaternary-active Washington fault zone in southwestern Utah. Those data, along with the earthquake recurrence and vertical slip-rate estimates derived from them, can be used to improve both deterministic seismic-source characterization models and probabilistic earthquake-hazard analyses in the rapidly urbanizing St. George, Utah, metropolitan area. Additionally, these data will be used to update the U.S. Geological Survey's *Quaternary Fault and Fold Database of the United States* and *National Seismic Hazard Maps*, and the Utah Geological Survey's *Quaternary Fault and Fold Database and Map of Utah.*

Stratigraphic and structural relations exposed in two trenches excavated across a fault scarp formed on a late Quaternary alluvial fan near Dutchman Draw in Arizona, revealed evidence for two surface-faulting earthquakes on the main strand of the Fort Pearce section. OxCal modeling of a combination of radiocarbon and optically stimulated luminescence ages constrain the timing of the earthquakes to the Holocene, one at 7.7 ± 2.4 ka (P2) and the other at 1.0 ± 0.6 ka (P1) (rounded to the nearest 100 years, two-sigma uncertainty). The closed-seismic-cycle recurrence interval between the two earthquakes (also modeled with OxCal) is 6.6 ± 2.4 kyr. Additionally, the trenches revealed indirect stratigraphic evidence permissive of at least one latest Pleistocene earthquake that may have occurred between about 14 and 17 ka. If a P3 earthquake did occur in that time interval, and the P2 earthquake occurred at 7.7 ± 2.4 ka, the length of the resulting P3–P2 recurrence interval would range from about 2.5 to 13.2 kyr, with a median value of about 7.9 kyr. The P2-P1 recurrence interval of 6.6 ± 2.4 kyr is within one sigma of the possible P3–P2 median value, suggesting that the P2–P1 recurrence interval may be generally representative of the average surface-faulting recurrence on the Fort Pearce section during latest Quaternary time.

We obtained net vertical displacement estimates at the Dutchman Draw site from a combination of scarp profiles, displaced stratigraphy exposed in trenches, and scarp free-face heights extrapolated from colluvial-wedge thicknesses. Displacements ranged from about 1.0 m (P1) to 2.4 m (P2). There are significant caveats associated with all three displacement estimation methods at the Dutchman Draw site; therefore, we consider the displacement values poorly constrained estimates. The vertical slip rate for the P2–P1 recurrence interval (6.6 ± 2.4 kyr) and the P1 net vertical displacement (1.0–1.2 m) is 0.11–0.29 mm/yr (average 0.2 mm/yr). This slip-rate range represents only the most recent closed seismic cycle, and should be treated with caution if used to extrapolate the long-term behavior of the Fort Pearce section.

Multiple regression relations recommended by the Working Group on Utah Earthquake Probabilities to estimate M_w resulted in magnitude estimates ranging from M_w 6.7 to 7.1 for three possible rupture scenarios for the Fort Pearce section. Available paleoseismic information is insufficient to fully characterize all possible Fort Pearce section rupture scenarios, but our limited analysis shows that the Fort Pearce section can produce future earthquakes of $M_w \geq 7$, with average recurrence intervals of several thousand years.

INTRODUCTION

The purpose of this paleoseismic trenching investigation was to develop new information on paleoearthquake timing and displacement for the Fort Pearce (formerly Northern; Knudsen, this volume) section of the late-Quaternary-active Washington fault zone in southwestern Utah. Those data, along with the earthquake recurrence and vertical slip-rate estimates derived from them can be used to improve both deterministic seismic-source characterization models and probabilistic earthquake-hazard analyses in the rapidly urbanizing St. George metropolitan area of Washington County, Utah. Additionally, these data will be used to update the U.S. Geological Survey's (USGS) *Quaternary Fault and Fold Database of the United States* (http://earthquake.usgs.gov/hazards/qfaults) and *National Seismic Hazard Maps* (http://earthquake.usgs.gov/hazards/index.php), and the Utah Geological Survey's (UGS) *Quaternary Fault and Fold Database and Map of Utah*.

The Washington fault zone is one of several north-south trending, down-to-the-west Quaternary normal faults that define the boundary between the Colorado Plateau and Basin and Range physiographic provinces in northern Arizona and southwestern Utah. Based on structural and geomorphic criteria, Menges and Pearthree (1983) subdivided the Washington fault zone from south to north into the Sullivan Draw, Mokaac, and Northern sections. The Northern section, redefined as the Fort Pearce section by Knudsen (this volume), trends into the St. George metropolitan area, and scarps on unconsolidated Quaternary deposits and soft bedrock are evidence of late Quaternary surface faulting; therefore, the Fort Pearce section is considered active and capable of producing future large, damaging earthquakes.

Recognizing the earthquake hazard presented by the Fort Pearce section to the St. George metropolitan area, the UGS initiated a 1:50,000-scale surficial geologic mapping project (Knudsen, this volume) to better define the Fort Pearce section's location, boundaries, and geometry. While conducting the mapping, the UGS identified an isolated fault scarp formed on a latest Quaternary alluvial fan near Dutchman Draw south of the Utah-Arizona border (figure 1). After site evaluation that included three-dimensional (3-D) tomographic seismic profiling, the UGS excavated and logged two trenches across the scarp, and excavated a third trench several meters west of the scarp to explore for possible antithetic faulting inferred from the seismic profiles. The two scarp trenches exposed the fault zone and associated fault-related geologic deposits that provide new information on the timing, recurrence, and displacement of the two most recent surface-faulting earthquakes on the main strand of the Fort Pearce section, and indirect evidence for at least one possible third, older earthquake. The third trench did not expose evidence of antithetic faulting and was not logged.

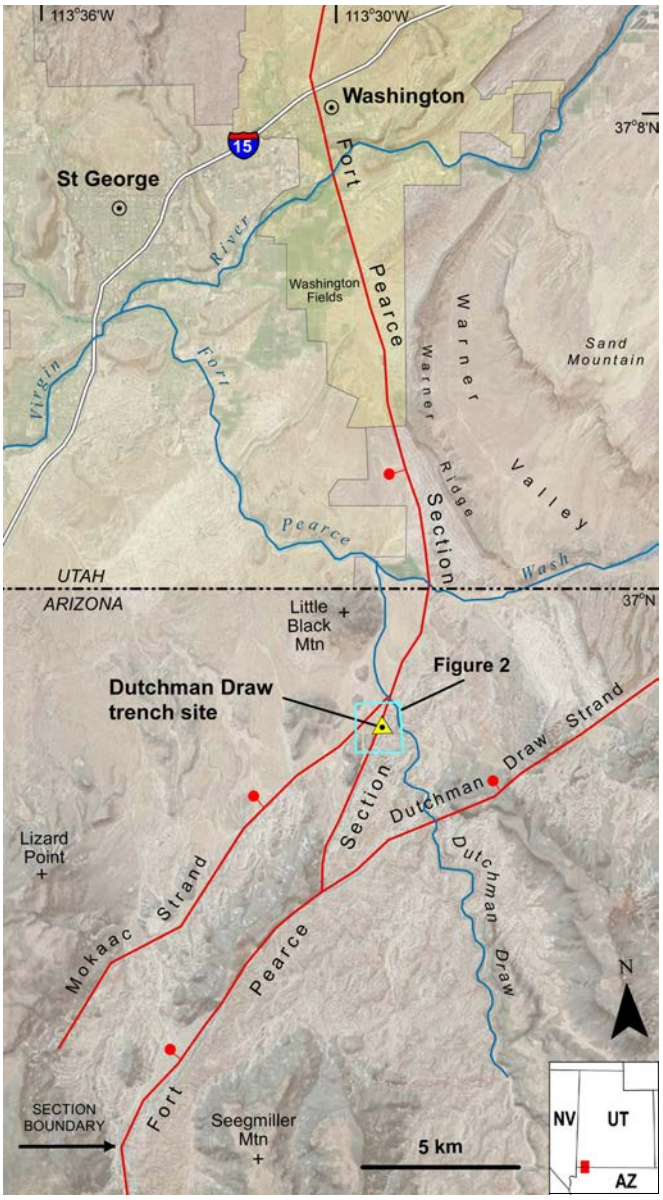

Figure 1. *Dutchman Draw trench site on the main strand of the Fort Pearce section of the Washington fault zone (fault shown by red lines, ball and bar on downthrown side of the fault). St. George and Washington City denoted by yellow shaded areas. Base map consists of Microsoft® Bing™ Maps aerial imagery and World Shaded Relief Map from the ESRI Resource Center.*

GEOLOGIC SETTING

The Dutchman Draw trench site is approximately 6 km south of the Utah-Arizona border near the southern end of the main strand of the Fort Pearce section (figure 1). We selected the site based on interpretation of 1:24,000-scale, color aerial photographs (Knudsen, this volume) and field reconnaissance along the fault in Utah and Arizona. The site is about 0.6 km south of Dutchman Draw (figure 1) at the mouth of a small unnamed ephemeral drainage where the fault displaces a late Quaternary alluvial fan (figure 2). The fault scarp is 2 to 4 m high (figure 3), and is continuous across the fan for approximately 100 m. The scarp is expressed as a single trace across most of the site before bifurcating to form two subparallel strands near its southern end (figure 4). There is no surface evidence of antithetic faulting. North and south of the site, scarps are formed on bedrock, but at the site, a stream cut dissects the fault scarp and exposes alluvial deposits that are at least 4 m thick in the fault footwall. The 3-D seismic profiling demonstrated that the scarp is not bedrock cored, and that unconsolidated alluvial-fan deposits extend to a depth of several meters on the fault hanging wall (Shengdong Liu, University of Utah Department of Geology and Geophysics, written communication, 2008). A second, subparallel fault trace to the east is well expressed in bedrock, but geologic mapping (Knudsen, this volume) shows that it does not displace Holocene/latest Quaternary unconsolidated deposits. Because the site is on the more remote southern part of the Fort Pearce section, it has received minimal human-caused disturbance.

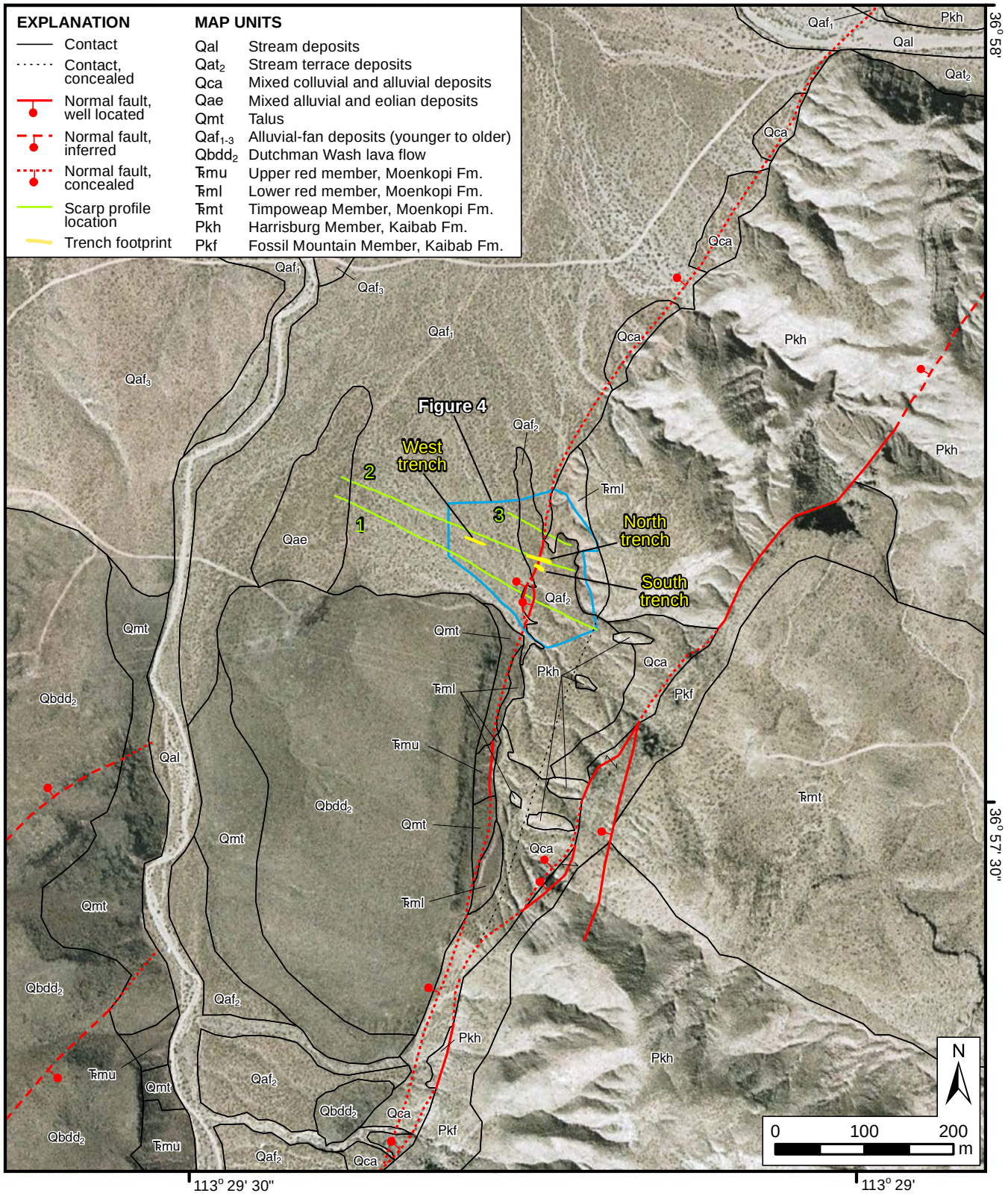

Figure 2. *Dutchman Draw trench site area geologic map showing the location of paleoseismic trenches and scarp profiles. Base map from Microsoft® Bing™ Maps. Bar and ball on downthrown side of fault. Blue box shows area of figure 4.*

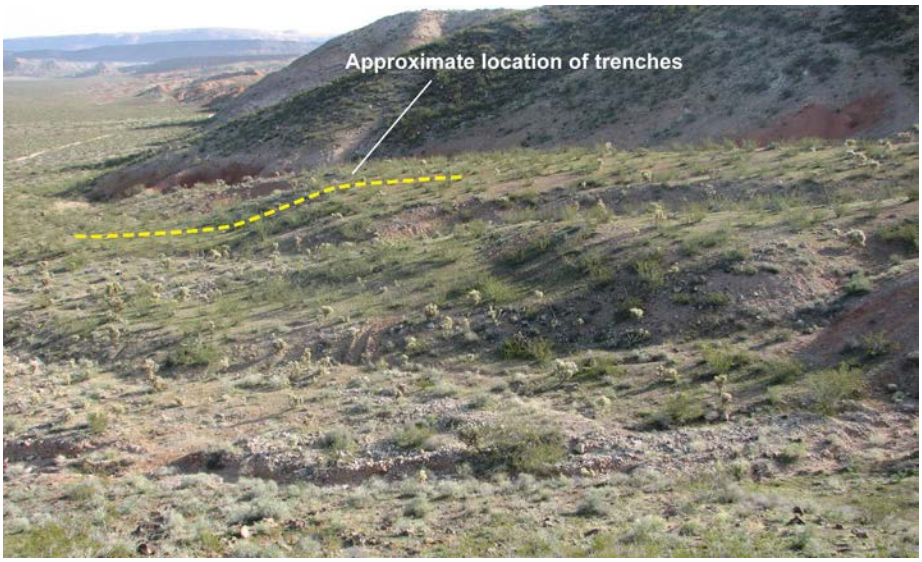

Figure 3. *Fault scarp (identified by yellow line) formed on a late Quaternary alluvial fan at the Dutchman Draw trench site. View is to the north. Photo taken in 2009.*

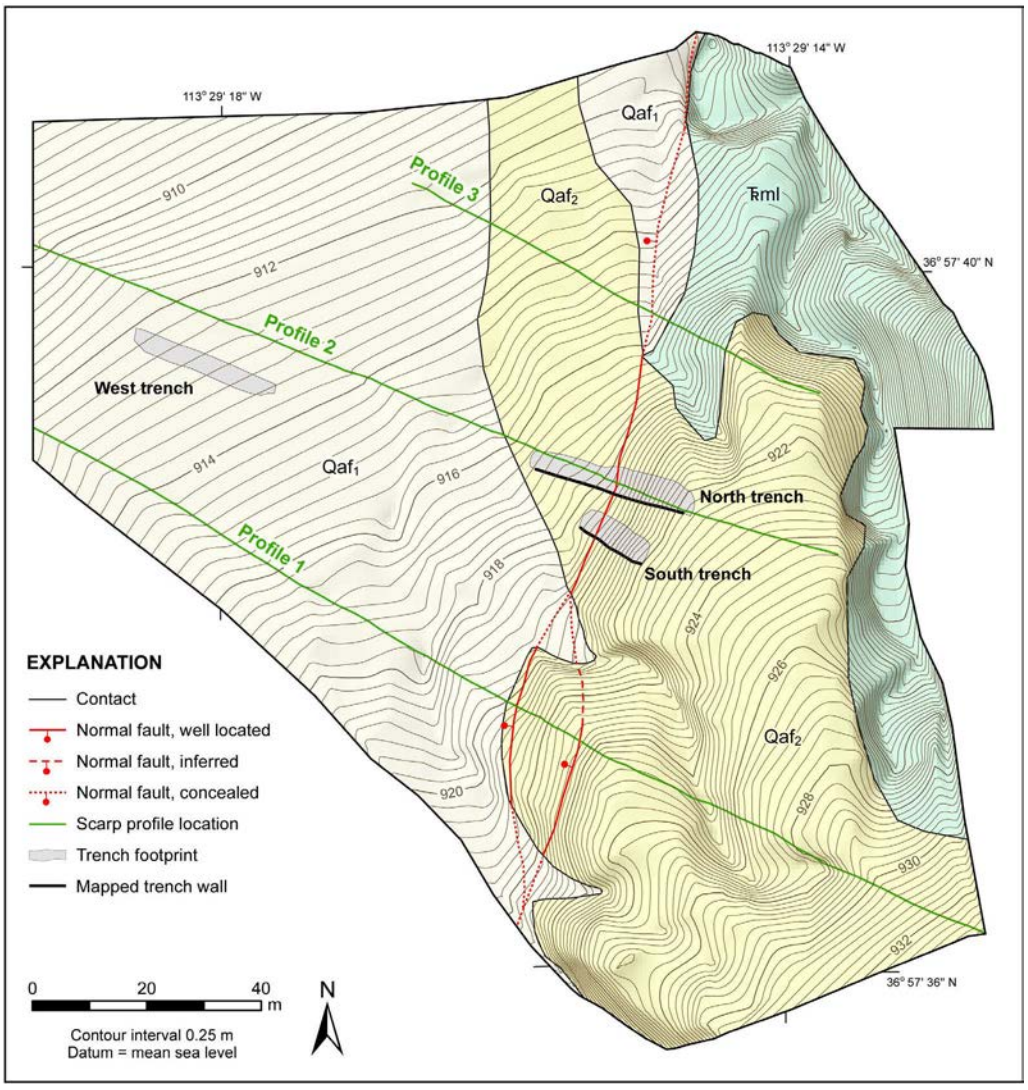

Figure 4. *Dutchman Draw trench site geologic and topographic map; topography mapped summer 2009. See figure 2 for explanation of geologic units; for detailed unit explanations, see unit descriptions for the Washington fault zone geologic map (Knudsen, this volume).*

TRENCHING

We excavated three trenches (North, South, and West) at the Dutchman Draw site (figures 2 and 4, and plate 1). The North and South trenches were roughly parallel, about 5 m apart, and normal to the main fault scarp. Both trenches exposed the fault zone and associated geologic units. Detailed trench logging demonstrated that the geologic units were common to both trenches (plate 1). We excavated the West trench in the fault hanging wall about 30 m west of the main fault scarp (figure 2) to explore for possible antithetic faulting indicated by the 3-D tomographic seismic profiles; however, no antithetic faults were discovered and we did not log the West trench.

We established meter-scale horizontal and vertical grid systems in the North and South trenches, and measured both horizontal and vertical distances from the east end of the North trench (plate 1). The grid system in the shorter South trench was tied to the grid system in the longer Northern trench; consequently, the east end of the South trench grid corresponds to horizontal station (h) 13 in the North trench and is numbered accordingly on plate 1. We logged the North and South trenches at a scale of 1:20 using a total station instrument (Trimble TTS 500) to measure geologic control points.

North Trench

Stratigraphy

The North trench exposed nine geologic units, with units 1 and 4 further subdivided into "a" and "b" subunits (plate 1; appendix A). Units 8 and 9 were the only units exposed in the fault footwall; unit 9 was not exposed on the fault hanging wall. Unit 9, the oldest stratigraphic unit in the trench, consists of steeply dipping to overturned red mudstone, siltstone, and fine-grained sandstone bedrock of the Triassic Moenkopi Formation. Unit 8 unconformably overlies unit 9, and consists of strongly indurated (chiefly gypsum cemented), coarse-grained, massively bedded alluvial sediments (appendix A). Because of its thickness, massive bedding, and strong cementation, we interpret unit 8 as an alluvial-fan deposit that likely consists of numerous individual debris-flow and debris-flood deposits; however, we were unable to map any stratigraphically continuous subunits in unit 8 in the North trench. The upper part of unit 8 yielded an optically stimulated luminescence (OSL) age of 48.66 ± 3.74 ka (see the Numerical Ages section below and appendices B and C for details regarding the radiocarbon [^{14}C] and OSL ages obtained from the North and South trenches).

The fault zone in the North trench contains tilted and sheared blocks of unit 8 (see Structure section below), west (downthrown side) of the main fault (NF1). Unit 8 is not otherwise exposed in the fault hanging wall. Unit 8 in the fault zone is in fault contact with unit 7, a strongly indurated, coarse-grained, massively bedded debris-flow deposit (plate 1, appendix A). Unit 6 is a moderately indurated, coarse-grained, thick-bedded debris-flow deposit with limited exposure in the North trench, but is more extensively exposed in the South trench. Unit 5 overlies units 6 and 7 in the fault hanging wall and unit 8 in the fault zone, and is a weakly indurated, coarse-grained debris-flow deposit. Units 5 through 9 predate the penultimate surface-faulting earthquake (P2) at the Dutchman Draw site.

Unit 4 consists of the colluvial-wedge (unit 4a) and associated crack-fill (unit 4b) deposits formed by fault-scarp erosion following the P2 earthquake. We obtained three stratigraphically consistent ^{14}C ages (6900–6200 cal yr B.P., 4420–4250 cal yr B.P., and 4330–4360 [2.7%] cal yr B.P. and 4150–4300 [92.7%] cal yr B.P. [2σ]; appendix B) from weakly organic, fine-grained horizons in unit 4a (plate 1). An OSL sample from near the bottom of the P2 colluvial wedge (plate 1) yielded an anomalously young age of 3.03 ± 0.34 ka when compared with the three ^{14}C ages (see discussion regarding why numerical ages may be out of stratigraphic order in the Numerical Ages section below).

Unit 3 is a weakly indurated debris-flow deposit (appendix A), which was deposited downslope from the toe of the fault scarp and conformably overlies unit 5 but does not overlie unit 4. Because units 3 and 4 occupy the same relative stratigraphic position in the North trench, deposition of unit 3 likely occurred close in time to deposition of unit 4.

Unit 2 is a weakly to moderately indurated, chiefly coarse-grained debris-flow/debris-flood deposit (appendix A) that buried units 3 and 4, and therefore postdates the P2 earthquake. The wavy to irregular contact at the base of unit 2 may in places be unconformable with the underlying deposits, such as between station h-17 and the main fault zone (plate 1). A thin, weakly developed paleosol (buried A horizon soil; s2 on plate 1) formed on unit 2 prior to the most recent surface-faulting earthquake (P1). Charcoal from the paleosol yielded a ^{14}C age of 1530–1280 cal yr B.P. The ^{14}C age from the charcoal is in correct stratigraphic order with the three older ^{14}C ages from unit 4a (P2 colluvial wedge). Unit 2 is overlain by unit 1a, the colluvial-wedge deposit formed by fault-scarp erosion following the P1 earthquake. Unit 1b is a crack-fill deposit related to the P1 earthquake (plate 1).

Other than the s2 paleosol, no other paleosols were recognized in the North trench. A weakly developed modern soil (s1) has formed on unit 8 in the fault footwall and on units 1a and 2 on the fault hanging wall (plate 1).

Structure

In the North trench, faulting was restricted to a 3-m-wide zone between station h-15 and h-18 (plate 1). The main fault (NF1) intersected the trench bottom at about station h-15.7, and consisted of a steeply dipping main trace with minor bifurcating secondary strands. The upper part of fault NF1 dips steeply to the east, before changing to a west dip with increasing depth in the trench. At about station h-16.8 (bottom of trench), the first of three interconnected, small-displacement,

east-dipping, high-angle reverse faults (NF2–NF4) formed a zone of secondary faulting that was about a meter wide at its greatest extent.

Two colluvial-wedge deposits (units 1a and 4a) and associated crack-fill deposits (units 1b and 4b) that formed adjacent to fault NF1 by post-earthquake fault scarp erosion provide stratigraphic evidence for two surface-faulting earthquakes (P1 and P2) on the Fort Pearce section main strand. Units 8 and 9 have been displaced beneath the bottom of the trench in the fault hanging wall. Units 5, 6, and 7 are displaced by the three small reverse faults (NF2–NF4). Evidence for reverse faulting extending above unit 5 was poorly expressed, and it is possible that the reverse faults were only active during the P2 earthquake. Unit 2, which overlies the P2 colluvial wedge and underlies the P1 colluvial wedge, was only displaced by fault NF1 during the P1 earthquake.

Geologic units 2 through 7 either were never deposited on the fault footwall or were removed by one or more episodes of post-earthquake erosion. Given that units 2 and 5 were exposed on the footwall in the South trench just 5 m distant (plate 1), erosion seems a likely explanation for their absence on the North trench footwall.

South Trench

Stratigraphy

The South trench exposed eight geologic units (plate 1) that correspond with the stratigraphic units in the North trench (plate 1; appendix A). Unit 8 is the oldest stratigraphic unit in the South trench, and it displayed better developed bedding than did the same unit in the North trench; consequently, we divided unit 8 in the South trench into four subunits (8a–8d; plate 1 and appendix A). Unit 8 is a strongly indurated (chiefly gypsum cemented), mostly coarse-grained, thick-bedded alluvial-fan deposit confined to the footwall of the main fault in the South trench (see Structure section below). Unit 8b yielded an OSL age of 54.07 ± 4.07 ka (plate 1).

Rotated and sheared blocks of what we interpret to be unit 8 were present in the South trench fault zone (see Structure section below); however, the blocks were highly sheared, making positive identification of the geologic unit from which they were derived difficult. Unit 7, a strongly indurated, coarse-grained, massively bedded debris-flow deposit (plate 1; appendix A), is in fault contact with unit 8. Unit 7 yielded an OSL age of 30.75 ± 2.21 ka in the North trench, making unit 7 approximately 23 kyr younger than unit 8. Unit 6 is a moderately indurated, coarse-grained debris-flow deposit that conformably overlies unit 7. A sample from near the top of unit 6 yielded an OSL age of 17.10 ± 1.38 ka (plate 1), making unit 6 about 14 kyr younger than unit 7. Units 6 and 7 were only exposed in the fault hanging wall. Unit 5 is a coarse-grained, weakly indurated debris-flow deposit, and is the oldest geologic unit present on both sides of the main fault in the South trench. A sample from near the top of unit 5 in the fault hanging wall yielded an OSL age of 13.80 ± 1.18 ka (plate 1), making unit 5 about 3 kyr younger than unit 6. Unit 5 overlies units 6 and 8 in the fault hanging wall and units 8a and 8b in the fault footwall, and is the youngest unit that predates the P2 earthquake.

Unit 4 consists of the colluvial-wedge (unit 4a) and associated crack-fill (unit 4b) deposits formed by erosion of the P2 earthquake fault scarp (see the North trench Stratigraphy section for details of the ^{14}C ages associated with unit 4). Unit 3 is a weakly indurated debris-flow deposit confined to the main fault hanging wall that conformably overlies unit 5, but does not overlie unit 4 (plate 1). Units 3 and 4 occupy the same relative stratigraphic position in the South trench, but because there are no numerical ages available for unit 3, it is not known if unit 3 is older, younger, or contemporaneous with unit 4. However, based on stratigraphic position, deposition of unit 3 likely occurred close in time to deposition of unit 4.

Unit 2 is a loose to moderately indurated, chiefly coarse-grained debris-flow/debris-flood deposit that overlies unit 4 (plate 1), and therefore postdates the P2 earthquake. Unit 2 yielded an OSL age of 4.22 ± 0.27 ka, which is younger than the youngest ^{14}C age obtained from the underlying P2 colluvial wedge (unit 4a) in the North trench, thus the OSL age is in correct stratigraphic sequence with the older ^{14}C ages. Erosion either prior to or contemporaneous with deposition of unit 2 truncated the upper part of the P2 colluvial wedge (unit 4a). Unit 2 is overlain by unit 1a, the P1 earthquake colluvial wedge (plate 1); therefore, unit 2 predates the P1 earthquake. Unit 2 is also present on the fault footwall, where it overlies units 8a and 5, and is displaced by P1 faulting on a secondary fault zone (see Structure section below). Erosion, either prior to or contemporaneous with deposition of unit 2, locally removed unit 5 from the fault footwall. Unit 1b is a crack-fill deposit related to the P1 earthquake (plate 1).

We identified no other paleosols or other organic-bearing units in the South trench. A modern soil (s1) is forming at the ground surface on units 1a and 2.

Structure

The South trench exposed three fault zones: a main, west-dipping zone (SF1) at about station h-17.8 (bottom of trench); a secondary, west-dipping zone (SF2) at about station h-13.5 (bottom of trench); and an east-dipping, small displacement reverse fault (SF3) west of the main fault zone at about station h-20 (bottom of trench) (plate 1).

Fault zone SF1 consists of a near-vertical to west-dipping principal shear and two interconnected, small-displacement, subsidiary reverse faults. Two colluvial-wedge deposits (units 1a and 4a) and associated crack-fill deposits (units 1b and 4b) that formed adjacent to fault zone SF1 provide evidence for two surface-faulting earthquakes on the Fort Pearce section.

Fault zone SF1 displaced unit 8 down-to-the-west to below the bottom of the trench in the fault hanging wall. Units 6 and 7 are exposed in the hanging wall of the main fault, but not in the footwall. In the footwall, units 2 and 5 directly overlie unit 8, indicating that units 6 and 7 were either (1) eroded from the footwall most likely following an earlier surface-faulting earthquake, or (2) were only deposited on the fault hanging wall, possibly by debris flows whose flow paths were controlled by a preexisting fault scarp on the displaced alluvial-fan surface. Unit 5 has been displaced by two surface-faulting paleoearthquakes (P1 and P2), and unit 2 by one paleoearthquake (P1).

Fault zone SF2 is in the footwall of the main fault zone, and represents a wide, debris-filled void across which the P1 earthquake produced a few tens of centimeters of displacement (plate 1). Fault zone SF2 displaces units 5 and 8 (both pre-P2 earthquake geologic units) and unit 2 (a post-P2 earthquake geologic unit) by roughly the same amount, indicating that fault zone SF2 was only active during the P1 earthquake. The fissure formed along fault zone SF2 is exceptionally wide for a fault with such small displacement. Additionally, between fault zones SF1 and SF2, there were several well-developed cracks also related to the P1 earthquake (plate 1). The cracks exhibited little or no vertical displacement, but some have open voids formed along them. Open voids are also present along both the SF1 and SF2 fault zones. We interpret the voids as evidence that the P1 earthquake is a geologically young event, and that there has not been sufficient time for the voids to collapse or completely fill with debris since the P1 earthquake.

Fault zone SF3 is a moderate- to high-angle reverse fault that bifurcates upward (plate 1). Fault zone SF3 displaces unit 5 tens of centimeters. Evidence that fault zone SF3 displaces units 2 and 3 is poorly expressed, and if such displacement did occur, it was significantly less than the displacement produced in unit 5. Therefore, fault zone SF3 was active during the P2 earthquake, but less so, if at all, during the P1 earthquake.

Numerical Ages

Geologic units in the North and South trenches yielded a combination of ^{14}C and OSL ages (briefly discussed above in the Stratigraphy sections) that helped constrain both the ages of the units and the timing of the two most recent surface-faulting earthquakes at the Dutchman Draw site.

Radiocarbon Ages

We found no datable organic material in the South trench, and no macroscopic charcoal in the North trench. However, the North trench did expose three thin, weakly organic stringers of fine-grained sediment within the P2 colluvial wedge (unit 4a), and a thin, weakly organic paleosol (s2) formed on unit 2 and buried by the P1 colluvial wedge (unit 1a; plate 1). Because all four horizons were thin (a few cm to 10 cm thick) and only weakly organic, we sampled them through their entire thickness to ensure that we collected sufficient material for ^{14}C dating. The likely origin of the organic colluvial-wedge stringers is erosion of pre-existing carbon-bearing material on the upthrown side of the fault following the P2 earthquake. The s2 paleosol was forming on unit 2 (a debris-flow deposit) at the time of the P1 earthquake, and was down dropped by the earthquake and subsequently buried by P1 colluvial-wedge sediment.

We submitted four bulk organic sediment samples from the North trench to PaleoResearch Institute (PRI) for separation and identification of plant macrofossils (appendix B). Sample NT-RC1 yielded charcoal consisting of Salicaceae (willow family) and unidentified hardwood (wood from a broad-leaved flowering tree or shrub, but too small for further identification). Sample NT-RC2 also yielded unidentified hardwood charcoal. Samples NT-RC3 and NT-RC4 both provided microcharcoal suitable for dating, but which could not be identified to family or genus. Following preparatory treatment of the charcoal (appendix B), PRI submitted the four charcoal samples to the Keck Carbon Cycle Accelerator Mass Spectrometry Facility at the University of California, Irvine, for accelerator mass spectrometry (AMS) ^{14}C dating. Table 1 presents the results of the PRI sample processing and subsequent AMS ^{14}C dating. The resulting age estimates are reported both as ^{14}C years before present (RCYBP) and as one- and two-sigma calendar calibrated ages (cal yr B.P.). The four ^{14}C ages are in correct stratigraphic order (plate 1).

Bioturbation, the mixing of younger or older carbon within an unconsolidated geologic unit by burrowing animals and/or root mixing, can result in anomalously young or old ^{14}C ages that are out of stratigraphic order. Additionally, reworking of older detrital carbon into a younger unconsolidated geologic deposit by erosion and redeposition of a pre-existing A horizon soil or other carbon-bearing deposit may yield an age that is too old and likewise stratigraphically inconsistent. We tried to minimize these dating uncertainties given the limited size of the organic-bearing horizons in the North trench (our sampling largely depleted the organic stringers in the P2 colluvial wedge and the most organic parts of the s2 paleosol), by avoiding collecting samples near obviously burrowed or otherwise bioturbated areas. Although not a guarantee that carbon mixing has not occurred, the fact that the four ^{14}C ages from the North trench are in proper age/stratigraphic order gives us confidence that the sampled deposits were not significantly contaminated by younger or older carbon. Additionally, during trench logging, we observed little evidence of burrowing or other bioturbation in the sampled geologic units.

Optically Stimulated Luminescence Ages

We collected seven OSL samples at the Dutchman Draw site: three from the North trench and four from the South trench (plate 1). We conducted the sampling in accordance with Utah State University Luminescence Laboratory (USULL) sampling protocol (http://www.usu.edu/geo/luminlab/how2osl.pdf), and submitted the samples to USULL for OSL dating.

Table 1. *AMS radiocarbon age results for carbon samples from the Dutchman Draw site trenches, Arizona. Samples analyzed at the Keck Carbon Cycle AMS Facility at the University of California, Irvine.*

Sample No.	Sample Identification	Geologic Unit	AMS ^{14}C Age[1] RCYBP	One-sigma Calibrated Age[2] (68.2%) cal yr B.P.	Two-sigma Calibrated Age[2] (95.4%) cal yr B.P.
PRI-09-61-NT-RC1	Salicaceae and unidentified hardwood charcoal	4a P2 colluvial wedge	5720 ± 150	6680–6390 (61.7%) 6370–6320 (6.5%)	6900–6200
PRI-09-61-NT-RC2	Unidentified hardwood charcoal	s2 paleosol on unit 2	1480 ± 70	1490–1470 (2.7%) 1420–1300 (65.5%)	1530–1280
PRI-09-61-NT-RC3	Microcharcoal	4a P2 colluvial wedge	3905 ± 20	4420–4350 (42.1%) 4330–4290 (26.1%)	4420–4250
PRI-09-61-NT-RC4	Microcharcoal	4a P2 colluvial wedge	3830 ± 20	4290–4270 (2.5%) 4250–4220 (22.1%) 4210–4150 (43.6%)	4360–4330 (2.7%) 4300–4150 (92.1%)

[1]*Reported in radiocarbon years before present (RCYBP) at one standard deviation measurement precision (68.2%), corrected for* ^{13}*C; present = 1950.*

[2]*See appendix B for details of PaleoResearch Institute* ^{14}*C ages and age calibration.*

See appendix C for details of USULL sample processing and dating procedures. Table 2 presents the OSL age estimates.

Optically stimulated luminescence determines the last time quartz or feldspar grains were exposed to sunlight (Gray and others, 2015; see also USULL website at http://www.usu.edu/geo/luminlab/whatis.html for details of the OSL dating technique). As sediment is transported, it is exposed to sunlight and zeroed of any previous luminescence signal. If insufficient sunlight exposure occurs, the quartz or feldspar grains may retain a luminescence signal that results in an OSL age that is too old. Similarly, OSL ages may be affected by bioturbation if material with a young luminescence signal is carried downward into older unconsolidated geologic units by burrowing or root mixing. Sample NT-OSL3 has an age that is too young given its stratigraphic context and the multiple stratigraphically consistent ^{14}C ages obtained from the same unit. A possible explanation for the anomalously young age is bioturbation of more recently deposited sediment downward into older material. The other OSL ages from the North and South trenches are in correct stratigraphic order.

Table 2. *OSL age results for sediment samples from the Dutchman Draw site trenches, Arizona. Samples analyzed at the Utah State University Luminescence Laboratory.*

Sample Number	Trench	Geologic Unit	OSL Age (ka)
NT-OSL1*	North	7 Debris-flow deposit	30.75±2.21
NT-OSL2*	North	8 Debris-flow deposit	48.66+3.74
NT-OSL3*	North	4b P2 Colluvial wedge	3.02±0.34
ST-OSL1*	South	2 Debris-flow deposit	4.22+0.27
ST-OSL2**	South	7 Debris-flow deposit	17.10±1.38
ST-OSL3**	South	8b Debris-flow deposit	54.07±4.07
ST-OSL4**	South	5 Debris-flow deposit	13.80±1.18

[1]*Reported in radiocarbon years before present (RCYBP; present = 1950).*

[2]*Calender years before present; present = 1950.*

[3]*Mean ± two sigma (two standard deviations). Reported ages are unmodelled values.*

[4]*Value that separates the higher half of the sample from the lower half.*

[5]*Value that occurs most frequently in the data set, i.e., the peak of the probability density function for the age value.*

PALEOSEISMOLOGY

Number of Earthquakes

Geologic units 1a, 1b, 4a, and 4b in both the North and South trenches (see Stratigraphy sections above; plate 1) provide direct stratigraphic evidence (tectonic colluvial-wedge and crack-fill deposits) for two Holocene surface-faulting earthquakes on the main strand of the Fort Pearce section of the

Washington fault zone. New geologic mapping performed for this study (Knudsen, this volume) redefines the Mokaac section (Pearthree, 1988) as a strand of the Fort Pearce section. Likewise, our new mapping redefines the Dutchman Draw fault (previously mapped as an independent structure; Pearthree [1988]) also as a strand of the Fort Pearce section. There are no paleoseismic data for either the Mokaac or Dutchman Draw strands to quantify the number or timing of past surface-faulting earthquakes on those structures. However, given their comparatively short lengths (both 16 km long) and the fact that they connect to the Fort Pearce section main strand, but not to each other (plate 1), we consider it most likely that the Mokaac and Dutchman Draw strands rupture synchronously with the main strand of the Fort Pearce section and do not rupture independently or together. However, we acknowledge that we have only a single paleoseismic data point for the Fort Pearce main section and no paleoseismic trenching information from the Mokaac and Dutchman Draw strands, thus our data are insufficient to characterize the multitude of possible rupture scenarios among and between the three structures. Therefore, although we consider it unlikely for geomorphic and geometrical reasons that the Mokaac and Dutchman Draw strands rupture either separately or together (along with a short intervening portion of the Fort Pearce section), the available data are too sparse to exclude that possibility.

Furthermore, in the absence of paleoseismic data for the Mokaac and Dutchman Draw strands, it is not known whether both strands rupture during all Fort Pearce main section earthquakes, or if they rupture less frequently (i.e., due to geometrical constraints, the Dutchman Draw strand may rupture only during northward-propagating earthquakes, whereas the Mokaac strand may rupture only during southward-propagating earthquakes; Knudsen, this volume). It may also be possible that an earthquake initiating at the south end of the main strand may divert onto the Dutchman Draw strand and not rupture the main strand farther north. Likewise, an earthquake initiating at the north end of the main strand may rupture southward and divert onto the Mokaac strand and not rupture the main strand farther south. Determining which of these scenarios (or others possible on this geometrically complex fault) may actually occur requires additional paleoseismic trenching information for the Mokaac and Dutchman Draw strands.

Based on the results of our trenching at the Dutchman Draw site on the Fort Pearce section main strand, we believe that the two surface-faulting earthquakes identified there represent a minimum number of surface-faulting earthquakes on the Fort Pearce section during the Holocene. It is possible that southward-propagating earthquakes on the Fort Pearce section may have diverted onto the Mokaac strand or northward-propagating earthquakes may have diverted on to the Dutchman Draw strand and therefore would not appear in the geologic record at the Dutchman Draw site. Again, we consider a Mokaac-strand or Dutchman Draw-strand independent rupture, or a combined Mokaac- and Dutchman Draw-strand synchronous rupture (which would also require rupture of 6 km of the main Fort Pearce strand) unlikely, but cannot categorically exclude the possibility; only additional paleoseismic information for the Mokaac and Dutchman Draw strands will resolve this issue.

The South trench contained indirect stratigraphic evidence for at least one possible latest Pleistocene surface-faulting earthquake. There, units 6 and 7 are present on the main fault hanging wall, but not on the footwall (plate 1). On the hanging wall, units 6 and 7 are overlain by units 2, 3, and 5 that consist of younger debris-flow deposits. Units 2 and 5 are also present on the fault footwall where they overlie unit 8. Those stratigraphic relations show that either units 6 and 7 were removed by erosion from the footwall prior to deposition of units 2 and 5, or alternatively, that units 6 and 7 were never deposited on the footwall. Because unit 5 overlies units 6 and 7 on the hanging wall, but overlies unit 8 on the footwall, units 6 and 7 may have been eroded from the footwall prior to deposition of unit 5. A surface-faulting earthquake that left units 6 and 7 exposed to erosion at an elevated position on the fault footwall, but at a lower elevation and protected from erosion on the fault hanging wall, could account for the stratigraphic relations observed in the South trench. Conversely, if a fault scarp was present at the site when units 6 and 7 were deposited, the scarp may have preferentially directed the unit 6 and 7 debris flows to the fault hanging wall and prevented deposition on the footwall. Either scenario requires at least one older (antepenultimate) surface-faulting earthquake at the site. Based on OSL ages of units 6 (17.10 ± 1.38 ka) and 5 (13.80 ± 1.18 ka), the older surface faulting would likely have occurred in the latest Pleistocene between about 17 and 14 ka. Evidence not supporting an older earthquake scenario is the absence of colluvial-wedge deposits representing older event(s) in the North and South trenches.

Stratigraphic evidence for a possible older surface-faulting earthquake is also expressed in the North trench, where units 2 and 5 are not present on the fault footwall. Where exposed on the hanging wall, units 2 and 5 show evidence of thinning toward the fault zone, implying that they were pinching out in that direction (plate 1). However, unit 5 overlies what we interpret to be a sheared block of unit 8 in the fault zone. Units 6 and 7 are also absent from the fault footwall and present on the hanging wall, where they do not show evidence of much thinning toward the fault zone. A possible explanation for these stratigraphic relations is that an older surface-faulting earthquake resulted in erosion of units 6 and 7 from the footwall and their preservation on the hanging wall. At a later time, the P3 scarp or other irregularity in the alluvial-fan surface influenced the flow paths of the debris flows that deposited units 2 through 5 and limited their deposition to the fault hanging wall. Conversely, since unit 5 overlies unit 8 in the fault zone, unit 5 and possibly unit 2 may have been deposited on the footwall, but were subsequently removed by erosion following the P2 earthquake.

OSL ages from the North and South trenches show that geologic units deposited prior to the P2 earthquake range in age from at least 54.07 ka to 13.80 ka (plate 1; table 2). Unconformable contacts between several of those units represent intervals of either non-deposition or erosion. For example, the contact between units 5 and 8b in the South trench footwall represents a hiatus of about 40 kyr, and evidence presented above indicates that the upper unit 8a contact is likely an erosional surface. Similarly, the contact between units 6 and 7 represents a hiatus of about 14 kyr, and the contact between units 4a and 5, a hiatus of about 8 kyr. Clearly, long periods of time elapsed between episodes of sediment deposition on the alluvial fan at the Dutchman Draw site. What remains unclear is how much erosion occurred in those long intervals that may have been earthquake driven, and how much, if any, stratigraphic evidence of older surface-faulting earthquakes may have been removed by erosion.

Earthquake Timing and Recurrence

Earthquake Timing

We used OxCal radiocarbon calibration and analysis software (version 4.1.7; Bronk Ramsey, 2010; using the IntCal09 radiocarbon age calibration curve [Reimer and others, 2009]) to model the timing of the P1 and P2 earthquakes and the duration of the closed seismic interval between the earthquakes (appendix D). The OxCal software (Bronk Ramsey, 2009) probabilistically models the time distribution of undated events (such as earthquakes) by incorporating stratigraphic ordering information for radiocarbon and luminescence ages (Bronk Ramsey, 2008) obtained from our trenches. We report earthquake time ranges, and elapsed time between earthquakes with two-sigma confidence intervals. Note that we report OSL ages as the mean and two-sigma uncertainty rounded to the nearest century in thousands of calendar years before the sample processing date (2009–2010). The ~60-year difference in the OSL sample age versus the reference standard for ^{14}C (1950) is minor compared to the OSL age uncertainties, and is accounted for in modeling of earthquake times in OxCal.

OxCal modeling of ^{14}C and OSL ages from the Dutchman Draw site constrains the timing of the P2 and P1 earthquakes to the early to middle Holocene and late Holocene, respectively. Earthquake P2 occurred at 7.7 ± 2.4 ka and P1 at 1.0 ± 0.6 ka. Table 3 shows the ^{14}C and OSL ages that we modeled in OxCal to constrain earthquake timing. Ages older than 17.1 ka (see table 2) were not used in the OxCal model because they do not impose significant constraints on earthquake timing within the stratigraphic context provided by the trenches. We rounded all ages to the nearest 10 years for use in the OxCal model. Table 4 shows the earthquake timing resulting from OxCal modeling at the Dutchman Draw site. All results are rounded to the nearest 100 years.

Earthquake Recurrence

The elapsed time between the P2 and P1 earthquakes represents a single closed seismic cycle (recurrence interval) for the Fort Pearce section of the Washington fault zone. The length of a seismic cycle represents the time required following a large stress-release earthquake (P2) for a fault to re-accumulate sufficient strain to generate a second large earthquake (P1) on the same fault section. Comparing the recurrence interval with the elapsed time since the most recent surface-faulting earthquake (MRE) gives an indication of where a fault lies in its current seismic cycle. However, the paleoearthquake timing information from the Dutchman Draw site is limited and only constrains the length of the most-recent seismic cycle for the main trace of the Fort Pearce section. The recurrence interval modeled by OxCal

Table 3. *Radiocarbon and OSL ages used in OxCal v. 4.1.7 (Bronk Ramsey, 2010; Reimer and others, 2009) to model earthquake timing at the Dutchman Draw site, Arizona.*

Sample Number	Trench	AMS ^{14}C Age[1] RCYBP	OSL Age (ka)	Calibrated Age[2,3] ± Two Sigma (cal yr B.P.)	Median[4] (cal yr B.P.)	Mode[5] (cal yr B.P.)
NT-RC1	North	5720 ± 150	--	6540 ± 340	6530	6490
NT-RC2	North	1480 ± 70	--	1390 ± 140	1380	1360
NT-RC3	North	3905 ± 20	--	4350 ± 80	4350	4360
NT-RC4	North	3830 ± 20	--	4220 ± 100	4220	4180
ST-OSL1	South	--	4.22 ± 0.27	4160 ± 540	4160	4160
ST-OSL2	South	--	17.10 ± 1.38	17,040 ± 2760	17,040	17,050
ST-OSL4	South	--	13.80 ± 1.18	13,020 ± 2360	13,020	13,040

[1]*Reported in radiocarbon years before present (RCYBP; present = 1950).*

[2]*Calender years before present; present = 1950.*

[3]*Mean ± two sigma (two standard deviations). Reported ages are unmodelled values.*

[4]*Value that separates the higher half of the sample from the lower half.*

[5]*Value that occurs most frequently in the data set, i.e., the peak of the probability density function for the age value.*

Table 4. *Earthquake timing and recurrence (one seismic cycle) at the Dutchman Draw site, Arizona.*

	Mean ± Two Sigma[1]	Median[1,2]	Mode[1,3]	95.4% Probability[1]
P1 Earthquake	1000 ± 600	1100	1300	1500 – 400
P2 Earthquake	7700 ± 2400	7300	6700	10,200 – 6200
P2 – P1 Interval	6600 ± 2400	6300	7800	9300 – 4900

[1]*All values in table reported as cal yr BP (present = 1950).*

[2]*Value that separates the higher half of the sample from the lower half.*

[3]*Value that occurs most frequently in the data set, i.e., the peak of the probability density function.*

between the P2 and P1 earthquakes is 6.6 ± 2.4 kyr (table 4), and the elapsed time since P1 is 1.0 ± 0.6 ka, indicating that the Fort Pearce section at the Dutchman Draw site may be early in its current seismic cycle. However, we do not know whether the P2–P1 recurrence interval approximates the average long-term recurrence of surface-faulting on the Fort Pearce section, or if it represents an outlier, a recurrence interval that is significantly longer or shorter than the long-term average recurrence. Therefore, while the single recurrence interval and MRE elapsed time at the Dutchman Draw site represent significant new paleoseismic information for the Fort Pearce section, caution is advised when using those data to extrapolate the long-term behavior of the section.

As a matter for speculation, stratigraphic relations in the South trench are permissive of at least one latest Pleistocene surface-faulting earthquake (see Number of Earthquakes section above). If a single older surface-faulting earthquake (P3) did occur sometime between 17.10 ± 1.38 ka and 13.80 ± 1.18 ka (see Earthquake Timing section above), and the P2 earthquake occurred at 7.7 ± 2.4 ka, the resulting P3–P2 recurrence interval would range from about 2.5 (12.6 ka–10.1 ka) to 13.2 kyr (18.5 ka–5.3 ka), with a median value of about 7.9 kyr (all values rounded to the nearest hundred years). By way of comparison, the P2–P1 mean recurrence of 6.6 kyr is 1.3 kyr from the P3–P1 possible mean recurrence of 7.9 kyr, or nearly within the P2–P1 one-sigma range (± 1.2 kyr), thus suggesting that the P2–P1 recurrence interval may be generally representative of the average surface-faulting recurrence on the Fort Pearce section during latest Pleistocene–Holocene time. Again, evidence for a P3 surface-faulting earthquake is not conclusive, and the length of a possible P3–P2 recurrence interval remains speculative.

Vertical Displacement

Scarp Profiles

We measured three profiles across the Dutchman Draw fault scarp (figures 2 and 4) using a survey-grade GPS (Trimble R8 GNSS) instrument. Profile 1 crossed the southern, bifurcated end of the scarp (figure 4) and immediately encountered uneven gullied terrain on the footwall alluvial-fan surface, which made projecting the surface slope back to the fault zone speculative. For that reason, profile 1 was not suitable for vertical offset analysis.

Profile 2 (figure 5) was the longest profile, extending 280 m from west of any anticipated antithetic faulting on the fault hanging wall, through the future location of the North trench, and as far east on the footwall alluvial-fan surface as possible before encountering gullied terrain. At profile 2, the scarp height was 3.7 m and the vertical surface offset (minimum net vertical slip) was 2.8 m (figure 5). The scarp-height and surface-offset measurements obtained from profile 2 are minimum values because material eroded from the scarp has buried the original alluvial-fan surface on the hanging wall to an unknown depth.

The profile 3 scarp is cored by bedrock (figure 4). The scarp height is 4.5 m and the vertical surface offset is 3.9 m (figure 6), both significantly larger than values obtained from profile 2 where the scarp is formed in alluvium. This variation may reflect differences in the way bedrock and alluvial scarps degrade over time, or the bedrock scarp may record more paleoearthquakes (see discussion of possible older surface-faulting earthquakes above). For that reason, we do not consider profile 3 suitable for vertical offset analysis.

Displaced Trench Stratigraphy

When geologic units in a trench are well exposed on both sides of a fault, it is possible to determine net vertical slip across the fault by projecting the same unit contact from the footwall and hanging wall to the main fault and measuring the vertical distance (displacement) between them. In addition, units that are exposed in the footwall but are not found in the hanging wall due to burial beneath the maximum feasible excavation depth provide evidence of minimum vertical displacement. Measurement reliability is improved when (1) the unit contact is relatively smooth and dips (slopes) at the same angle on both sides of the fault, (2) the portions of the contact selected for projection are outside any zone of tilting or deformation associated with faulting, and (3) a sufficient length of contact is exposed on both sides of the fault to ensure that the projections can be aligned to accurately reflect the continua-

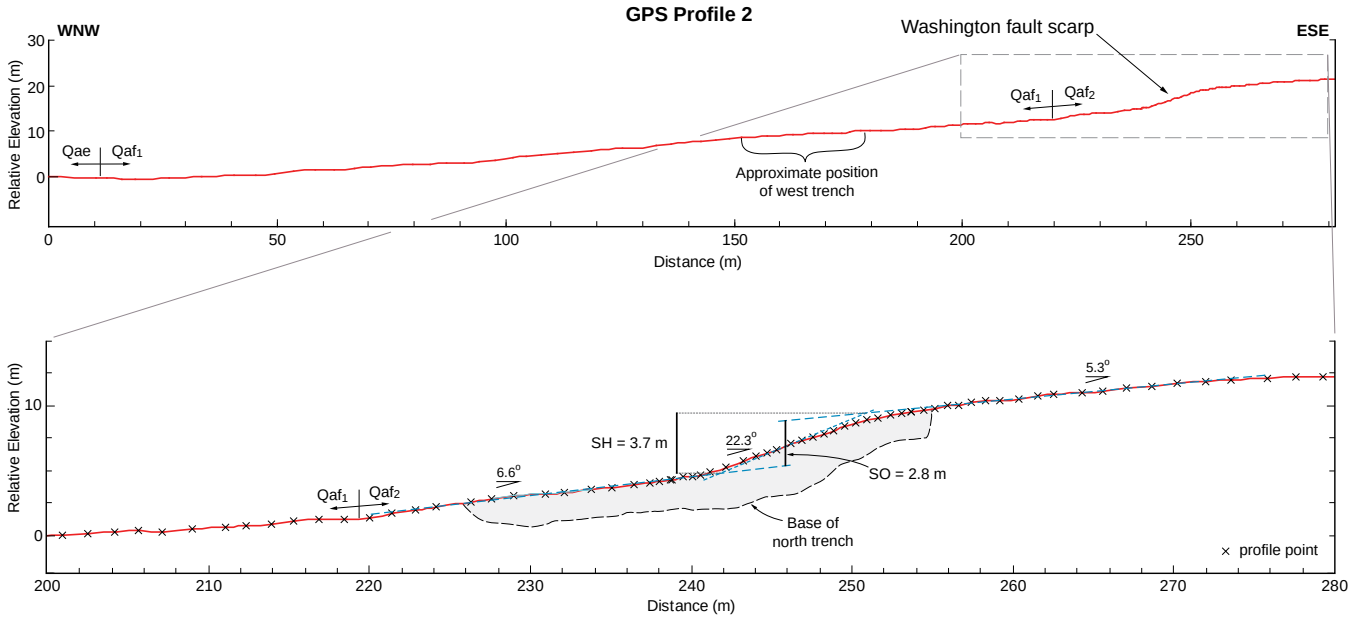

Figure 5. *Dutchman Draw trench site scarp profile #2; profile measured summer 2009. See figure 2 for explanation of geologic units. View to the north. SH = scarp height, SO = surface offset. See figure 4 for profile location.*

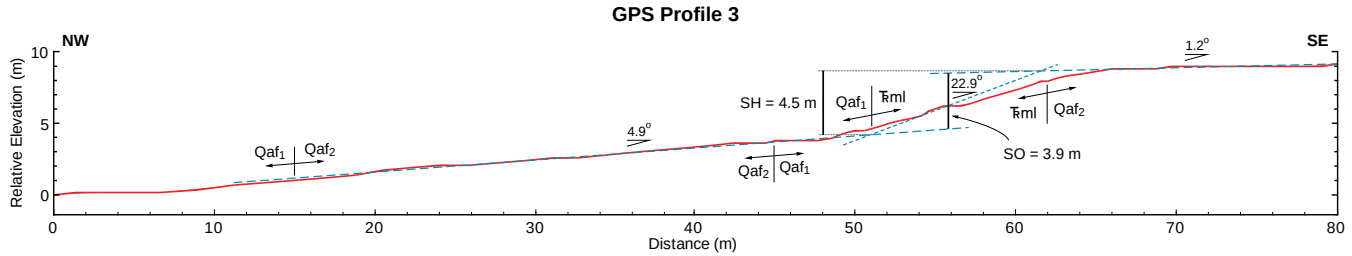

Figure 6. *Dutchman Draw trench site scarp profile #3; profile measured summer 2009. See figure 2 for explanation of geologic units. View to the north. SH = scarp height, SO = surface offset. See figure 4 for profile location.*

tion of the contact to the fault zone. All three of these conditions are problematic in the Dutchman Draw trenches.

The North trench (plate 1) did not expose any geologic units common to both the footwall and hanging wall; therefore, trench stratigraphy could not be used to estimate net vertical slip across the fault. The fact that the surface on late Pleistocene alluvial-fan deposits of unit 8 appears to be fairly well preserved in the east end of the trench, and the equivalent fan surface is buried west of the fault, implies ≥ 4 m of vertical displacement since unit 8 was deposited. In the South trench, units 2 and 5 are present on both sides of the fault; however, (1) both units have been affected by post-faulting erosion making their contacts undulatory and irregular, (2) exposures of both units on the footwall east of fault SF2 (and therefore outside the fault displacement zone) are limited (plate 1), and (3) the slopes of the upper contacts (paleosurfaces) on either side of the main fault are different, indicating that in addition to being affected by erosion, the units also may be affected by fault-related deformation. Given these caveats, we consider the measurements of net vertical slip based on displaced stratigraphy in the South trench to be "rough estimates" only and not precise measurements of net vertical displacement.

Unit 5 has been displaced by both the P1 and P2 earthquakes. Projecting the unit 5 upper contact to the main fault from (1) east of fault SF2 on the footwall, and (2) west of the small reverse faults (SF3) in the hanging wall resulted in a "best estimate" vertical net slip of about 2.3 m for two earthquakes. Projections of the unit 5 lower contact from the hanging wall and footwall to the main fault zone were at such widely divergent angles that a reliable estimate of net slip could not be made. Unit 2 has been displaced by only the P1 earthquake. Projecting the unit 2 lower contact from the footwall and hanging wall to the fault zone resulted in a net vertical displacement "best estimate" for the P1 earthquake of about 1 m. The upper contact of unit 2 is too irregular to provide a reliable displacement measurement.

Colluvial-Wedge Thickness

Ostenna (1984) stated that ". . . for large displacements, the thicknesses of the colluvial wedge preserved should approach half the initial free face height." Numerous factors can affect the height of a surface-faulting scarp free face, but in general, in the absence of antithetic faulting or significant back-rotation or drag along the fault, free face height can be

used as a rough proxy for fault slip during a surface-faulting earthquake (McCalpin, 2009). The logs for the North and South trenches (plate 1) show that the P1 and P2 colluvial wedges are not the same size. In both trenches, the P2 wedge is both thicker and longer in cross section than the P1 wedge. The P2 wedge in the North trench has been somewhat affected by erosion and is much affected by erosion in the South trench. The maximum thickness of the P2 colluvial wedge in the North trench is 1.2 m, which implies an initial free face height of about 2.4 m. The P2 wedge in the South trench is too modified by erosion to provide a good measurement of wedge thickness. The P1 wedge in the North trench is 0.5 m thick, and in the South trench is 0.6 m thick, implying an initial free-face height of 1.0 to 1.2 m. The colluvial-wedge thicknesses in the trenches show that the P2 earthquake produced approximately twice as much slip as the P1 earthquake. However, we consider both measurements poorly constrained and to represent only approximate values of net vertical slip for the P1 and P2 earthquakes.

Vertical Slip Rate

Slip rate provides a measure of fault activity; generally, the higher the slip rate, the more active the fault. Slip rates may be calculated horizontally (typical for strike-slip faults), vertically (typical for normal-slip faults), or in a down-dip direction (net slip) when the fault's dip at depth is known. A vertical slip rate measures how fast two sides of a fault are slipping vertically relative to one another, and is commonly determined from vertically offset features whose ages are known. A vertical slip rate for a closed seismic cycle is calculated by dividing per event net vertical displacement by the time length of the previous recurrence interval. It is generally preferable to calculate slip rates for multiple "closed" seismic cycles to better estimate the average slip behavior of the fault.

The new paleoseismic information obtained at the Dutchman Draw site defines just one closed seismic cycle (P2–P1 mean recurrence interval = 6.6 ± 2.4 kyr) on the main strand of the Fort Pearce section. The "best estimate" vertical displacement resulting from the P1 earthquake determined from the South trench is 1.0–1.2 m; therefore, the vertical slip rate for the most recent closed seismic cycle is:

$$1000 \text{ to } 1200 \text{ mm} 6600 \pm 2400 \text{ yr} = \textit{0.11–0.29} \text{ mm/yr}$$

As stated above, where sufficient data are available, it is preferable to calculate an average slip rate that incorporates multiple closed seismic cycles and cumulative net vertical slip to provide a more stable measure of long-term fault activity. Since that is not possible at the Dutchman Draw site, caution is advised when using the single closed-seismic-cycle vertical slip rate reported here to extrapolate the long-term behavior of the Fort Pearce section. Also note that this slip rate is applicable only to the main strand of the Fort Pearce section and does not include slip that may have occurred during synchronous rupture on the Mokaac or Dutchman Draw stands.

Paleoearthquake Magnitude Estimates

Paleomagnitude Scaling Relations

Paleoearthquake magnitude estimates are typically based on magnitude scaling relations that variously incorporate surface rupture length (SRL), average displacement (AD), maximum displacement (MD), fault rupture area (RA), slip rate (SR), or seismic moment (M_0). The proper relations for calculating paleoearthquake magnitudes within a particular tectonic regime has been and continues to be a topic of active research and discussion (e.g., see Lund [2012] and Stirling and Goded [2012]). The Working Group on Utah Earthquake Probabilities (WGUEP) (Wong and others, 2011, 2012), which at the time of this report is conducting an ongoing project to develop time-independent and time-dependent earthquake forecasts for the Wasatch Front region (see http://geology.utah.gov/ghp/workgroups/wguep.htm), has performed a rigorous analysis of magnitude scaling relations to determine which of the many available relations are most appropriate for their study region (which includes parts of the Basin and Range and Middle Rocky Mountains physiographic provinces).

The WGUEP grouped the faults in their study region into category A, B, and C faults based on the quantity/reliability of displacement data and whether or not the fault is segmented (WGUEP, written communication, 2015). Based on the WGUEP criteria, the Fort Pearce section of the Washington fault zone is a category B fault (segmented with limited per event displacement data). The paleomagnitude scaling relations recommended by the WGUEP to best characterize epistemic uncertainty in magnitude for category B faults in their study region are:

- Hanks and Kanamori (1979) – Moment magnitude (**M**) for all fault types
- Wells and Coppersmith (1994) – SRL all fault types
- Stirling and others (2002) – Censored instrumental SRL, all fault types
- Wesnousky (2008) – SRL all fault types

Although the WGUEP study is still a work in progress, based on their careful evaluation of available scaling relations and the similarity of our study area to theirs, we adopt the current WGUEP fault category B regressions for this investigation.

Regression Parameters

For this study, we use two SRL values (straight line tip-to-tip length) representing three possible rupture scenarios on the Fort Pearce section. The three rupture scenarios are:

- Fort Pearce section end to end. Includes any synchronous rupture on the sub-parallel Mokaac and Dutch-

man Draw strands, which are presumed to merge with the main strand at seismogenic depth. Length 37 km.

- Northern tip of the Fort Pearce section to the southern tip of the Mokaac strand. Length 37 km.

- Southern tip of the Fort Pearce section to the northern tip of the Dutchman Draw strand. Length 25 km.

Although not discussed further here because we consider the possibility unlikely for geomorphic and geometric reasons, a fourth rupture scenario that includes the combined Mokaac and Dutchman Draw sections (each 16 km long) and the intervening portion of the Fort Pearce section main strand (6 km) would be 38 km long. Paleomagnitude estimates for this scenario would be similar (slightly larger) than those obtained for the 37-km-long rupture scenarios described above.

The WGUEP (written communication, 2015) uses a range of fault dips (50 ± 15 degrees) and seismogenic depths (15 ± 3 km) to estimate uncertainty in fault parameters in their study region; we adopt the WGUEP values for this study. Because considerable variation exists in the vertical slip estimates between the P1 (1–1.2 m) and P2 (2.4 m) earthquakes at the Dutchman Draw site, for purposes of estimating paleoearthquake magnitudes, we use a range of vertical slip at the Dutchman Draw site of 1–2.4 m, and consider this range of displacements to approximate AD for each event.

Paleomagnitude Estimates

Hanks and Kanamori (1979) – seismic moment for all fault types: The Hanks and Kanamori (1979) regression relates M_o to **M** as follows:

$$M_o = \mu \text{ x} L \text{x} W \text{x} D$$

where

M_o = seismic moment

μ = shear modulus (3.00^{11} dynes/cm^2)

L = SRL (km)

W = down-dip width of fault (km)

D = net (down dip) displacement (m)

and

$$\mathbf{M} = 2/3 \log M_o - 10.7$$

Using the fault parameters above, the Hanks and Kanamori (1979) regression provides estimates of **M** (rounded to the nearest 0.1 magnitude unit) that range from 6.8 to 7.4.

Wells and Coppersmith (1994) – SRL all fault types: Regressions developed by Wells and Coppersmith (1994) for a variety of fault parameters (SRL, AD, MD, RA) from a worldwide earthquake data set, have long been considered industry standards. However, the earthquake dataset used for these regressions is now out of date, and magnitudes tend to be systematically lower than those estimated from more modern regressions (Stirling and Goded, 2012; WGUEP, written communication, 2015). The WGUEP included the Wells and Coppersmith (1994) SRL all fault types regression in its study to estimate the lower bound of earthquake magnitudes possible within its study region.

The Wells and Coppersmith (1994) SRL all fault types regression is:

$$M_w = 5.08 + (1.16 \text{ x } \log \text{SRL})$$

Using SRLs of 25 and 37 km, the Wells and Coppersmith (1994) regression provides estimates of M_w (rounded to the nearest 0.1 magnitude unit) that range from 6.7 to 6.9.

Stirling and others (2002) – censored instrumental SRL relation: Stirling and others (2002) developed their censored instrumental SRL relation to compare pre-instrumental (pre-1900) and prehistoric earthquake magnitudes with those for instrumental surface-faulting earthquakes to understand why the Wells and Coppersmith (1994) regressions systematically underestimate the magnitudes of many large-magnitude earthquakes (Stirling and Goded, 2012). Stirling and others (2002) expanded and updated the all-fault-type Wells and Coppersmith (1994) earthquake dataset, and systematically removed (censored) small SRL events from the dataset. The results were significantly larger magnitudes than those obtained from the Wells and Coppersmith (1994) regressions (Stirling and Goded, 2012).

The Stirling and others (2002) censored instrumental SRL relation is:

$$M_w = 5.88 + (0.8 \text{ x } \log \text{SRL})$$

Using SRLs of 25 and 37 km, the Stirling and others (2002) regression provides estimates of M_w (rounded to the nearest 0.1 magnitude unit) that range from 7.0 to 7.1.

Wesnousky (2008) – SRL all fault types: Wesnousky (2008) developed a SRL all-fault-type regression using a dataset of 37 worldwide, surface-rupturing, continental earthquakes with rupture lengths greater than 15 km and for which there were both maps and measurements of coseismic displacement along the strike of the rupture.

The Wesnousky (2008) SRL all-fault-type relation is:

$$M_w = 5.30 + (1.02 \text{ x } \log \text{SRL})$$

Using SRLs of 25 and 37 km, the Wesnousky's (2008) regression provides estimates of M_w (rounded to the nearest 0.1 magnitude unit) that range from 6.7 to 6.9.

Summary

Using the multiple paleomagnitude regressions recommended by the WGUEP to determine earthquake magnitudes for various rupture scenarios of the Fort Pearce section of the Washington fault zone resulted in earthquake magnitude estimates ranging from M_w 6.7 to 7.4, depending on the regression used and the rupture parameters selected. Available paleoseismic data are not sufficient to fully characterize all the possible rupture scenarios for the Fort Pearce section; however, it is clear from the limited analysis above, that the Fort Pearce section is capable of generating $M_w \geq 7$ earthquakes in the future.

SUMMARY AND CONCLUSIONS

Trenching at the Dutchman Draw site provides the following new paleoseismic information for the Fort Pearce section of the Washington fault zone:

1. The Fort Pearce section has experienced at least two Holocene surface-faulting earthquakes, one in the early to middle Holocene at about 7.7 ± 2.4 ka (P2) and the other in the late Holocene at about 1.0 ± 0.6 ka (P1).

2. The resulting single, closed-seismic-cycle recurrence interval (P2–P1 earthquakes) is 6.6 ± 2.4 kyr. It is unknown if this recurrence interval approximates the long-term average recurrence of large surface-faulting earthquakes on the Fort Pearce section. This recurrence interval represents only the most recent closed seismic cycle, and should be treated with caution if used to extrapolate the long-term behavior of the Fort Pearce section.

3. There is indirect stratigraphic evidence in the trenches permissive of at least one latest Pleistocene earthquake that may have occurred between about 14 and 17 ka; however, any resulting tectonic colluvial-wedge deposits have either been removed by erosion or faulted below the bottom of the trenches.

4. If a single P3 surface-faulting earthquake did occur between 13.8 ± 1.2 and 17.1 ± 1.4 ka, and the P2 earthquake occurred at 7.7 ± 2.4 ka, the length of the resulting P3–P2 recurrence interval would range from about 2.5 to 13.2 kyr, with a median value of about 7.9 kyr. The P2–P1 recurrence interval is 6.6 ± 2.4 kyr, placing it within one-sigma (1.2 kyr) of the possible P3–P2 median value of 7.9 kyr, thus suggesting that the P2–P1 recurrence interval may be representative of the average surface-faulting recurrence on the Fort Pearce section during latest Pleistocene-Holocene time.

5. Net vertical displacement estimates at the Dutchman Draw site range from about 1.0 m (P1) to 2.4 m (P2). The late Pleistocene alluvial-fan surface formed on unit 8 is displaced ≥ 4 m by at least three surface-faulting earthquakes. We obtained these estimates from a combination of scarp profiles, displaced trench stratigraphy, scarp free-face heights extrapolated from colluvial-wedge thicknesses, and the fact that geologic units exposed in the fault footwall are displaced below the bottom of the trench in the fault hanging wall. There are significant caveats associated with all these methods and we consider these displacement values poorly constrained estimates.

6. The vertical slip rate for the P2–P1 recurrence interval (6.6 ± 2.4 kyr) and a P1 net vertical displacement (1.0–1.2 m) is 0.11–0.29 mm/yr. This slip-rate range is representative of only the most recent closed seismic cycle on the main strand of the Fort Pearce section at the Dutchman Draw site, and should be treated with caution if used to extrapolate the long-term behavior of this part of the Washington fault zone.

7. Multiple magnitude scaling relations provide paleomagnitude estimates at the Dutchman Draw site ranging from M_w 6.7 to 7.4, depending on the regression and rupture parameters selected. The scaling relations demonstrate that the Fort Pearce section of the Washington fault zone is likely capable of producing future **M** ≥ 7 earthquakes.

In conclusion, the Fort Pearce section of the Washington fault zone has generated multiple (minimum of two), large (M_w 6.7 to 7.4) surface-faulting earthquakes during the Holocene Epoch. Therefore, the Fort Pearce section is an active, hazardous fault that represents significant seismic hazard (both ground rupture and strong ground shaking) in southwestern Utah's rapidly developing St. George basin (metropolitan area). The Washington fault zone is a complex fault in a complex geologic setting; current paleoseismic data for the fault represents the minimum information necessary to evaluate seismic hazard, to better define the hazard represented by the Washington fault zone, we recommend additional detailed paleoseismic investigations be performed on both the Fort Pearce section and other sections of the fault zone.

ACKNOWLEDGMENTS

We thank Phil Pearthree and Jeri Young, Arizona Geological Survey, and Tony Crone, U.S. Geological Survey, for their visits to the Dutchman Draw trench site and insightful comments on the geology exposed in the trenches. We thank Phil Pearthree, Arizona Geological Survey, and Steve Bowman, Utah Geological Survey, for their careful reviews of the report manuscript and trench logs. We thank Rosenberg Associates for funding the ^{14}C ages obtained for the Dutchman

Draw North trench. We also thank Professor Gerald Schuster, formerly of the University of Utah Department of Geology and Geophysics, and his graduate student Shengdong Liu for performing the 3-D tomographic seismic profiling of the fault scarp at the Dutchman Draw site.

REFERENCES

Birkeland, P.W., Machette, M.N., and Haller, K.M., 1991, Soils as a tool for applied Quaternary research: Utah Geological and Mineral Survey Miscellaneous Publication 91-3, 63 p.

Bronk Ramsey, C., 2008, Depositional models for chronological records: Quaternary Science Reviews, v. 27, no. 1-2, p. 42–60.

Bronk Ramsey, C., 2009, Bayesian analysis of radiocarbon dates: Radiocarbon, v. 51, no. 1, p. 337–360.

Bronk Ramsey, C., 2010, OxCal Program, v. 4.1.7: Radiocarbon Accelerator Unit, University of Oxford, UK; Online, https://c14.arch.ox.ac.uk/oxcal.html.

Gray, H.J., Mahan, S.A., Rittenour, T., and Nelson, M.S., 2015, Guide to luminescence dating techniques and their application for paleoseismic research, *in* Lund, W.R., editor, Proceedings Volume Basin and Range Province Seismic Hazard Summit III: Utah Geological Survey Miscellaneous Publication 15-5, CD.

Hanks, T.C., and Kanamori, H, 1979, A moment magnitude scale: Journal of Geophysical Research, v. 84, no. B5, p. 2348–2350.

Lund, W.R., editor, 2012, Basin and Range Province Earthquake Working Group II—Recommendations to the U.S. Geological Survey National Seismic Hazard Mapping Program for the 2014 update of the National Seismic Hazard Maps: Utah Geological Survey Open-File Report 591, 17 p.

McCalpin, J.P., 2009, Chapter 3—Paleoseismology in extensional tectonic environments, in McCalpin, J.P., editor, Paleoseismology (2nd edition): Burlington, Massachusetts, Academic Press (Elsevier), p. 171–269.

Menges, C.M., and Pearthree, P.A., 1983, Map of neotectonic (latest Pliocene-Quaternary) deformation in Arizona: Arizona Geological Survey Open-File Report 83-22, 48 p., 4 plates, scale 1:500,000.

Ostenaa, D., 1984, Relationships affecting estimates of surface fault displacement based on scarp-derived colluvial deposits [abs.]: Geological Society of America, Abstracts with Programs, v. 16, no. 5, p. 327.

Pearthree, P.A., compiler, 1998, Quaternary fault data and map for Arizona: Arizona Geological Survey Open-File Report 98-24, 122 p., 1 plate in pocket, scale 1:750,000.

Reimer, P.J., Baillie, M.G.L., Bard, E., Bayliss, A., Beck, J.W., Blackwell, P.G., Bronk Ramsey, C., Buck, C.E., Burr, G.S., Edwards, R.L., Friedrich, M., Grootes, P.M., Guilderson, T.P., Hajdas, I., Heaton, T.J., Hogg, A.G., Hughen, K.A., Kaiser, K.F., Kromer, B., McCormac, F.G., Manning, S.W., Reimer, R.W., Richards, D.A., Southon, J.R., Talamo, S., Turney, C.S.M., van der Plicht, J., and Weyhenmeyer, C.E., 2009, IntCal09 and Marine09 radiocarbon age calibration curves, 0-50,000 years cal BP: Radiocarbon, v. 51, no. 4, p. 1111–1150.

Stirling, M.W., and Goded, T., 2012, Magnitude scaling relationships, GEM Faulted Earth and Regionalization Global Components: GNS Science Miscellaneous Series 42, 40 p., online, http://www.nexus.globalquakemodel.org.

Stirling, M., Rhoades, D., and Berryman, K., 2002, Comparison of earthquake scaling relations derived from data of the instrumental and preinstrumental era: Bulletin of the Seismological Society of America, v. 92, no. 2, p. 812–830.

Wells, D.L., and Coppersmith, K.J., 1994, New empirical relationships among magnitude, rupture length, rupture width, rupture area, and surface displacement: Bulletin of the Seismological Society of America, v. 84, no. 4, p. 974–1002.

Wesnousky, S.G., 2008, Displacement and geometrical characteristics of earthquake surface ruptures—issues and implications for seismic-hazard analysis and the process of earthquake rupture: Bulletin of the Seismological Society of America, v. 98, no. 4, p. 1609–1632.

Wong, I., Lund, W., DuRoss, C., Arabasz, W., Pechmann, J., Crone, A., Luco, N., Personius, S., Petersen, M., Olig, S., and Schwartz, D., 2011, The Working Group on Utah Earthquake Probabilities (WGUEP)—background and goals [abs.]: Seismological Research Letters, v. 82, no. 2, p. 345–346.

Wong, I., Lund, W., DuRoss, C., Thomas, P., Arabasz, W., Crone, A., Hylland, M., Luco, N., Olig, S., Pechmann, J., Personius, S., Petersen, M., Schwartz, D., and Smith, R., 2012, Forecasting large earthquakes along the Wasatch Front, Utah [abs]: AEG News, 2012 Annual Meeting Program with Abstracts, v. 55, p. 85.

APPENDICES

APPENDIX A
DUTCHMAN DRAW SITE TRENCH GEOLOGIC UNIT DESCRIPTIONS

Unit	Genesis	Color[1]		Texture[2] (wt. percent)			Max. Clast (cm)	Density/ Consistency[3]	Clast/Matrix Supported[4]	Cementation			Lower Boundary	Soil Development Thickness (cm)	North Trench		South Trench	
		Dry	Moist	Fines	Sand	Gravel				Strength	Type	Morphology[5]			Footwall	Hanging Wall	Footwall	Hanging Wall
1_a	P1 colluvium	7.5YR6/4	7.5YR4/6	30	50	20	20	loose	–	none	–	I	clear	weak A horizon, <10 cm	–	x	–	x
1_b	P1 crack fill	7.5YR6/4	7.5YR4/6	30	50	20	10	loose	–	none	–	?	abrupt	none	–	x	–	x
2	debris flow	7.5YR6/4	7.5YR4/6	20	35	45	15	loose	matrix	weak	carbonate	I+	clear/gradual	weak A horizon, 10-15 cm	–	x	x	x
3	debris flow	7.5YR6/4	7.5YR4/4	15	25	60	20	loose	variable	weak	carbonate	I+	clear	none	–	x	–	–
4_a	P2 colluvium	7.5YR7/3	7.5YR5/4	20	25	55	20	loose	clast	weak	carbonate	I+	clear	none	–	x	–	x
4_b	P2 crack fill	7.5YR7/3	7.5YR5/4	30	30	40	10	loose	matrix	weak	carbonate	?	abrupt	none	–	x	–	x
5	debris flow	7.5YR6/4	7.5YR5/6	20	50	30	15	loose/medium	matrix	weak	carbonate	I+	abrupt	none	–	x	x	x
6	debris flow	7.5YR7/4	7.5YR5/6	20	50/30	30/50	20	medium	variable	moderate	gypsum	II-	clear	none	–	–	–	x
7	debris flow	7.5YR8/4	7.5YR6/6	50	35	15	10	hard	na	strong	gypsum	II+	not exposed	none	–	–	–	x
8	old alluvial fan undifferentiated	7.5YR7/4	7.5YR5/6	20	30	50	15	dense	variable	strong	gypsum	II+	not exposed	none	–	–	–	x
8_a	old alluvial fan	5YR7/4	5YR6/6	20	30	50	20	dense	variable	strong	gypsum	II+	clear	none	–	–	x	–
8_b	old alluvial fan	5YR7/4	5YR6/6	25	60	15	5	dense	–	strong	gypsum	II+	abrupt	none	–	–	x	–
8_c	old alluvial-fan	5YR5/6	5YR4/6	25	50	25	35	dense	–	strong	gypsum	II+	abrupt	none	–	–	x	–
8_d	old alluvial-fan	5YR5/6	5YR4/6	30	60	10	35	dense	–	strong	gypsum	II+	not exposed	none	–	–	x	–
9	Moenkopi Fm.	10R3/4	10R3/4	–	–	–	–	–	–	–	–	–	not exposed	none	x	–	–	–

[1]Munsell Soil Color Chart year 2000 revised edition.

[2]Textural information may not be representative of entire unit due to vertical and horizontal lithological heterogeneity. Clast sizes: fines (silt and clay), <0.074mm (#200 sieve); sand, >0.074 mm <4.76 mm (# 4 sieve); gravel, 4.76 mm-76 mm; cobbles, 76 mm-305 mm; boulders >305 mm. Weight percentage reported for clast-size fractions are field estimates.

[3]Density terms (very loose–very dense) describe coarse-grained units (>50% retained on the #200 sieve) and consistency terms (very soft–very hard) describe fine-grained units (< 50% retained on the #200 sieve).

[4]Visual estimate for units with ≥ 30% gravel content.

[5]Cement morphology stages follow table A-6 in UGS Miscellaneous Publication 91-3 (Birkeland and others, 1991).

APPENDIX B

EXAMINATION OF BULK SOIL AND AMS RADIOCARBON ANALYSIS OF CARBON FROM THE DUTCHMAN DRAW TRENCHES, WASHINGTON FAULT ZONE, ARIZONA

(Analyses performed by PaleoResearch Institute, Golden, Colorado)

EXAMINATION OF BULK SOIL AND AMS RADIOCARBON ANALYSIS OF MATERIAL FROM THE DUTCHMAN DRAW TRENCH SITE ON THE WASHINGTON FAULT, ARIZONA

By

Kathryn Puseman

With Assistance from
R. A. Varney

PaleoResearch Institute
Golden, Colorado

PaleoResearch Institute Technical Report 09-61

Prepared For

Utah Geological Survey (Microcharcoal Recovery)
Salt Lake City, Utah

and

Rosenberg Associates (AMS Radiocarbon Dating)
St. George, Utah

November 2009

INTRODUCTION

A total of four bulk soil samples from the Dutchman Draw Trench site on the Washington Fault in northwest Arizona were examined to recover organic fragments suitable for radiocarbon analysis. These samples were recovered from soil stringers in the PE wedge, as well as from paleosol beneath the Most Recent Event (MRE) wedge in the North paleoseismic trench. Botanic components and detrital charcoal were identified, and potentially radiocarbon datable material was separated. Two of the samples did not yield sufficient macroscopic charcoal for dating; therefore, they were processed to recover microscopic charcoal to obtain a radiocarbon date.

METHODS

Flotation and Charcoal Identification

After removing calcium carbonates with hydrochloric acid (10%), the samples were screened through a 250 micron mesh sieve. The material remaining in the screen was retained for macroscopic examination, while the material that passed through the screen was saved for possible microscopic charcoal extraction. The dried screen contents were examined under a binocular microscope at a magnification of 10x. Charcoal fragments were separated from the water-screened sample matrix, broken to expose a fresh cross-section, and examined under a binocular microscope at a magnification of 70x.

Macrofloral remains, including charcoal, were identified using manuals (Core, et al. 1976; Martin and Barkley 1961; Panshin and Zeeuw 1980; Petrides and Petrides 1992) and by comparison with modern and archaeological references. Because charcoal and possibly other botanic remains were to be submitted for radiocarbon dating, clean laboratory conditions were used during flotation and identification to avoid contamination. All instruments were washed between samples, and samples were protected from contact with modern charcoal.

Microcharcoal Extraction

The next step is to recover microscopic charcoal from sediments for the purpose of obtaining an AMS radiocarbon age. Microscopic charcoal fragments are far superior to humates because they provide dates with the same precision as those obtained from larger pieces of charcoal, with the single exception that the individual pieces of microscopic charcoal are not identified to taxon. A chemical extraction technique based on that used for pollen, and relying upon heavy liquid extraction, has been modified to recover microscopic charcoal for the purpose of obtaining an AMS radiocarbon age. Two of the samples did not yield sufficient macroscopic charcoal for radiocarbon dating; therefore, the fraction of the sample that passed through the 250 micron mesh sieve during initial screening was further processed to obtain microscopic charcoal.

The samples were rinsed until neutral, then a small quantity of sodium hexametaphosphate was added to each sample, which was then filled with reverse osmosis, deionized (RODI) water and allowed to settle according to Stoke's Law. After two hours the

supernatant, containing clay, was poured off and the samples were rinsed with RODI water three more times, being allowed to settle according to Stoke's Law to remove more clays. Once the clays had been removed, the samples were freeze dried. Sodium polytungstate (SPT), with a density of 1.8, was used for the flotation process. The samples were mixed with SPT and centrifuged at 1500 rpm for 10 minutes to separate organic from inorganic remains. The supernatant containing pollen, organic remains, and microscopic charcoal was decanted. Sodium polytungstate again was added to the inorganic fraction to repeat the separation process until all visible charcoal had been recovered. The charcoal was recovered from the sodium polytungstate and rinsed thoroughly with RODI water. At this stage, the microcharcoal samples joined the macroscopic charcoal samples for chemistry pre-treatment.

AMS Radiocarbon Dating

Wood and charcoal samples submitted for radiocarbon dating are identified and weighed prior to selecting subsamples for pre-treatment. The remainder of each subsample that proceeds to pre-treatment, if there is any, is permanently curated at PaleoResearch. The subsample selected for pre-treatment is first subjected to hot (at least 110°C), 6N hydrochloric acid (HCl), with rinses to neutral between each HCl treatment, until the supernatant is clear. This removes iron compounds and calcium carbonates that would hamper removal of humate compounds later. Next the samples are subjected to 5% potassium hydroxide (KOH) to remove humates. Once again, the samples are rinsed to neutral and re-acidified with pH 2 HCl between each KOH step. This step is repeated until the supernatant is clear, signaling removal of all humates. After humate removal, each sample is made slightly acidic and left that way for the next step. Charcoal samples (but not wood samples) are subjected to a concentrated, hot nitric acid bath, which removes all modern and recent organics. This treatment is not used on unburned or partially burned wood samples because it oxidizes the submitted sample of unknown age.

Each submitted sample is then freeze-dried using a vacuum system, freezing out all moisture at -98°C. Each individual sample is combined with cupric oxide (CuO) and elemental silver (Ag^o) in a quartz tube, then flame sealed under vacuum.

Standards and laboratory background samples also are treated in the same manner as the wood and charcoal samples of unknown age. A radiocarbon “dead” EUA wood blank from Alaska that is more than 70,000 years old (currently beyond the detection capabilities of AMS) is treated using the same chemical processing as the samples of unknown age in order to calibrate the laboratory correction factor. Standards of known age, such as Two Creeks wood that dates to 11,400 RCYBP and others from the Third International Radiocarbon Intercomparison (TIRI), are also processed simultaneously to establish the laboratory correction factor. Each wood standard is run in a quantity similar to the submitted samples of unknown age and sealed in a quartz tube after the requisite pre-treatment.

Once all the wood standards, blanks, and submitted samples of unknown age are prepared and sealed in their individual quartz tubes, they are combusted at 820°C, soaked for an extended period of time at that temperature, and then slowly allowed to cool to enable the chemical reaction that extracts carbon dioxide ($C0_2$) gas.

Following this last step, all samples of unknown age, the wood standards, and the laboratory backgrounds are sent to the Keck Carbon Cycle AMS Facility at the University of California, Irvine, where the $C0_2$ gas is processed into graphite. The graphite in these samples

is then placed in the target and run through the accelerator, which produces the numbers that are converted into the radiocarbon date presented in the data section. Dates are presented as conventional radiocarbon ages, as well as calibrated ages using Intcalc04 curves on Oxcal version 3.10.

RADIOCARBON REVIEW

When interpreting radiocarbon dates from non-annuals such as trees and shrubs, it is important to understand that the radiocarbon date reflects the age of that portion of the tree/shrub when it stopped exchanging carbon with the atmosphere, not necessarily the date that the tree/shrub died or was burned. Trees and shrubs grow bigger each year from the cambium, where a new layer or ring of cells is added each year. During photosynthesis new cells take in atmospheric carbon dioxide, which includes radiocarbon. The radiocarbon taken in will reflect the radiocarbon present in the atmosphere during that season of growth. Once the sapwood in a tree has been converted into heartwood, the metabolic process stops for that inner wood. Once this happens, no new carbon atoms are acquired, and the radiocarbon that is present starts to decay. Studies have shown that there is little to no movement of carbon-bearing material from one ring to another. As a result, wood from different parts of the tree will yield different radiocarbon dates. The outer rings exhibit an age close to the cutting or death date of the tree, while the inner rings will reflect the age of the tree. Because the younger, outer rings burn off first when a log or branch is burned, it is the older, inner rings that typically are what is left remaining in a charcoal assemblage (Puseman 2009; Taylor 1987).

DISCUSSION

The Dutchman Draw Trench site is located on the Washington Fault in northwest Arizona. Samples were collected from three soil stringers in the PE wedge, as well as from paleosol beneath the MRE wedge. Sample NT-RC-1 was taken from the lower soil stringer in the PE wedge (Table 1). This sample yielded small fragments of Salicaceae and unidentified hardwood charcoal weighing a total of 0.0006 g. This charcoal reflects a woody member of the willow family and possibly another type of hardwood (Tables 2 and 3). Recovery of a few charred insect fecal pellets suggests that some of the burned wood contained insects. An AMS radiocarbon date of 5720 ± 150 RCYBP (PRI-09-61-NT-RC1) was returned for the combined charcoal, with a two-sigma calibrated age range of 6900-6200 CAL yr. BP (Table 4, Figure 1). Sample RC1 also yielded a moderate amount of uncharred rootlets from modern plants, a few uncharred bone fragments, and two snail shell fragments.

Sample NT-RC-3 was collected from the middle soil stringer in the PE wedge, while sample NT-RC-2 represents the upper soil stringer. No macroscopic charcoal fragments were present in either of these two samples; therefore, AMS radiocarbon dates were obtained on microscopic charcoal (microcharcoal) recovered from this sample. Sample NT-RC-3 yielded a date of 3905 ± 20 RCYBP (PRI-09-61-NT-RC3) and a two-sigma calibrated age range of 4420-4250 CAL yr. BP (Figure 2). Sample NT-RC-4 from the upper soil stringer yielded a date of 3830 ± 20 RCYBP (PRI-09-61-NT-RC4). This date calibrates to 4360-4330 and 4300-4150 CAL yr. BP at the two-sigma level (Figure 3).

Paleosol from beneath the MRE wedge was collected as sample NT-RC-2. This sample contained 16 fragments of hardwood charcoal too small for identification weighing 0.0009 g. A $\delta^{13}C$ value of -9.9 $^{o}/_{o}$ reported as part of the AMS dating process, suggests that this hardwood charcoal represents a wood with a C4 photosynthetic pathway, such as *Atriplex* (saltbush). The hardwood charcoal returned a date of 1480 ± 70 RCYBP (PRI-09-61-NT-RC2), with a two-sigma calibrated age range of 1530-1280 CAL yr. BP (Figure 4). A moderate amount of uncharred rootlets from modern plants, several insect chitin fragments, and numerous worm casts also were noted.

SUMMARY AND CONCLUSIONS

Examination of bulk samples from the Dutchman Draw trench site resulted in recovery of macroscopic and microscopic charcoal submitted for AMS radiocarbon dating. Pieces of willow family and unidentified hardwood charcoal from the lowest soil stringer in the PE wedge returned a date of 5720 ± 150 BP. Microscopic charcoal extracted from samples NT-RC-3 (middle soil stringer) and NT-RC-4 (upper stringer) yielded dates of 3905 ± 20 BP and 3830 ± 20 BP, respectively. A date of 1480 ± 70 BP was returned for unidentified hardwood charcoal from paleosol beneath the MRE wedge.

TABLE 1
PROVENIENCE DATA FOR SAMPLES FROM THE DUTCHMAN DRAW TRENCH SITE, ARIZONA

Sample No.	Provenience/ Description	Analysis
NT-RC-1	Sediment from lower soil stringer in PE Wedge	Macrofloral AMS ^{14}C Date
NT-RC-3	Sediment from middle soil stringer in PE Wedge	Macrofloral Microcharcoal AMS ^{14}C Date
NT-RC-4	Sediment from upper soil stringer in PE Wedge	Macrofloral Microcharcoal AMS ^{14}C Date
NT-RC-2	Sediment from paleosol beneath MRE wedge in alluvial fan	Macrofloral AMS ^{14}C Date

TABLE 2
MACROFLORAL REMAINS FROM THE DUTCHMAN DRAW TRENCH SITE, ARIZONA

Sample No.	Identification	Part	Charred		Uncharred		Weights/ Comments
			W	F	W	F	
NT-RC-1	Liters Floated						1.00 L
	Light Fraction Weight						0.57 g
	FLORAL REMAINS:						
	Rootlets					X	Moderate
	CHARCOAL/WOOD:						
	Salicaceae and Unidentified hardwood - small**	Charcoal		X			0.0006 g
	NON-FLORAL REMAINS:						
	Bone					X	Few
	Insect fecal pellet		X	X			Few
	Rock/Gravel					X	Few
	Snail shell					2	
NT-RC-3	Liters Floated						0.20 L
	Light Fraction Weight						0.42 g
	FLORAL REMAINS:						
	Rootlets					X	Few
	NON-FLORAL REMAINS:						
	Rock/Gravel					X	Moderate
NT-RC-4	Liters Floated						0.40 L
	Light Fraction Weight						0.30 g
	FLORAL REMAINS:						
	Rootlets					X	Moderate
	NON-FLORAL REMAINS:						
	Rock/Gravel					X	Numerous
NT-RC-2	Liters Floated						1.00 L
	Light Fraction Weight						6.70 g
	FLORAL REMAINS:						
	Rootlets					X	Moderate
	CHARCOAL/WOOD:						
	Unidentified hardwood - small**	Charcoal		16			0.0009 g

Table 2 Continued

Sample No.	Identification	Part	Charred		Uncharred		Weights/ Comments
			W	F	W	F	
NT-RC-2	NON-FLORAL REMAINS						
	Insect	Chitin				37	
	Rock/Gravel					X	Moderate
	Worm casts				X	X	Numerous

W = Whole
F = Fragment
X = Presence noted in sample
L = Liters
g = grams
** = Submitted for AMS radiocarbon dating

TABLE 3
INDEX OF MACROFLORAL REMAINS RECOVERED FROM
THE DUTCHMAN DRAW TRENCH SITE, ARIZONA

Scientific Name	Common Name
CHARCOAL/WOOD:	
Salicaceae	Willow family
Unidentified hardwood - small	Wood from a broad-leaved flowering tree or shrub, fragments too small for further identification

TABLE 4
RADIOCARBON RESULTS FOR SAMPLES FROM
THE DUTCHMAN DRAW TRENCH SITE, ARIZONA

Sample No.	Sample Identification	AMS ^{14}C Date*	1-sigma Calibrated Date (68.2%)	2-sigma Calibrated Date (95.4%)
PRI-09-61-NT-RC1	Salicaceae and unidentified hardwood charcoal	5720 ± 150 RCYBP	6680-6390 6370-6320 CAL yr. BP	6900-6200 CAL yr. BP
PRI-09-61-NT-RC3	Microcharcoal	3905 ± 20 RCYBP	4420-4350 4330-4290 CAL yr. BP	4420-4250 CAL yr. BP
PRI-09-61-NT-RC4	Microcharcoal	3830 ± 20 RCYBP	4290-4270 4250-4220 4210-4150 CAL yr. BP	4360-4330 4300-4150 CAL yr. BP
PRI-09-61-NT-RC2	Unidentified hardwood charcoal	1480 ± 70 RCYBP	1490-1470 1420-1300 CAL yr. BP	1530-1280 CAL yr. BP

* Reported in radiocarbon years at 1 standard deviation measurement precision (68.2%), corrected for δ^{13}C

FIGURE 1. PRI RADIOCARBON AGE CALIBRATION

Laboratory Number: PRI-09-61-NT-RC1
Sample Identification: Salicaceae and unidentified hardwood charcoal
Conventional AMS ^{14}C Date: 5720 ± 150 RCYBP
1-sigma Calibrated Date (68.2%): 6680-6390; 6370-6320 CAL yr. BP
2-sigma Calibrated Date (95.4%): 6900-6200 CAL yr. BP

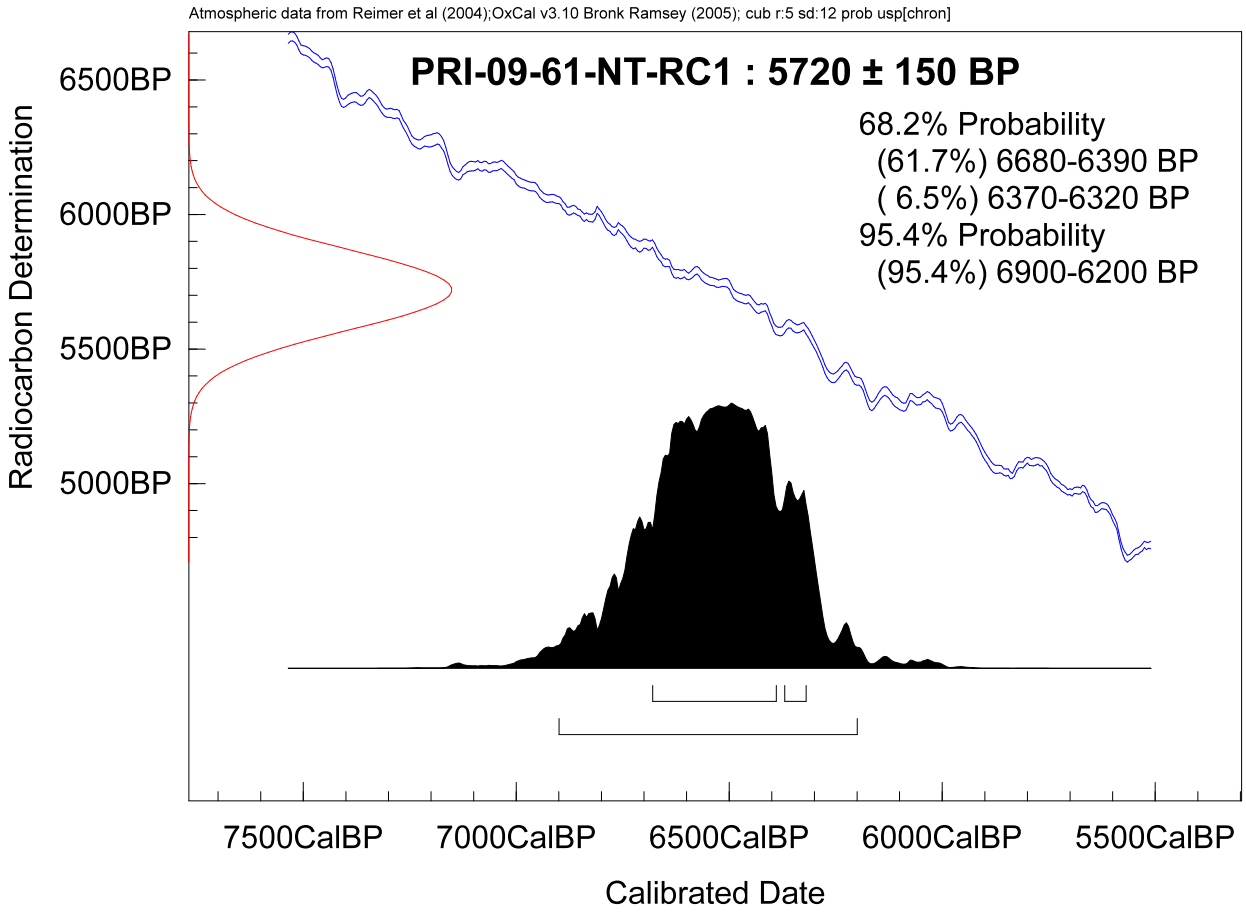

Intercept Statement. PaleoResearch Institute utilizes OxCal3.10 (Bronk Ramsey, 2005) for radiocarbon calibration, which is a probability-based method for determining conventional ages. We prefer this method over the intercept-based alternative because it provides our clients with a calibrated date that reflects the probability of its occurrence within a given distribution (reflected by the amplitude (height) of the curve), as opposed to individual point estimates (Telford 2004). As a result, the probability-based method offers more stability to the calibrated values than those derived from intercept-based methods that are subject to adjustments in the calibration curve (Telford 2004).

References

Telford, R. J., E. Heegaard, and H. J. B. Birks, 2004, *The Holocene* 14(2), pp. 296-298.

FIGURE 2. PRI RADIOCARBON AGE CALIBRATION

Laboratory Number: PRI-09-61-NT-RC3
Sample Identification: Microcharcoal
Conventional AMS ^{14}C Date: 3905 ± 20 RCYBP
1-sigma Calibrated Date (68.2%): 4420-4350; 4330-4290 CAL yr. BP
2-sigma Calibrated Date (95.4%): 4420-4250 CAL yr. BP

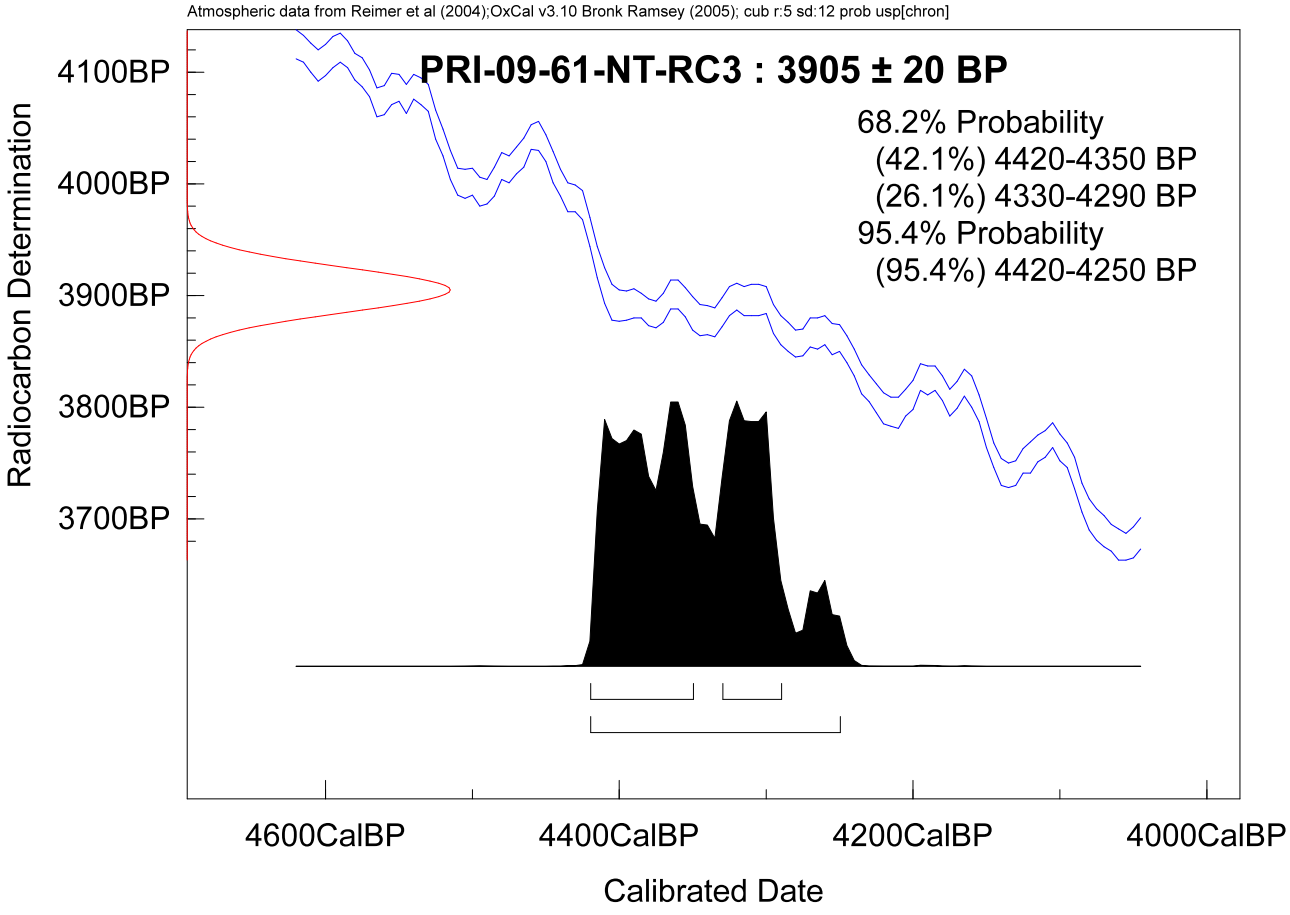

Intercept Statement. PaleoResearch Institute utilizes OxCal3.10 (Bronk Ramsey, 2005) for radiocarbon calibration, which is a probability-based method for determining conventional ages. We prefer this method over the intercept-based alternative because it provides our clients with a calibrated date that reflects the probability of its occurrence within a given distribution (reflected by the amplitude (height) of the curve), as opposed to individual point estimates (Telford 2004). As a result, the probability-based method offers more stability to the calibrated values than those derived from intercept-based methods that are subject to adjustments in the calibration curve (Telford 2004).

References

Telford, R. J., E. Heegaard, and H. J. B. Birks, 2004, *The Holocene* 14(2), pp. 296-298.

FIGURE 3. PRI RADIOCARBON AGE CALIBRATION

Laboratory Number: PRI-09-61-NT-RC4
Sample Identification: Microcharcoal
Conventional AMS ^{14}C Date: 3830 ± 20 RCYBP
1-sigma Calibrated Date (68.2%): 4290-4270; 4250-4220; 4210-4150 CAL yr. BP
2-sigma Calibrated Date (95.4%): 4360-4330; 4300-4150 CAL yr. BP

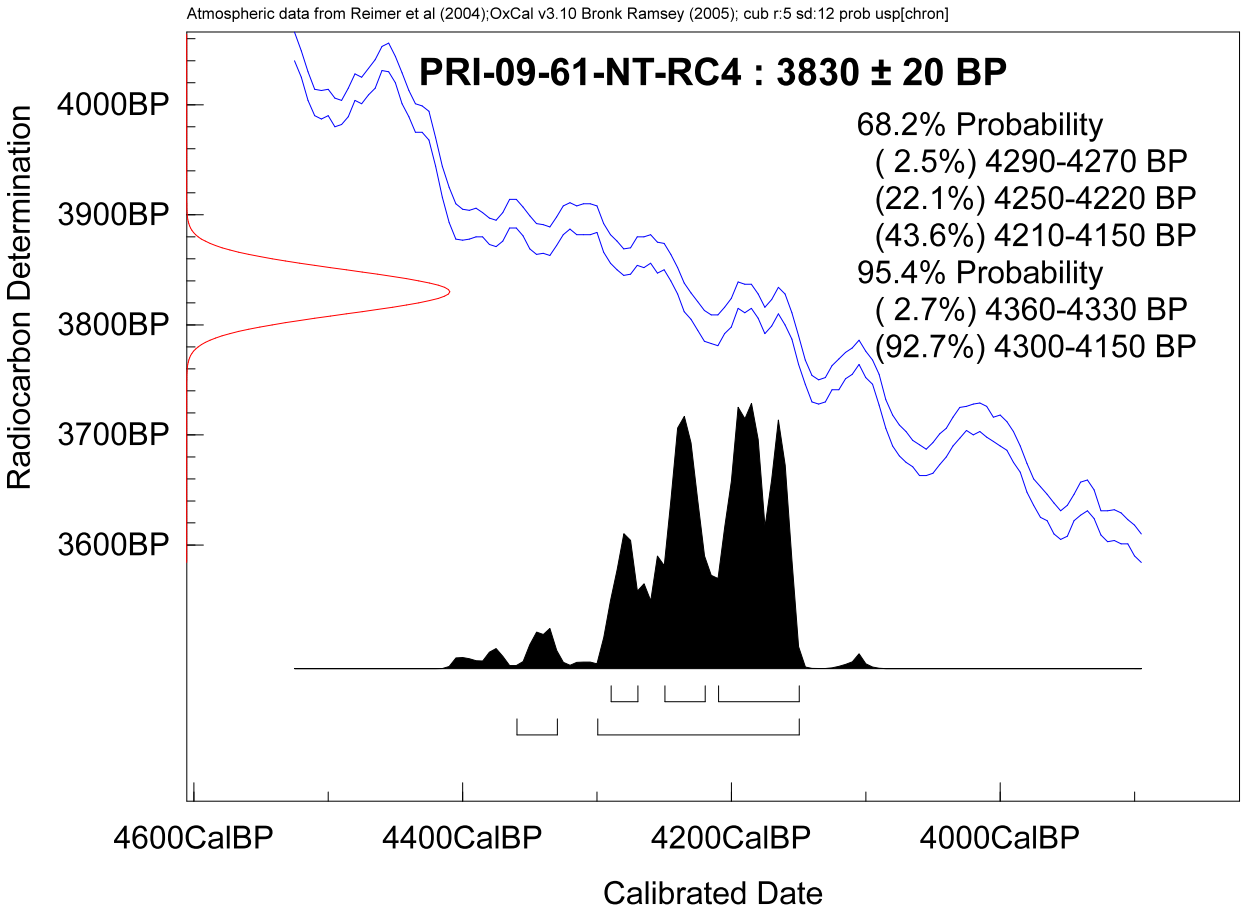

Intercept Statement. PaleoResearch Institute utilizes OxCal3.10 (Bronk Ramsey, 2005) for radiocarbon calibration, which is a probability-based method for determining conventional ages. We prefer this method over the intercept-based alternative because it provides our clients with a calibrated date that reflects the probability of its occurrence within a given distribution (reflected by the amplitude (height) of the curve), as opposed to individual point estimates (Telford 2004). As a result, the probability-based method offers more stability to the calibrated values than those derived from intercept-based methods that are subject to adjustments in the calibration curve (Telford 2004).

References

Telford, R. J., E. Heegaard, and H. J. B. Birks, 2004, *The Holocene* 14(2), pp. 296-298.

FIGURE 4. PRI RADIOCARBON AGE CALIBRATION

Laboratory Number: PRI-09-61-NT-RC2
Sample Identification: Unidentified hardwood charcoal
Conventional AMS ^{14}C Date: 1480 ± 70 RCYBP
1-sigma Calibrated Date (68.2%): 1490-1470; 1420-1300 CAL yr. BP
2-sigma Calibrated Date (95.4%): 1530-1280 CAL yr. BP

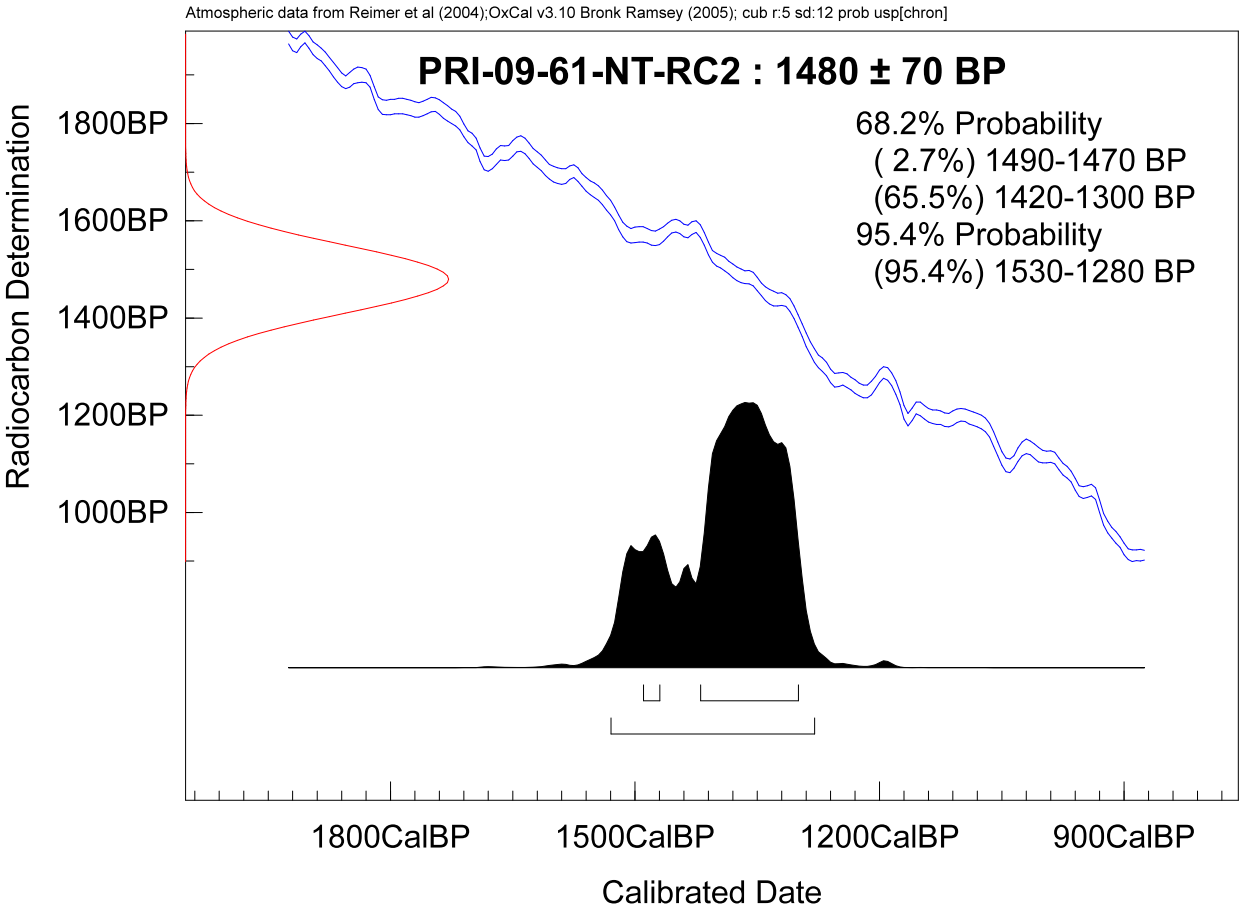

Intercept Statement. PaleoResearch Institute utilizes OxCal3.10 (Bronk Ramsey, 2005) for radiocarbon calibration, which is a probability-based method for determining conventional ages. We prefer this method over the intercept-based alternative because it provides our clients with a calibrated date that reflects the probability of its occurrence within a given distribution (reflected by the amplitude (height) of the curve), as opposed to individual point estimates (Telford 2004). As a result, the probability-based method offers more stability to the calibrated values than those derived from intercept-based methods that are subject to adjustments in the calibration curve (Telford 2004).

References

Telford, R. J., E. Heegaard, and H. J. B. Birks, 2004, *The Holocene* 14(2), pp. 296-298.

REFERENCES CITED

Puseman, Kathryn
2009 Choose Your Wood Wisely: Bigger Isn't Always Better. Paper presented at the Ninth Biennial Rocky Mountain Anthropological Conference, Western State College of Colorado, Gunnison.

Taylor, R. E.
1987 *Radiocarbon Dating: An Archaeological Perspective*. Academic Press, Inc., Orlando.

Telford, R.J., E. Heegaard, and H.J.B. Birks
2004 The Intercept is a Poor Estimate of a Calibrated Radiocarbon Age. *The Holocene* 14(2):296-298.

APPENDIX C

UTAH STATE UNIVERSITY
LUMINESCENCE LABORATORY OSL AGES,
DUTCHMAN DRAW TRENCH SITE,
WASHINGTON FAULT ZONE, ARIZONA

USU LUMINESCENCE LABORATORY
1770 north research park way, suite 123, north logan, ut, 84341

FINAL OSL AGE REPORT

Project: Washington Fault, Utah Geological Survey **Project #:** 068
Scientists: William Lund
Report by: Tammy Rittenour
Date: 01 September 2010

OSL Age Information[1]

USU #	Sample #	Location	Num. of aliquots[2]	Equivalent Dose[3] (De), Gy	Dose Rate (Gy/ka)	OSL Age[4] (ka)
NT-OSL 1	USU-554	unit 5b, hanging wall	**26** (35)	51.52 ± 6.08	1.68 ±0.07	**30.75 ± 2.21**
NT-OSL 2	USU-555	unit 5, foot wall	**26** (33)	55.72 ± 8.36	1.10 ±0.05	**48.66 ± 3.74**
NT-OSL 3	USU-556	fault scarp colluv, P2	**23** (35)	6.92 ± 1.59	2.30 ±0.10	**3.02 ± 0.34**
ST-OSL 1	USU-557	btwn P2 and P1 colluv	**25** (31)	7.53 ± 0.07	1.78 ±0.08	**4.22 ± 0.27**
ST-OSL 2	USU-788	South trench, unit 5a	**22** (31)	25.06 ± 5.11	1.47 ± 0.07	**17.10 ± 1.38**
ST-OSL 3	USU-789	South trench, unit 5e	**24** (40)	57.18 ± 9.33	1.06 ± 0.05	**54.07 ± 4.07**
ST-OSL 4	USU-790	South trench, unit 4	**20** (32)	17.20 ± 4.31	1.25 ± 0.06	**13.80 ± 1.18**

[1]Age analysis using the single-aliquot regenerative-dose procedure of Murray and Wintle (2000) on 1-mm small-aliquots (SA) of quartz sand.

[2]Number of aliquots used for age calculation, number of aliquots measured in parentheses.

[3]De calculated using the central age model of Galbraith et al (1999), error on De is 1 standard deviation.

[4]Error on age includes random and systematic errors calculated in quadrature.

Dose Rate Information[1]

USU #	Sample #	Depth (m)	Grain size (µm)	*In-situ* H_2O%[2]	U (ppm)	Th (ppm)	K_2O%	Rb_2O (ppm)	Cosmic[3] (Gy/ka)
NT-OSL 1	USU-554	2.0	90-150	1.0%	1.8±0.1	3.3±0.3	1.06±0.03	41.6±1.7	0.19±0.02
NT-OSL 2	USU-555	0.68	90-150	0.3%	1.3±0.1	1.9±0.2	0.57±0.01	21.8±0.9	0.23±0.02
NT-OSL 3	USU-556	1.9	90-150	0.9%	1.9±0.1	5.8±0.5	1.59±0.04	61.4±2.5	0.19±0.02
ST-OSL 1	USU-557	0.46	90-150	1.4%	1.7±0.1	4.3±0.4	1.08±0.03	49.0±2.0	0.23±0.02
ST-OSL 2	USU-788	2.25	90-125	2.0%	1.6±0.1	3.2±0.3	0.84±0.02	33.7±1.3	0.18±0.02
ST-OSL 3	USU-789	1.5	75-150	0.6%	0.9±0.1	1.9±0.2	0.61±0.02	22.6±0.9	0.20±0.02
ST-OSL 4	USU-790	1	75-150	1.0%	1.6±0.1	2.5±0.2	0.58±0.01	21.5±0.9	0.22±0.02

[1]Radioelemental concentrations determined by ICP-MS and ICP-AES techniques from ALS Chemex, dose rate is derived from concentrations by conversion factors from Aitken (1985) and Adamiec and Aitken (1998).

[2]Assumed 3±3%wt H_2O for USU-554:-557 and *in-situ* ±3%wt H_2O for USU-788:-790 to represent moisture content over burial history.

[3]Contribution of cosmic radiation to the dose rate was calculated by using sample depth, elevation, and longitude/latitude following Prescott and Hutton (1994).

Equivalent dose distributions: Probability density functions

USU-554

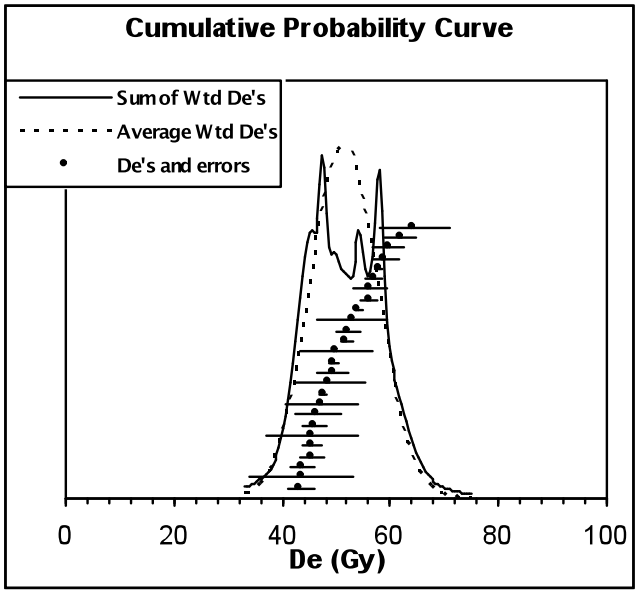

USU-555

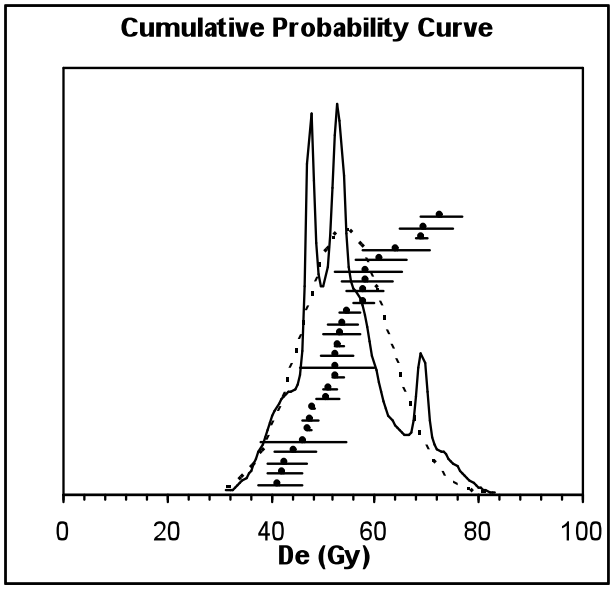

USU-556

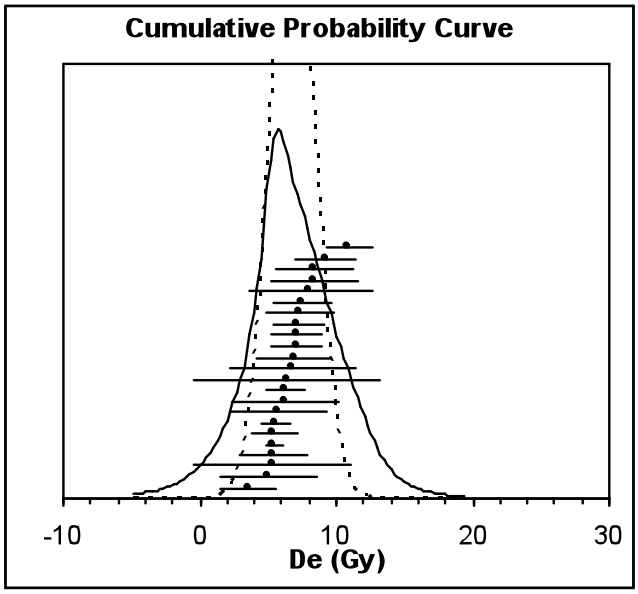

USU-557

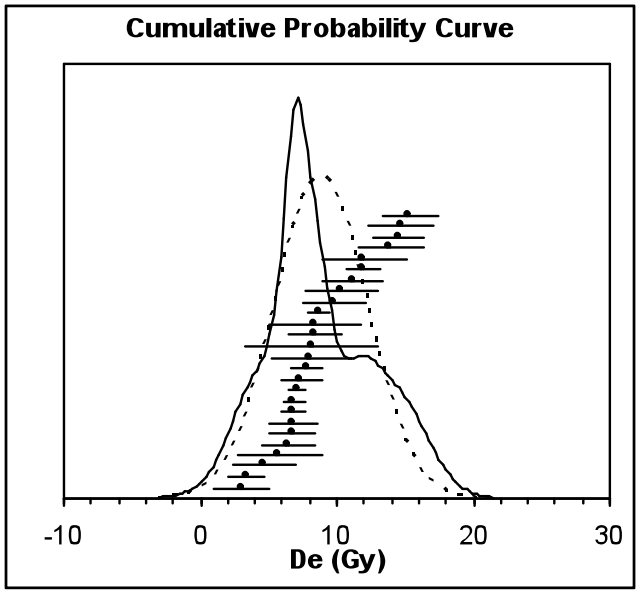

Equivalent dose distributions: Probability density functions (con't)

USU-788

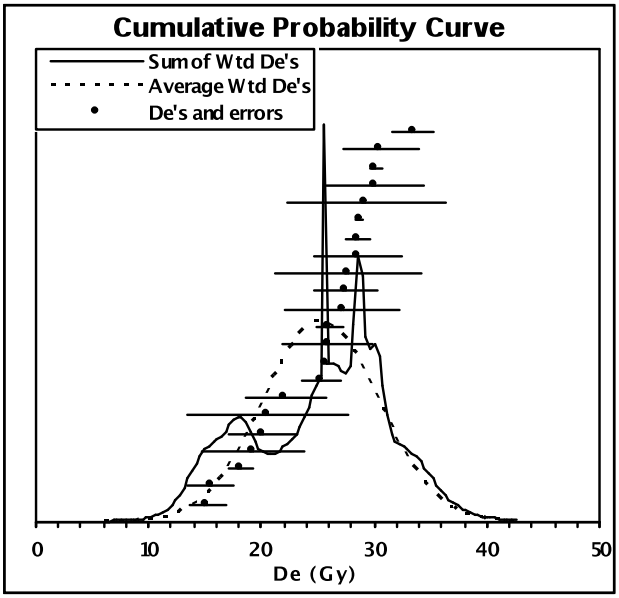

USU-789

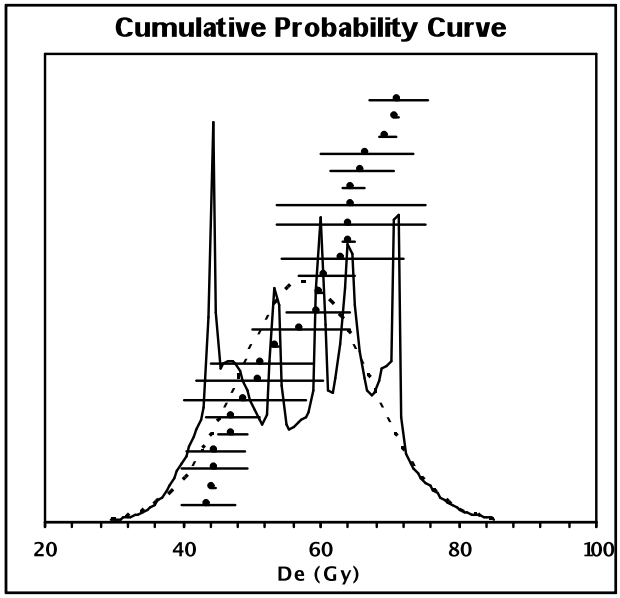

USU-790

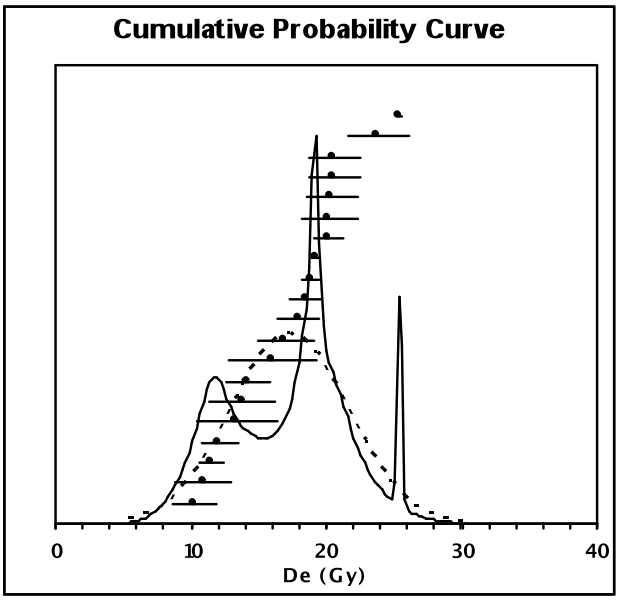

USU LUMINESCENCE LABORATORY
1770 north research park way, suite 123, north logan, ut, 84341

Procedures for sample processing and age analysis:

All samples were opened and processed under dim amber safelight conditions within the lab. Sample processing follows standard procedures involving sieving, gravity separation and acid treatments with HCl and HF to isolate the quartz component of a narrow grain-size range, usually 90-150 µm*. The purity of the samples is checked by measurement with infra-red stimulation to detect the presence of feldspar. Sample processing procedures follow those outlined in Aitken (1998) and described in Rittenour et al. (2003, 2005).

The USU Luminescence Lab follows the latest single-aliquot regenerative-dose (SAR) procedures for dating quartz sand (Murray and Wintle, 2000, 2003; Wintle and Murray, 2006). The SAR protocol includes tests for sensitivity correction and brackets the equivalent dose (De) the sample received during burial by irradiating the sample at five different doses (below, at, and above the De, plus a zero dose and a repeated dose to check for recuperation of the signal and sensitivity correction). The resultant data are fit with a saturating exponential curve from which the De is calculated on the mean, Central Age Model (CAM) or the Minimum Age Model (MAM) of Galbraith et al. (1999) or Juyal et al. (2006), depending on the distribution of De results and evidence for partial bleaching*. In cases where the samples have significant positive skew, ages are calculated based on a MAM. OSL age is reported at 1σ or 2σ standard error* and is calculated by dividing the De (in grays, gy) by the environmental dose rate (gy/ka) that the sample has been exposed to during burial.

Dose-rate calculations were determined by chemical analysis of the U, Th, K and Rb content using ICP-MS and ICP-AES techniques by ALS Chemex, Elko NV and conversion factors from Aitken (1985) and Adamiec and Aitken (1998). The contribution of cosmic radiation to the dose rate was calculated using sample depth, elevation, and latitude/longitude following Prescott and Hutton (1994). Dose rates are calculated based on water content, sediment chemistry, and cosmic contribution (Aitken, 1998).

Under the collaborative agreement to analyze samples at the USU Luminescence Lab, please consider including Dr. Rittenour as a co-author on resultant publications. Contact me for additional information and help with describing the OSL technique when you plan your publication.

Dr. Tammy Rittenour

Director
USU Luminescence Lab
1770 N Research parkway, suite 123
North Logan, UT 84341

Assistant Professor
Department of Geology, Utah State University
4505 Old Main Hill
Logan, UT 84322-4505

tammy.rittenour@usu.edu
ph (435) 213-5756, fax (435) 797-1588
http://www.usu.edu/geo/luminlab/

* these parameters are sample dependent, see first page of report for specific sample information

References cited:

Adamiec, G., Aitken, M., 1998. Dose-rate conversion factors: update. Ancient TL 16, 37-50.

Aitken, M.J. 1985: Thermoluminescence Dating: New York, Academic Press, 359 p.

Aitken, M.J. 1998: An Introduction to Optical Dating: The dating of Quaternary sediments by the use of photon-stimulated luminescence. New York, Oxford University Press, 267 p.

Galbraith, R.F., Roberts, R.G., Laslett, G.M., Yoshida, H., Oleey, J.M., 1999. Optical dating of single and multiple grains of quartz from Jinmium Rock Shelter, northern Australia: Part I, experimental design and statistical models. Archaeometry 41, 339-364.

Goble, R.J. and Rittenour, T.M., 2006, A linear modulation OSL study of the unstable ultrafast component in samples from glacial lake Hitchcock, Massachusetts, USA: Ancient TL 24, 37-46.

Juyal, N., Chamyal, L.S., Bhandari, S., Bhushan, R., Singhvi, A.K., 2006. Continental record of the southwest monsoon during the last 130 ka: evidence from the southern margin of the Thar Desert, India. Quaternary Science Reviews 25, 2632-2650.

Prescott, J. R., Hutton, J.T., 1994. Cosmic ray contributions to dose rates for luminescence and ESR dating: Radiation Measurements 23, 497-500.

Murray, A.S., Wintle, A.G., 2000. Luminescence dating of quartz using an improved single aliquot regenerative-dose protocol. Radiation Measurements 32, 57-73.

Murray, A.S., Wintle, A.G., 2003. The single aliquot regenerative dose protocol: potential for improvements in reliability. Radiation Measurements 37, 377-381.

Olley, J.M., Pietsch, T., Roberts, R.G., 2004. Optical dating of Holocene sediments from a variety of geomorphic settings using single grains of quartz: Geomorphology 60, 337-358.

Rittenour, T.M., Goble, R.J., Blum, M.D., 2003, An Optical Age Chronology of Fluvial Deposits in the Northern Lower Mississippi Valley: Quaternary Science Reviews, v. 22, p. 1105-1110.

Rittenour, T.M., Goble, R.J., Blum, M.D., 2005, Development of an OSL chronology for late Pleistocene channel belts in the lower Mississippi valley: Quaternary Science Reviews, v.24, p.2539-2554.

Rittenour, T.M. 2008. Luminescence dating of fluvial deposits: applications to geomorphic, paleoseismic and archaeological research. Boreas, 37, 613-635.

Wintle, A.G. Murray, A.S., 2006, A review of quartz optically stimulated luminescence characteristics and their relevance in single-aliquot regenerative protocols: Radiation Measurements, v. 41, p. 369-391.

APPENDIX D
DUTCHMAN DRAW TRENCH SITE
OXCAL MODEL

The OxCal model for the Dutchman Draw trench site was created using OxCal calibration and analysis software version 4.1.7 (Bronk Ramsey, 2010), and the IntCal09—Northern Hemisphere calibration curve of Reimer and others (2009). The model includes "C_Date" for luminescence ages, "R_Date" for radiocarbon ages, and "Boundary" for undated events (paleoearthquakes). The model components are arranged in sequence based on the stratigraphic position of the luminescence and radiocarbon samples. The "Difference P2–P1" command computes the two-sigma recurrence interval between the P1 and P2 paleoearthquakes. The "Difference MRE elapse time" command computes the elapsed time since the most recent surface-faulting earthquake (P1) to 2011. The model is in reverse stratigraphic order (oldest ages at the top), following the order in which the ages and events are evaluated in OxCal.

```
Plot()
 {
  Sequence("Washington fault OxCal Model, Version 3")
  {
   Boundary("Sequence start");
   C_Date("OSLS2 17.1",-15091,1380);
   C_Date("OSLS4 13.1",-11071,1180);
   Zero_Boundary("1");
   Boundary("P2 earthquake");
   R_Date("R1 6540+/-340",5720,150);
   R_Date("R3 4350+/-80",3905,20);
   R_Date("R4 4220+/-100",3830,20);
   C_Date("OSLS1 4.2",-2211,270);
   R_Date("R2 1390+/-140",1480,70);
   Boundary("P1 earthquake");
   Zero_Boundary("2");
   Boundary("Begin historical record",1847 AD);
   C_Date("2011",2011,0);
  };
  Page( );
  Difference("P2-P1", "P2", "P1");
  Difference("MRE elapse time", "2011", "P1");
 };
```

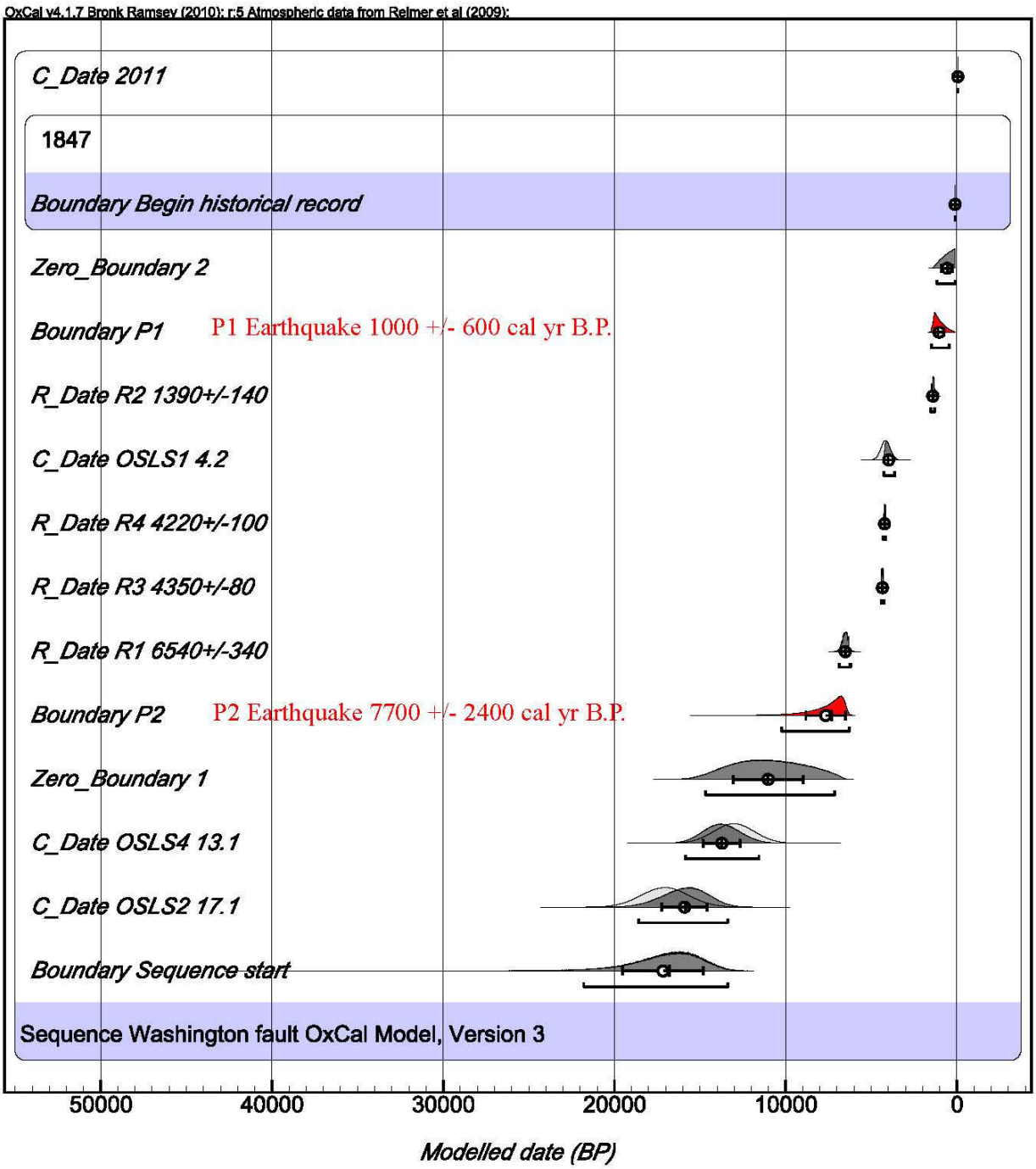

Stratigraphic ordering and age controls for the Dutchman Draw site using OxCal v. 4.1.7 (Bronk Ramsey, 2010) and the IntCal09—Northern Hemisphere calibration curve of Reimer and others (2009). Probability density functions are for radiocarbon and luminescence ages and the modeled paleoearthquake time ranges (two sigma). Light gray shaded areas represent pre-modeling distributions; dark-gray areas represent modeled distributions using stratigraphic ordering information. Horizontal bars show two-sigma age ranges for post-modeling distributions.

LONG-TERM VERTICAL SLIP-RATE ESTIMATES FROM DISPLACED MAFIC VOLCANIC FLOWS, FORT PEARCE AND SULLIVAN DRAW SECTIONS, WASHINGTON FAULT ZONE, MOHAVE COUNTY, ARIZONA

by

William R. Lund and Tyler R. Knudsen

Utah Geological Survey
Cedar City, Utah

This report is part of Utah Geological Survey Miscellaneous Publication 15-6, *Surficial Geologic Mapping and Paleoseismic Investigations of the Washington Fault Zone, Washington County, Utah, and Mohave County, Arizona*—Paleoseismology of Utah, Volume 27.

Bibliographic citation for this report: Lund, W.R., and Knudsen, T.R., 2015, Long-term vertical slip-rate estimates from displaced mafic volcanic flows, Fort Pearce and Sullivan Draw sections, Washington fault zone, Mohave County, Arizona, *in* Lund, W.R., editor, 2015, Surficial geologic mapping and paleoseismic investigations of the Washington fault zone, Washington County, Utah, and Mohave County, Arizona—Paleoseismology of Utah, Volume 27: Utah Geological Survey Miscellaneous Publication 15-6, p. 93–112, CD.

CONTENTS

ABSTRACT 89
INTRODUCTION 89
Purpose and Scope of Work 89
Geologic Setting 91
Previous Investigations 91
GEOCHEMISTRY 91
$^{40}AR/^{39}AR$ RADIOMETRIC AGES 92
VOLCANIC FLOW CORRELATION 93
VERTICAL SLIP-RATE ESTIMATES 93
DISCUSSION 95
CONCLUSIONS 95
ACKNOWLEDGMENTS 96
REFERENCES 96
APPENDICES 97
Appendix A Geochemical analyses of mafic volcanic rock samples from the footwall and hanging wall of the Washington fault zone, Mohave County, Arizona 98
Appendix B Variation diagrams of mafic volcanic rock samples from the footwall and hanging wall of the Washington fault zone, Mohave County, Arizona 101
Appendix C $^{40}Ar/^{39}Ar$ radiometric ages of mafic volcanic rock samples from the footwall and hanging wall of the Washington fault zone, Mohave County, Arizona 105

FIGURES

Figure 1. Mafic volcanic flow remnants along the southern part of the Fort Pearce section and northern end of the Sullivan Draw section of the Washington fault zone, Mohave County, Arizona 90
Figure 2. Classification of mafic volcanic rock samples collected along the southern part of the Fort Pearce section and northern end of the Sullivan Draw section of the Washington fault zone, Mohave County, Arizona 91
Figure 3. Sections of the Hurricane and Washington fault zones 95

TABLES

Table 1. Radiometric ages available for mafic volcanic flows along southern part of the Fort Pearce section and northern end of the Sullivan Draw section of the Washington fault zone in Arizona prior to this investigation. 92
Table 2. Newly acquired $^{40}Ar/^{39}Ar$ radiometric ages for mafic volcanic flows along the southern part of the Fort Pearce section and northern end of the Sullivan Draw section of the Washington fault zone. 92
Table 3. Long-term vertical slip-rate estimates for southern part of the Fort Pearce section and northern end of the Sullivan Draw section of the Washington fault zone in Arizona determined from displaced volcanic flows. 94

LONG-TERM VERTICAL SLIP-RATE ESTIMATES FROM DISPLACED MAFIC VOLCANIC FLOWS, FORT PEARCE AND SULLIVAN DRAW SECTIONS, WASHINGTON FAULT ZONE, MOHAVE COUNTY, ARIZONA

by William R. Lund and Tyler R. Knudsen

ABSTRACT

The Utah Geological Survey conducted an investigation of mafic volcanic flow remnants along the southern part of the Fort Pearce section and extreme northern end of the Sullivan Draw section of the Washington fault zone in Arizona. The purpose of the investigation was to determine if flow remnants on the upthrown and downthrown sides of the faults are geochemically (trace elements and major oxides) correlative, and if so, obtain radiometric ages ($^{40}Ar/^{39}Ar$) for the correlative remnants and combine the new age information with flow displacement estimates to calculate long-term (post-early to middle Quaternary) vertical slip-rate estimates for the sections. New long-term slip-rate estimates will help improve seismic source zone characterization models for the fault sections, and provide important information for future probabilistic seismic hazard analyses in southwestern Utah and northwestern Arizona.

Earlier workers speculated that some or all of the volcanic flows along the Fort Pearce (formerly Northern) and Sullivan Draw sections of the Washington fault zone in northern Arizona are correlative across the fault. The close physical proximity of displaced flow remnants shows that the Seegmiller Mountain and East Mesa flows are displaced by the Sullivan Draw and Fort Pearce (Dutchman Draw strand) sections, respectively; however, evidence that other flows are correlative across the fault has been lacking. Our new geochemical analyses, radiometric ages, and geologic mapping provide evidence that a likely correlation exists across the fault between either the East or West Mesa flows (but not both) and the Dutchman Draw-1 flow remnant. A possible correlation also exists between the Seegmiller Mountain flow and the Dutchman Draw-2 flow remnant. The correlation with the Dutchman Draw-1 remnant captures the vertical slip across the entire Fort Pearce section (main, Mokaac, and Dutchman Draw strands). The displaced northwestern end of the East Mesa flow provides a vertical slip-rate estimate for only one splay of the multi-splay Dutchman Draw strand. The southwestern end of the Seegmiller Mountain flow is displaced across the Sullivan Draw section, and provides a vertical slip-rate estimate for the extreme northern end of that section.

The correlation of the East and West Mesa flows with the Dutchman Draw-1 flow remnant resulted in vertical slip-rate estimates of 0.25 and 0.38 mm/yr, respectively. Only one of those estimates can be correct because the East and West Mesa flows are not correlative with each other. The possible correlation between the Seegmiller Mountain flow and the Dutchman Draw-2 flow remnant provides a vertical slip-rate estimate for the main strand of the Fort Pearce section of 0.30 mm/yr. The vertical slip-rate estimate for the Sullivan Draw section is 0.04 mm/yr, and the slip-rate estimate for one splay of the Dutchman Draw strand is also 0.04 mm/yr.

The composite long-term (post-middle Quaternary) vertical slip-rate estimate for the Fort Pearce section of 0.25–0.38 mm/yr is somewhat higher than the vertical slip rate determined from paleoseismic data at the Dutchman Draw trench site for the most recent closed seismic cycle on the main strand of the Fort Pearce section of 0.11–0.29 mm/yr (mean 0.20 mm/yr). The Seegmiller Mountain–Dutchman Draw-2 long-term vertical slip-rate estimate for the main strand of the Fort Pearce section of 0.30 mm/yr generally matches the upper bound of the Dutchman Draw trench site single seismic cycle rate. A long-term Fort Pearce-section slip rate of approximately 0.3 mm/yr is also generally similar with the long-term vertical slip rate of the Shivwits section of the Hurricane fault several kilometers to the east.

INTRODUCTION

Purpose and Scope of Work

The Utah Geological Survey (UGS) conducted an investigation of mafic volcanic flow remnants along the southern part of the Fort Pearce (formerly Northern; see Knudsen, this volume) section and at the extreme northern end of the Sullivan Draw section of the Washington fault zone in Arizona (figure 1). The purpose of the investigation was to determine if the flow remnants on the upthrown and downthrown sides of the faults are correlative, and if so, combine that information with age and displacement information to calculate long-term (post-early to middle Quaternary) vertical slip rates for the sections.

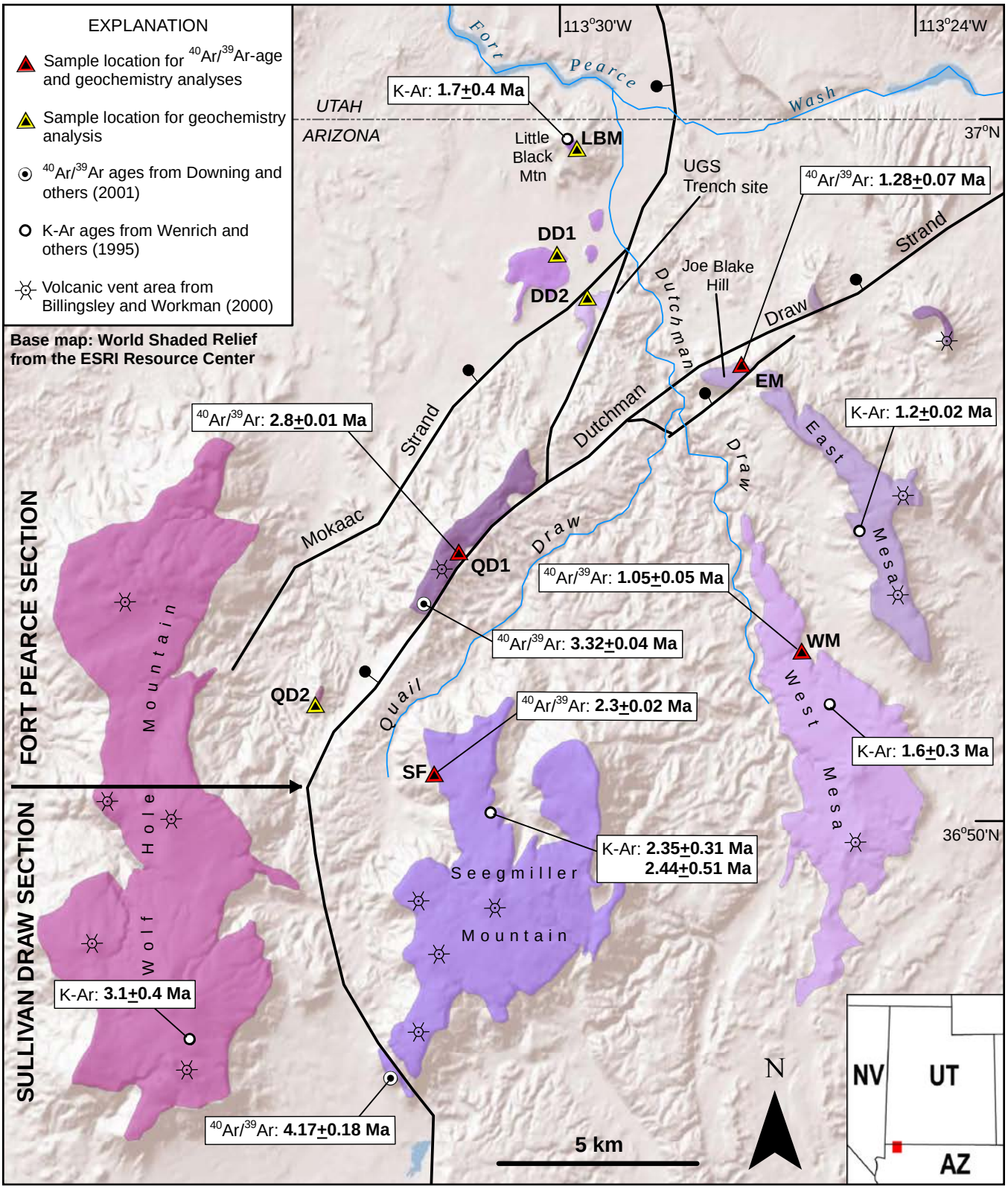

Figure 1. *Mafic volcanic flow remnants along the southern part of the Fort Pearce section and northern end of the Sullivan Draw section of the Washington fault zone, Mohave County, Arizona. Bar and ball on downthrown side of faults.*

The investigation scope of work included:

- Collecting eight samples from selected flow remnants for geochemical analysis (appendix A), and analyzing the geochemical data using IgPet software to classify the remnants by rock type (figure 2) and establish potential geochemical correlations using trace element and major oxide variation diagrams (appendix B).

- Collecting four samples from the potentially correlative flow remnants for $^{40}Ar/^{39}Ar$ radiometric age analysis (appendix C).

- Combining the new and existing age information with flow displacement estimates to calculate long-term vertical slip-rate estimates for the sections.

The resulting new long-term vertical slip-rate estimates can be compared with shorter-term rates estimated from paleoseismic trenching investigations (e.g., Lund and others, this volume). Together, these data will improve seismic source zone characterization models for the fault sections, and provide important information for future probabilistic seismic hazard analyses in southwestern Utah and northwestern Arizona.

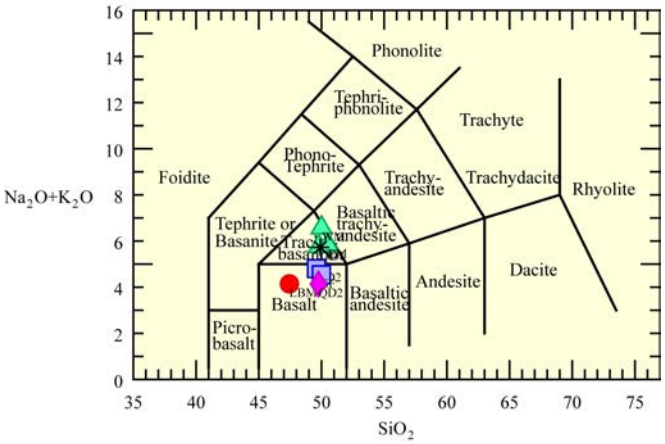

Figure 2. *Classification of mafic volcanic rock samples collected along the southern part of the Fort Pearce section and northern end of the Sullivan Draw section of the Washington fault zone, Mohave County, Arizona (after LeBas and others, 1986).* △ *= DD1, EM, WM;* ♦ *=QD2;* □ *= DD2, SF;* ● *= LBM;* ✳ *= QD1.*

Geologic Setting

Lund (this volume) summarizes the general geologic setting of southwestern Utah and provides an overview of the Washington fault zone. Knudsen (this volume) provides details of the geology along the Fort Pearce section, and more general information on the geology of the adjacent Sullivan Draw section. Readers interested in additional information about the geology of the Fort Pearce section are directed to those reports, and to the geologic map and the reference lists accompanying them.

Figure 1 shows the relation of mafic volcanic flow remnants to the southern part of the Fort Pearce section and northern end of the Sullivan Draw section in Arizona. The figure also shows the locations of geochemical and radiometric age analyses conducted for this investigation, and the locations of previously existing flow remnant radiometric age information. It is important to note on figure 1 that cinder cone sources for the mafic volcanic flows are present on both the fault footwall and hanging wall.

Previous Investigations

Numerous workers (e.g., Hamblin and Best, 1970; Petersen, 1983; Billingsley and Workman, 2000; Billingsley and Graham, 2003) mapped mafic volcanic flows (figure 1) on both the southeast (upthrown) and northwest (downthrown) sides of the Fort Pearce section of the Washington fault zone in northern Arizona, and speculated that some of the volcanic flows are displaced by the Washington fault zone. Erosion of the soft sedimentary rocks on which the more resistant flows were extruded has left the flows as mostly isolated remnants capping hills and mesas (inverted topography) on both sides of the fault. Aerially extensive flow remnants cap Seegmiller Mountain (SF), West Mesa (WM), and East Mesa (EM) on the fault footwall. Smaller remnants either within or northwest of the fault zone on the fault hanging wall are present near Quail Draw (Quail Draw-1 [QD1] and Quail Draw-2 [QD2]), Joe Blake Hill (EM), Little Black Mountain (LBM), and at a cluster of low hills west of Dutchman Draw (Dutchman Draw-1 [DD1] and Dutchman Draw-2 [DD2]) (figure 1). The close physical proximity of displaced flow remnants shows that the Seegmiller Mountain and East Mesa flows are displaced across the Sullivan Draw section and the Dutchman Draw strand of the Fort Pearce section, respectively; however, evidence that other flows are correlative across the fault has been lacking.

Recognizing the nature of the inverted topography created by the volcanic flows, Hamblin (1963, 1970) used the height of the flows above the current elevation of the Virgin River in the St. George basin as a proxy for flow age. Wenrich and others (1995) obtained a pair of K-Ar radiometric ages for the Seegmiller Mountain flow, and individual K-Ar ages for the Wolf Hole Mountain, Little Black Mesa, East Mesa, and West Mesa flows (figure 1, table 1). Downing and others (2001) obtained an $^{40}Ar/^{39}Ar$ total gas age for the Seegmiller Mountain flow, and an $^{40}Ar/^{39}Ar$ plateau age for the Quail Draw-1 flow remnant which they interpreted to be displaced Seegmiller Mountain flow.

GEOCHEMISTRY

We collected eight samples from mafic volcanic flows along the southern part of the Fort Pearce section and northern end of the Sullivan Draw section in Arizona for geochemi-

Table 1. *Radiometric ages available for mafic volcanic flows along southern part of the Fort Pearce section and northern end of the Sullivan Draw section of the Washington fault zone in Arizona prior to this investigation.*

Location[1]	Radiometric age (Ma)	Reference
East Mesa flow	1.4 + 0.25 (K-Ar)	Wenrich and others (1995)
West Mesa flow	1.6 + 0.3 (K-Ar)	Wenrich and others (1995)
Little Black Mountain flow	1.7 + 0.4 (K-Ar)	Wenrich and others (1995)
Seegmiller Mountain flow	2.35 + 0.31 and 2.44 + 0.51 (K-Ar)	Wenrich and others (1995)
Wolf Hollow Mountain flow	3.1 + 0.4 (K-Ar)	Wenrich and others (1995)
Quail Draw-1 flow	3.32 + 0.04 ($^{40}Ar/^{39}Ar$)	Downing and others (2001)
Seegmiller Mountain flow	4.17 + 0.18 ($^{40}Ar/^{39}Ar$)	Downing and others (2001)

[1]*See figure 1 for flow locations.*

cal analysis (figure 1). The GeoAnalytical Lab at Washington State University (http://www.sees.wsu.edu/Geolab/index.html) analyzed the samples; results of the geochemical analyses are presented in appendix A.

Robert Biek (UGS, written communication, 2012) used the geochemical data to classify the rock types of the eight samples using the igneous rock classification system of LeBas and others (1986). Samples DD1, EM, QD1, and WM classify as trachybasalt and samples DD2, LBM, QD2, and SF classify as basalt (figure 2). Biek also plotted correlation diagrams to compare combinations of trace elements and major oxides (Rb vs. Sr, Sr vs. Zr, Ba vs. Cr, Nd vs. Nb, TiO_2 vs. P_2O_5, TiO_2 vs. SiO_2) between samples (appendix B). The correlation diagrams show a strong geochemical affinity between samples DD1, EM, and WM, and a possible affinity between samples DD2, QD1, and SF (R. Biek, UGS, written communication, 2012).

^{40}AR/^{39}AR RADIOMETRIC AGES

We collected four samples for $^{40}Ar/^{39}Ar$ radiometric age analysis at locations EM, QD1, SF, and WM (figure 1). The New Mexico Geochronology Research Laboratory (http://geoinfo.nmt.edu/labs/argon/home.html) at the New Mexico Institute of Mining and Technology analyzed the samples; the resulting age estimates with one-sigma uncertainty are shown in table 2. The sample analysis spectra are presented in appendix C.

Comparison of the new $^{40}Ar/^{39}Ar$ ages (table 2) with pre-existing radiometric ages (table 1) shows that:

1. The new $^{40}Ar/^{39}Ar$ age for the East Mesa flow is younger than but overlaps in time with the Wenrich and others (1995) K-Ar age for that flow. Wenrich and others (1995) did not report whether the uncertainty associated with their ages is one or two sigma.

2. The new $^{40}Ar/^{39}Ar$ age for the West Mesa flow is younger and more precise than the Wenrich and others (1995) K-Ar age for that flow, and the uncertainty ranges for the two ages do not overlap. Wenrich and others (1995) did not report whether the uncertainty associated with their ages is one or two sigma.

3. The new $^{40}Ar/^{39}Ar$ age for the Seegmiller Mountain flow is about 1.85 myr younger than the Downing and others (2001) $^{40}Ar/^{39}Ar$ age for that flow, but the new age does overlap in time with the two Wenrich and others (1995) K-Ar ages for the flow. The reason for the large discrepancy between the new and old $^{40}Ar/^{39}Ar$ ages for the Seegmiller Mountain flow is unknown. The uncertainty reported for the Downing and others (2001) ages is one sigma; Wenrich and others (1995) did not report whether the uncertainty associated with their ages is one or two sigma.

4. The Downing and others (2001) $^{40}Ar/^{39}Ar$ age for the Quail Draw-1 flow remnant is about 540 kyr older than the newly acquired $^{40}Ar/^{39}Ar$ age for that flow, and the uncertainty limits for the two ages do not overlap. Wenrich and others (1995) did not report whether the uncertainty associated with their ages is one or two sigma.

Table 2. *Newly acquired $^{40}Ar/^{39}Ar$ radiometric ages for mafic volcanic flows along the southern part of the Fort Pearce section and northern end of the Sullivan Draw section of the Washington fault zone.*

Sample[1]	Location	$^{40}Ar/^{39}Ar$ Age[2,3] (Ma)
EM	East Mesa flow	1.211 + 0.015
WM	West Mesa flow	1.05 + 0.05
SF	Seegmiller Mountain flow	2.32 + 0.02
QD1	Quail Draw-1 flow	2.779 + 0.017

[1] *See figure 1 for sample locations.*

[2]*Age analyses performed by the New Mexico Geochronology Research Laboratory – see appendix C.*

[3]*Ages are reported at with one-sigma uncertainty.*

VOLCANIC FLOW CORRELATION

Trace-element and major oxide correlation diagrams (appendix B) show a strong geochemical affinity between the Dutchman Draw-1 flow remnant on the Fort Pearce section hanging wall and the East Mesa and West Mesa flows on the fault footwall (figure 1). Although less pronounced, the correlation diagrams also indicate a possible correlation between the Seegmiller Mountain flow on the fault footwall and the Dutchman Draw-2 and Quail Draw-1 flow remnants on the fault hanging wall (R. Biek, UGS, written communication, 2012) (figure 1).

The $^{40}Ar/^{39}Ar$ and K-Ar radiometric ages available for the volcanic flows (tables 1 and 2) provide additional insight regarding flow correlations across the fault. Although the East and West Mesa flows have a strong geochemical affinity and overlapping K-Ar ages, the new $^{40}Ar/^{39}Ar$ ages for those flows are significantly different, and their uncertainty limits do not overlap. Billingsley and Graham (2003) mapped the geology of lower Hurricane Wash and vicinity, and showed that the East and West Mesa flows are sourced from different volcanic centers. In addition, the West Mesa flow is typically about 100 m lower than the East Mesa flow, indicating that substantial erosion of the landscape occurred between the eruption of the East Mesa and West Mesa flows. Similar geochemistry implies that the two flows may have been derived from a similar (same?) magma source, but significantly different ages (erupted as much as 350 kyr apart) and landscape positions indicate that the two flows are not directly correlative. A radiometric age is not available for the Dutchman Draw-1 flow remnant to help define its relation to the East and West Mesa flows. The Dutchman Draw-1 remnant is geochemically similar to both the East and West Mesa flows, but in the absence of a radiometric age to further clarify the relation, the remnant could correlate with either flow.

Geochemistry is also permissive of a possible correlation between the Seegmiller Mountain flow on the fault footwall, and the Quail Draw-1 and Dutchman Draw-2 flow remnants on the fault hanging wall (R. Biek, UGS, written communication, 2012) (appendix B). However, neither the K-Ar ages nor the $^{40}Ar/^{39}Ar$ ages available for the Seegmiller Mountain flow overlap in time with the two Quail Draw-1 flow radiometric ages (tables 1 and 2). So once again, geochemistry shows that the flows likely share a similar magma source, but their ages indicate that the flows were erupted at significantly different times and therefore are not directly correlative. The Dutchman Draw-2 flow remnant is geochemically similar to both the Seegmiller Mountain and Quail Draw-1 flows, but lacking a radiometric age to better define the correlation, the Dutchman Draw-2 remnant could be correlative with either of the former, but not both.

One splay of the Dutchman Draw strand displaces the northwestern end of the East Mesa flow at Joe Blake Hill, and the Sullivan Draw section displaces the southwestern end of the Seegmiller Mountain flow (figure 1). In both instances, the displaced flow remnants are closely adjacent to each other, and are clearly correlative.

Based on the geochemistry, radiometric ages, and geologic relations of the volcanic flows on the footwall and hanging wall of the Fort Pearce section in Arizona, we conclude that a likely correlation exists between either the East or West Mesa flows and the Dutchman Draw-1 flow remnant, and that a possible correlation exists between either the Seegmiller Mountain or Quail Draw-1 flow and the Dutchman Draw-2 flow remnant (figure 1). The East/West Mesa–Dutchman Draw-1 correlation encompasses the entire vertical slip across the Fort Pearce section (main, Dutchman Draw, and Mokaac strands). The possible Seegmiller Mountain–Dutchman Draw-2 correlation encompasses the slip only on the main strand of the Fort Pearce section. A Quail Draw-1–Dutchman Draw-2 correlation provides no information on fault slip since both flow remnants are on the hanging wall of the Fort Pearce section main trace. The displaced northwestern end of the East Mesa flow provides only a partial slip rate for the Dutchman Draw strand of the Fort Pearce section, since the flow is only displaced across a single splay of the multi-splay strand. New UGS mapping (Knudsen, this volume) shows that the southwestern end of the Seegmiller Mountain flow is displaced across the Sullivan Draw section, so the vertical slip-rate estimate determined there applies to the entire section.

VERTICAL SLIP-RATE ESTIMATES

New information on volcanic flow geochemistry, new and existing radiometric flow ages, and elevation estimates for displaced correlative flows allowed us to calculate vertical slip-rate estimates for the Washington fault zone in northern Arizona (table 3). We obtained elevation data for the displaced flows from Google Earth color aerial imagery dated 10/2/2011. Locations where we measured flow elevations were (1) carefully evaluated on aerial imagery (chiefly Google Earth color and black-and-white aerial photographs of multiple vintages) to avoid areas of landsliding or other topographic complications, and (2) the closest suitable points on the flow remnants to each other. Nevertheless, uncertainties associated with the elevation measurements are large. Horizontal distances separating some correlated flows are measured in multiple kilometers, while other flows are immediately adjacent to each other across a fault (table 3). Additionally, based on geologic mapping (Billingsley and Workman, 2000; Billingsley and Graham, 2003; Knudsen, this volume), the flows originated chiefly in the east on the fault footwall and flowed downslope to the west toward the fault hanging wall prior to faulting. Our slip-rate estimates do not account for differences in pre-faulting topography (i.e., the original elevation difference between measuring points due to higher elevations in the east and lower elevations in the west). For widely separated flow remnants, differences in pre-faulting topography may

Table 3. *Long-term vertical slip-rate estimates for the southern part of the Fort Pearce section and northern end of the Sullivan Draw section of the Washington fault zone in Arizona determined from displaced volcanic flows.*

Correlated Flows	Elev. A[1] (m)	Elev. B[1] (m)	Elevation Difference (m)	Horizontal Distance[2] (km)	Radiometric Age[3,4] (Ma)	Vertical Slip Rate (mm/yr)	Vertical Slip Across
Seegmiller Mountain Flow–Dutchman Draw-2 Flow Remnant	1700	1000	700	9.2	2.32 ± 0.02	0.30[5]	Fort Pearce section main strand
West Mesa Flow–Dutchman Draw-1 Flow Remnant	1300	900	400	7.9	1.05 ± 0.05	0.38[5]	Fort Pearce section composite
East Mesa Flow–Dutchman Draw-1 Flow Remnant	1200	900	300	6.3	1.211 ± 0.015	0.25[5]	Fort Pearce section composite
East Mesa Flow–East Mesa Flow	1220	1170	50	Adjacent	1.211 ± 0.015	0.04	Dutchman Draw strand single splay
Seegmiller Mountain Flow–Seegmiller Mountain Flow	1800	1710	90	Adjacent	2.32 ± 0.02	0.04	Sullivan Draw section

[1]Elevation obtained from Google Earth imagery dated 10/2/2011, and rounded to the nearest 100 m for widely separated correlative flow remnants and to the nearest 10 m for closely adjacent remnants.

[2]Straight line distance between elevation points (map distance) measured on Google Earth imagery dated 10/2/2011.

[3]New $^{40}Ar/^{39}Ar$ radiometric ages obtained for this study (see appendix C). See table 1 for older radiometric ages available for some flows.

[4]The time of onset of faulting is unknown, but is less than the ages of the flows used for slip-rate calculations; therefore, the resulting slip-rate estimates are underestimated by an unknown amount. The greater the time interval between eruption and faulting, the greater the effect on slip rate.

[5]Horizontal distances between elevation points measured in multiple kilometers. Based on geologic mapping, the flows originated in the east and flowed downslope to the west prior to faulting. The reported slip rates do not account for the effect of pre-faulting topography (i.e., original elevation difference between the two measurement points due to downslope movement of flows), so we consider displacement to be overestimated, which results in overestimated slip-rate values. It is assumed, but cannot be confirmed, that the flows did not cascade over a pre-existing fault escarpment which would also result in an overestimation of displacement. The extent to which the topographic and timing effects may balance each other is unknown.

amount to tens of meters of elevation change from east to west, which would increase apparent displacement and result in overestimated slip rates. Flow remnants close to the Washington fault zone on the fault hanging wall may be tilted toward the fault, which would also tend to increase apparent displacement and likewise contribute to overestimating slip rates. We have no information regarding whether the flows cascaded over a pre-existing fault escarpment. For purposes of our calculations, we assume that they did not, but if they did, our displacement estimates would be too high and result in higher-than-justified slip rates. To help account for uncertainties in our elevation measurements, we rounded the measurements to the nearest 100 m for widely separated flow remnants and to the nearest 10 m for remnants closely spaced across faults. Therefore, we consider the elevation differences between correlated flow remnants reported in table 3 to be poorly constrained estimates, but estimates that reflect best currently available information.

Also affecting our slip-rate calculation is the timing of the surface faulting that displaced the flows following their eruption. We do not know how much time elapsed between eruption and the onset of faulting. Therefore, we must base our slip-rate estimates on flow ages and not on the shorter interval since faulting commenced. As a consequence, our time estimates are too long and result in underestimated slip rates. The greater the length of time between eruption and onset of faulting, the greater the potential effect on slip rate. The extent to which topographic and timing effects balance each other is unknown.

We calculated five long-term, vertical slip-rate estimates for the Washington fault zone: two "composite" rates that include the main trace and the Mokaac, and Dutchman Draw strands of the Fort Pearce section (only one of which can be correct—see discussion in Volcanic Flow Correlation section above), one rate across only the main trace of the Fort Pearce section, one rate at the extreme northern end of the Sullivan Draw section, and a rate for one splay of the multiple-splay Dutchman Draw strand of the Fort Pearce section (table 3). The two composite vertical slip-rate estimates for the Fort Pearce section are 0.25 and 0.38 mm/yr, respectively (only one correct). The rate for the main strand of the Fort Pearce section is 0.30 mm/yr. The vertical slip-rate estimate for the Sullivan Draw section is 0.04 mm/yr, significantly lower than

the estimates for the adjacent Fort Pearce section. Because the Seegmiller Mountain flow remnants displaced across the Sullivan Draw section are directly adjacent to each other, the effect of downslope movement of the flow prior to faulting is negligible. The low Sullivan Draw slip rate may indicate that (1) slip on the Sullivan Draw section is generally lower than on the Fort Pearce section (Knudsen, this volume), (2) slip dies out rapidly at the end of the section, but may be higher farther south within the section, or (3) fault drag or other unrecognized near-fault perturbation may be affecting the rate. The slip rate for the Dutchman Draw strand is also 0.04 mm/yr, but is limited to a single splay of that multi-splay strand, and therefore does not represent all of the slip across that strand. Again, the proximity of the flow remnants on either side of the fault makes the effect of pre-faulting topography negligible.

DISCUSSION

The Fort Pearce section lies several kilometers west of and generally parallel to the Shivwits section of the Hurricane fault (figure 3). Amoroso and others (2004) used the displaced Moriah Knoll basalt flow to calculate a maximum middle Quaternary (0.85 Ma) to present vertical slip rate of 0.15 to 0.25 mm/yr for the Shivwits section. Lund and others (2007) determined long-term vertical slip rates for the Ash Creek and Anderson Junction sections of the Hurricane fault in Utah (figure 3) from displaced volcanic flows. Middle Quaternary (0.63–1.08 Ma) slip rates ranged from 0.37 to 0.57 mm/yr, and a displaced flow on the Anderson Junction section yielded a late Quaternary (0.353 Ma–present) vertical slip rate of 0.21 mm/yr.

The distribution and age of volcanic flows displaced across the Fort Pearce section allowed us to obtain a composite vertical slip-rate estimate for the Fort Pearce section (main, Mokaac, and Dutchman Draw strands) of either 0.25 or 0.38 mm/yr (only one can be correct), which is generally similar to the long-term vertical slip rates obtained for Hurricane fault sections to the east. The vertical slip rate determined from paleoseismic trenching data for the most recent seismic cycle on the Fort Pearce section main strand is 0.11–0.29 mm/yr (Lund and others, this volume), which is generally comparable to the long-term (early Quaternary) slip rate (0.30 mm/yr) determined for the Fort Pearce section main strand from displaced volcanic flows (table 3). Thus, the single-seismic-cycle vertical slip rate determined from paleoseismic trenching data on the Fort Pearce section main strand may be characteristic of late Quaternary slip on the section.

CONCLUSIONS

The principal conclusions resulting from this investigation of long-term vertical slip rates determined from displaced volcanic flows along the Fort Pearce and Sullivan Draw sections of the Washington fault zone include the following:

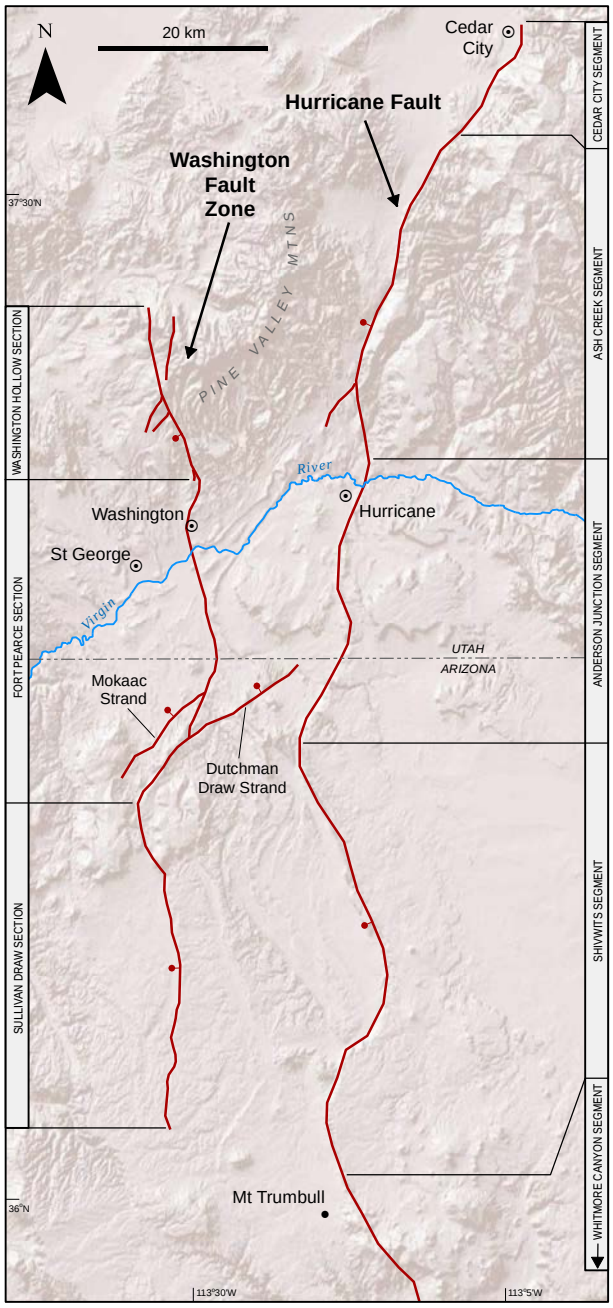

Figure 3. *Sections of the Hurricane and Washington (after Knudsen, this volume) fault zones. Bar and ball on downthrown side of faults. Base map: World Shaded Relief from the ESRI Resource Center.*

1. New information on trace-element and major oxide geochemistry combined with new and existing radiometric flow ages allowed correlation of some mafic volcanic flows across the Washington fault zone in Arizona. Estimates of elevation differences obtained from Google Earth imagery for the correlated flows displaced across the fault, combined with the flow ages, permitted calculation of five vertical slip-rate estimates for the Fort Pearce and Sullivan Draw sections. The estimates include two composite slip rates across the main trace and Mokaac and Dutchman Draw strands of the Fort Pearce section (0.25 and 0.38 mm/yr [only

one correct—see Discussion section]), a slip rate across the main trace of the Fort Pearce section (0.30 mm/yr), a rate for the northern end of the Sullivan Draw section (0.04 mm/yr), and a rate across one splay of the multi-splay Dutchman Draw strand (0.04 mm/yr).

2. The vertical slip-rate estimates do not account for differences in elevation between displaced flow remnants due to pre-faulting topography. In instances where flows traveled long distances downslope following their eruption, the pre-faulting elevation difference between flow remnants may amount to tens of meters. Differences in pre-fault topography would tend to make the vertical slip-rate estimates maximum values. It is unknown if some flows cascaded across pre-existing fault scarps.

3. Timing of the onset of surface faulting following eruption of the volcanic flows is unknown, but is less than the ages of the flows used to make the slip-rate calculations. Therefore, available timing data tend to underestimate slip-rates values. The longer the interval between eruption and onset of faulting, the greater the underestimation of slip rates.

4. Vertical slip-rate estimates determined from displaced volcanic flows along the Fort Pearce section of the Washington fault zone show that the long-term (since the middle Quaternary) vertical slip rate on the Fort Pearce section has likely been ~0.3 mm/yr. The long-term vertical slip-rate estimate for the Fort Pearce section is roughly comparable with the vertical slip rate reported by Amoroso and others (2004) for the Shivwits section of the Hurricane fault, and to late Quaternary slip rates reported by Lund and others (2008) for the Anderson Junction and Ash Creek sections of the Hurricane fault.

ACKNOWLEDGMENTS

We thank Robert Biek, UGS Geologic Mapping Program, for classifying the mafic volcanic rock samples collected along the southern part of the Fort Pearce section and northern end of the Sullivan Draw section, and for preparing the variation diagrams for those rock samples which allowed us to correlate volcanic flows across the Washington fault zone. Careful reviews by Phil Pearthree, Arizona Geological Survey, and Steve Bowman, Utah Geological Survey, greatly improved this report.

REFERENCES

Amoroso, L., Pearthree, P.A., and Arrowsmith, J.R., 2004, Paleoseismology and neotectonics of the Shivwits section of the Hurricane fault, northwestern Arizona: Bulletin of the Seismological Society of America, v. 94, no. 5, p. 1919-1942, doi: 10.1785/012003241.

Billingsley, G.H., and Graham, S.E., 2003, Geologic map of the lower Hurricane Wash and vicinity, Mojave County, northwestern Arizona: U.S. Geological Survey Miscellaneous Field Studies Map 2396, scale 1:31,680.

Billingsley, G.H., and Workman, J.B., 2000, Geologic map of the Littlefield 30′ x 60′ quadrangle, Mojave County, northwestern Arizona: U.S. Geological Survey Geologic Investigations Series Map I-2628, scale 1:100,000.

Downing, R.F., Smith, E.I., Orndorff, R.L., Spell, T.L., and Zanetti, K.A., 2001, Imaging the Colorado Plateau—Basin and Range transition zone using basalt geochemistry, geochronology, and geographic information systems, *in* Erskine, M.C., Faulds, J.E., Bartley, J.M., and Rowley, P.D., editors, The geologic transition, High Plateaus to Great Basin—a symposium and field guide (The Mackin Volume): Utah Geological Association and Pacific Section of the American Association of Petroleum Geologists, Utah Geological Association Publication 30, p. 127–154.

Hamblin, W.K., 1963, Late Cenozoic basalts of the St. George basin, Utah, *in* Heylmun, E.B., editor, Geology of the southwestern transition between the Basin-Range and Colorado Plateau, Utah: Intermountain Association of Petroleum Geologists, Guidebook to the Geology of Southwestern Utah, p. 84–89.

Hamblin, W.K., 1970, Late Cenozoic basalt flows of the western Grand Canyon, *in* Hamblin, W.K., and Best, M.G., editors, The western Grand Canyon region: Utah Geological Society Guidebook to the Geology of Utah, no. 23, p. 21–37.

Hamblin, W.K., and Best, M.G., 1970, Road log, *in* Hamblin, W.K., and Best, M.G., editors, The western Grand Canyon region: Utah Geological Society Guidebook to the Geology of Utah, no. 23, p. 93–153.

LeBas, M.J., LeMaitre, R.W., Streckeisen, A., and Zanettin, B., 1986, A chemical classification of volcanic rocks based on the total alkali-silica diagram: Journal of Petrology, v. 27, p. 745–750.

Lund, W.R., Hozik, M.J., and Hatfield, S.C., 2007, Paleoseismic investigation and long-term slip history of the Hurricane fault in southwestern Utah—Paleoseismology of Utah, Volume 14: Utah Geological Survey Special Study 119, 81 p.

Peterson, S.M., 1983, The tectonics of the Washington fault zone, northern

Mohave County, Arizona: Brigham Young University Geology Studies, v. 30, part 1, p. 83–94.

Wenrich, K.J., Billingsley, G.H., and Blackerby, B.A., 1995, Spatial migration and compositional changes of Miocene-Quaternary magmatism in the western Grand Canyon: Journal of Geophysical Research, v. 100, p. 10,417–10,440.

APPENDICES

APPENDIX A

GEOCHEMICAL ANALYSES OF MAFIC VOLCANIC ROCK SAMPLES FROM THE FOOTWALL AND HANGING WALL OF THE WASHINGTON FAULT ZONE, MOHAVE COUNTY, ARIZONA

Analyses performed in 2012

by the

GeoAnalytical Laboratory at Washington State University

See figure 1 for sample locations

Geochemical analysis as reported by the GeoAnalytical Laboratory at Washington State University. (http://www.sees.wsu.edu/Geolab/index.html)

OXIDE/ELEMENT	SAMPLES							
	LBM	DD1	DD2	EM	WM	QD1	SF	QD2
Unnormalized Major Elements (Weight %)								
SiO_2	46.55	48.00	48.74	49.39	49.30	49.18	49.41	49.35
TiO_2	2.063	2.012	1.772	1.965	2.071	1.775	1.591	1.717
Al_2O_3	12.06	16.58	15.75	17.92	17.50	16.06	15.70	14.20
FeO*	10.93	9.40	11.11	9.27	9.60	9.69	11.26	10.47
MnO	0.181	0.152	0.172	0.157	0.155	0.163	0.176	0.173
MgO	12.57	5.15	7.88	4.56	4.76	7.33	8.11	9.74
CaO	10.29	9.77	8.79	9.05	8.90	9.10	8.86	10.09
Na_2O	2.71	3.57	3.42	3.58	4.26	3.93	3.44	2.97
K2O	1.35	1.98	1.30	2.12	2.21	1.71	1.04	1.13
P_2O_5	0.502	0.712	0.441	0.694	0.778	0.555	0.357	0.392
Sum	99.21	97.33	99.38	98.71	99.54	99.48	99.94	100.24
SO_3 >/=	0.00	0.17	0.06	0.00	0.00	0.01	0.00	0.00
Normalized Major Elements (Weight %)								
SiO_2	46.92	49.32	49.04	50.03	49.53	49.43	49.44	49.23
TiO_2	2.079	2.068	1.783	1.991	2.080	1.784	1.592	1.713
Al_2O_3	12.15	17.04	15.85	18.16	17.58	16.14	15.71	14.17
FeO*	11.02	9.66	11.18	9.39	9.64	9.74	11.27	10.44
MnO	0.183	0.156	0.173	0.159	0.155	0.164	0.176	0.173
MgO	12.67	5.29	7.93	4.62	4.79	7.37	8.11	9.72
CaO	10.38	10.04	8.85	9.17	8.94	9.14	8.86	10.07
Na_2O	2.74	3.67	3.44	3.63	4.27	3.95	3.44	2.96
K_2O	1.37	2.03	1.31	2.15	2.22	1.72	1.04	1.13
P_2O_5	0.506	0.732	0.444	0.703	0.781	0.558	0.357	0.392
Total	100.00	100.00	100.00	100.00	100.00	100.00	100.00	100.00
Unnormalized Trace Elements (ppm)								
Ni	358	46	150	14	27	95	142	160
Cr	736	80	250	11	23	276	304	597
Sc	28	23	23	22	22	25	26	29
V	245	202	202	211	206	211	207	238
Ba	705	1057	749	688	780	619	789	626
Rb	24	24	14	24	26	18	13	19
Sr	591	930	609	902	940	750	480	469
Zr	190	234	167	239	251	213	142	159
Y	23	25	22	26	26	22	22	24
Nb	49.2	42.0	29.9	46.3	45.6	45.0	22.8	32.3
Ga	17	22	21	21	22	21	21	18
Cu	91	41	67	38	41	67	60	77
Zn	94	93	109	90	97	95	105	90
Pb	5	6	5	8	7	8	4	5
La	40	45	26	48	49	39	23	32
Ce	74	90	53	80	98	78	51	59
Th	5	5	3	7	6	6	4	5
Nd	32	42	24	36	45	31	22	25
U	3	2	2	1	2	2	3	2
sum tr.	3308	3008	2527	2510	2712	2620	2441	2666
in %	0.33	0.30	0.25	0.25	0.27	0.26	0.24	0.27

sum m+tr	99.54	97.63	99.63	98.96	99.81	99.75	100.18	100.50
M+Toxides	99.64	97.69	99.69	99.02	99.87	99.81	100.24	100.58
*Major elements are normalized on a volatile-free basis, with total Fe expressed as FeO.								
NiO	455.3	58.2	191.4	17.8	34.5	120.5	181.1	203.7
Cr_2O_3	1076.2	116.5	365.0	15.8	33.2	404.0	443.9	873.1
Sc_2O_3	42.9	34.7	35.1	34.4	33.7	37.7	39.7	44.5
V_2O_3	359.7	297.2	297.6	310.7	302.9	310.3	304.2	349.4
BaO	786.7	1180.0	836.3	767.7	870.4	690.6	880.6	698.9
Rb_2O	26.2	25.7	15.1	26.4	28.0	19.2	14.4	20.8
SrO	698.4	1099.5	720.6	1066.6	1111.5	886.5	568.0	554.5
ZrO_2	256.0	316.6	225.6	322.2	339.2	287.3	192.1	214.6
$Y2O_3$	29.2	32.1	28.1	32.4	32.5	28.3	28.1	30.1
Nb_2O_5	70.4	60.1	42.8	66.2	65.2	64.4	32.6	46.2
Ga_2O_3	23.4	29.6	28.0	27.6	29.8	28.8	27.7	24.6
CuO	114.4	50.8	84.1	46.9	51.4	83.7	75.6	96.1
ZnO	117.4	117.0	136.9	112.1	121.7	118.7	131.9	113.1
PbO	5.1	6.4	5.6	8.2	7.3	8.1	4.5	5.2
La_2O_3	46.8	52.8	30.8	55.8	57.7	46.2	26.9	37.1
CeO_2	91.3	110.3	64.5	98.5	120.7	96.3	62.7	72.9
ThO_2	5.2	6.0	3.4	7.6	6.1	7.1	4.0	6.0
Nd_2O_3	36.7	49.1	27.8	42.5	51.9	36.2	25.8	28.8
U_2O_3	3.3	1.8	2.3	1.3	2.1	2.2	2.8	2.1
Cs_2O	0.0	0.0	0.0	0.0	0.0	0.0	0.0	0.0
As_2O_5	0.0	0.0	0.0	0.0	0.0	0.0	0.0	0.0
W_2O_3	0.0	0.0	0.0	0.0	0.0	0.0	0.0	0.0
sum tr.	4245	3644	3141	3061	3300	3276	3046	3422
in %	0.42	0.36	0.31	0.31	0.33	0.33	0.30	0.34

APPENDIX B

VARIATION DIAGRAMS FOR MAFIC VOLCANIC ROCK SAMPLES FROM THE FOOTWALL AND HANGING WALL OF THE WASHINGTON FAULT ZONE, MOHAVE COUNTY, ARIZONA

(Diagrams prepared by R.F. Biek, UGS, 2012 using IgPet software by Terra Soft, Inc.)

See figure 1 for sample locations

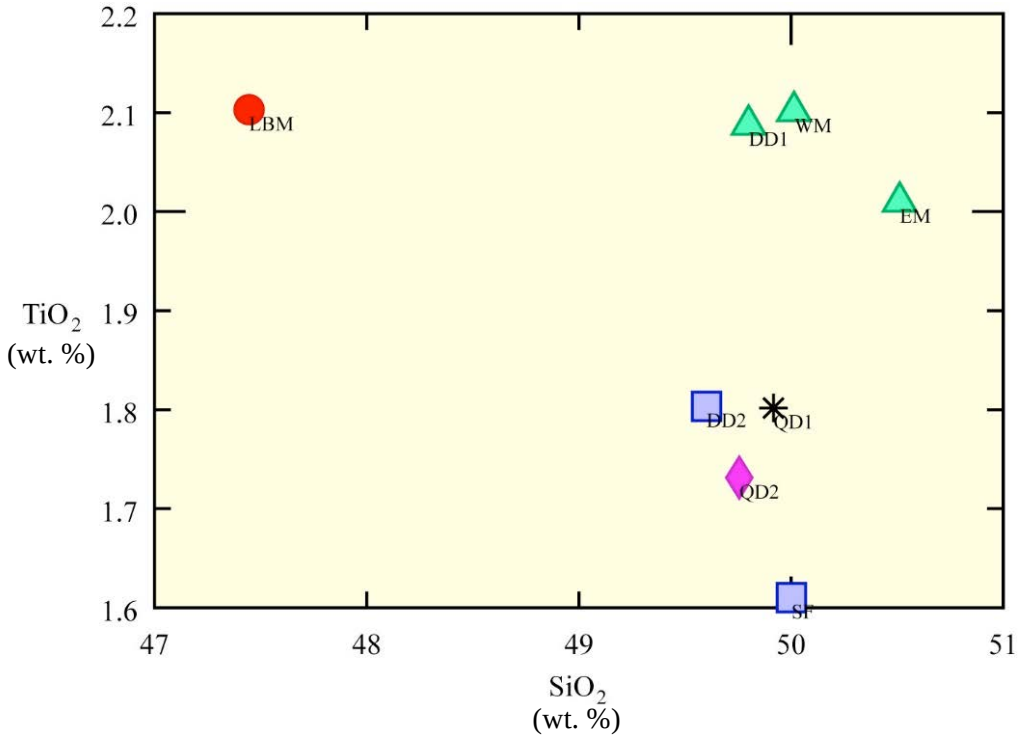
2.2
2.1
2.0
1.9
1.8
1.7
1.6
TiO2 (wt. %)
47
48
49
50
51
SiO2 (wt. %)
LBM
DD1
WM
EM
DD2
QD1
QD2
SF

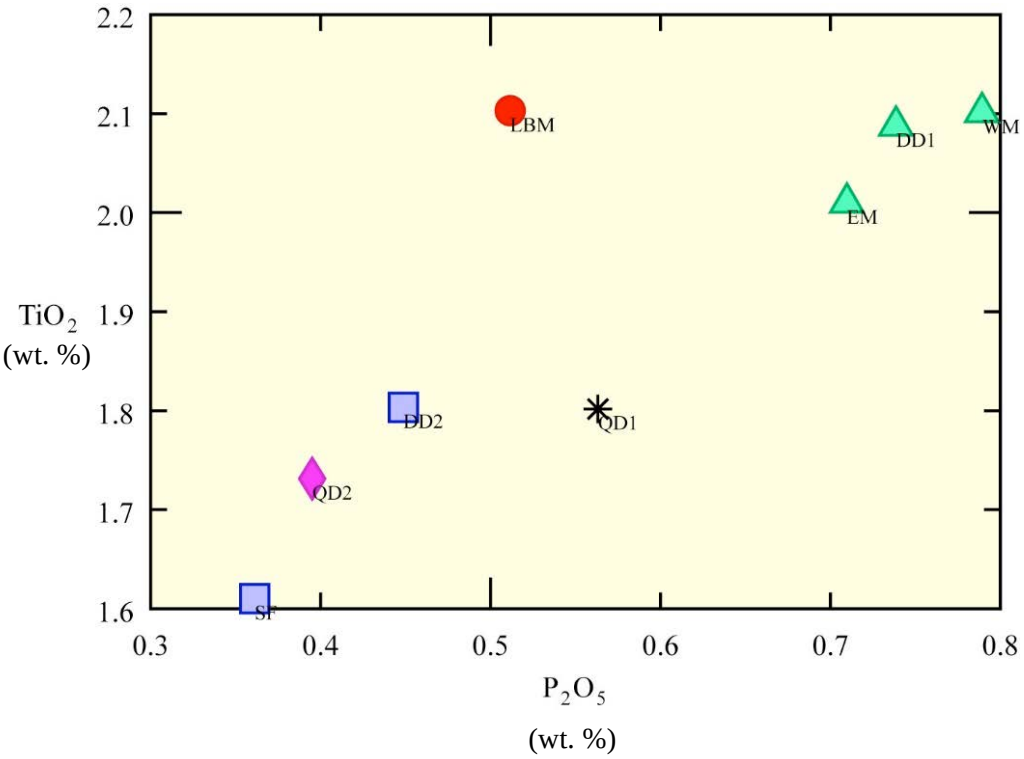
2.2
2.1
2.0
1.9
1.8
1.7
1.6
TiO2 (wt. %)
0.3
0.4
0.5
0.6
0.7
0.8
P2O5 (wt. %)
LBM
DD1
WM
EM
DD2
QD1
QD2
SF

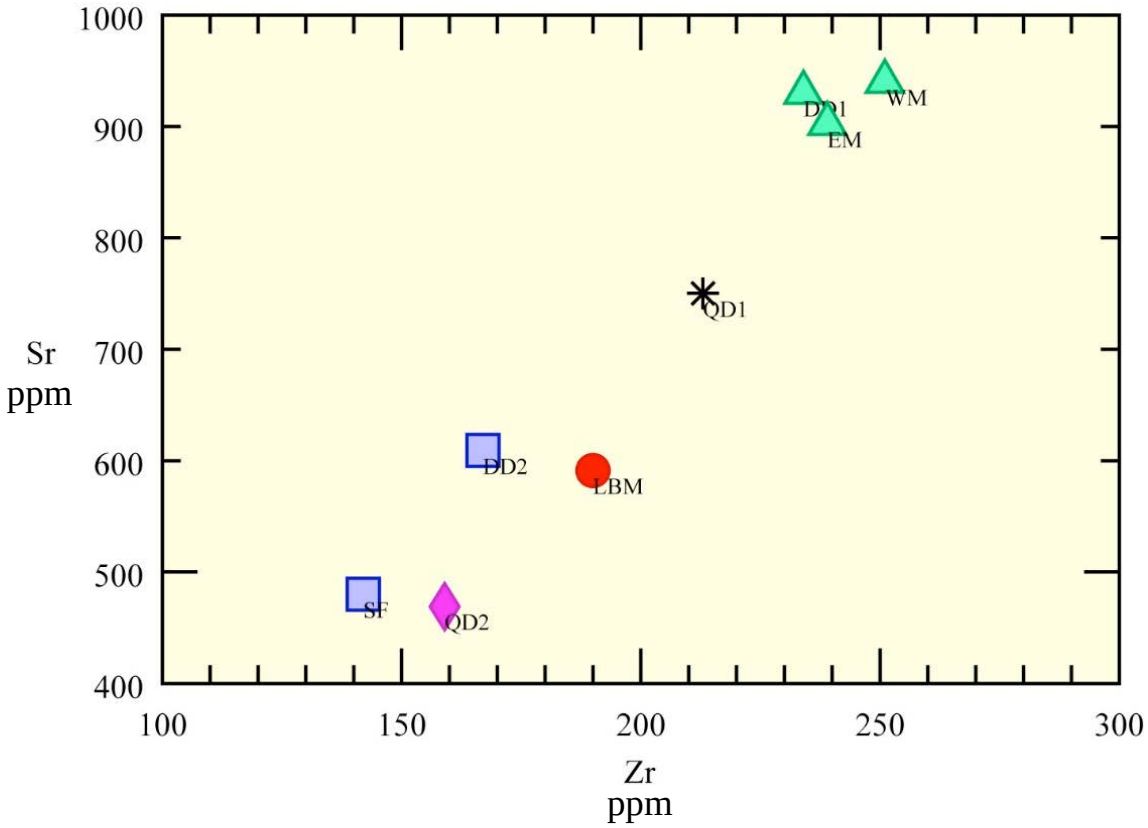
1000
900
800
700
600
500
400
Sr
ppm
100
150
200
250
300
Zr
ppm
WM
DD1
EM
QD1
DD2
LBM
SF
QD2

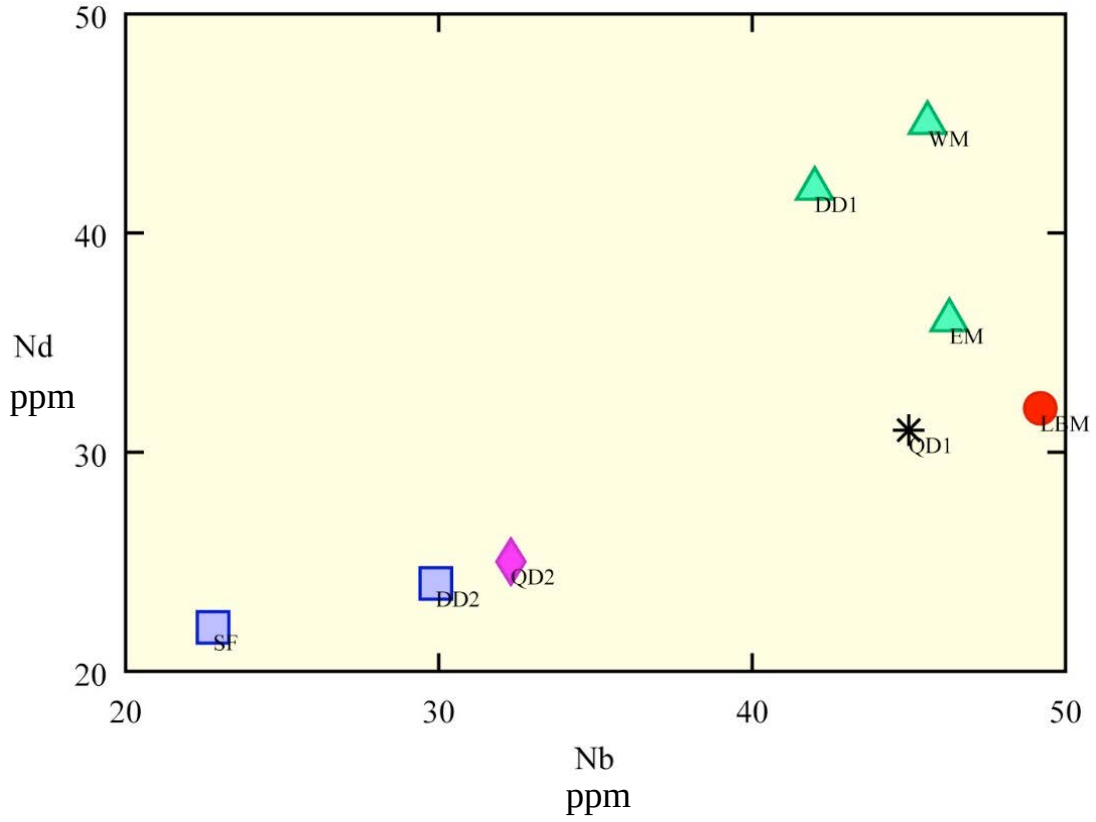
50
40
30
20
Nd
ppm
20
30
40
50
Nb
ppm
WM
DD1
EM
LBM
QD1
QD2
DD2
SF

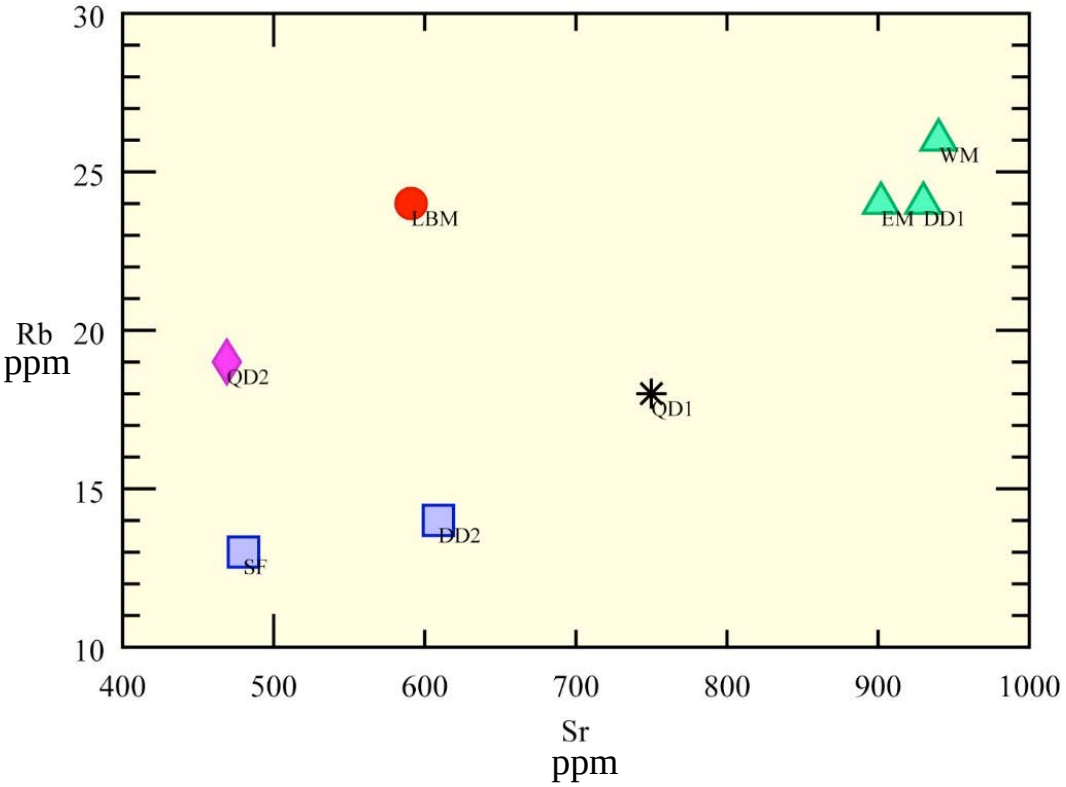
30
25
20
15
10
Rb
ppm
400
500
600
700
800
900
1000
Sr
ppm
WM
LBM
EM
DD1
QD2
QD1
DD2
SF

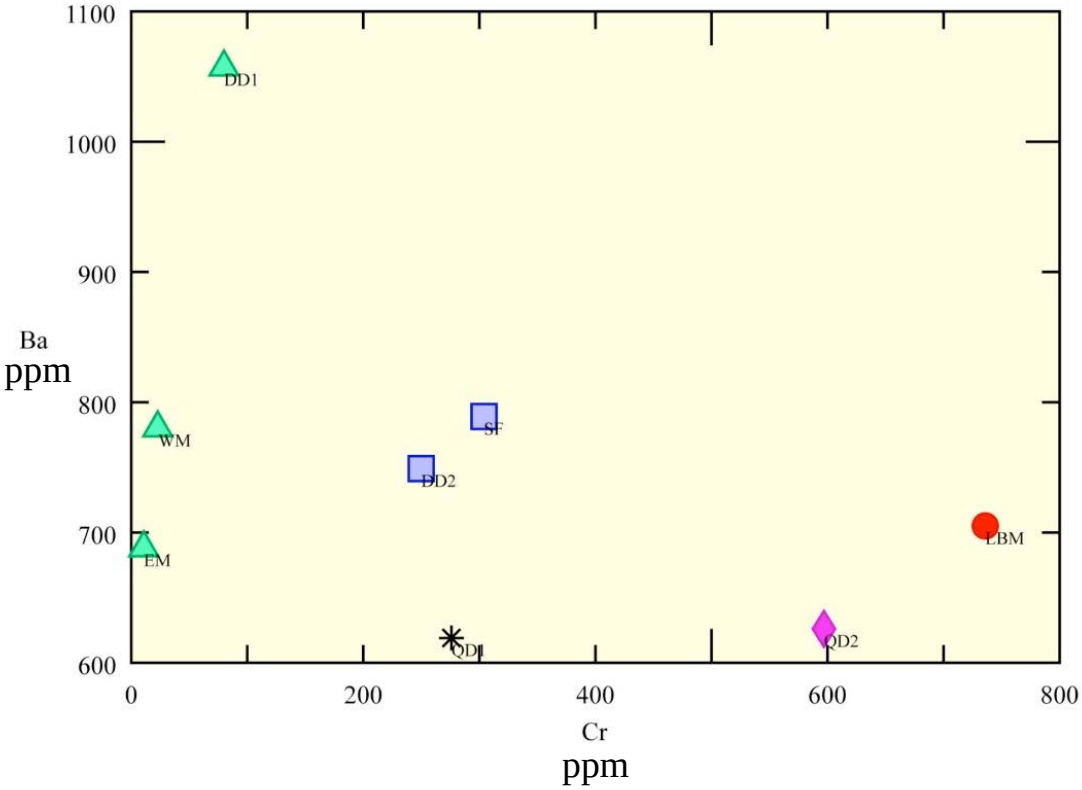
1100
1000
900
800
700
600
Ba
ppm
0
200
400
600
800
Cr
ppm
DD1
WM
SF
DD2
EM
LBM
QD2
QD1

APPENDIX C

$^{40}AR/^{39}AR$ RADIOMETRIC AGES FOR MAFIC VOLCANIC ROCK SAMPLES FROM THE FOOTWALL AND HANGING WALL OF THE WASHINGTON FAULT ZONE, MOHAVE COUNTY, ARIZONA

Analyses performed in 2012

by the

New Mexico Geochronology Research Laboratory

at the

New Mexico Institute of Mining and Technology

See figure 1 for sample locations

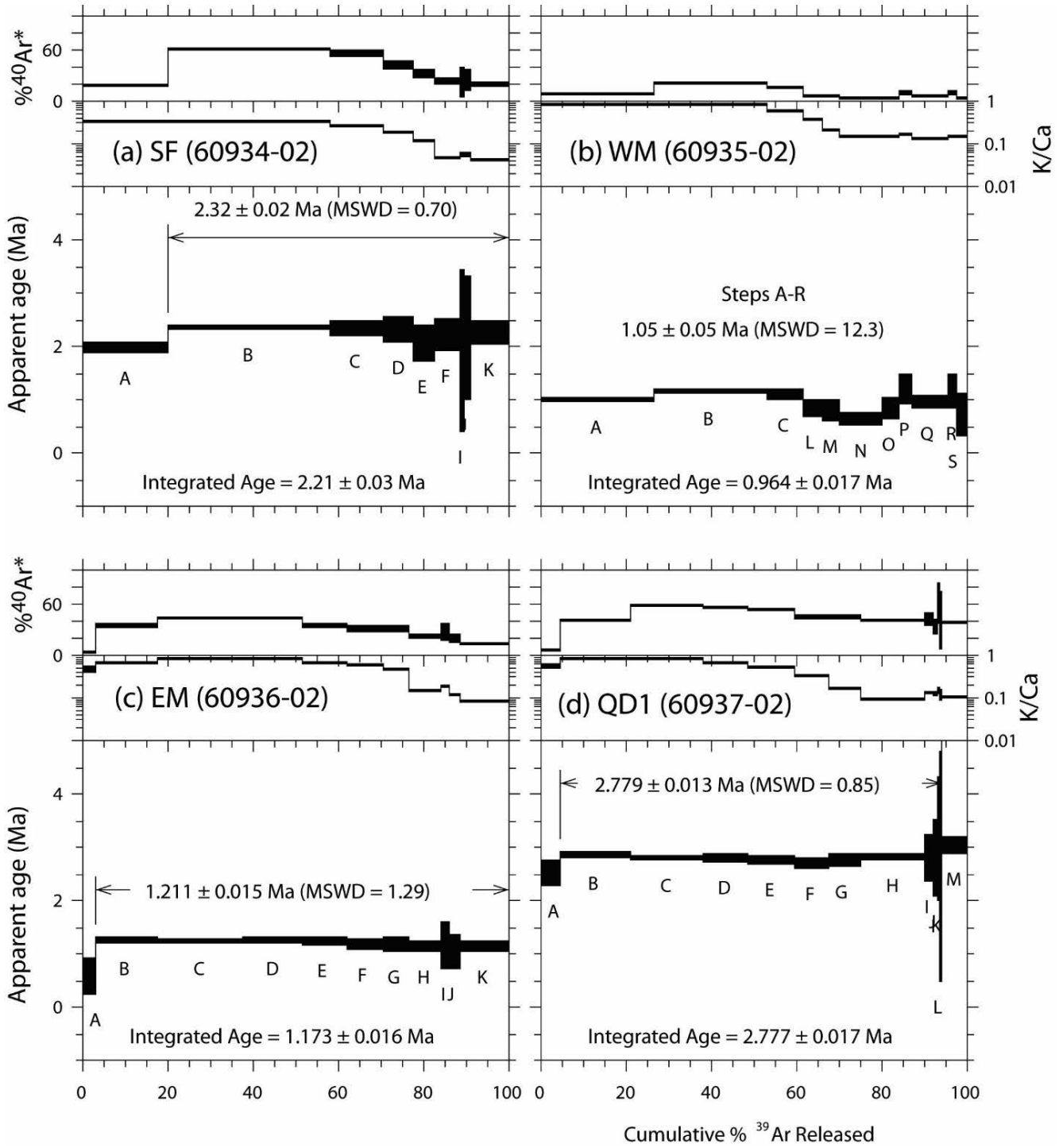

Weighted mean (plateau) ages are between arrows (ages reported in text for dated volcanic flows). The integrated age represents the equivalent age expected from conventional K/Ar dating.

SURFACE-FAULT-RUPTURE-HAZARD INVESTIGATION FOR A PORTION OF THE SOUTHERN PARKWAY (STATE ROUTE 7) NORTHERN EXTENSION, FORT PEARCE SECTION, WASHINGTON FAULT ZONE, WASHINGTON COUNTY, UTAH

by

David B. Simon[1], David R. Black[2], Jonathan R. Hanson[2], and Peter D. Rowley[3]

[1]Simon Associates, LLC., Salt Lake City, Utah
(formerly Simon-Bymaster, Inc.)
[2]Rosenberg Associates, Inc., St. George, Utah
[3]Geologic Mapping, Inc., New Harmony, Utah

This report is the work of non-UGS authors. Although review comments have been incorporated, this document does not conform to UGS technical, editorial, or policy standards. The Utah Department of Natural Resources, Utah Geological Survey, makes no warranty, expressed or implied, regarding the suitability of this product for a particular use. The Utah Department of Natural Resources, Utah Geological Survey, shall not be liable under any circumstances for any direct, indirect, special, incidental, or consequential damages with respect to claims by users of this product.

This report is part of Utah Geological Survey Miscellaneous Publication 15-6, *Surficial Geologic Mapping and Paleoseismic Investigations of the Washington Fault Zone, Washington County, Utah, and Mohave County, Arizona*—Paleoseismology of Utah, Volume 27.

Bibliographic citation for this chapter: Simon, D.B., Black, D.K., Hanson, J.R., and Rowley, P.D., 2015, Surface-fault-rupture-hazard investigation for a portion of the Southern Parkway (State Route 7) northern extension, Fort Pearce section, Washington fault zone, Washington County, Utah, *in* Lund, W.R., editor, 2015,Surficial geologic mapping and paleoseismic investigations of the Washington fault zone, Washington County, Utah, and Mohave County, Arizona—Paleoseismology of Utah, Volume 27: Utah Geological Survey Miscellaneous Publication 15-6, p. 117–184., 14 plates, CD.

CONTENTS

ABSTRACT 111
INTRODUCTION 111
GEOLOGIC SETTING 112
INVESTIGATIVE METHODS 113
Task 1 – Geologic Mapping 113
Task 2 – Literature Review 113
Task 3 – Evaluation of Aerial Photographs 113
Task 4 – Field Reconnaissance 113
Task 5 – Subsurface Exploration 113
GENERAL SITE CONDITIONS 118
GEOLOGY 118
LINEAMENT ANALYSIS 118
Lineaments L-1 and L-2 118
Lineament L-3 119
Lineament L-4 119
SUBSURFACE EXPLORATION 120
FAULTING 120
Trench T-1 120
Trench T-1 Earthquake Timing 122
Trench T-1 Radiocarbon Ages 122
Trench T-1 OSL Ages 122
Trench T-1 Summary – Earthquake Timing 122
Trench T-2 123
Trench T-3 124
Trench T-4 124
Trench T-4 Radiocarbon Ages 124
Trench T-4 OSL Ages 124
Trench T-4 Summary – Earthquake Timing 125
Trench T-5 125
Trench T-5 Anthropologic Hearth 125
Trench T-5 Radiocarbon Ages 125
Trench T-5 OSL Ages 126
Trench T-6 126
Trench T-7 127
Trench T-8 127
Trenches T-9 and T-10 128
Trench T-11 128
Trench T-12 128
Trench T-13 128
Washington Fields Trench WFT-1 128
WFT-1 General 128
WFT-1 Radiocarbon Ages 129
WFT-1 OSL Ages 129
Trench WFT-1 – Summary 129
INVESTIGATION RESULTS 130
ACKNOWLEDGMENTS 131
REFERENCES 131
APPENDICES 133
Appendix A PaleoResearch Institute Report – Organic Recovery and AMS Dates for the Washington Fault, Phase III Corridor Project, Southern Utah 134
Appendix B Utah State University Luminescence Laboratory Final OSL Age Report 153
Appendix C Western GeoArch Research Ages – Trench T-5 159

FIGURES

Figure 1. Location of proposed transportation corridor and study area 112
Figure 2. Surface-fault-rupture-hazard special study area map 112
Figure 3. Geologic map index 114
Figure 4. Geologic map legend 114
Figure 5. Geologic map of the north part of the study area 115
Figure 6. Geologic map of the center part of the study area 116
Figure 7. Geologic map of the south part of the study area 117
Figure 8. Lineaments identified from aerial photographs and topographic maps 119
Figure 9. Displacement within trench WFT-1 130

TABLES

Table 1. Aerial photographs examined for this investigation 118
Table 2. Site geologic units 118
Table 3. Purpose of trenches 121
Table 4. Summary of trench data 121
Table 5. Displacements per surface-faulting earthquake 122
Table 6. Trench T-1 AMS radiocarbon ages 123
Table 7. Trench T-1 OSL ages 123
Table 8. Displacements for faults f1-f5 in trench T-4 125
Table 9. Displacements for faults f6-f7 in trench T-4 125
Table 10. Trench T-4 OSL ages 125
Table 11. Trench T-5 radiocarbon ages 126
Table 12. Trench T-5 OSL ages 127
Table 13. Trench WFT-1 radiocarbon ages 129
Table 14. Trench WFT-1 OSL ages 129

PLATES

Plate 1. T-1 trench log 163
Plate 2. T-2 trench log 164
Plate 3. T-3 trench log 165
Plate 4. T-4 trench log 166
Plate 5. T-5 trench log 167
Plate 6. T-6 trench log 168
Plate 7. T-7 trench log 169
Plate 8. T-8 trench log 170
Plate 9. T-9 trench log 171
Plate 10. T-10 trench log 172
Plate 11. T-11 trench log 173
Plate 12. T-12 trench log 174
Plate 13. T-13 trench log 175
Plate 14. WFT-1 trench log 176

SURFACE-FAULT-RUPTURE-HAZARD INVESTIGATION FOR A PORTION OF THE SOUTHERN PARKWAY (STATE ROUTE 7) NORTHERN EXTENSION, FORT PEARCE SECTION, WASHINGTON FAULT ZONE, WASHINGTON COUNTY, UTAH

by David B. Simon, David R. Black, Jonathan R. Hanson, and Peter D. Rowley

ABSTRACT

The Fort Pearce section of the Washington fault zone is well documented within the study area and exhibits geomorphology suggestive of Holocene-age surface faulting. About 2.2 miles (3.5 km) of the proposed Utah Department of Transportation (UDOT) Southern Parkway (State Route 7) transportation corridor closely parallels the Washington fault zone. The purpose of this investigation was to (1) characterize past surface faulting within the study area, and (2) utilize the history of past surface-faulting as a scientific basis for providing engineering geologic recommendations to UDOT to mitigate impacts of future surface faulting on the transportation corridor.

The purposes of the engineering geologic recommendations were to (1) protect public health, safety, and welfare from future surface faulting on the Washington fault zone, and (2) minimize placement of the transportation corridor along identified Holocene fault traces to reduce damage to three proposed elevated interchange structures from future surface-faulting earthquakes.

Faults documented during this investigation were complex, consisting of multiple strands, areas of upward-diverging fault splays, and areas of local thrusting. Results of the subsurface exploration indicate the faults documented in the study area are Holocene-age; therefore, the faults were considered "active" for the purpose of siting the elevated interchanges associated with the proposed transportation corridor.

We documented multiple surface-faulting earthquakes during this investigation. As many as five surface-faulting earthquakes over the past 67,750 ± 4560 yr years have produced at least 23 feet (7 m) of cumulative displacement, resulting in a slip rate over that time period of about 0.004 in/yr (0.1 mm/yr). Average displacement per surface-faulting earthquake is about 4.3 feet (1.3 m).

Some faults documented during this investigation have evidence for Holocene displacement that appears to correlate with the P1 (1000 ± 600 cal yr B.P.) and P2 (7700 ± 2400 cal yr B.P.) earthquakes documented during the Dutchman Draw, Arizona, paleoseismic investigation conducted by the Utah Geological Survey near the south end of the Fort Pearce section of the Washington fault zone.

Due to the proximity to Holocene-age faulting, two proposed interchange structures were relocated in accordance with building setback criteria previously established by the Utah Geological Survey. Where feasible, proposed roadway crossings of Holocene-age faults will be near perpendicular.

INTRODUCTION

This report presents the findings of an engineering geology consultant's surface-fault-rupture-hazard investigation of a portion of the Holocene-active (Lund and others, this volume) Fort Pearce section of the Washington fault zone, performed for the Utah Department of Transportation (UDOT) Southern Parkway (State Route [SR] 7) northern extension project in the St. George metropolitan area, Washington County, Utah. The 3.8-mile-long (6.1 km) transportation corridor extends from the existing terminus of the Southern Parkway at Airport Parkway (road to St. George Airport), north to Washington Dam Road (figure 1), and includes three elevated interchanges: one near the south end of the transportation corridor, one near the central part of the corridor at Warner Valley Road, and the third near the northern part of the transportation corridor.

The proposed transportation corridor closely parallels the Washington fault zone for approximately 2.2 miles (3.5 km), a distance that includes the proposed central and northern interchanges. The center and north interchanges and the transportation corridor right of way lie within a surface-faulting-special-study zone established by Lund and others (2007) for the Washington fault (figure 2).

The purpose of this investigation was to (1) characterize past surface faulting within the study area, and (2) use the history of past surface-faulting as a scientific basis for providing engineering geologic recommendations to UDOT to mitigate the impact of future surface faulting on the transportation corridor.

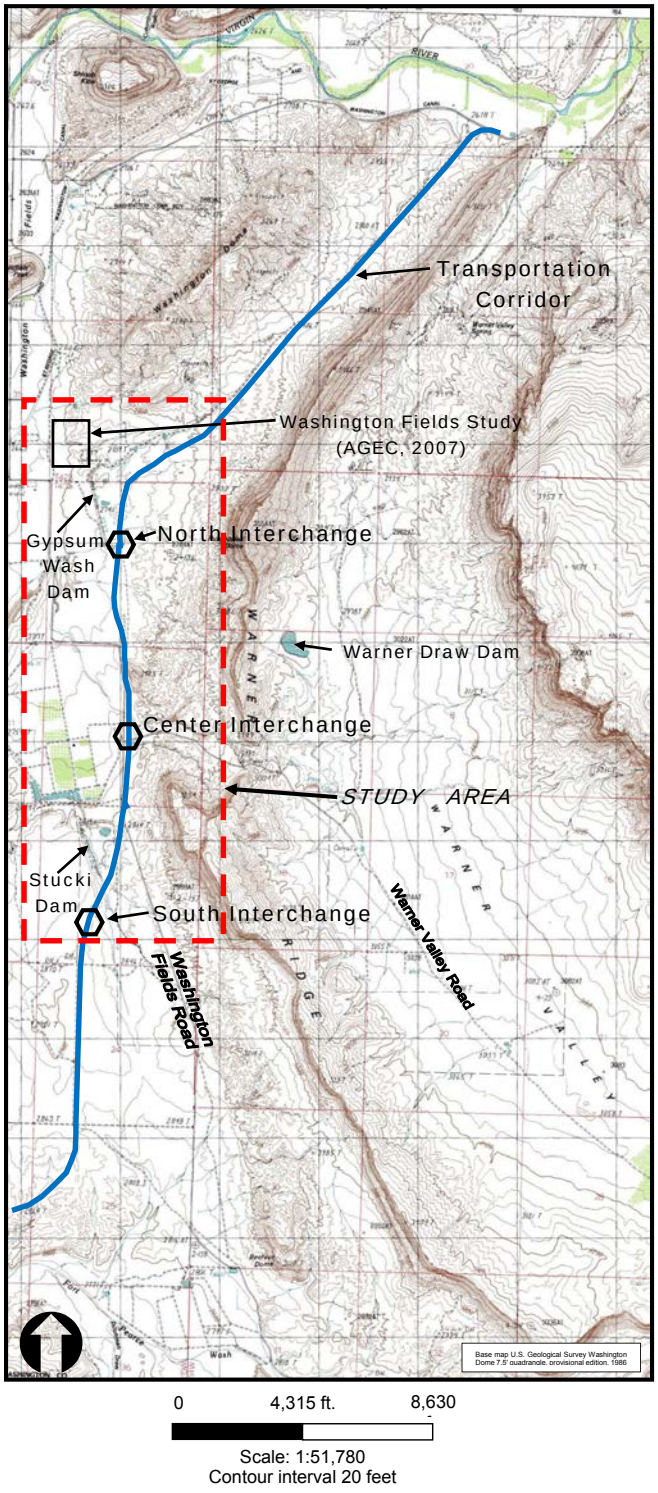

Figure 1. *Location of proposed transportation corridor and study area.*

The purposes of the engineering geologic recommendations were to (1) protect public health, safety, and welfare from future surface faulting on the Washington fault zone, and (2) minimize placement of the transportation corridor along identified Holocene fault traces to reduce damage to three proposed elevated interchange structures from future surface-faulting earthquakes.

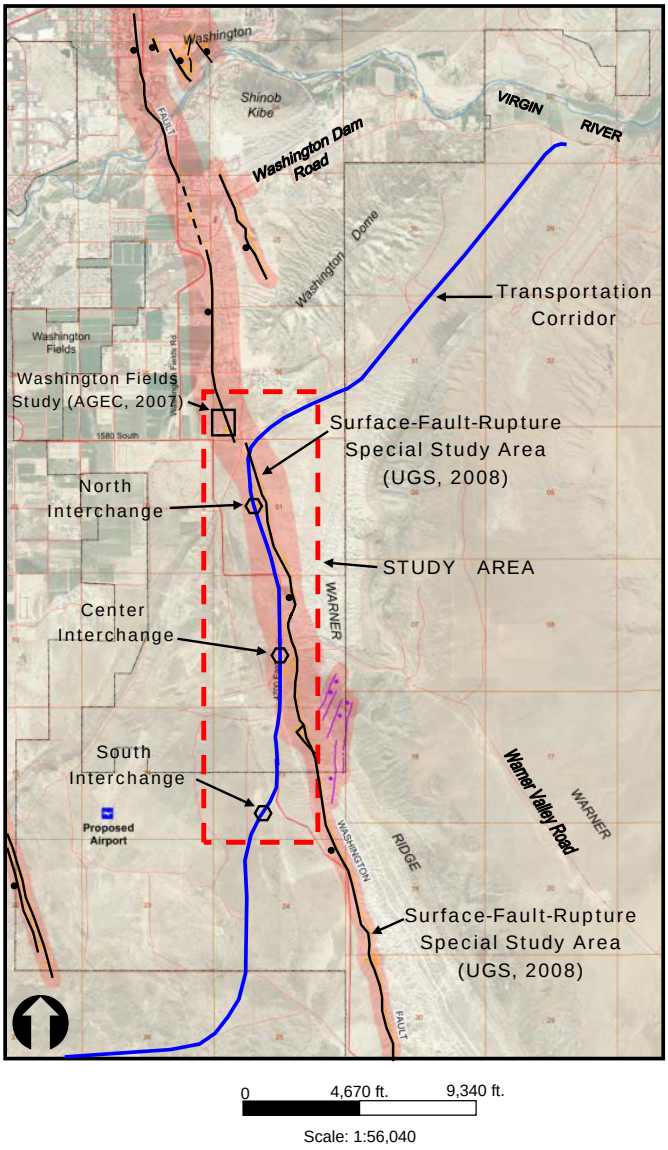

Figure 2. *Surface-fault-rupture hazard special study area map (modified from Lund and others, 2008).*

This report focuses on the geologic and paleoseismic aspects of the investigation, and does not present or discuss the engineering geologic design recommendations provided to UDOT, which included structural setbacks from the Washington fault zone and a recommendation to relocate the central and northern interchange structures.

GEOLOGIC SETTING

The Washington fault zone is one of several north-south trending, down-to-the-west Quaternary normal faults in the structural and seismic transition between the Colorado Plateau and Basin and Range physiographic provinces in northern Arizona and southwestern Utah. Based on structural, geologic, and geomorphic criteria, Knudsen (this volume) subdivided the Washington fault zone in Utah from north to

south into the Washington Hollow, Fort Pearce, and Sullivan Draw sections.

The Fort Pearce section extends for about 23 miles (37 km) from near Washington City in southwestern Utah to the southern margin of the St. George basin in northwestern Arizona (Knudsen, this volume), and includes the study area of this investigation. Scarps formed on unconsolidated basin-fill deposits and soft bedrock are evidence of late Quaternary surface faulting (Lund and others, this volume). Because the geomorphology of the St. George basin is dominated by erosion, fault scarps on unconsolidated deposits are rare and isolated. Many scarps on unconsolidated deposits along the Fort Pearce section in Utah and Arizona appear to be bedrock cored (Knudsen, this volume).

Lund and others (this volume) conducted a detailed paleoseismic investigation near the south end of the Fort Pearce section at the Dutchman Draw site, Arizona, about 6 miles (10 km) south of this study area. Paleoearthquake timing at Dutchman Draw was constrained, by a combination of radiocarbon (^{14}C) and optically stimulated luminescence (OSL) ages, to the Holocene: one earthquake at about 7700 ± 2400 cal yr B.P. (penultimate or P2 earthquake) and a second earthquake at about 1000 ± 600 cal yr B.P. (most recent or P1 earthquake). Additionally, the trenches revealed indirect stratigraphic evidence permissive of, but not conclusive for, a third older earthquake (P3) that may have occurred between 13.8 ± 1.18 and 17.1 ± 1.38 ka (Lund and others, this volume).

More detailed geologic overviews of the Washington fault zone, including the physiographic and seismic setting and fault zone characteristics, are provided by Hayden (2005), Lund and others (2008), Rosenberg Associates (2009), Knudsen (this volume), and Lund and others (this volume).

INVESTIGATIVE METHODS

This investigation consisted of five principal tasks.

Task 1 – Geologic Mapping

Rosenberg Associates (2009) prepared a geologic strip map for the proposed corridor (figures 3–7). The map served as a geologic base map for the study area, and was used to develop a surface-fault-rupture-hazard investigation for the proposed transportation corridor and raised interchange structures.

Task 2 – Literature Review

We reviewed available published geologic literature concerning rock units, faulting, and seismicity in the area. In addition to published literature, unpublished technical reports addressing surface faulting were reviewed for the northern part of the study area in the Washington Fields area (Applied Geotechnical Engineering Consultants [AGEC], 2007), and for flood-retention structures near the north/north-central parts of the transportation corridor (Earth Sciences Associates [ESA], 1982, 1983; see also Bowman and others, 2011).

In 2007, AGEC performed a surface-fault-rupture-hazard investigation in the Washington Fields area in the north part of the study area (figure 1). The AGEC (2007) investigation included excavating five trenches to identify the main trace of the Washington fault zone. AGEC located the main trace of the fault zone and concluded there was displacement of Holocene-age geologic units.

In 1982, ESA (1982, 1983) conducted a seismic safety investigation of eight dams in southwest Utah. Two of the dams, Gypsum Wash and Stucki Dams, are within the study area (figure 1). Trenches excavated near the southwest corner of Gypsum Wash Dam exposed offsets in "young-appearing" sedimentary deposits that were estimated by ESA, based on soil morphology, to be Holocene-age. Using soil morphology, the ESA (1982) investigation assigned an age of 1000 to 1500 years to the youngest alluvium and a late Pleistocene age of 10,000 to 25,000 years to older alluvial-fan sediments. ESA (1982) concluded there was no potential for surface-fault offset at Stucki Dam. At Gypsum Wash Dam, ESA (1983) concluded there was direct evidence of 2 inches (~5 cm) of displacement during the past 1500 years and 4 or more feet (~1.2 m) during what was estimated to be the past 10,000 to 25,000 years.

Task 3 – Evaluation of Aerial Photographs

We examined two sets of stereoscopic aerial photographs of the study area for photo lineaments which might indicate surface faulting (table 1).

Task 4 – Field Reconnaissance

We performed a field reconnaissance of the study area to document evidence of surface faulting and evaluate geologic units and pertinent surface features. Data generated during the field reconnaissance was incorporated in the Task 1 geologic maps.

Task 5 – Subsurface Exploration

We excavated thirteen trenches to evaluate subsurface deposits for the presence of faulting. Trench locations are shown on figures 5–7. The trenches, totaling about 3600 feet (1100 m) in length, were excavated by a track-mounted excavator with a 3-foot-wide (90 cm) bucket to depths up to 15 feet (4.6 m) below existing ground surface. Following excavation, trenches were logged and surveyed to a horizontal accuracy of about one inch (~2.5 cm) by Utah licensed professional surveyors (Rosenberg Associates, St. George, Utah).

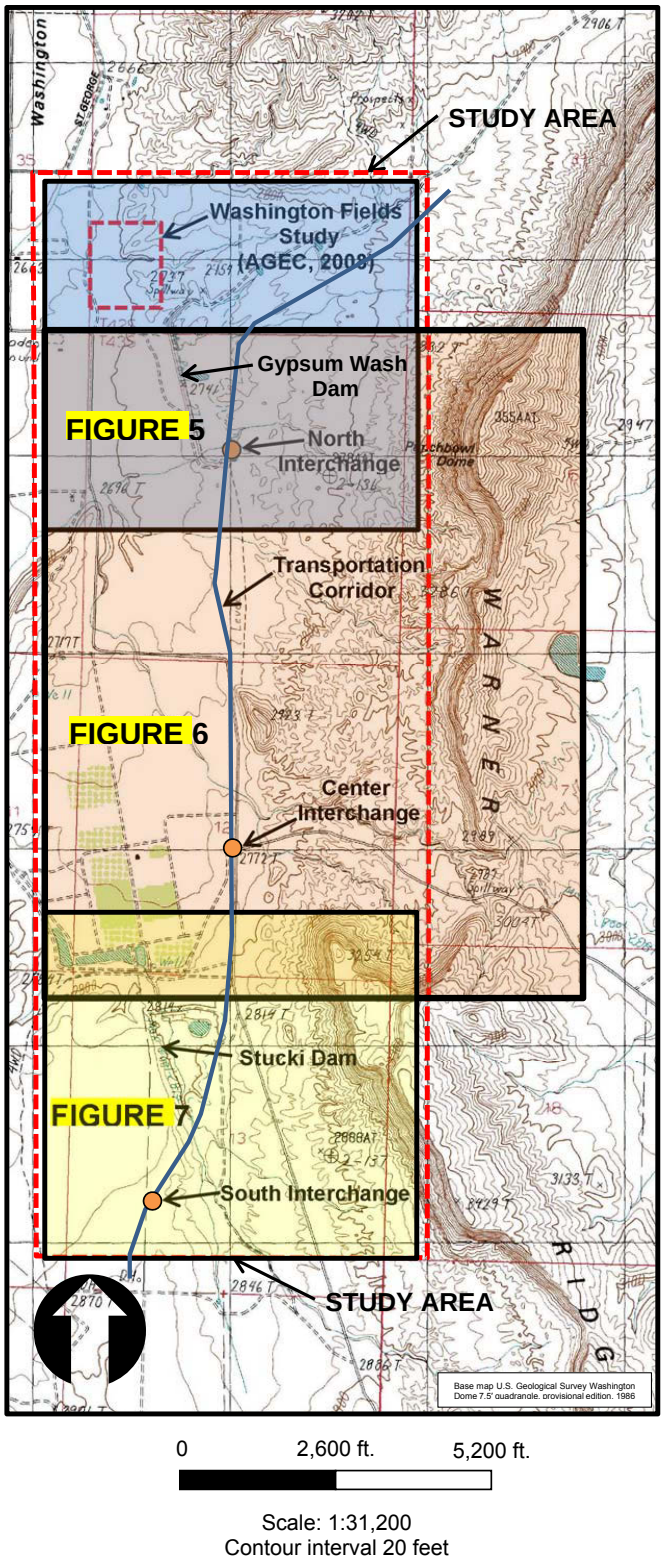

Figure 3. *Geologic map index.*

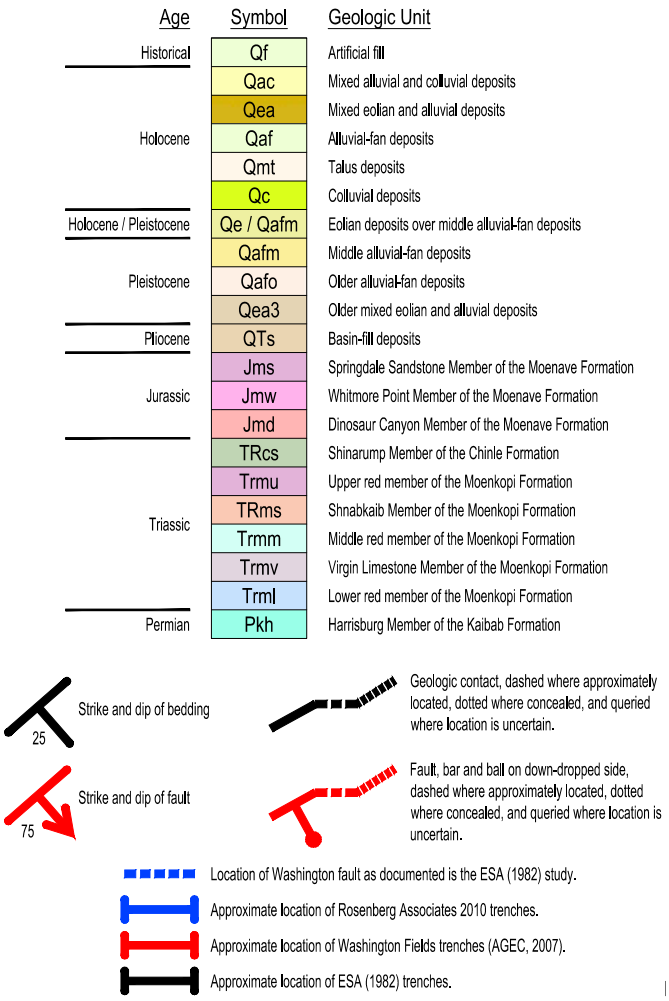

Figure 4. *Geologic map legend.*

The AGEC (2007) surface-fault-rupture hazard investigation in the Washington Fields area (figure 1) included excavating five trenches to locate the main trace of the Washington fault zone. In trench WFT-1 (north wall), AGEC (2007) documented a 13-foot-wide (3.9 m) fault zone consisting of at least three west-dipping faults. The Utah Geological Survey (UGS) (Lund and others, 2008) conducted a reconnaissance-level investigation of the trench and exposed faults in the north wall of the trench and reported the following:

1. Colluvial-wedge deposits provided evidence for at least three surface-faulting earthquakes that displaced mixed alluvial-colluvial-eolian deposits from about 1 foot (~0.3 m) to just less than 3.2 feet (1 m).

2. The most recent earthquake displaced a buried organic soil horizon (Bkb) and an overlying weakly indurated sand deposit.

3. One fault strand extended to within 10 inches (25 cm) of the existing ground surface, where it was buried by a modern eolian sand deposit.

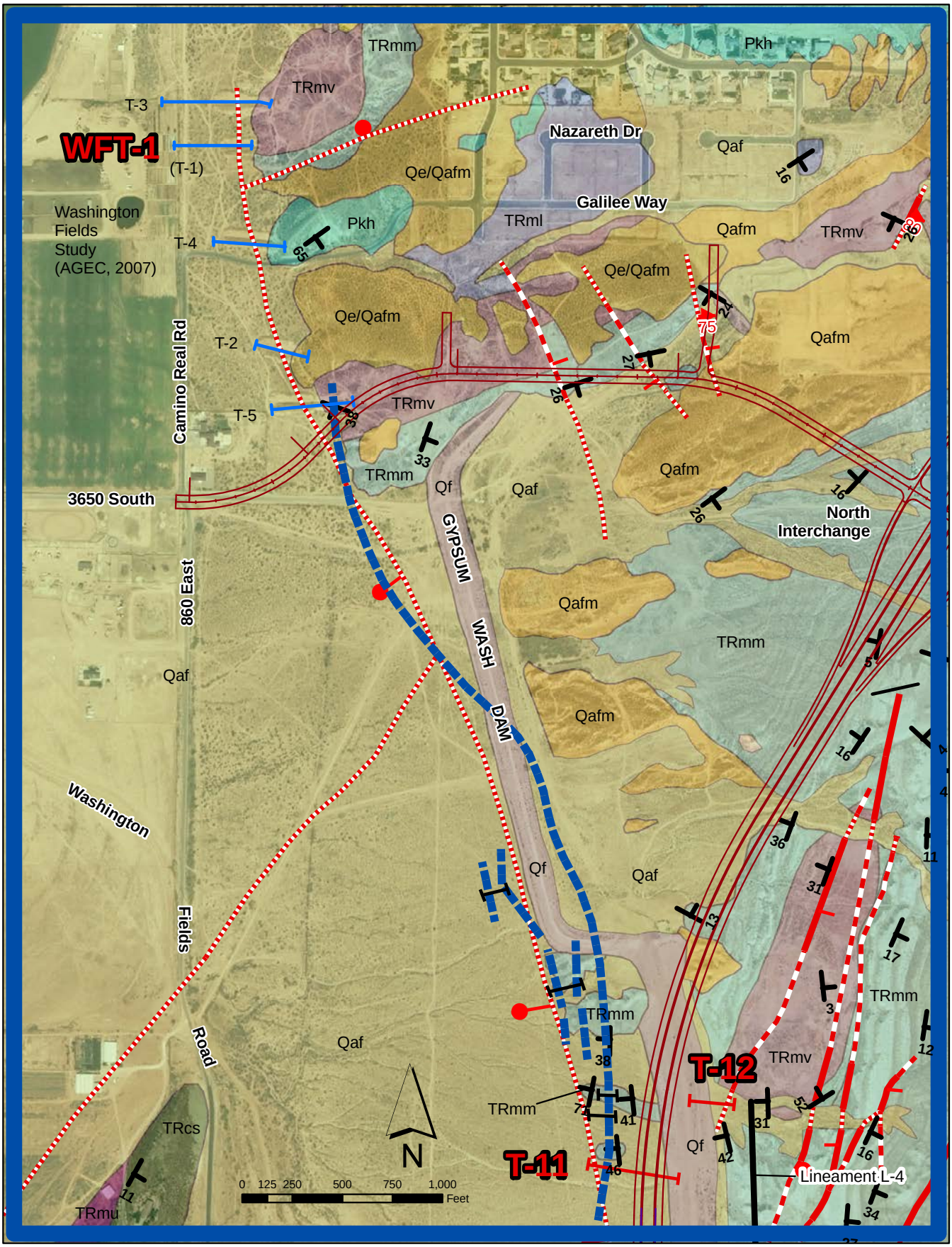

Figure 5. *Geologic map of the north part of study area. See figure 4 for geologic map legend.*

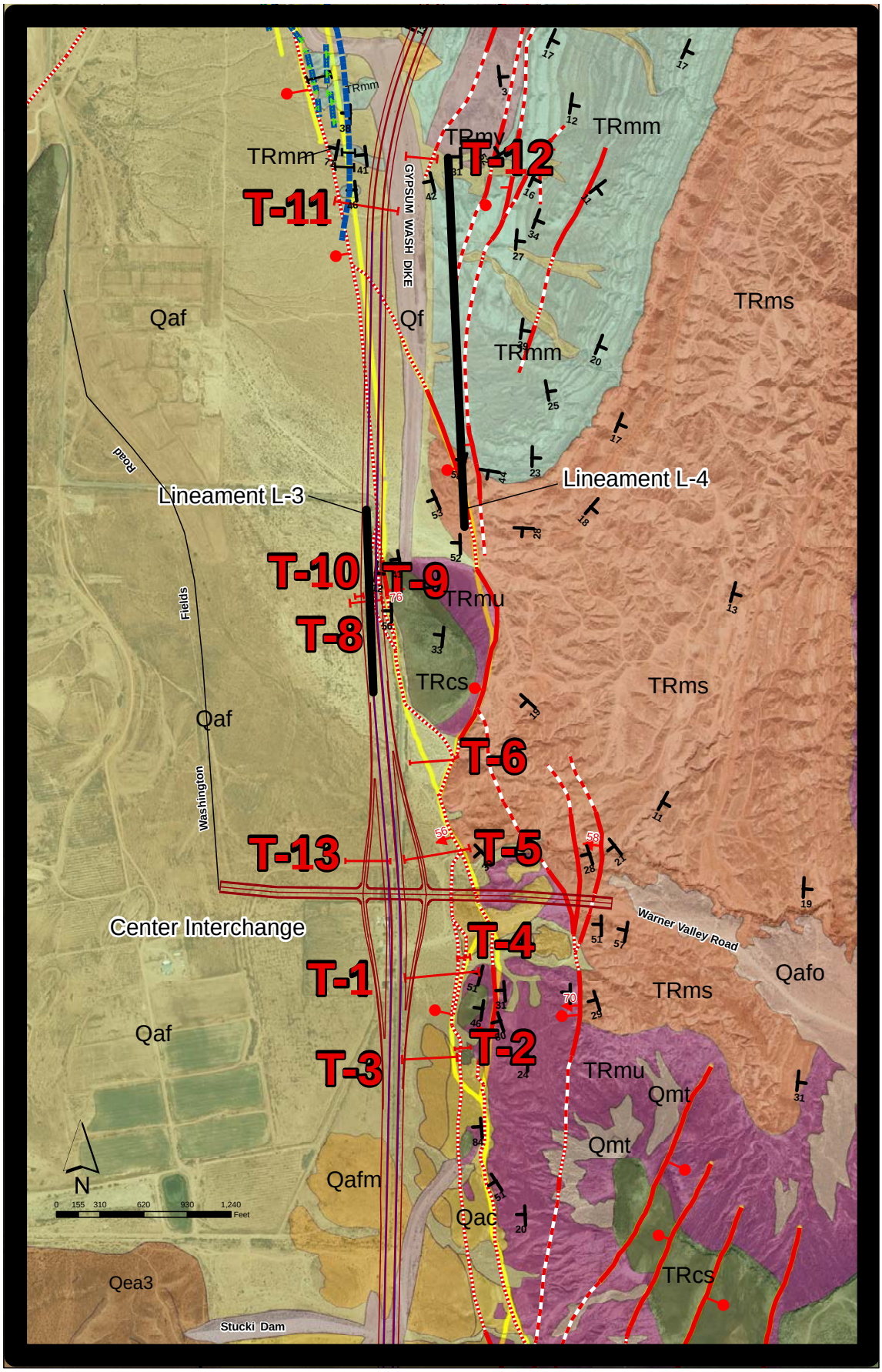

Figure 6. *Geologic map of the central part of study area. See figure 4 for geologic map legend.*

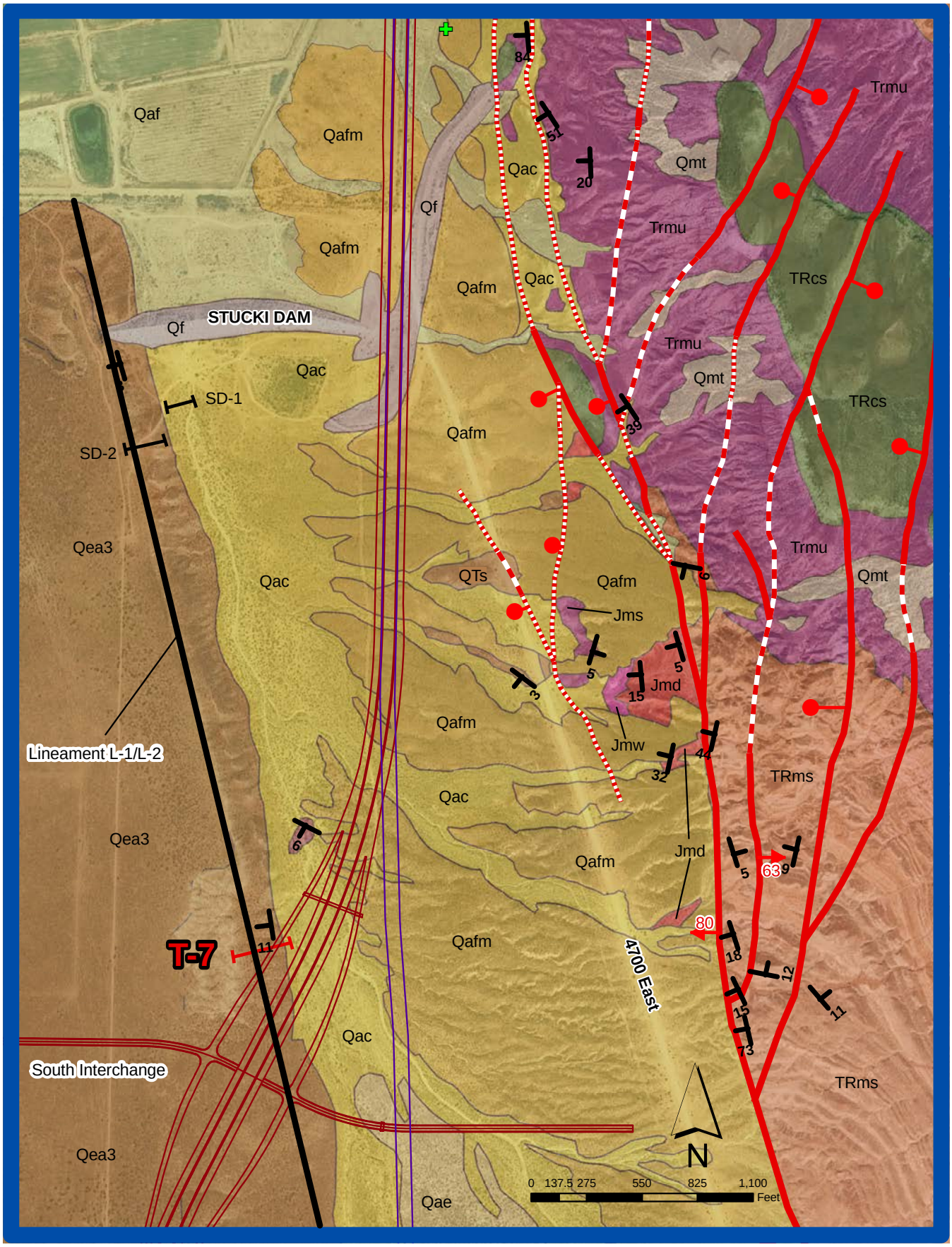

Figure 7. *Geologic map of the south part of study area. See figure 4 for geologic map legend.*

Table 1. *Aerial photographs examined for this investigation.*

SOURCE[1]	DATE	PHOTOGRAPHS	SCALE
BLM	07-19-2000	1-14 nos. 4 through 10	1:24,000
ESA (1982) (see also Bowman and others, 2011)	10-23-1982	AM: 6-3 through 6-7[2]	1:24,000
		PM: 6-1 through 6-12[2]	1:24,000

[1]*Both sets of aerial photographs consist of stereoscopic photo pairs.*

[2]*Low-sun angle photographs.*

During the AGEC (2007) investigation, the UGS obtained samples of alluvial deposits from the north wall of trench T-1 for OSL age analysis. At that time, the UGS understood that the trenches were to be backfilled following logging; therefore, due to time constraints, the UGS only generated a reconnaissance-level trench log (William Lund, UGS, verbal communication, 2010).

In the absence of a detailed log and with ages from only one trench, the UGS considered the uncertainty too great to adequately characterize the timing of surface faulting on the Washington fault zone (William Lund, UGS, verbal communication, 2010). Fortunately for this investigation, the AGEC (2007) trenches in the Washington Fields area were not backfilled. As part of this investigation, we cleaned and logged about 102 feet (31 m) of the north wall of AGEC trench WFT-1 (plate 14), and used the 2007 UGS OSL ages to help evaluate the time of past surface faulting on the Fort Pearce section.

Materials exposed in the trenches are described on the trench logs (plates 1 through 14), and were classified, when applicable, in accordance with the Unified Soil Classification System (ASTM D 2488). Color designations follow standard Munsell Soil Color notations. Trench excavations and field logs were reviewed by William Lund and Tyler Knudsen, geologists with the UGS.

GENERAL SITE CONDITIONS

The study area is primarily undeveloped. Three single-family residential structures are adjacent to the west side of Washington Fields Road immediately south of the intersection with Warner Valley Road (figure 1). Undeveloped residential subdivisions are present north of the northern interchange. Vegetation along the transportation corridor consists of a sparse ground cover of native grass, sage brush, and low mesquite. Numerous west-trending ephemeral drainages cross the study area.

GEOLOGY

The distribution of the geologic units along the transportation corridor is shown on figures 5–7; figure 4 is a legend for the geologic maps. Most of the corridor is underlain by Quaternary-age unconsolidated surficial deposits of windblown, fluvial, and alluvial-fan origin; these deposits cover bedrock units of Triassic and Jurassic age (Hayden, 2005; Biek and others, 2009; Rosenberg Associates, 2009; Knudsen, this volume). Detailed descriptions of the geologic units observed in the exploratory trenches are presented on plates 1 through 14, and are summarized in table 2.

Table 2. *Site geologic units.*

Geologic Unit	Geologic Age	Approximate age (years before present)
Fault-scarp-derived colluvium	Holocene	≤ 1500
Pedogenic A-horizon	Holocene	≤ 2500
Alluvium, younger	Holocene	≤ 10,000
Alluvium, older	Holocene to Pleistocene	≤ 150,000
Bedrock units	Triassic	248–206 million

LINEAMENT ANALYSIS

We examined topographic maps and stereoscopically paired aerial photographs of the study area for the presence of lineaments which might indicate surface faulting. Lineaments suggestive of faulting primarily corresponded to previously mapped traces of the Washington fault zone (Hayden, 2005; Biek and others, 2009; Rosenberg Associates, 2009), and consisted of north-northeast trending linear topography, alignment of vegetation, and linear color contrasts. We identified four lineaments not associated with previously mapped faults. The lineaments are shown on figure 8.

Lineaments L-1 and L-2

Lineaments L-1 consists of a north-south oriented linear ridge and lineament L-2 consists of a north-south oriented linear saddle near the middle of the ridge (figures 7 and 8); the paired lineaments are strongly expressed on aerial photographs. The lineaments, which cross the transportation corridor at the proposed location of the south interchange (figures 1 and 7), were described by Rosenberg Associates (2009) as follows:

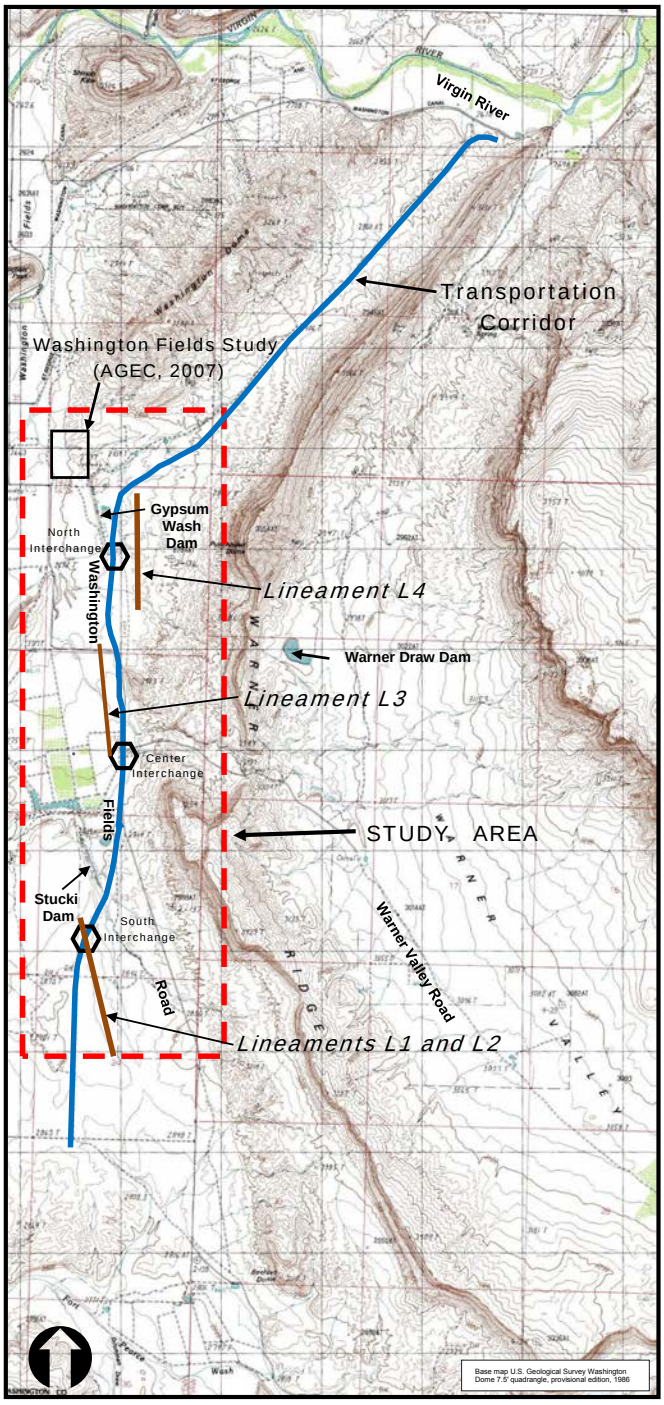

Figure 8. *Lineaments identified from aerial photographs and topographic maps.*

During this investigation we mapped a new fault, defined by a linear scarp, not recognized previously, that parallels and lies about a half mile west of the main strand of the Washington fault zone. ESA (1982, 1983) noted that the scarp was a "suspicious feature" that might be fault related. ESA (1982, 1983) excavated two trenches across the feature when they were studying the Stucki Dam, but did not document any faults and concluded that the feature was not a fault. It is possible that the ESA trenches were not deep enough.

The new fault is poorly exposed in the basin-fill sediments that are overlain by a caliche-capped pediment surface in the southern part of the map. North of the linear scarp, the fault is concealed (dotted), but is projected northward to truncate the northeast end of a bedrock hogback made up of the upper part of the Moenkopi Formation and the lower part of the Chinle Formation. It appears the subsidiary fault joins the main strand in the northern part of the map, but is buried beneath younger surficial deposits and its trace is conjectural.

The new fault crosses the transportation corridor and Interchange 9 near the south edge of the map area. Displacement along the fault is down to the east, antithetic to the main strand of the Washington fault zone. The two faults create a graben filled in with sediment derived from erosion of material on the upthrown sides. Antithetic faults and grabens on the downthrown sides of large normal faults are common. We interpret this fault to be part of the Washington fault zone.

Lineament L-3

Lineament L-3 (figure 8) appears on aerial photographs as a weakly to moderately expressed linear tonal contrast in an area of young alluvium. The lineament is about 245 feet (74.7 m) north of the center interchange (figure 6), and was described by Rosenberg Associates (2009):

> Although we were not able to corroborate photo lineaments in the area of the Gypsum Wash Dam, we did map a north-trending lineament about 0.2 miles (0.3 km) long, whose south end is 0.25 miles (0.4 km) north of Interchange 10 (figure 6). This feature has no surface topographic expression but appears on aerial photographs as a tonal linear feature in an area of young alluvial deposits (Qaf on figure 6) about 100 feet (30.5 m) west of the exposed main trace of the fault. We interpret the lineament to be associated, in some manner, with the main splay of the Washington fault zone.

Lineament L-4

Lineament L-4 (figure 8) consists of a linear slope strongly expressed on aerial photographs and topographic maps (Rosen-

berg Associates, 2009). The linear slope is immediately east of the Gypsum Wash Dam and about 990 feet (300 m) east of the corridor at the north interchange (figures 1 and 5).

SUBSURFACE EXPLORATION

The purpose of the subsurface exploration was to (1) evaluate the origin of the lineaments identified in the Rosenberg Associates (2009) investigation, and (2) assess the part of the study area situated within the surface-fault-rupture special study area established for the Washington fault zone by the UGS (Lund and others, 2008). Note that grid systems in the investigation trenches (plates 1–14) are in feet. Horizontal distances along the trench wall are stationed and reported as 0+00 (hundreds of feet + feet; e.g., 1+95 = 195 feet from the grid origin point in the trench).

Initially, six trenches were excavated to:

1. Evaluate subsurface deposits for the presence of faulting.

2. Verify the presence or absence of mapped faults within the study area as indicated by others (Hayden, 2005; Biek and others, 2009; Rosenberg Associates, 2009; Knudsen, this volume).

3. Intercept faults that project into the study area.

4. Intercept lineaments identified from aerial photographs and topographic maps.

5. Provide the minimum footage of trenching necessary, such that surface-fault rupture within the study established for the Washington fault zone by the UGS (Lund and others, 2008) could be assessed.

Due to documentation of faults in the initial six trenches, we excavated seven additional trenches to:

1. Further refine fault locations (or confirm the absence of faulting).

2. Accurately define construction restriction areas.

3. Provide additional exposures for evaluating the age of movement along particular faults.

Table 3 summarizes the primary purpose of each trench.

Materials exposed in the trenches are described on plates 1 through 14. The length and orientation of each trench, and whether or not a fault was documented within the trench, are presented in table 4.

FAULTING

We identified faults in nine of the 13 trenches excavated for this investigation (table 3) as well as in trench WFT-1 of the AGEC (2007) Washington Fields investigation. Displacement of bedrock and alluvial units ranged from about 3 inches (8 cm) to about 5 feet (1.5 m). Table 5 shows the number of surface-faulting earthquakes and average displacement per surface-faulting earthquake as interpreted from the trenches.

We identified multiple surface-faulting earthquakes in trenches T-1, T-2, T-4, and WFT-1. Due to the absence of correlative stratigraphy across the faults in trenches T-1 and T-2, the displacement across the faults in those trenches could not be determined. The trench depth at each fault location in trenches T-1 and T-2 represents the minimum cumulative displacement at that particular fault exposure.

To constrain the ages of surface-faulting earthquakes, selected samples were submitted to Paleo Research Institute (Golden, Colorado) for charcoal extraction and atomic mass spectrometry (AMS) ^{14}C analysis (AMS analysis performed at Keck Carbon Cycle AMS Facility at the University of California, Irvine) and to the Utah State University Luminescence Laboratory for OSL age analysis. Results of the AMS and OSL analyses are presented in appendices A and B, respectively.

Trench T-1

The purpose of trench T-1 (figure 6, plate 1) was to locate the main trace of the Washington fault zone and to evaluate the area east of the center interchange for the presence of faults. We documented a fault, trending N. 30° W. and dipping from about 40° SW to near vertical in the trench at station 0+98 (plate 1). The fault corresponds to the main trace of the Washington fault zone as mapped by others (Hayden, 2005; Biek and others, 2009; Rosenberg Associates, 2009; Knudsen, this volume). Displacement along the fault is normal slip (west side down), juxtaposing Triassic-age bedrock (upper red member of the Moenkopi Formation) against Holocene-age alluvial deposits. The local easterly dip of the fault is likely the result of near-surface overturning of the down-to-the-west normal fault due to the fault splaying/diverging near the surface where overburden pressures are essentially negligible.

We identified two fault-scarp-derived colluvial wedges (units 14 and 15, plate 1) adjacent to the west side of the fault. The upper wedge (unit 15) is overlain by about 4.6 feet (1.4 m) of unfaulted alluvial sediments (unit 16, plate 1). The source material for the colluvial-wedge units may be bedrock of the upper red member of the Moenkopi Formation (unit 1a, plate 1). However, the colluvial-wedge units resemble loess deposits, and, in fact, may well be loess, in which case the wedge source material may be either (1) wind-blown silt that was deposited against a post-earthquake bedrock scarp, or (2) an eolian deposit formerly present on the east side of the fault that was

Table 3. *Purpose of trenches.*

Trench	Purpose					
	Evaluate subsurface deposits for the presence of faulting.	Evaluate Surface-Fault-Rupture Special Study Area for the presence of faulting.	Verify the presence or absence of mapped faults within the study area as indicated by others.	Evaluate lineaments identified from aerial photographs and topographic maps.	Supplemental trench to provide additional exposures for evaluating age of fault movement.	Generate detailed log so ages obtained by the UGS could be utilized for evaluating age of movement.
T-1	■	■	■			
T-2	■	■	■			
T-3	■	■	■			
T-4	■				■	
T-5	■	■	■			
T-6	■	■	■			
T-7	■			■		
T-8	■			■		
T-9	■			■		
T-10	■			■		
T-11	■	■	■			
T-12	■			■		
T-13	■	■				
WFT-1 North Wall						■

Table 4. *Summary of trench data.*

Trench	Trench Orientation	Length (m)	Fault Documented	Plate No.
T-1	S. 85° W.	164	X	1
T-2	S. 85° W.	33	X	2
T-3	S. 87° W.	124		3
T-4	S. 87° W.	128	X	4
T-5	S. 80° W.	137		5
T-6	S. 55° W. to S. 86° W.	104	X	6
T-7	S. 77° W.	128		7
T-8	S. 81° W.	74	X	8
T-9	N. 89° W.	19	X	9
T-10	S. 79° W.	16	X	10
T-11	N. 80° W.	144	X	11
T-12	S. 89° W.	69	X	12
T-13	N. 90° W.	55		13
WFT-1 North Wall	N. 89° W.	23	X	14

Table 5. *Displacements per surface-faulting earthquake.*

Trench	Number of Surface-Faulting Earthquakes	Average Displacement Per Surface-Faulting Earthquake
T-1	2	≥ 3.3 ft (1 m)
T-2	unknown	Could not be determined
T-4	2	3.3 ft (1 m)
T-6	unknown	Could not be determined
WFT-1	5	4.3 ft (1.3 m)

subsequently completely eroded during and after formation of the fault colluvium.

Cumulative displacement could not be determined due to the absence of bedrock on the west side of the fault (hanging wall) and the absence of the faulted alluvial units on the east side of the fault (footwall). Based on trench depth and the absence of bedrock on the hanging wall, minimum cumulative displacement is equal to the depth of the trench at the location of the fault (~6.6 ft [2 m]).

In general, free face height is a rough proxy for fault slip during a surface-faulting earthquake. Ostenna (1984) stated that "…for large displacements, the thicknesses of the colluvial wedge preserved should approach half the initial free face height." In trench T-1, the colluvial wedge is about 1.5 feet (0.5 m) thick, which would indicate corresponding displacements of about 3 feet (0.9 m).

Trench T-1 Earthquake Timing

To constrain the time of faulting in trench T-1, samples from units 14, 15, and 16 (plate 1) were submitted for ^{14}C analysis (appendix A) and samples from units 14 and 15 (plate 1) for OSL age analysis (appendix B).

Trench T-1 radiocarbon ages: The ^{14}C ages from trench T-1 are presented in table 6. Samples from the upper colluvial wedge (unit 15, plate 1, sample S2), the lower colluvial wedge (unit 14, plate 1, sample S3), and the overlying alluvial deposit (unit 11, plate 1, sample S1 were submitted for charcoal extraction and AMS ^{14}C analysis. All three samples were expected to be Holocene age. However, AMS ages for the upper (sample S2) and lower (sample S3) colluvial wedges were anomalously young and stratigraphically inverted.

Sample S1 (unit 16; plate 1) contained sufficient particulate organics to yield a ^{14}C age of 2140 ± 15 radiocarbon years before present (RCYBP) (appendix A, table 2). This age calibrates to 2160–2060 calendar years before present (cal yr B.P.; appendix A). Sample S2 (unit 15, plate 1) contained a small quantity of *Pinus* charcoal, which was selected for analysis in preference to continuing the extraction process to recover particulate organics. Sample S2 produced a ^{14}C age of 205 ± 15 RCYBP, which calibrates to multiple ages of 300–260 (25.6%), 190–140 (47.1%), and 20–(-11) (22.7%) cal yr B.P. Sample S3 (unit 14, plate 1) yielded a ^{14}C age of 465 ± 15 RCYBP on particulate organics, which calibrates to 530-500 cal yr B.P. (appendix A, table 2).

The very recent ages reported for colluvial-wedge units 14 and 15 (table 6) indicate that there has probably been considerable mixing (bioturbation) and intrusion of young carbon, and likely contamination by "bomb carbon" associated with atmospheric atomic bomb testing at the Nevada Test Site, about 135 miles southwest of St. George, Utah. St. George is downwind of the Nevada Test Site, which detonated atmospheric atomic bombs between January 1951 and July 1962. Winds carrying significant radioactive fallout over the St. George area following atmospheric atomic bomb tests is well documented (Fuller, 1984).

Trench T-1 OSL ages: OSL samples of the upper (unit 15, plate 1, sample S2) and lower (unit 14; sample S3) colluvial-wedge units were submitted to the Utah State University Luminescence Laboratory for OSL age analysis (appendix B). The OSL ages are in correct stratigraphic order, and are 6.76 ± 1.94 and 8.27 ± 1.21 ka, respectively (table 7).

Trench T-1 Summary – Earthquake Timing

The fault in trench T-1 does not extend to the surface and is overlain by about 4.6 feet (1.4 m) of unfaulted alluvial sediments. The very recent and stratigraphically inverted ^{14}C ages reported for units 14 and 15 (table 6) indicate that there has been considerable mixing of young carbon into the unconsolidated deposits, likely including atomic bomb carbon; therefore, the ^{14}C age results from trench T-1 are inconclusive.

The OSL ages are stratigraphically consistent and suggest the colluvial-wedge units (14 and 15, plate1) may either (1) collectively form a single complex wedge that corresponds to the P2 (7700 ± 2400 ka) surface-faulting earthquake at the Dutchman Draw, Arizona, site (Lund and others, this volume), or (2) represent two paleoearthquakes, the older of which may correspond to surface-faulting earthquake P3 at Dutchman Draw (Lund and others, this volume). Given the large (2σ) uncertainty limits associated with the OSL ages, the ages of both wedge deposits overlap with the Dutchman Draw P2 earthquake, and it is not possible to resolve which of the two alternatives is correct.

Table 6. *Trench T-1 AMS radiocarbon ages.*

Relative Stratigraphic Age	Sample	Geologic Unit		Station	Age	
					RCYBP	cal yr B.P.[1]
oldest	S3	14	fault-derived colluvium	1+03	465 ± 15	530–500
↓	S2	15	fault-derived colluvium	1+03.5	205 ± 15	300–260 (25.6%) 190–140 (47.1%) 20–(-11) (22.7%)
youngest	S1	16	alluvium	1+04.	2140 ± 15	2160–2060

[1]*Two-sigma uncertainty.*

Table 7. *Trench T-1 OSL ages.*

Relative Stratigraphic Age	Sample	Geologic Unit		Station	OSL Age (ka) (2σ)
younger	S2	15	fault-derived colluvium	1+03.5	6.76 ± 1.94
older	S3	14	fault-derived colluvium	1+03	8.27 ± 1.21

Possible reasons for the absence of a geomorphic scarp and/or a colluvial wedge representative of the P1 surface-faulting earthquake at Dutchman Draw include (from most to least probable):

1. The P1 colluvial wedge and fault scarp formed in the loose, unconsolidated, chiefly eolian basin-fill sediments that underlie the study area, and the scarp was rapidly eroded. Several workers (Lund and others, 2008, 2010; Knudsen, this volume) note that erosion is the principal geomorphic process active in the St. George basin.

2. The P1 surface-faulting earthquake represents a partial rupture (e.g., Crone and others, 1987; DuRoss, 2008; Wesnousky, 2008) of the Fort Pearce section, which originated at the south end of the section and died out before reaching the study area.

3. The trench may not have crossed the fault trace associated with the P1 surface-faulting earthquake.

4. The P1 surface-faulting earthquake at Dutchman Draw (south end of the Fort Pearce section) may be due to spill-over rupture from a northward propagating surface-faulting earthquake on the Sullivan Draw segment to the south (Pearthree, 1997), and the spill-over rupture did not extend northward as far north as trench T-1(speculative, no data to support this hypothesis).

Trench T-2

The purpose of trench T-2 (figure 6, plate 2) was to locate the main trace of the Washington fault zone, and to evaluate the area east of the center interchange for the presence of faults. We identified a zone of faults (f1-f5) between stations 0+05 and 0+12 (plate 2). The primary fault (f5), at station 0+12, trends N. 8° W., dips about 65° E., and thrusts Triassic-age bedrock (Petrified Forest and Shinarump Conglomerate Members of the Chinle Formation and upper red member of the Moenkopi Formation) over Holocene to perhaps late Pleistocene-age alluvial sediments. These faults are overlain by alluvium (unit 7, plate 2) that is about 6 inches (15 cm) thick, containing a weakly developed Bkb pedogenic horizon.

The Washington fault zone is a well-documented normal fault (west side down), and the thrust fault in trench T-2 (fault f5, plate 2) is likely due to compressional forces in an area where the main fault bends to the east. Displacement along faults f1-f5 could not be determined. Minimum cumulative displacement (~3.4 m) is equal to at least the depth of the trench near the faulted units.

Faults f1-f5 extend to the base of unit 7, the youngest stratigraphic unit in the trench. We submitted two alluvial samples from the west side (footwall) of the thrust fault (unit 6; plate 2) to Paleo Research Institute for charcoal extraction and subsequent AMS ^{14}C analysis at the Keck Carbon Cycle AMS Facility at the University of California, Irvine (appendix A). Unit 6 alluvium was anticipated to be Holocene to perhaps late Pleistocene.

Ages during the atomic bomb testing era (1950s–1980s) to modern are reported as Fraction Modern. The particulate organics extracted from sample T2-S1 appeared very similar to those recovered from trench T-1; however, the sample contained very young carbon, yielding a Fraction Modern of

1.058100 ± 0.00150. This age calibrates to between December 1955 and July 1957, indicating that there has been considerable mixing of modern carbon associated with nuclear bomb testing.

Without an age for unit 6 (nor is there is an age for unit 7), constraining the time of faulting along fault f5 is not possible. However, the following data suggest fault f5 is Holocene-age, and could represent the P1 surface-faulting earthquake (1000 ± 600 cal yr B.P.) at Dutchman Draw (Lund and others, this volume).

1. Faults f1-f5 extend to the base of the youngest unit in the trench, and within about 6 inches (15 cm) of the ground surface.

2. There is an eroded geomorphic fault scarp associated with the fault (plate 2).

3. Based on soil morphology, the ESA (1982) study assigned an age of 1000 to 1500 years to the youngest alluvium in the area, and a late Pleistocene age (10,000 to 25,000 years) to the older alluvial-fan sediments in the area. Faults f1-f5 displace all but the youngest unit in the trench.

A sixth fault, f6, trends N. 15° W. and dips 88° E. at station 0+42.5. This fault displaces the Triassic-age Petrified Forest Member of the Chinle Formation and a Holocene to perhaps late Pleistocene alluvial deposit. The fault is overlain by about 12 feet (3.7 m) of unfaulted and stratigraphically continuous alluvial sediments. Without an age for unit 3, constraining the time of faulting on fault f6 was not possible; however, considering depth of burial of f6, the displacement on f6 is older than the most recent displacement of faults f1-f5, and represents a second, older surface-faulting earthquake.

Trench T-3

The purpose of trench T-3 (figure 6, plate 3) was to locate the main trace of the Washington fault zone, and to evaluate the area east of the center interchange for the presence of faults. Unfaulted and stratigraphically continuous alluvial sediments were documented throughout the entire length (502 ft [153 m]) of trench T-3 (plate 3). Trench depth was about 15 feet (4.6 m). Geomorphic and stratigraphic similarities to trench T-5, from which Holocene ages were obtained for the alluvial sediments, suggest the alluvial sediments in trench T-3 are Holocene, but older than the P1 surface-faulting earthquake at the Dutchman Draw, Arizona, site (Lund and others, this volume).

Trench T-4

The purpose of trench T-4 (figure 6, plate 4) was to refine the location of the fault identified in trench T-1, and to provide additional exposures for evaluating the age of movement along the Fort Pearce section. Trench T-4 was about 100 feet (30.4 m) north of trench T-1, and was one of the more significant trenches with regard to fault exposures. Trench T-4 crosses a 50-foot-long (15 m), moderately eroded, north-south trending fault scarp. To the north, the fault scarp was likely removed during construction of Warner Valley Road, and to the south by erosion from adjacent ephemeral drainages.

We identified seven faults in trench T-4 (plate 4), which represent at least two surface-faulting earthquakes. The faults presumably coalesce at relatively shallow depths (i.e., ± 50 ft [15 m]). Displacement along faults f1, f2, f3, f4, f6, and f7 is normal with the west side down. Fault f5 (station 0+32.5) is an antithetic fault, with the east side down. The faults juxtapose (1) the Shinarump Conglomerate Member of the Chinle Formation against Holocene-age alluvium, and (2) Holocene alluvium against Holocene alluvium.

Faults f1-f5 (stations 0+21 to 0+32.5) comprise a zone of faulting with net cumulative vertical displacement of about 5.2 feet (1.6 m). Only one colluvial wedge, associated with fault f4, was documented in the trench (unit 11, plate 4). Faults f1-f5 extend to within 1.5 to 2 feet (0.5 to 0.6 m) of the ground surface, and are overlain by units 11, 12, and 13, among the youngest alluvial units in the east part of the trench. Cumulative displacements for faults f1-f5 are presented in table 8, which indicates at least two surface-faulting earthquakes, the youngest of which produced about 4 feet (1.2 m) of displacement.

Cumulative displacements for faults f6-f7 are presented in table 9, which also indicates at least two surface-faulting earthquakes, the youngest of which produced 1.7 feet (0.5 m) of displacement. Faults f6 and f7 displace unit 13, and therefore are younger than faults f1-f5, and represents a second surface-faulting earthquake.

Trench T-4 Radiocarbon Ages

We submitted a sample from the colluvial wedge (unit 11, plate 4) and one sample of the underlying alluvial unit (unit 9, plate 4) to Paleo Research Institute for charcoal extraction and subsequent AMS ^{14}C analysis at the Keck Carbon Cycle AMS Facility at the University of California, Irvine (appendix A). The sediments sampled were expected to be Holocene age. However, very recent ages (1951 to 1957) (appendix A, table 2) were reported for the trench T-4 samples, which we attribute to modern organic contamination from bioturbation, and contamination by atomic bomb carbon.

Trench T-4 OSL Ages

We submitted a sample of the f4 colluvial wedge (unit 11, plate 4; sample S11) and the overlying unit (unit 12; sample S12) to the Utah State University Luminescence Laboratory for OSL age analysis (appendix B). The OSL ages were 10,970 ± 1850 and 7710 ± 2280 years, respectively (table 10).

Table 8. *Displacements for faults f1-f5 in trench T-4.*

	Unit		Displacement
Oldest	2	alluvium	5.2 ft (1.6 m)
↓	3	alluvium	4.0 ft (1.2 m)
	4	alluvium	4.0 ft (1.2 m)
Youngest	5	alluvium	4.0 ft (1.2 m

Table 9. *Displacements for faults f6-f7 in trench T-4.*

	Unit		Displacement
Oldest	2	alluvium	2.2 ft (0.7 m)
	3	alluvium	2.2 ft (0.7 m)
	4	alluvium	1.7 ft (0.5 m)
	5	alluvium	1.7 ft (0.5 m)
	6	alluvium	1.7 ft (0.5 m)
↓	8	alluvium	1.7 ft (0.5 m)
Youngest	9	alluvium	1.7 ft (0.5 m)

Table 10. *Trench T-4 OSL ages.*

Relative Stratigraphic Age	Sample	Geologic Unit		OSL Age (ka)
younger	S10	12	alluvium	7.71 ± 2.28
older	S11	11	Colluvial wedge	10.97 ± 1.85

Trench T-4 Summary – Earthquake Timing

The OSL age for the f4 colluvial wedge (unit 11, plate 4) is 10.97 ± 1.85 ka. At the 2σ confidence level, the age of unit 11 overlaps the age of the P2 surface-faulting earthquake (7700 ± 2400 cal yr B.P.) at the Dutchman Draw, Arizona, site (Lund and other, this volume). Therefore, it appears that faults f1-f5 are associated with the P2 surface-faulting earthquake at Dutchman Draw. Displacement associated with the P2 earthquake at Dutchman Draw was about 8 feet (2.4 m). Displacement across the f4 fault zone is 5.2 feet (1.6 m), which is consistent with variations in slip along strike in a surface-faulting earthquakes on a normal-slip fault (DuRoss, 2008).

Faults f6-f7 displace a younger geologic deposit (unit 13, plate 4) than do faults f1-f5; therefore, faults f6-f7 represents a second, most recent surface-faulting earthquake. An OSL age of 7.71 ± 2.28 ka from unit 12 (plate 4), which overlies unit 11 and underlies unit 13, places a maximum limiting age on the timing of the most recent earthquake. The younger event exposed in trench T-4 likely corresponds with the P1 surface-faulting earthquake (1000 ± 600 cal yr B.P.) at the Dutchman Draw, Arizona, site (Lund and other, this volume); however, based on available age information, we can only say that the most recent event is younger than 7.71 ± 2.28 ka. Displacement associated with the P1 surface-faulting earthquake at Dutchman Draw was 3.3 to 4 feet (1.0–1.2 m). Displacement across faults f6-f7 is 1.7 feet (0.5 m), which again is consistent with variations in slip along strike in a surface-faulting earthquakes on a normal-slip fault (DuRoss, 2008).

Trench T-5

The purpose of trench T-5 (figure 6, plate 5) was to locate the main trace of the Washington fault zone and to evaluate the area east of the center interchange for the presence of faults. The trench extended to an average depth of about 10 feet (3 m) (plate 5); however, near station 0+55, the trench was about 20 feet (6.1 m) deep.

We documented stratigraphically continuous bedrock (Shnabkaib Member of the Moenkopi Formation) in the eastern part of the trench (stations 0+00 to 0+60), and unbroken and stratigraphically continuous alluvial sediments extend throughout the entire length of the trench (plate 5). No faults were identified in the trench, which is problematic because the main trace of the Washington fault zone was identified in trench T-4 about 875 feet (266 m) to the south and also in trench T-6 about 650 feet (198 m) to the north of trench T-5 (figure 6).

Prior to deepening trench T-5 at station 0+45, we initially thought there was a fault at station 0+44, which juxtaposed Shnabkaib bedrock against alluvial unit 3. Unit 3 has a colluvial-wedge-like geometry and included two 6-inch (15-cm)-long sandstone clasts along the contact between units 1c and 3 (plate 5). Deepening the trench in this area exposed unit 1a, which was stratigraphically continuous below units 1c and 3, precluding the possibility of faulting. AGEC (2007) encountered a similar anomaly in the Washington Fields area, with the absence of faults in trenches centered between adjacent trenches in which faults were observed.

Trench T-5 Anthropologic Hearth

An anthropologic hearth was discovered in unit 10, at about station 1+43 (plate 5). We also observed several areas of anthropologic charcoal staining within alluvial unit 8 between stations 0+50 and 0+58. Unit 10 is stratigraphically above unit 8 and is therefore a younger deposit.

Bighorn Archaeological Consultants, LLC and Western GeoArch Research (WGR) investigated the archaeological significance of the hearth and cultural charcoal staining (appendix C). WGR submitted eight samples from the anthropologic hearth and cultural charcoal staining to Beta Analytical for charcoal extraction and AMS ^{14}C age analysis, and two samples of unit 8 and one sample of unit 10 to the University of Illinois at Chicago Luminescence Laboratory for OSL age analysis (appendix C).

Trench T-5 radiocarbon ages: Table 11 presents a summary of the WGR (2011) ^{14}C ages. A ^{14}C age of 2030 ± 40 RCYBP

Table 11. *Trench T-5 radiocarbon ages.*

Big Horn Sample Designation	Geologic Unit	Trench Station	Feature	Age	
				Conventional ^{14}C age (RCYBP)[1]	Average calendar calibrated years before present (cal yr B.P.)[2]
FS06	Unit 8	0+73.8	cultural charcoal	5150 ± 40	5875 ± 115
FS09	Unit 8	0+56.0	cultural charcoal	4980 ± 40	5745 ± 135
FS19	Unit 8	0+58.7	cultural general charcoal	5400 ± 40	6205 ± 85
FS29	Unit 10	1+40.0	cultural hearth	1900 ± 40	1830 ± 100
FS31	Unit 10	1+43.0	disseminated cultural charcoal layer directly below hearth feature (sample FS29).	2030 ± 40	2000 ± 110
FS34	Unit 8	0+18.0	cultural charcoal stained sediment above regolith at base of unit 4	4640 ± 40	5380 ± 60
FS113 (feature 11)	Unit 8	0+50.5	cultural charcoal stain/hearth	5730 ± 40	6530 ± 110
FS115 (feature 10)	Unit 8	0+56.7	cultural charcoal stain/hearth	5360 ± 40	6140 ± 140

[1]*The conventional ^{14}C age represents the measured ^{14}C age corrected for isotopic fractionation, calculated using the delta ^{13}C. The conventional ^{14}C age is not calendar calibrated (WGR, 2011).*

[2]*Weighted average of multiple intercepts calculated using OxCal (http://c14.arch.ox.ac.uk); two-sigma (2σ) uncertainty (WGR, 2011).*

(2000 ± 110 cal yr B.P.) was obtained for the hearth at station 1+43 in unit 10 (sample FS31; appendix C). A significantly smaller accumulation of charcoal, about a foot (0.3 m) above the FS31 sample at station 1+40 in unit 10, produced a ^{14}C age of 1900 ± 40 RCYBP (1830 ± 100 cal yr B.P.) (sample FS29). Radiocarbon ages obtained from unit 8 (plate 5) between stations 0+50 and 0+75 range from 5745 ± 135 cal yr B.P. (sample FS09) to 6205 ± 85 cal yr B.P. (sample FS19) (plate 5). A ^{14}C age from unit 8 at station 0+17 was 5380 ± 60 cal yr B.P. (plate 5).

Trench T-5 OSL ages: Table 12 presents a summary of the WGR (2011) OSL ages. Sample A (9940 ±1030) and sample C (12,910 ± 1415) were collected from unit 8 (plate 5), and both are significantly older than the anthropogenic ^{14}C ages obtained from charcoal staining in that unit, and therefore are stratigraphically inverted (see Trench T-5 and tables 11 and 12 for ^{14}C and OSL ages). Samples A and C may have undergone only partially bleaching when deposited to form unit 8, and therefore would produce an age older than the time of unit 8 deposition. Therefore, the anthropogenic ^{14}C ages provide a more reliable estimate of the age of unit 8.

OSL sample E (4830 ± 430) collected from unit 10 below a manuport (a natural object which has been moved from its original context by human activity but otherwise remains unmodified) near the anthropomorphic hearth at station 1+43, is older than the ^{14}C ages obtained from charcoal associated with the hearth. Therefore, the ^{14}C and OSL ages obtained from unit 10 are stratigraphically consistent, and OSL sample E provides a reliable estimate for the age of the sediments below the hearth.

Alluvial units west of the hearth at about station 1+45 (chiefly units 11–13), which is where we expected to find faulting in trench T-5, are not displaced and provide geologic evidence for the absence of faulting in that part of the trench. Unit 8, which may be as old at 12,910 ± 1415, disappears into the trench bottom at station 0+90, so it is unknown if unit 8 is faulted in the subsurface to the west. However, units 11–13 are older than unit 10, which has a minimum age based on OSL sample E of 4830 ± 430, thus indicating that faulting has not occurred since at least 4830 ± 430 years ago.

Trench T-6

The purpose of trench T-6 (figure 6, plate 6) was to locate the main trace of the Washington fault zone and to evaluate the area east of the center interchange for the presence of faults. The main trace of the Washington fault zone fault was identified at station 0+27.5 (plate 6). The fault trends N. 6° W. and dips about 80° E., and juxtaposes Triassic bedrock (Shnabkaib Member of the Moenkopi Formation) against Holocene alluvium.

Displacement along the fault is largely normal slip (west side down). The easterly dip to the fault is the result of near-surface overturning of the down-to-the-west normal fault due to the fault splaying/diverging near the surface where overburden

Table 12. *Trench T-5 OSL ages.*

Big Horn Sample Designation	Geologic Unit[1]	Trench Station	Feature	OSL Age
OSL A[2]	Unit 8[2]	0+55.5	upper bracket of a typical charcoal staining (Area 3) (FS113, FS09, FS1115, FS19, FS06)	9940 ± 1030
OSL C	Unit 8	0+56.5	lower bracket of a typical charcoal staining (Area 3) (FS113, FS09, FS115, FS19, FS06)	12,910 ± 1415
OSL E	Unit 10	1+43.2	cultural staining immediately below a cobble-size manuport on the floor of the south wall in the SE corner of the south block; near the block floor in stratum 10a	4830 ± 430

[1]*Unit 8 is stratigraphically below Unit 10*

[2]*OSL A is 1.1 feet above OSL C.*

pressures are negligible. Displacement along the fault could not be determined. Cumulative displacement is equal to at least the depth of the trench (8.6 feet [2.6 m]) near the faulted units.

Unit 5 is the oldest faulted alluvial deposit in the trench. Stratigraphically, alluvial unit 4 is older than unit 5 (station 0+70, plate 6). Unit 9 is the youngest faulted alluvial unit, and faulting extends to the base of unit 10, the youngest stratigraphic unit in the trench. No age is available for unit 10; therefore, constraining the time of faulting in the trench is not possible.

However, geologic mapping along the Washington fault zone (Knudsen, this volume) indicates that the alluvial units exposed at the surface near trench T-6 are Holocene, and because the fault extends to the base of the youngest unit in the trench, it is possible the fault is late Holocene-age, and could represent the Dutchman Draw P1 surface faulting earthquake (1000 ± 600 cal yr B.P.) (Lund and others, this volume).

Trench T-7

The purpose of trench T-7 (figure 7, plate 7) was to intercept lineaments L-1 and L-2 (figures 7 and 8). Lineaments L-1 consists of a north-south oriented linear ridge and lineament L-2 is represented by a north-south oriented linear saddle near the middle of the ridge (figures 7 and 8). Trench T-7 was about 425 feet (129 m) long, and extended from the youngest valley-fill sediments on the east, to the top of the linear ridge on the west. Stratigraphically continuous Pleistocene (Rosenberg Associates, 2009) basin-fill sediments were documented throughout the entire length of the trench (plate 7). The basin-fill sediments dip about 10° W.

The absence of displacement within the Pleistocene basin-fill sediments in trench T-7 provides evidence of the absence of faulting and absence of a tectonic subsurface feature associated with lineaments L1 and L2. We attribute the linear ridge (lineament L1) to erosion by north-south trending ephemeral drainages. The north-south oriented linear saddle near the middle of the ridge (lineament L2) is the result of differential erosion between soft, erosion-prone sand (units 9–14 and unit 16, plate 7) and more resistant calcium-carbonate-cemented sediments (units 8, 15, and 17, plate 7).

Trench T-8

The purpose of trench T-8 (figure 6, plate 8) was to intercept lineament L-3 (figures 6 and 8). Lineament L-3 appears on aerial photographs as a weak to moderate linear tonal contrast, with no surface topographic expression, in an area of young alluvium. The main trace of the Washington fault zone is about 40 feet (12 m) east of the east end of trench T-8, adjacent to the east side of Washington Fields Road.

Bedrock was exposed along the entire length of the trench (plate 8). The Petrified Forest Member of the Chinle Formation extended from about station 0+00 to 0+64. The Dinosaur Canyon Member of the Moenave Formation was present west of station 0+64.

Bedding was oriented near vertical and many bedding planes exhibited shearing. The contact between the two bedrock units is defined by a 5-foot-wide (1.5 m) zone of fault breccia. Starting at about station 0+15, the bedrock units are unconformably overlain by unfaulted and stratigraphically continuous alluvial sediments.

We identified seven fault traces in trench T-8 between stations 0+00 and 1+50. The faults are confined to the near-vertical and highly sheared bedrock units. The absence of displacement within the alluvial sediments, uniform slope of the ground surface, and contact between the bedrock and alluvial units provide evidence that there is not a subsurface feature associated with the lineament L-3

Trench T-8 was within a center-pivot irrigation system, which is visible on 1982 aerial photographs, but not on 2000 aerial photographs. Based on trench observations and the former center pivot, we interpret lineament L3 to be associated with agricultural irrigation activity.

Trenches T-9 and T-10

The purpose of trenches T-9 and T-10 (figure 6, plates 9 and 10) was to further refine the locations of the faults documented in trench T-8, intercept lineament L-3 (figures 6 and 8), and to provide additional exposures for evaluating the age of movement along the faults. The exposures in trenches T-9 and T-10 were very similar to trench T-8, the various faults exposed in trenches T-9 and T-10 were similarly confined to near-vertical and highly sheared bedrock units as was observed in T-8. The bedrock units in trenches T-9 and T-10 were overlain by unfaulted and stratigraphically continuous alluvial sediments.

The absence of displacement within the alluvial sediments, uniform slope of the ground surface, and contact between the bedrock and alluvial units provide further evidence that there is not a subsurface feature associated with the lineament L-3 (see discussion under Trench T-8).

Trench T-11

The purpose of trench T-11 (figure 6, plate 11) was to locate the main trace of the Washington fault zone, to confirm the findings of the ESA (1982) report regarding faulting in this area, and to evaluate the area near the north interchange for the presence of faults.

We identified six faults in trench T-11 (plate 11), five of which were confined to bedrock of the middle red member of the Moenkopi Formation, and do not displace overlying Holocene alluvium (faults f1-f5). However, fault f6 at about station 4+22, displaces Holocene and perhaps late Pleistocene alluvium, and juxtaposes alluvium against Moenkopi Formation bedrock. The location of fault f6 corresponds reasonably well with the primary trace of the Washington fault zone as documented by others (ESA, 1982, 1983; Hayden, 2005; Rosenberg Associates, 2009; Knudsen, this volume). Cumulative displacement along fault f6 could not be determined due to the absence of bedrock on the hanging wall and the absence of the faulted alluvial units on the footwall. Based on trench depth, minimum cumulative displacement is equal to the depth of the trench (8 ft [2.4 m]) at the location of the fault.

Trench T-12

The purpose of trench T-12 (figure 6, plate 12) was to intercept lineament L-4 (figures 6 and 8) documented in the Rosenberg Associates (2009) study. Lineament L-4 consists of a strongly expressed linear slope on aerial photographs and topographic maps (Rosenberg Associates, 2009), located immediately east of the Gypsum Wash Dam.

We identified 18 bedrock faults in trench T-12 with displacements ranging from 0.2 to 6.5 feet (0.1 to 2 m) (plate 12). None of the faults correspond to lineament L-4. Faults f1-f13 extend to the base of the youngest alluvial deposits in the trench. Faults f14-f18 extend to the base of fill associated with Gypsum Wash Dam, where alluvial sediments were removed during construction of the dam. Based on the presence of extensive fill associated with Gypsum Wash Dam and proximity to the dam, we attribute lineament L-4 (linear slope) to grading associated with construction of the dam (located adjacent to the west end of trench T-12).

Trench T-13

The purpose of trench T-13 (figure 6, plate 13) was to evaluate the area west of the north interchange for the presence of faults. Trench T-13 is on the west side of Washington Fields Road and is a continuation of trench T-5 on the east side of the road. Unfaulted and stratigraphically continuous alluvial sediments were documented throughout the entire length of trench T-13 (plate 13).

The depth of trench T-13 was about 15 feet (4.6 m). Ages of the alluvial deposits are not known. However, based on soil morphology, ESA (1982), assigned an age of 1000 to 1500 years to the youngest alluvium; also, geologic mapping (Knudsen, this volume) indicates the alluvial deposits near trench T-13 are of Holocene age.

Washington Fields Trench WFT-1

WFT-1 General

Washington Fields is near the north end of the study area (figures 1 and 5). Trenching by AGEC (2007) at Washington Fields exposed the main trace of the Washington fault zone. The UGS conducted a reconnaissance-level investigation of the fault exposure in AGEC's (2007) Washington Fields trench WFT-1. At that time, the UGS understood that the trenches were to be backfilled following logging; therefore, due to time constraints, the UGS only generated a reconnaissance-level trench log (William Lund, Utah Geological Survey, verbal communication, 2010), and collected five samples for OSL age analysis from sediments thought to represent fault-scarp colluvium in the north trench wall (Lund and others, 2008).

Based on the OSL data, the UGS concluded that the Washington fault zone has experienced a minimum of three surface-faulting earthquakes in the past ~75,600 years, with the most recent surface faulting earthquake occurring shortly before 18,600 years, the penultimate surface faulting earthquake occurring shortly before 30,700 years, and a third surface faulting earthquake occurring shortly before 67,800 years (Lund and others, 2008). However, due to the absence of a detailed trench log and ages from only one location, the UGS considered the uncertainty in the ages too great to adequately characterize the timing of surface faulting on the Washington fault zone (William Lund, UGS, verbal communication, 2010).

At the time of this investigation, we discovered that trench WFT-1 was not backfilled following the AGEC (2007) investigation, and we logged the trench exposure for this investigation to provide a detailed log (plate 14) so that the UGS OSL ages could be reinterpreted and used to evaluate the age of movement of the Washington fault zone at this location

We identified nine faults over a width of about 31 feet (9.4 m) in the north wall of trench WFT-1 (plate 14), many of which likely coalesce at relatively shallow depths (~50 ft [15 m]). The faults dip between 80° W. to vertical, and displacement along the faults is normal slip (west side down), juxtaposing Holocene alluvium against Holocene to late Pleistocene-age alluvium. There are no scarps associated with the faults.

WFT-1 Radiocarbon Ages

We submitted two samples of alluvial sediment and one sample of fault-scarp-derived colluvium to Paleo Research Institute for charcoal extraction and AMS ^{14}C age analysis at the Keck Carbon Cycle AMS Facility at the University of California, Irvine (appendix A). The AMS ages from trench WFT-1 are presented in table 13.

The three samples submitted for AMS analysis yielded young ages. Samples S1 and S2 are stratigraphically inverted, which we attribute to modern organic contamination from bioturbation. Of importance is that three relatively young ages were obtained, consistent with two of the youngest stratigraphic units in the trench. However, as discussed below, the ages are not consistent with OSL ages.

WFT-1 OSL Ages

We collected two samples for OSL age dating from trench WFT-1 (appendix B). Our new OSL ages and the original UGS OSL ages (Lund and others, 2008) are presented in table 14. The OSL ages are significantly older than the AMS ^{14}C ages (table 13). Additionally, the OSL ages for units 2 (67,750 ± 4560) and 4 (75,570 ± 5130) (plate 14) are inverted; unit 4 is stratigraphically higher (younger) than unit 2.

Trench WFT-1 – Summary

The ^{14}C and OSL ages in trench WFT-1 are very different and problematic in regard to determining the timing of earthquakes at this site. Alluvial unit 9 is faulted and underlies unit 11, a fault-scarp-derived colluvial wedge associated with fault f5 (station 0+46.5, plate 14). The relatively old OSL ages for units 9 (18,590 ±1160) and unit 11 (4170 ±1360), which are within 1.7 and 1.0 feet (0.52 and 0.3 m), respectively, of the ground surface, do not appear to be stratigraphically reason-

Table 13. *Trench WFT-1 radiocarbon ages.*

Relative Stratigraphic Age	Sample	Geologic Unit		Age 2σ	
				RCYBP	cal yr B.P.[1]
youngest	S1	11	colluvial wedge	645 ± 15	670–630 (38.8%) 600–560 (56.6%)
↓	S2	9	alluvium	530 ± 15	560–510
oldest	S3	8	alluvium	925 ± 15	920–790

[1]*Two-sigma uncertainty.*

Table 14. *Trench WFT-1 OSL ages.*

Relative Stratigraphic Age	Sample	Geologic Unit		OSL Age
youngest	WF S-5 [1]	11	colluvial wedge	4170 ± 1360
↓	WF S-4 [1]	8	alluvium in-filling	7020± 1480
	WD 3 [2]	9	alluvium	18,590 ± 1,160
	WD 5 [2]	8	alluvium	30,810 ± 2110
	WD 4 [2]	7	alluvium	30,590 ± 2100
	WD 1 [2]	2	alluvium in-filling	67,750 ± 4560
oldest	WD 2 [2]	4	alluvium	75,570 ± 5130

[1]*Sample obtained during this investigation.*

[2]*Sample obtained by the UGS (Lund and others, 2008).*

able; however, they are stratigraphically consistent (younger above older). In contrast, we consider the young ^{14}C ages more reasonable for such shallow alluvial deposits.

The ^{14}C age of unit 11 (670–640 cal yr B.P [38.8%], 600–560 cal yr B.P. [56.6%]) is within the age range of the P1 surface-faulting earthquake at the Dutchman Draw, Arizona, site (1000 ± 600 cal yr B.P.; Lund and others, this volume) at the 2σ confidence level. Therefore, unit 11 may represent the Dutchman Draw P1 earthquake. The absence of a fault scarp suggests the scarp formed in the loose, unconsolidated sediments characteristic of the Washington Fields area was subsequently rapidly eroded.

The significantly older OSL age for unit 11 (4170 ± 1360) suggest the P1 surface-faulting earthquake at Dutchman Draw (Lund and others, this volume) is not present in trench WFT-1. The age of unit 11 (4170 ± 1360) overlaps at the 2σ confidence level with the age of the P2 surface-faulting earthquake at the Dutchman Draw site (7700 ± 2400), suggesting that unit 11 also represents the Dutchman Draw P2 earthquake, and that the P1 earthquake is not present in this trench. It could not be resolved during this investigation which set of ages, ^{14}C or OSL, is representative of faulting in this trench.

Figure 9 presents displacements for the four geologic units for which displacements could be measured, from oldest (unit 2) to youngest (unit 8).

Figure 9 shows:

1. The average displacement per surface-faulting earthquake between units 2, 4, 6, and 8 (three displacement intervals) is about 4.4 feet (1.3 m). Unit 8, the youngest alluvial unit, is displaced about 10 feet (3 m), which is about twice the average displacement of the other older units, and therefore may represent two earthquakes. If so, there may have been as many as five earthquakes in the past ~67,750 years. Note that we use the OSL age for unit 2 for this analysis, rather than the older OSL age of ~75,570 from unit 4, which is a stratigraphically younger unit (inverted ages).

2. There has been at least 23 feet (7 m) of cumulative displacement in the past ~67,750 years; average displacement (assuming five earthquakes) per surface-faulting earthquake was about 4.6 feet (1.4 m).

3. The average vertical slip rate on the Washington fault zone at this site over the past ~67,750 years is about 0.004 in/yr (0.1 mm/yr).

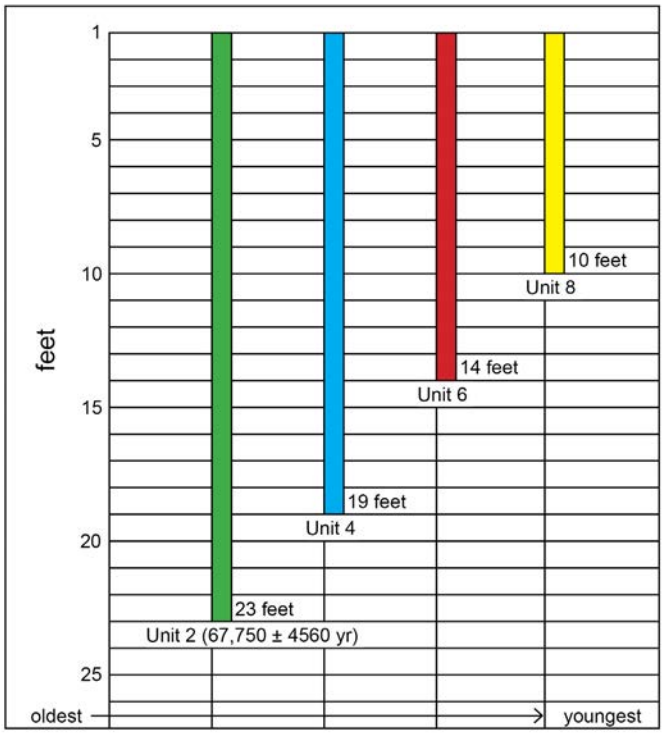

Figure 9. *Displacements within trench WFT-1.*

INVESTIGATION RESULTS

1. Most of the proposed Southern Parkway (State Route 7) northern extension is underlain by Holocene- to perhaps late Pleistocene-age unconsolidated alluvial deposits; these deposits cover bedrock formations of Triassic and Jurassic age.

2. Faults documented during this investigation were relatively complex, consisting of multiple strands, areas of upward-diverging fault splays, and areas of local thrusting.

3. Results of the subsurface exploration indicate the faults documented in the study area are Holocene; therefore, the faults are considered "active" for the purpose of siting proposed elevated structures associated with the transportation corridor.

4. Because the geomorphology of the St. George basin is dominated by erosion, fault scarps preserved on unconsolidated deposits were rare and isolated.

5. Multiple surface-faulting earthquakes were identified in trenches T-1, T-2, T-4, and WFT-1.

6. As many as five surface faulting earthquakes may have occurred on the Fort Pearce section over the past ~67,750 years.

7. There has been at least 23 feet (7 m) of cumulative displacement on the Washington fault in the past ~67,750 years at the Washington Fields site.

8. The average vertical slip rate over the past ~67,750 years is about 0.004 in/yr (0.10 mm/yr).

9. Some paleoearthquakes documented during this investigation appear to correlate with both the P1 (1000 ± 600 cal yr B.P.) and P2 (7700 ± 2400 cal yr B.P.) earthquakes documented on the Fort Pearce section at the Dutchman Draw, Arizona, paleoseismic investigation site (Lund and other, this volume).

10. Based on data from trench WFT-1, average displacement (assuming five earthquakes) per surface-faulting earthquake was about 4.6 feet (1.4 m).

11. Due to the proximity to Holocene faulting, two of the interchange structures were relocated in accordance with building setback criteria in Christenson and others (2003). Where feasible, proposed roadway crossings of the faults will be near perpendicular.

ACKNOWLEDGMENTS

We are grateful to William Lund and Tyler Knudsen with the UGS Southern Utah Regional Office for valuable advice, discussions, and information concerning trench exposures and local geology, and most importantly for providing field reviews of all trench excavations and trench logs. Thoughtful and thorough reviews by William Lund, Tyler Knudsen, Steve Bowman, and Mike Hylland, UGS, and Phil Pearthree, Arizona Geological Survey, greatly improved the figures and text. The authors are also appreciative to Rosenberg Associates (St. George, Utah) for providing graphical support, licensed land survey support, and GIS services for this investigation.

REFERENCES

Applied Geotechnical Engineering Consultants, 2007, Surface fault rupture hazard study, proposed Zippy LLC, 47-acre site, Washington Fields, Washington, Utah (AGEC Project No. 2070301): Sandy, Utah, unpublished consultant's report dated June 11, 2007, prepared for Zippy LLC c/o Rosenberg Associates, St. George, Utah, 14 p.

Biek, R.F., Rowley, P.D., Hayden, J.M., Hacker, D.B., Willis, G.C., Hintze, L.F., Anderson, R.E., and Brown, K.D., 2009, Geologic map of the St. George and east part of the Clover Mountains 30′ x 60′ quadrangles, Washington and Iron Counties, Utah: Utah Geological Survey Map 242, 101 p., 2 plates, scale 1:100,000.

Bowman, S.D, Young, B.W., and Unger, C.D., 2011, Compilation of 1982–83 seismic safety investigation reports of eight SCS dams in southwestern Utah (Hurricane and Washington fault zones) and low-sun-angle aerial photography, Washington and Iron Counties, Utah, and Mohave County, Arizona—Paleoseismology of Utah, Volume 21: Utah Geological Survey Open-File Report 583, 4 p., 6 DVD set.

Christenson, G.E., Batatian, L.D., and Nelson, C.V., 2003, Guidelines for evaluating surface-fault-rupture hazards in Utah: Utah Geological Survey Miscellaneous Publication 03-6, 14 p.

Crone, A.J., Machette, M.N., Bonilla, M.G., Lienkaemper, R.K., Pierce, K.L., Scott, W.E., and Buckman, R.C., 1987, Surface faulting accompanying the Borah Peak earthquake and segmentation of the Lost River fault, central Idaho: Bulletin of the Seismological Society of America, v. 77, no. 3, p. 739–770.

DuRoss, C.B., 2008, Holocene vertical displacement on the central segments of the Wasatch fault zone, Utah: Bulletin of the Seismological Society of America, v. 98, no. 6, p. 2918–2933.

Earth Science Associates, 1982, Phase I report, seismic safety investigation of eight SCS dams in southwestern Utah: Portland, Oregon, unpublished consultant's report for the U.S. Soil Conservation Service, dated December 1982, ESA project no. D118.

Earth Science Associates, 1983, Phase II report, seismic safety investigation of eight SCS dams in southwestern Utah: Portland, Oregon, unpublished consultant's report for the U.S. Soil Conservation Service, dated February 1983, ESA project no. D118.

Fuller, J.G., 1984, The day we bombed Utah—America's most lethal secret: New York, New York, New American Library, (ISBN 0-453-00457-1), 262 p.

Hayden, J.M., 2005, Geologic map of the Washington Dome quadrangle, Washington County, Utah: Utah Geological Survey Map 209, 29 p., 2 pl., scale 1:24,000.

Lund, W.R., Knudsen, T.R., and Sharrow, D.L., 2010, Geologic hazards of the Zion National Park geologic-hazard study area, Washington and Kane Counties, Utah: Utah Geological Survey Special Study 133, 95 p., 9 plates, DVD.

Lund, W.R., Knudsen, T.R., Vice, G.S., and Shaw, L., 2008, Geologic hazards and adverse construction conditions, St. George–Hurricane metropolitan area, Washington County, Utah: Utah Geological Survey Special Study 127, 105 p., DVD.

Ostenaa, D., 1984, Relationships affecting estimates of surface fault displacement based on scarp-derived colluvial deposits [abs.]: Geological Society of America Abstracts with Programs, v. 16, no. 5, p. 327.

Pearthree, P.A., compiler, 1997, Fault number 1004c, Washington fault zone, Sullivan Draw section, *in* Quaternary fault and fold database of the United States: Online, http://earthquakes.usgs.gov/hazards/qfaults, accessed October 13, 2013.

Rosenberg Associates, 2009, Surface-fault-rupture hazard evaluation, Task I, Interchange 10 and 11, Southern Parkway, Rosenberg Associates' project no. 5507-P3 09R036.G, September 3, 2009: Pleasant Grove, Utah, unpublished consultant's report for Horrocks Engineering.

Wesnousky, S.G., 2008, Displacement and geometrical characteristics of earthquake surface ruptures—issues and implications for seismic-hazard analysis and the process of earthquake rupture: Bulletin of the Seismological Society of America, v. 98, no. 4, p. 1609–1632.

Western GeoArch Research, LLC., 2011, Geoarchaeological assessment of 42ws5277 and a proposed detention basin in the Southern Parkway study area, Washington, Utah: Driggs, Idaho, unpublished consultant's report prepared for Horrocks Engineers Inc. and the Utah Department of Transportation, March 2011, 70 p.

APPENDICES

APPENDIX A

PaleoResearch Institute Report
Organic Recovery and AMS Dates for the
Washington Fault, Phase III Corridor Project, Southern Utah

By

Linda Scott Cummings

With Assistance from
R. A. Varney

PaleoResearch Institute
Golden, Colorado

PaleoResearch Institute Technical Report 09-143

Prepared For

Rosenberg Associates
St. George, Utah

November, 2009

INTRODUCTION

Eleven sediment samples from four trenches (T-1, T-2, T-4, and WFT) across the Washington Fault in Southern Utah were examined to recover particulate organics that might include microscopic charcoal and/or pollen for radiocarbon dating. Upon recovery of this material, AMS radiocarbon dating was performed.

METHODS

Organic Extraction

Now it is possible to recover microscopic charcoal, pollen, and other organics from sediments for the purpose of obtaining an AMS radiocarbon age. Microscopic charcoal fragments are far superior to humates because they provide dates with the same precision as those obtained from larger pieces of charcoal, with the single exception that the individual pieces of microscopic charcoal are not identified to taxon. Recovery of pollen and other organics also provides the opportunity to obtain a date on sediments that are determined, in the field, to pose little or no risk of contamination by materials more recent than the event on which the date is desired.

A chemical extraction technique based on that used for pollen, and relying upon heavy liquid extraction, has been modified to recover microscopic charcoal for the purpose of obtaining an AMS radiocarbon age. After removing calcium carbonates with hydrochloric acid (10%), the samples were screened through 150 micron mesh. Samples were rinsed until neutral, then a small quantity of sodium hexametaphosphate was added to each sample, which was then filled with reverse osmosis, deionized (RODI) water and allowed to settle according to Stoke's Law. After two hours the supernatant, containing clay, was poured off and the sample was rinsed with RODI water three more times, being allowed to settle according to Stoke's Law to remove more clays. Once the clays had been removed, the samples were freeze dried. Sodium polytungstate (SPT), with a density of 1.8, was used for the flotation process. The samples were mixed with SPT and centrifuged at 1500 rpm for 10 minutes to separate organic from inorganic remains. The supernatant containing pollen, organic remains, and microscopic charcoal was decanted. Sodium polytungstate was again added to the inorganic fraction to repeat the separation process until all visible charcoal had been recovered. The organics were recovered from the sodium polytungstate and rinsed thoroughly with RODI water. At this stage, the particulate organics received standard acid-base-acid chemical pre-treatment.

AMS Radiocarbon Dating

Each sample selected for pre-treatment is first subjected to hot (at least 110 °C), 6N hydrochloric acid (HCl), with rinses to neutral between each HCl treatment, until the supernatant is clear. This removes iron compounds and calcium carbonates that would hamper removal of humate compounds later. Next the samples are subjected to 5% potassium hydroxide (KOH) to remove humates. Once again, the samples are rinsed to neutral and re-acidified with pH 2 HCl between each KOH step. This step is repeated until the supernatant is clear, signaling removal

of all humates. After humate removal, each sample is made slightly acidic and left that way for the next step.

Each submitted sample is then freeze-dried using a vacuum system, freezing out all moisture at -98 °C. Each individual sample is combined with cupric oxide (CuO) and elemental silver (Ag^o) in a quartz tube, then flame sealed under vacuum.

Standards and laboratory background samples also are treated in the same manner as the wood and charcoal samples of unknown age. A radiocarbon "dead" EUA wood blank from Alaska that is more than 70,000 years old (currently beyond the detection capabilities of AMS) is treated using the same chemical processing as the samples of unknown age in order to calibrate the laboratory correction factor. Standards of known age, such as Two Creeks wood that dates to 11,400 RCYBP and others from the Third International Radiocarbon Intercomparison (TIRI), are also processed simultaneously to establish the laboratory correction factor. Each wood standard is run in a quantity similar to the submitted samples of unknown age and sealed in a quartz tube after the requisite pre-treatment.

Once all the wood standards, blanks, and submitted samples of unknown age are prepared and sealed in their individual quartz tubes, they are combusted at 820 °C, soaked for an extended period of time at that temperature, and then slowly allowed to cool to enable the chemical reaction that extracts carbon dioxide ($C0_2$) gas.

Following this last step, all samples of unknown age, the wood standards, and the laboratory backgrounds are sent to the Keck Carbon Cycle AMS Facility at the University of California, Irvine, where the $C0_2$ gas is processed into graphite. The graphite in these samples is then placed in the target and run through the accelerator, which produces the numbers that are converted into the radiocarbon date presented in the data section. Dates are presented as conventional radiocarbon ages, as well as calibrated ages using Intcalc04 curves on Oxcal version 3.10.

RESULTS AND DISCUSSION

Alluvial fan sediments from three trench excavations across the Washington Fault in southern Utah were sampled to recover particulate organics for AMS radiocarbon dating (Table 1). Organics expected in these sediments are primarily microscopic charcoal and pollen. Chemical pretreatment should remove the more mobile organics that typically constitute the humate and humic fractions. Samples were screened through 250 micron mesh to remove rootlets.

Trench 1

Sediments from T-1 were expected to be of Holocene age. Samples S-1, S-2, and S-3 represent alluvial fan sediments from Trench 1. Sample T1-S1 yielded sufficient particulate organics to date. A radiocarbon date of 2140 ± 15 RCYBP (PRI-09-143-T1-S1) is reported on these particulate organics (Table 2). This date calibrates to 2300-2270; 2160-2060 CAL yr. BP at the two-sigma level (Figure 1). It is slightly older than the date of 1480 ± 70 RCYBP reported

for the paleosol beneath the Most Recent Event (MRE) wedge at the Dutchman Draw trench site (Puseman 2009). This date is younger than the dates reported from the other trenches examined at the Dutchman Draw trench site.

Sample T1- S2 yielded a small quantity of *Pinus* charcoal, which was selected for dating in preference to continuing the extraction process to recover particulate organics. Sample T1-S2 yielded a radiocarbon date of 205 ± 15 RCYBP (PRI-09-143-T1-S2), which calibrates to 300-260; 190-140, or 20-present CAL yr. BP (Figure 2) at the two-sigma level. The very recent date reported on pine charcoal for this sediment indicates that there has been a considerable amount of mixing, bioturbation, or intrusion of modern to very recent material into these sampled alluvial deposits. Any pine wood large enough to burn, whether in a campfire or in a natural fire, is likely to have been at least several decades to more than 100 years old, indicating that the intrusion of organic material into these deposits could have happened at almost any time in the past 200 years, with at least a slight bias towards the present.

Sample T1-S3 yielded a radiocarbon date of 465 ± 15 RCYBP (PRI-09-143-T1-S3) on particulate organics extracted from the alluvium, which calibrates to 530-500 CAL yr. BP (Figure 3) at the two-sigma level. Once again, these alluvial sediments appear to have been heavily bioturbated, mixed, and or suffered from intrusion of modern to recent material, although this mixing appears to have happened earlier than that noted for sample T1-S2.

Trench 2

Trench T-2 sampled alluvial fan sediments that were expected to represent latest Pleistocene to early Holocene deposits. The particulate organics extracted from sample T2-S1 appeared very similar to those recovered from Trench 1, although this sample contained very modern carbon, yielding a Fraction Modern of 1.058100 ± 0.00150 (PRI-09-143-T2-S1). Dates during the atomic bomb testing era to modern are reported as Fraction Modern. This date calibrates between December 1955 and July 1957 at the two-sigma level (Figure 4), indicating that the carbon recovered from these sediments originated in this brief year-and-a-half interval. Due to rapidly changing quantities of ^{14}C in the atmosphere since the beginning of atomic bomb testing, dates during this interval can calibrate to very short periods.

Sample T2-S2 yielded no particulate carbon, indicating that this portion of the alluvium probably was not compromised by the intrusion of more recent or modern carbon. Unfortunately, it also did not contain carbon from the period of deposition and therefore, yielded no radiocarbon date.

Trench 4

Trench 4 is represented by three samples, two of which were expected to be of Holocene age. Sample T4-S3 yielded a Fraction Modern of 1.051200 ± 0.001700 (PRI-09-143-T4-S3), which calibrates to October 1955 to May 1957 at the two-sigma level (Figure 5). This date indicates that these sediments suffered a disturbance that introduced organic particles, including pollen, that were alive during this interval.

Sample T4-S4 also yielded a very recent date with a Fraction Modern of 0.998200 ± 0.001300 (PRI-09-143-T4-S4) on particulate organics, which calibrates to November 1951 to July 1955 at the two-sigma level (Figure 6). This date calibrates to a time only slightly before that reported for samples T2-S1 and T4-S3, as it ends July 1955, while the dates from the other two samples begin in December 1955 and October 1955, respectively.

Sample T4-S5 yielded a modern date of 1.004500 ± 0.001700 (PRI-09-143-T4-S5) on particulate organics, which calibrates to May 1952 to October 1955 at the two sigma level, which overlaps with the date obtained from sample T4-S4 very well and the other modern dates very slightly (Figure 7).

All three samples examined from Trench 4 yielded very recent dates, indicating that these alluvial sediments have been compromised with particulate organics very recently. The consistency of these dates, as well as the near overlap with the date from Trench 2 suggests fault activity in or around 1955 in this area. The slight difference in the calibrated dates suggests there might have been multiple shocks during this historic period. At a minimum there appears to have been a significant disturbance to the area in the early to middle 1950s that is recorded in these radiocarbon dates. It is unlikely that additional samples from this exposure/location in the alluvial deposits will yield radiocarbon dates indicative of earlier fault activity unless field work can identify different exposures.

Washington Fault Trench

Colluvial sediments in the Washington Fault Trench are expected to yield Holocene dates. All three samples from this trench yielded particulate organics, which were radiocarbon dated. Sample WFT-S1 yielded a date of 645 ± 15 RCYBP (PRI-09-143-WFT-S1) on particulate organics, which calibrates to 670-630; 600-560 CAL yr. BP at the two-sigma level, suggesting disturbance around 600 years ago (Figure 8).

Sample WFT-S2 yielded a date of 530 ± 15 RCYBP (PRI-09-143-WFT-S2) on particulate organics, which calibrates to 560-510 CAL yr. BP, which is slightly younger than the date obtained from sample WFT-S1 and suggests disturbance around or slightly more than 500 years ago (Figure 9).

Sample WFT-S3 yielded a date of 925 ± 15 RCYBP (PRI-09-143-WFT-S3) on particulate organics, which calibrates to 920-790 CAL yr. BP (Figure 10). This date provides evidence of disturbance, which might be fault activity, at this time.

The three dates obtained from the Washington Fault Trench suggest fault activity or at least a significant disturbance to these colluvial sediments late in the Holocene, within the past approximately 900 years.

CONCLUSIONS

Radiocarbon dating of alluvial and colluvial sediments from Trenches 1, 2, 4, and the Washington Fault Trench in southern Utah has provided dates that appeared, on first

examination, to not relate to faulting activity. However, upon final examination of these dates, definite trends are visible. All but one of these dates is on particulate organics, which include pollen. The oldest date is reported on alluvial sediments from T1-S1 (2140 ± 15 RCYBP), suggesting that this is the oldest fault activity represented by these samples. This is an older date than that reported for the youngest wedge examined from Dutchman Draw, which overlies a weakly developed soil, providing an end date for that soil formation. Next, dates from the Washington Fault Trench are reported as 925 ± 15 RCYBP (sample WFT-S3), 645 ± 15 RCYBP (sample WFT-S1), and 530 ± 15 RCYBP (sample WFT-S2), suggesting a series of faults in the late Holocene. A date of 465 ± 15 RCYBP (sample T1-S3) falls in line with these dates. A date of 205 ± 15 RCYBP (sample T1-S2) on pine charcoal might reflect a fault or disturbance almost any time within the past 200, but more likely 150, years. Finally, recovery of very recent dates between November 1951 and July 1957 from samples T2-S1, T4-S3, T4-S4, and T4-S5 indicates that these locations have been disturbed, possibly by faulting, very recently, probably in the early to middle 1950s, which resulted in intrusion of particulate organics, including pollen, into the sediments at that time.

TABLE 1
PROVENIENCE DATA FOR SAMPLES FROM TRENCH EXCAVATIONS ACROSS THE WASHINGTON FAULT, SOUTHERN UTAH

Sample No.	Trench	Depth (ft.)	Anticipated Age	Provenience/ Description	Analysis
S-1	T-1		Holocene	Alluvial fan sediments	Particulate organics recovery AMS ^{14}C Date
S-2				Alluvial fan sediments	Charcoal ID AMS ^{14}C Date
S-3				Alluvial fan sediments	Particulate organics recovery AMS ^{14}C Date
S-1	T-2		Latest Pleistocene to Holocene	Alluvial fan sediments	Particulate organics recovery AMS ^{14}C Date
S-2				Alluvial fan sediments	Particulate organics recovery No date possible
S-3	T-4		Holocene	Alluvial fan sediments	Particulate organics recovery AMS ^{14}C Date
S-4				Alluvial fan sediments	Particulate organics recovery AMS ^{14}C Date
S-5			Latest Pleistocene to Holocene	Alluvial fan sediments	Particulate organics recovery AMS ^{14}C Date
S-1	WFT	1.0	Holocene	Colluvial sediments	Particulate organics recovery AMS ^{14}C Date
S-2		1.4		Colluvial sediments	Particulate organics recovery AMS ^{14}C Date
S-3		2.4		Colluvial sediments	Particulate organics recovery AMS ^{14}C Date

TABLE 2
RADIOCARBON RESULTS FOR SAMPLES FROM TRENCH EXCAVATIONS ACROSS THE WASHINGTON FAULT, SOUTHERN UTAH

Sample No.	Sample Identification	AMS ^{14}C Date*	1-sigma Calibrated Date (68.2%)	2-sigma Calibrated Date (95.4%)	$\delta^{13}C$** ($^{o}/_{oo}$)
PRI-09-143-T1-S1	Microcharcoal	2140 ± 15 RCYBP	2155-2110 2080-2070 CAL yr. BP	2300-2270 2160-2060 CAL yr. BP	-13.4
PRI-09-143-T1-S2	*Pinus* charcoal	205 ± 15 RCYBP	290-280 180-150 10-(-11) CAL yr. BP	300-260 190-140 20-(-11) CAL yr. BP	-19.7
PRI-09-143-T1-S3	Microcharcoal	465 ± 15 RCYBP	525-505 CAL yr. BP	530-500 CAL yr. BP	-14.2
PRI-09-143-T2-S1	Microcharcoal	-450 ± 15 RCYBP	Apr. 1956-Mar. 1957	Dec. 1955-July 1957	-22.6
PRI-09-143-T4-S3	Microcharcoal	1.051200 ± 0.001700 FM	February to December 1956	October 1995 to May 1957	-29.0
PRI-09-143-T4-S4	Microcharcoal	0.998200 ± 0.001300 FM	March 1952 to April 1954	November 1951 to July 1955	-28.0
PRI-09-143-T4-S5	Microcharcoal	1.004500 ± 0.001700 FM	December 1952 to January 1955	May 1952 to October 1955	-20.0
PRI-09-143-WFT-S1	Microcharcoal	645 ± 15 RCYBP	660-640 590-565 CAL yr. BP	670-630 600-560 CAL yr. BP	-27.7
PRI-09-143-WFT-S2	Microcharcoal	530 ± 15 RCYBP	545-525 CAL yr. BP	560-510 CAL yr. BP	-27.8
PRI-09-143-WFT-S3	Microcharcoal	925 ± 15 RCYBP	910-850 840-790 CAL yr. BP	920-790 CAL yr. BP	-26.7

* Reported in radiocarbon years at 1 standard deviation measurement precision (68.2%), corrected for $\delta^{13}C$

** $\delta^{13}C$ values are measured by AMS during the ^{14}C measurement for use during the ^{14}C calculation and should not be used for dietary or paleoenvironmental interpretations.

FM = Fraction Modern. Recent dates (falling within the time after atomic testing began) are reported as Fraction Modern because calibrations can only be done using Fraction Modern for this time period. Years BP are calculated as prior to 1950 rather than the current year

FIGURE 1. PRI RADIOCARBON AGE CALIBRATION

Laboratory Number: PRI-09-143-T1-S1
Sample Identification: Microcharcoal
Conventional AMS ^{14}C Date: 2140 ± 15 RCYBP
1-sigma Calibrated Date (68.2%): 2155-2110; 2080-2070 CAL yr. BP
2-sigma Calibrated Date (95.4%): 2300-2270; 2160-2060 CAL yr. BP
$\delta^{13}C$ ($^{o}/_{oo}$): -13.4 (Measured for ^{14}C calculation, not valid for dietary or paleoenvironmental interpretations)

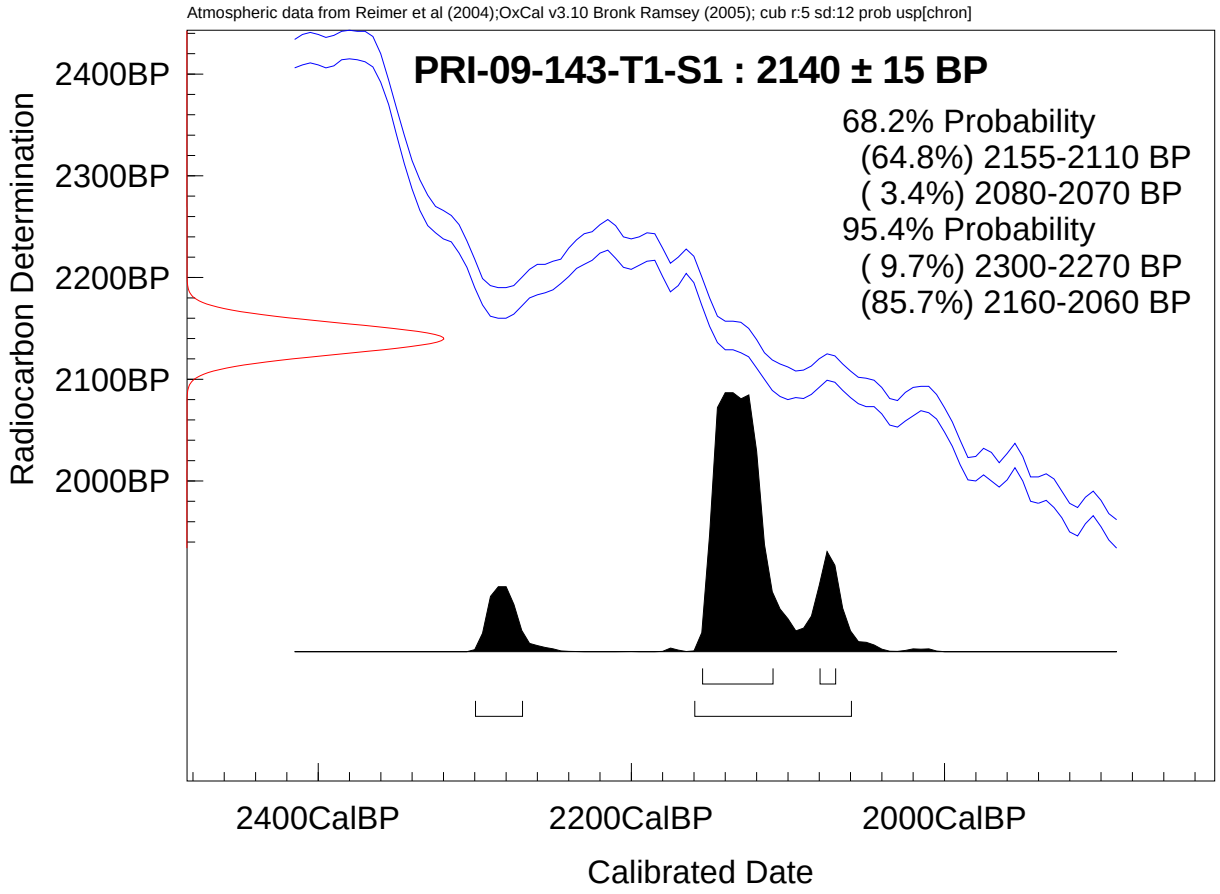

Intercept Statement. PaleoResearch Institute utilizes OxCal3.10 (Bronk Ramsey, 2005) for radiocarbon calibration, which is a probability-based method for determining conventional ages. We prefer this method over the intercept-based alternative because it provides our clients with a calibrated date that reflects the probability of its occurrence within a given distribution (reflected by the amplitude (height) of the curve), as opposed to individual point estimates {Telford, 2004 #4527}. As a result, the probability-based method offers more stability to the calibrated values than those derived from intercept-based methods that are subject to adjustments in the calibration curve {Telford, 2004 #4527}.

References

Telford, R. J., E. Heegaard, and H. J. B. Birks, 2004, *The Holocene* 14(2), pp. 296-298.

PaleoResearch Institute
2675 Youngfield Street, Golden, CO 80401
(303) 277-9848 • Fax (303) 462-2700
www.paleoresearch.com

FIGURE 2. PRI RADIOCARBON AGE CALIBRATION

Laboratory Number: PRI-09-143-T1-S2
Sample Identification: *Pinus* charcoal
Conventional AMS ^{14}C Date: 205 ± 15 RCYBP
1-sigma Calibrated Date (68.2%): 290-280; 180-150; 10-(-11) CAL yr. BP
2-sigma Calibrated Date (95.4%): 300-260; 190-140; 20-(-11) CAL yr. BP
$\delta^{13}C$ ($^{o}/_{oo}$): -19.7 (Measured for ^{14}C calculation, not valid for dietary or paleoenvironmental interpretations)

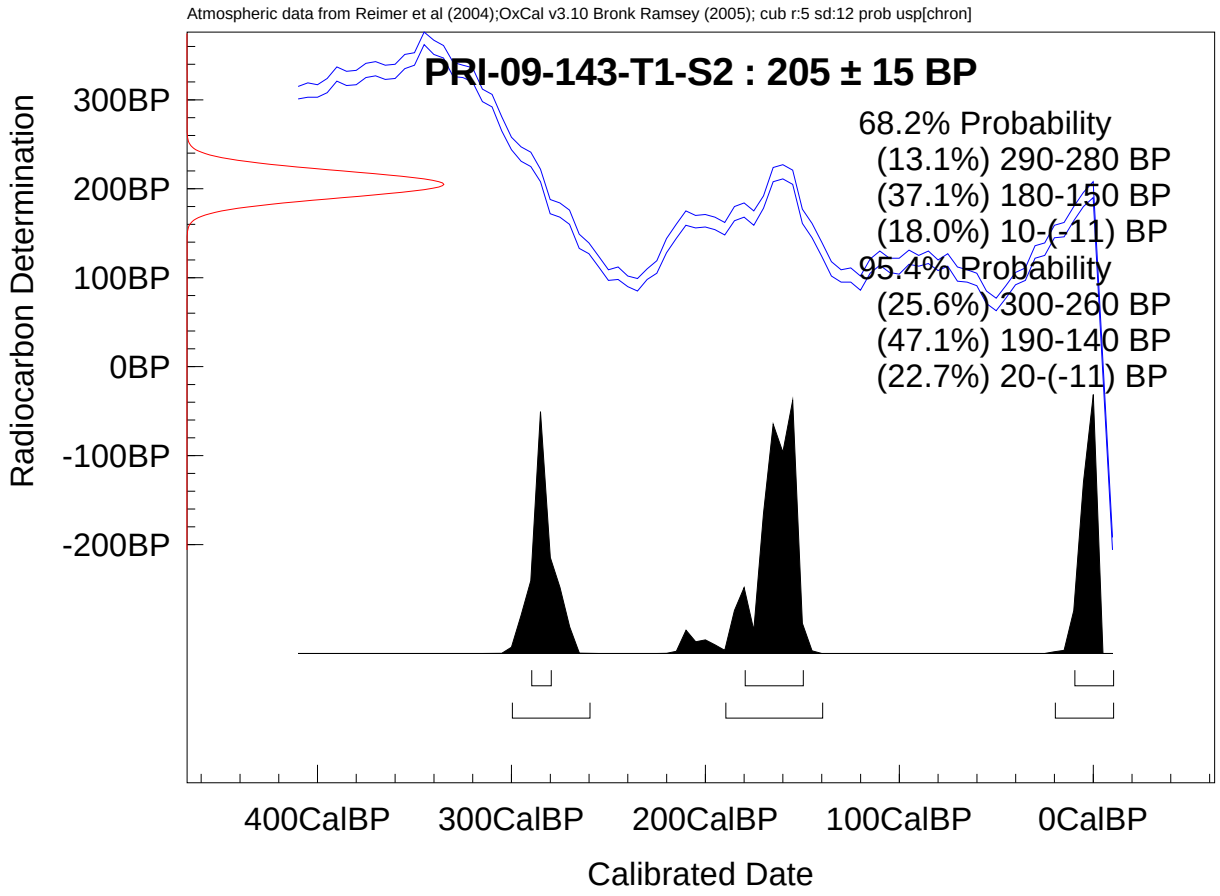

Intercept Statement. PaleoResearch Institute utilizes OxCal3.10 (Bronk Ramsey, 2005) for radiocarbon calibration, which is a probability-based method for determining conventional ages. We prefer this method over the intercept-based alternative because it provides our clients with a calibrated date that reflects the probability of its occurrence within a given distribution (reflected by the amplitude (height) of the curve), as opposed to individual point estimates {Telford, 2004 #4527}. As a result, the probability-based method offers more stability to the calibrated values than those derived from intercept-based methods that are subject to adjustments in the calibration curve {Telford, 2004 #4527}.

References

Telford, R. J., E. Heegaard, and H. J. B. Birks, 2004, *The Holocene* 14(2), pp. 296-298.

PaleoResearch Institute
2675 Youngfield Street, Golden, CO 80401
(303) 277-9848 • Fax (303) 462-2700
www.paleoresearch.com

FIGURE 3. PRI RADIOCARBON AGE CALIBRATION

Laboratory Number: PRI-09-143-T1-S3
Sample Identification: Microcharcoal
Conventional AMS ^{14}C Date: 465 ± 15 RCYBP
1-sigma Calibrated Date (68.2%): 525-505 CAL yr. BP
2-sigma Calibrated Date (95.4%): 530-500 CAL yr. BP
$\delta^{13}C$ ($^{o}/_{oo}$): -14.2 (Measured for ^{14}C calculation, not valid for dietary or paleoenvironmental interpretations)

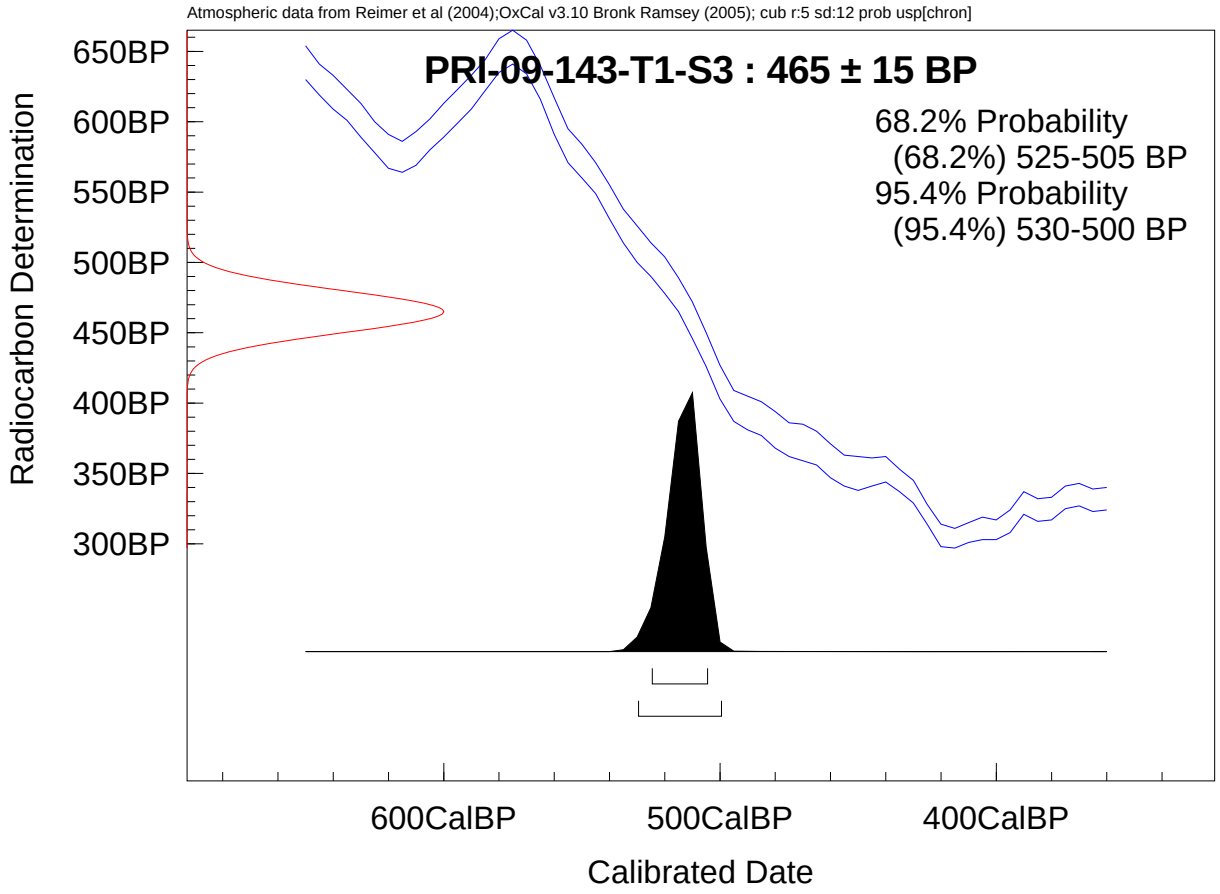

Intercept Statement. PaleoResearch Institute utilizes OxCal3.10 (Bronk Ramsey, 2005) for radiocarbon calibration, which is a probability-based method for determining conventional ages. We prefer this method over the intercept-based alternative because it provides our clients with a calibrated date that reflects the probability of its occurrence within a given distribution (reflected by the amplitude (height) of the curve), as opposed to individual point estimates {Telford, 2004 #4527}. As a result, the probability-based method offers more stability to the calibrated values than those derived from intercept-based methods that are subject to adjustments in the calibration curve {Telford, 2004 #4527}.

References

Telford, R. J., E. Heegaard, and H. J. B. Birks, 2004, *The Holocene* 14(2), pp. 296-298.

PaleoResearch Institute
2675 Youngfield Street, Golden, CO 80401
(303) 277-9848 • Fax (303) 462-2700
www.paleoresearch.com

FIGURE 4. PRI CALIBOMB RADIOCARBON AGE CALIBRATION

Laboratory Number: PRI-09-143-T2-S1
Sample Identification: Microcharcoal
Calibration of with NH_zone2.14c dataset

1-sigma Calibrated Date:	Probability:	2-sigma Calibrated Date:	Probability:
April 1956-March 1957	100.00%	December 1955-July 1957	100.00%

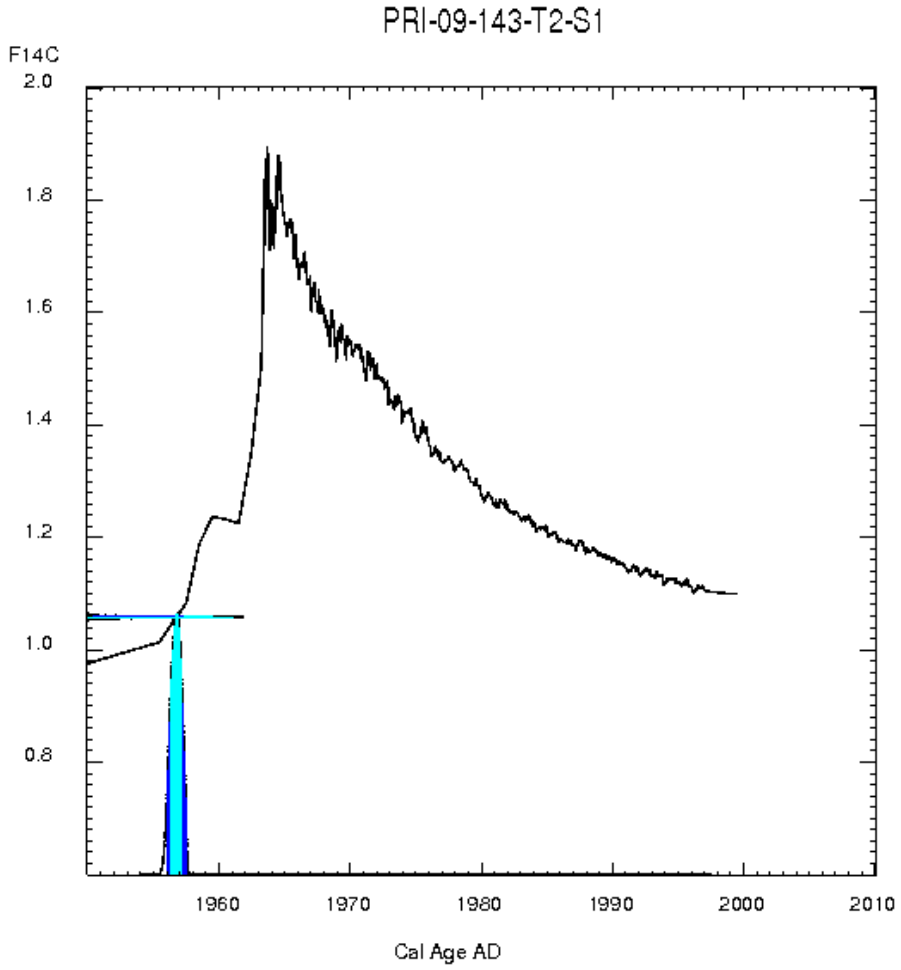

References

Hua, Q. and M. Barbetti, 2004, Review of Tropospheric Bomb ^{14}C Data for Carbon Cycle Modeling and Age Calibration Purposes", *Radiocarbon* 46:1273-1298.

FIGURE 5. PRI CALIBOMB RADIOCARBON AGE CALIBRATION

Laboratory Number: PRI-09-143-T4-S3
Sample Identification: Microcharcoal
Calibration of 1.051200 ± 0.001700 with NH_zone2.14c dataset

1-sigma Calibrated Date:	Probability:	2-sigma Calibrated Date:	Probability:
February-December 1956	100.00%	October 1955-May 1957	100.00%

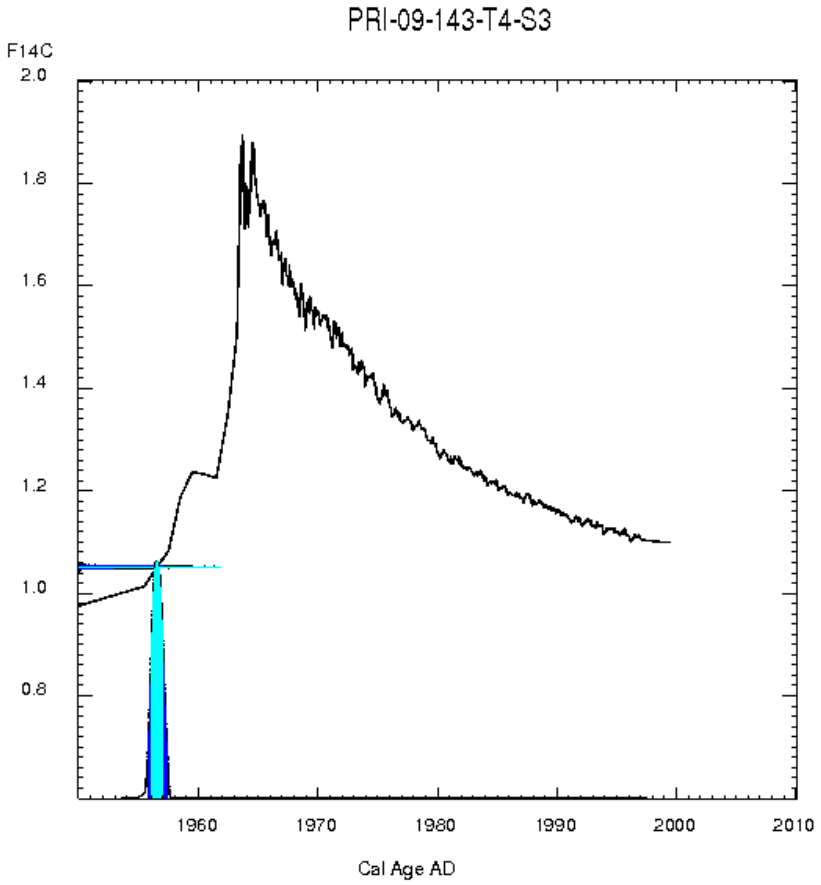

References

Hua, Q. and M. Barbetti, 2004, Review of Tropospheric Bomb ^{14}C Data for Carbon Cycle Modeling and Age Calibration Purposes", *Radiocarbon* 46:1273-1298.

FIGURE 6. PRI CALIBOMB RADIOCARBON AGE CALIBRATION

Laboratory Number: PRI-09-143-T4-S4
Sample Identification: Microcharcoal
Calibration of 0.998200 ± 0.001300 with NH_zone2.14c dataset

1-sigma Calibrated Date:	Probability:	2-sigma Calibrated Date:	Probability:
March 1952-April 1954	100.00%	November 1951-July 1955	100.00%

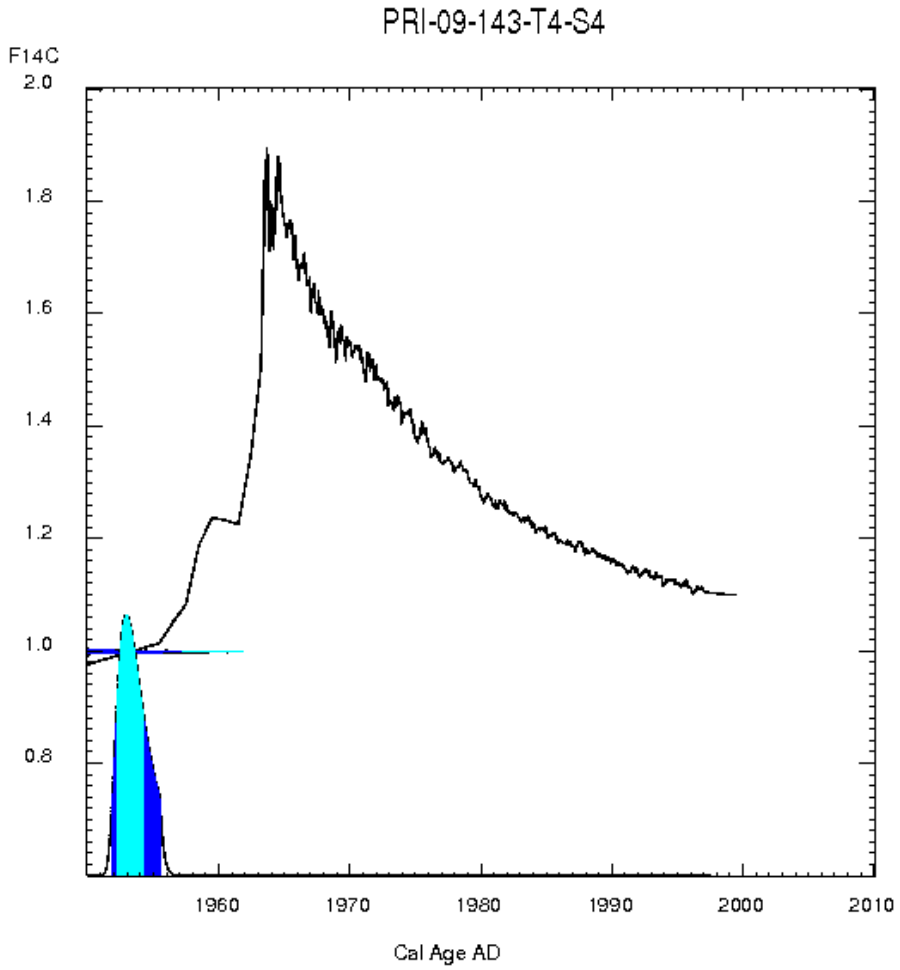

References

Hua, Q. and M. Barbetti, 2004, Review of Tropospheric Bomb ^{14}C Data for Carbon Cycle Modeling and Age Calibration Purposes", *Radiocarbon* 46:1273-1298.

FIGURE 7. PRI CALIBOMB RADIOCARBON AGE CALIBRATION

Laboratory Number: PRI-09-143-T4-S5
Sample Identification: Microcharcoal
Calibration of 1.004500 ± 0.001700 with NH_zone2.14c dataset

1-sigma Calibrated Date:	Probability:	2-sigma Calibrated Date:	Probability:
December 1952-January 1955	100.00%	May 1952-October 1955	100.00%

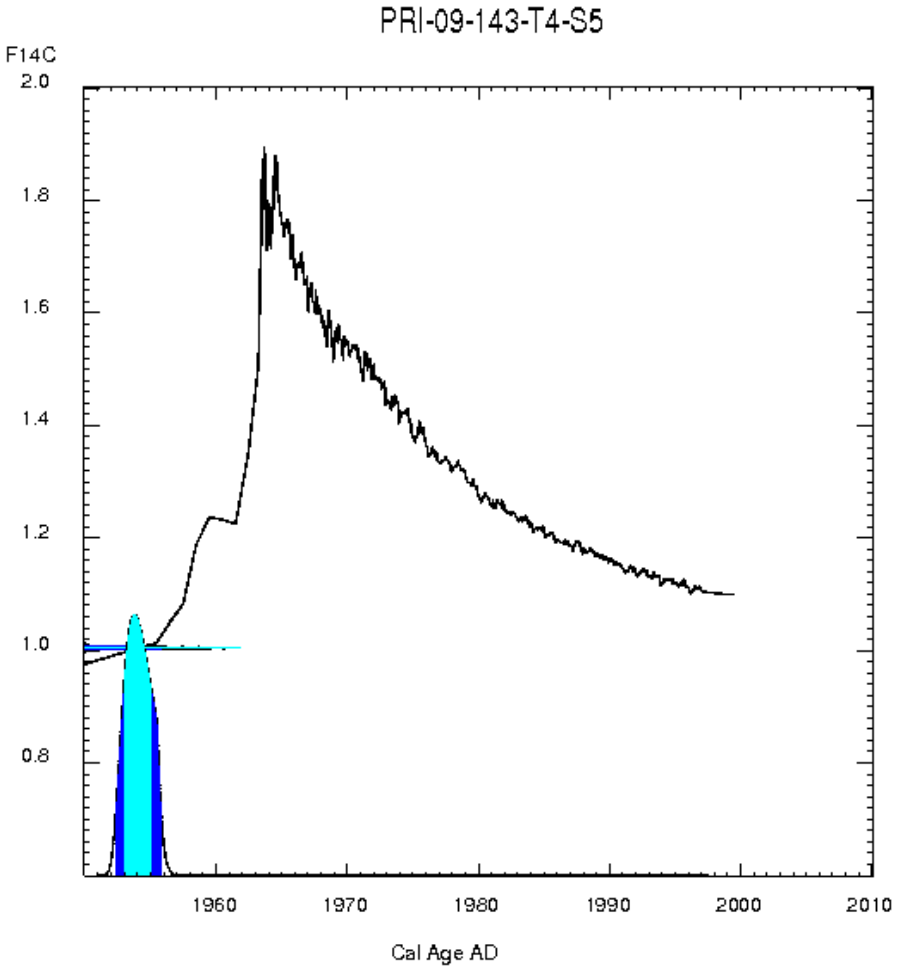

References

Hua, Q. and M. Barbetti, 2004, Review of Tropospheric Bomb ^{14}C Data for Carbon Cycle Modeling and Age Calibration Purposes", *Radiocarbon* 46:1273-1298.

FIGURE 8. PRI RADIOCARBON AGE CALIBRATION

Laboratory Number: PRI-09-143-WFT-S1
Sample Identification: microcharcoal
Conventional AMS ^{14}C Date: 645 ± 15 RCYBP
1-sigma Calibrated Date (68.2%): 660-640; 590-565 CAL yr. BP
2-sigma Calibrated Date (95.4%): 670-630; 600-560 CAL yr. BP
$\delta^{13}C$ ($^{o}/_{oo}$): -27.7 (Measured for ^{14}C calculation, not valid for dietary or paleoenvironmental interpretations)

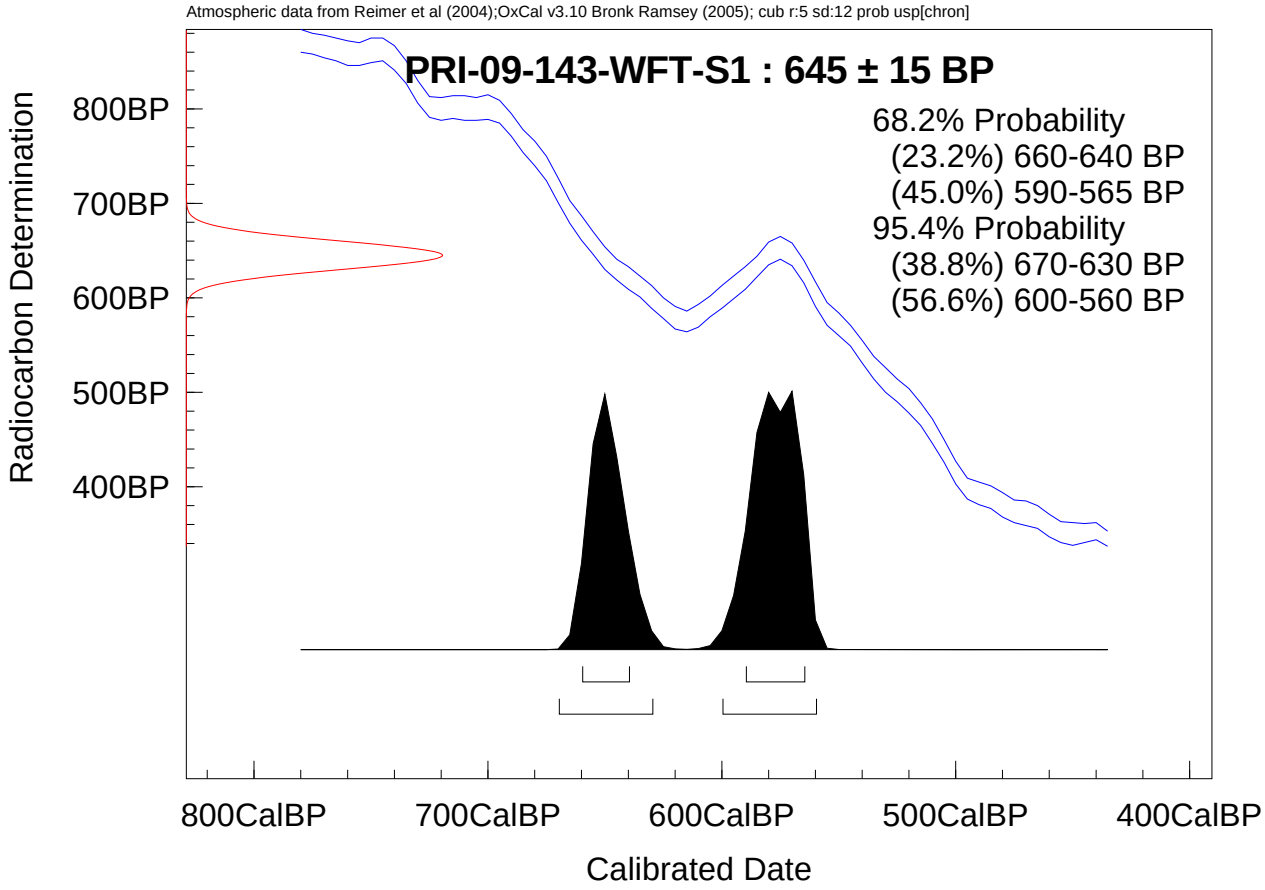

Intercept Statement. PaleoResearch Institute utilizes OxCal3.10 (Bronk Ramsey, 2005) for radiocarbon calibration, which is a probability-based method for determining conventional ages. We prefer this method over the intercept-based alternative because it provides our clients with a calibrated date that reflects the probability of its occurrence within a given distribution (reflected by the amplitude (height) of the curve), as opposed to individual point estimates (Telford 2004). As a result, the probability-based method offers more stability to the calibrated values than those derived from intercept-based methods that are subject to adjustments in the calibration curve (Telford 2004).

References

Telford, R. J., E. Heegaard, and H. J. B. Birks, 2004, *The Holocene* 14(2), pp. 296-298.

FIGURE 9. PRI RADIOCARBON AGE CALIBRATION

Laboratory Number: PRI-09-143-WFT-S2
Sample Identification: Microcharcoal
Conventional AMS ^{14}C Date: 530 ± 15 RCYBP
1-sigma Calibrated Date (68.2%): 545-525 CAL yr. BP
2-sigma Calibrated Date (95.4%): 560-510 CAL yr. BP
$\delta^{13}C$ ($^{o}/_{oo}$): -27.8 (Measured for ^{14}C calculation, not valid for dietary or paleoenvironmental interpretations)

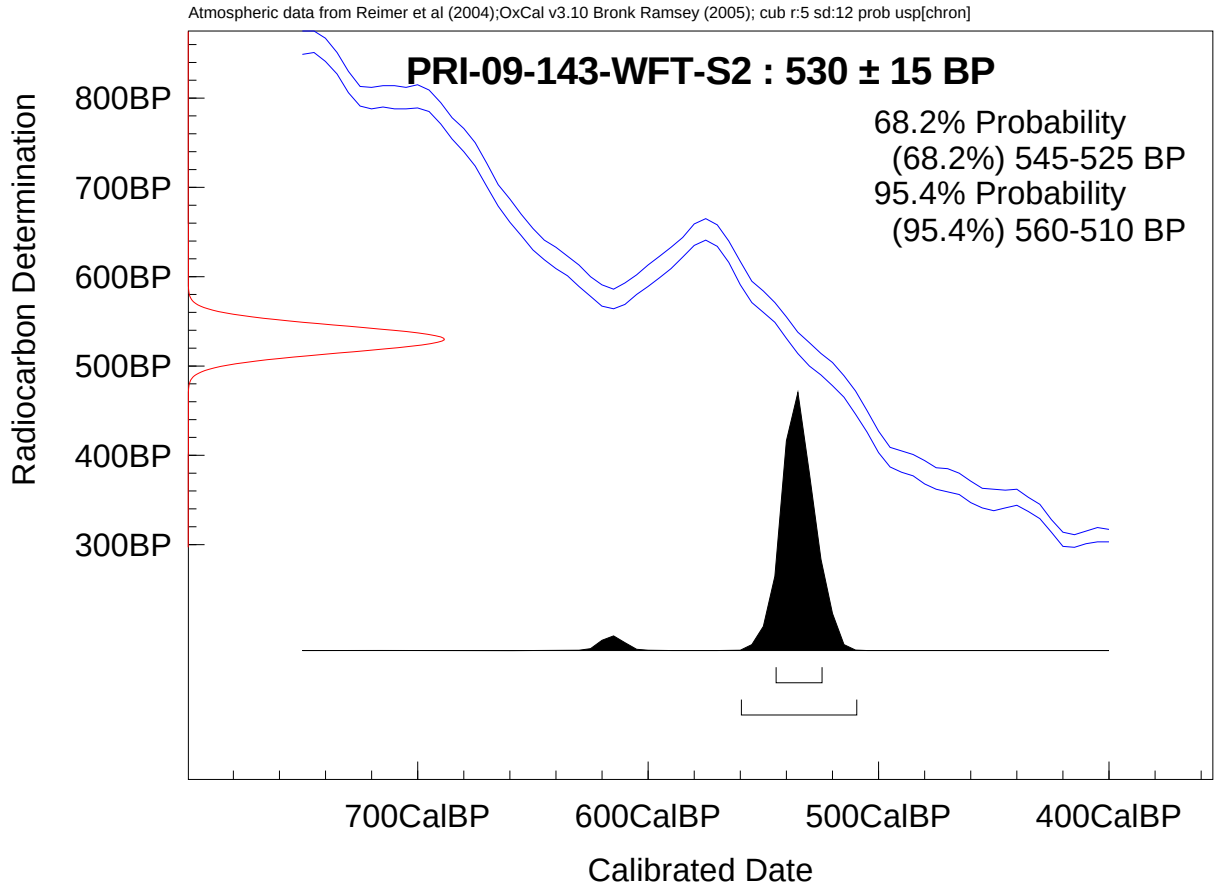

Intercept Statement. PaleoResearch Institute utilizes OxCal3.10 (Bronk Ramsey, 2005) for radiocarbon calibration, which is a probability-based method for determining conventional ages. We prefer this method over the intercept-based alternative because it provides our clients with a calibrated date that reflects the probability of its occurrence within a given distribution (reflected by the amplitude (height) of the curve), as opposed to individual point estimates (Telford 2004). As a result, the probability-based method offers more stability to the calibrated values than those derived from intercept-based methods that are subject to adjustments in the calibration curve (Telford 2004).

References

Telford, R. J., E. Heegaard, and H. J. B. Birks, 2004, *The Holocene* 14(2), pp. 296-298.

PaleoResearch Institute
2675 Youngfield Street, Golden, CO 80401
(303) 277-9848 • Fax (303) 462-2700
www.paleoresearch.com

FIGURE 10. PRI RADIOCARBON AGE CALIBRATION

Laboratory Number: PRI-09-143-WFT-S3
Sample Identification: Microcharcoal
Conventional AMS ^{14}C Date: 925 ± 15 RCYBP
1-sigma Calibrated Date (68.2%): 910-850; 840-790 CAL yr. BP
2-sigma Calibrated Date (95.4%): 920-790 CAL yr. BP
$\delta^{13}C$ ($^{o}/_{oo}$): -26.7 (Measured for ^{14}C calculation, not valid for dietary or paleoenvironmental interpretations)

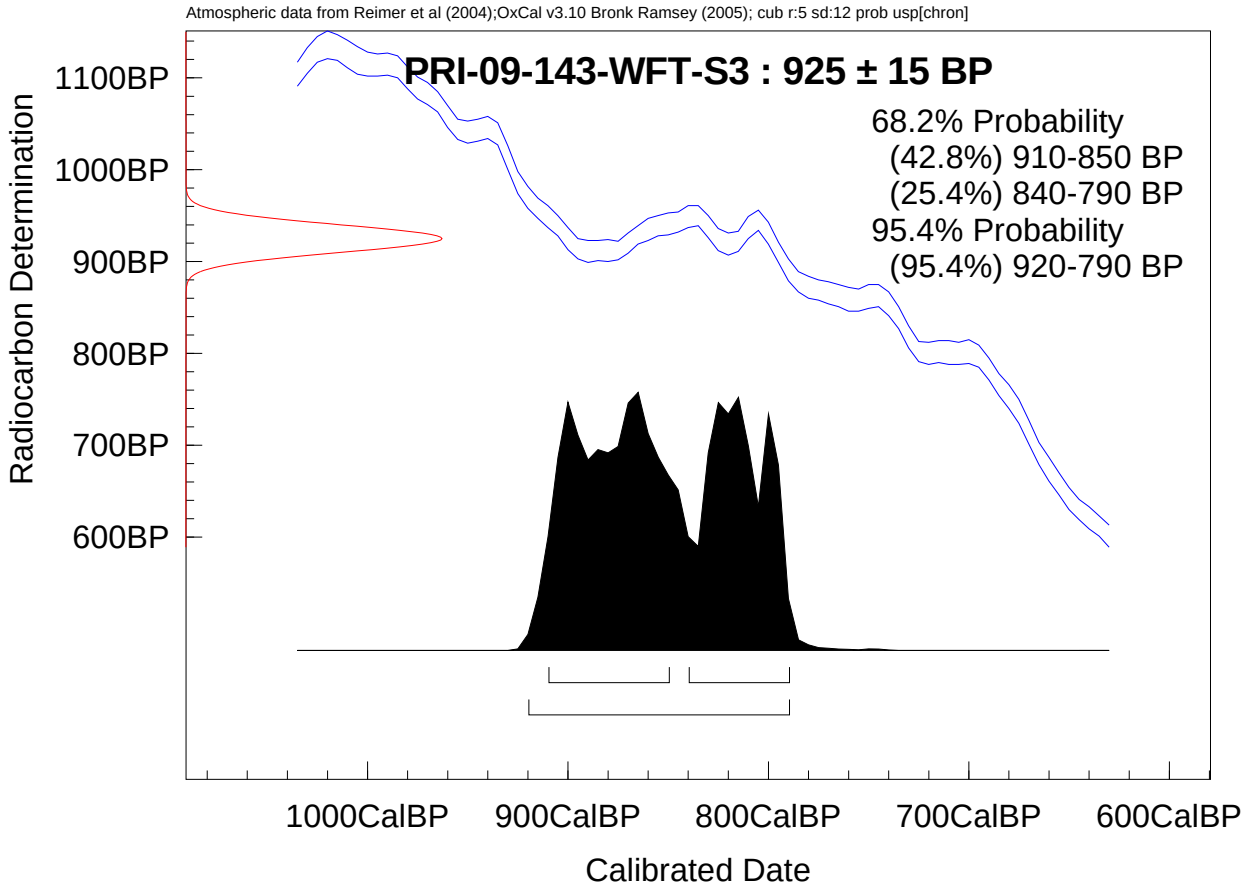

Intercept Statement. PaleoResearch Institute utilizes OxCal3.10 (Bronk Ramsey, 2005) for radiocarbon calibration, which is a probability-based method for determining conventional ages. We prefer this method over the intercept-based alternative because it provides our clients with a calibrated date that reflects the probability of its occurrence within a given distribution (reflected by the amplitude (height) of the curve), as opposed to individual point estimates (Telford 2004). As a result, the probability-based method offers more stability to the calibrated values than those derived from intercept-based methods that are subject to adjustments in the calibration curve (Telford 2004).

References

Telford, R. J., E. Heegaard, and H. J. B. Birks, 2004, *The Holocene* 14(2), pp. 296-298.

PaleoResearch Institute
2675 Youngfield Street, Golden, CO 80401
(303) 277-9848 • Fax (303) 462-2700
www.paleoresearch.com

REFERENCES CITED

Puseman, Kathryn

2009 *Examination of Bulk Soil and AMS Radiocarbon Analysis of Material from the Dutchman Draw Trench Site on the Washington Fault, Arizona*. PaleoResearch Institute, Golden. PRI Technical Report 09-61.

Telford, R.J., E. Heegaard, and H.J.B. Birks

2004 The Intercept is a Poor Estimate of a Calibrated Radiocarbon Age. *The Holocene* 14(2):296-298.

APPENDIX B

Utah State University Luminescence Laboratory Final OSL Age Report

USU LUMINESCENCE LABORATORY
http://usu.edu/geo/luminlab
1770 North Research Parkway, Suite 123, North Logan, Utah 84341

FINAL OSL AGE REPORT

Project: Washington Fault, Utah Geological Survey **Project #:** 068
Scientists: David Simon, Simon Bymaster Inc. and William Lund, UGS
Report by: Tammy Rittenour **Report Date:** August 5, 2013

Optically Stimulated Luminescence Age Information[1]

USU num.	Sample num.	Num. of aliquots[2]	Equivalent Dose, De (Gy)[3]	Overdispersion (%); Skew[4]	Dose Rate (Gy/ka)	OSL Age (ka)[5]
USU-1119	WV T1 OSL-2	**21** (57)	16.83 ±4.56	29.7 ± 6.3; 0.86*	2.49 ±0.11	**6.76 ± 1.94**
USU-1120	WV T1 OSL-3	**20** (47)	20.37 ± 2.28	16.6 ± 5.6; -0.42	2.47 ± 0.11	**8.27 ± 1.21**[6]
USU-1121	WV T4 OSL-10	**23** (48)	19.12 ± 5.35	35.2 ± 6.6; 1.56*	2.48 ± 0.11	**7.71 ± 2.28**
USU-1122	WV T4 OSL-11	**21** (60)	26.05 ± 3.64	31.0 ± 5.7; 0.80*	2.37 ± 0.11	**10.97 ± 1.85**
USU-1123	WV WF-4	**21** (36)	14.10 ± 2.65	50.3 ± 8.8; 0.91*	2.01 ± 0.09	**7.02 ± 1.48**
USU-1124	WV WF-5	**24** (69)	7.37 ± 2.29	43.1 ± 8.9; 0.32	1.77 ± 0.08	**4.17 ± 1.36**

[1]Age analysis using the single-aliquot regenerative-dose procedure of Murray and Wintle (2000) on 1-2-mm small-aliquots of quartz sand. Samples were preheated to 240°C and 160-220°C and held for 10 seconds for regenerative and test doses, respectively.

[2]Number of aliquots used for age calculation, number of aliquots measured in parentheses. Rejection of small-aliquots follows standard rejection criteria (see Rittenour 2005 for example).

[3]De calculated using the Minimum Age Model of Galbraith et al. (1999) unless otherwise noted, excel macros written by Sebastian Hout. Error on De is 2-sigma standard error.

[4]Overdispersion (OD) represents the scatter in De beyond calculated uncertainties for entire dataset. (*) indicates critical skew based on 1-sigma standard error of skew (Bailey and Arnold, 2006). MAM used to calculate De when OD is >20% and/or skew is significantly positive.

[5]Error on age is 2-sigma standard error.

[6]De calculated using the Central Age Model of Galbraith et al. (1999); excel macros written by Sebastian Hout. Error on De is 2-sigma standard error.

USU LUMINESCENCE LABORATORY http://usu.edu/geo/luminlab
1770 North Research Parkway, Suite 123, North Logan, Utah 84341

Dose Rate Information[1]

USU num.	Sample num.	Depth (m)	Grain size (µm)	*In-situ* H_2O (%)[2]	U (ppm)	Th (ppm)	%K	Rb (ppm)	Cosmic (Gy/ka)[3]
USU-1119	WV T1 OSL-2	1.7	90-150	0.36%	2.2±0.2	5.9±0.5	1.41±0.04	54.3±2.2	0.19±0.02
USU-1120	WV T1 OSL-3	2.0	90-150	0.41%	2.0±0.1	5.6±0.5	1.46±0.04	55.9±2.2	0.19±0.02
USU-1121	WV T4 OSL-10	0.52	90-150	0.55%	2.1±0.2	6.3±0.6	1.36±0.03	51.4±2.1	0.23±0.02
USU-1122	WV T4 OSL-11	1.04	90-150	0.51%	2.1±0.2	6.0±0.5	1.29±0.03	47.2±1.9	0.21±0.02
USU-1123	WV WF-4	0.5	90-125	0.14%	1.0±0.1	3.4±0.3	1.34±0.03	47.1±1.9	0.23±0.02
USU-1124	WV WF-5	0.43	90-150	0.24%	0.8±0.1	3.2±0.3	1.16±0.03	41.7±1.7	0.23±0.02

[1]Radioelemental concentrations determined by ICP-MS and ICP-AES techniques from ALS Chemex, dose rate is derived from concentrations by conversion factors from Guerin et al. (2011).
[2]Assume 3±3%wt H_2O is representative of burial history.
[3]Contribution of cosmic radiation to the dose rate was calculated by using sample depth, elevation, and longitude/latitude following Prescott and Hutton (1994).

Equivalent dose distributions: Probability density functions

USU-1119, WV T1 OSL-2

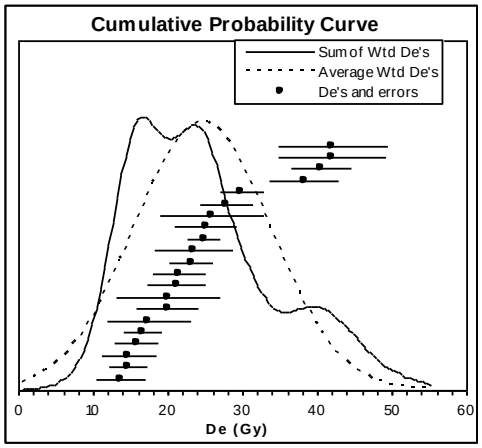

USU-1120, WV T1 OSL-3

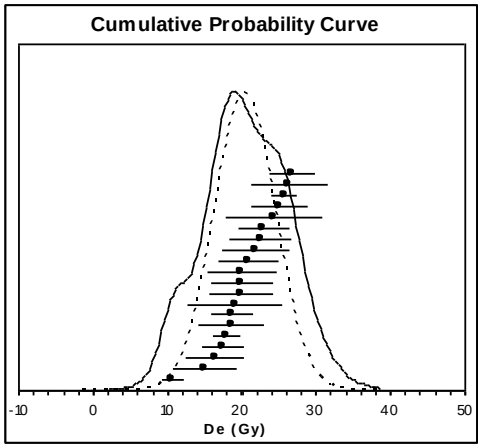

Project: Washington Fault, Utah Geological Survey
Scientists: David Simon, Simon Bymaster Inc. and William Lund, UGS
Report by: Tammy Rittenour

Project #: 068
Report date: August 5, 2013

USU LUMINESCENCE LABORATORY
http://usu.edu/geo/luminlab
1770 North Research Parkway, Suite 123, North Logan, Utah 84341

Equivalent dose distributions: Probability density functions (con't)

USU-1121, WV T4 OSL-10

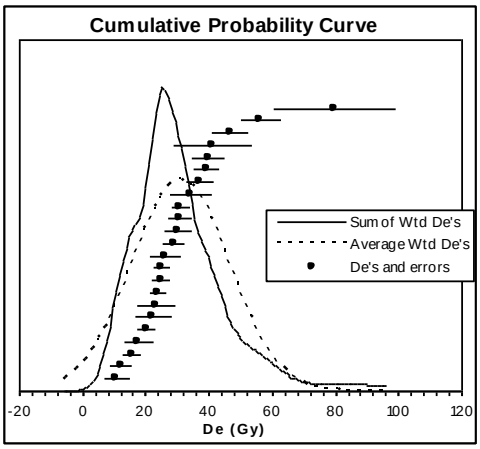

USU-1122, WV T4 OSL-11

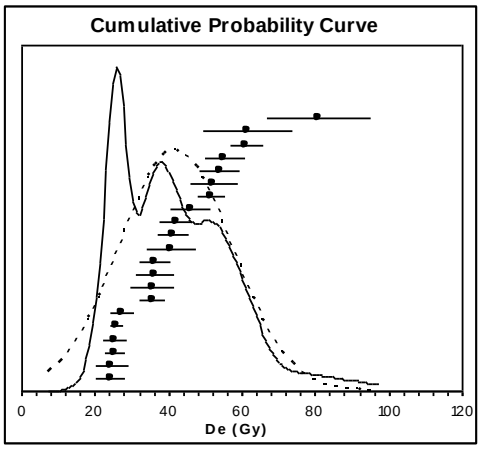

USU-1123, WV WF-4

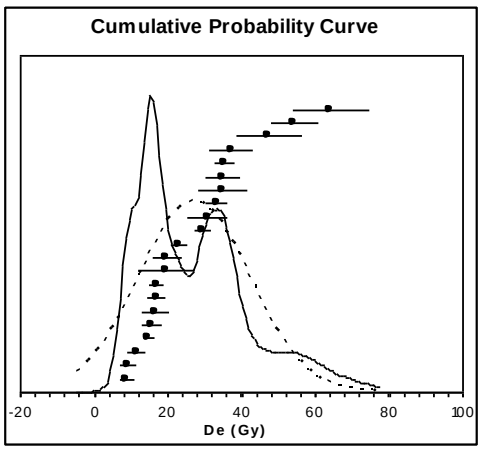

USU-1124, WV WF-5

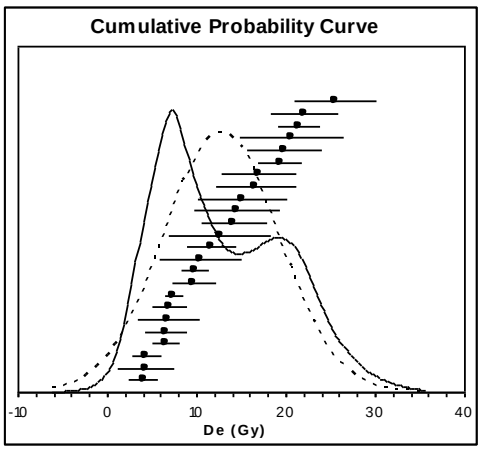

Project: Washington Fault, Utah Geological Survey
Scientists: David Simon, Simon Bymaster Inc. and William Lund, UGS
Report by: Tammy Rittenour

Project #: 068
Report date: August 5, 2013

Procedures for sample processing and age analysis:

All samples were opened and processed under dim amber safelight conditions within the lab. Sample processing follows standard procedures involving sieving, gravity separation and acid treatments with HCl and HF to isolate the quartz component of a narrow grain-size range, usually 90-150 µm*. The purity of the samples is checked by measurement with infra-red stimulation to detect the presence of feldspar. Sample processing procedures follow those outlined in Aitken (1998) and described in Rittenour et al. (2003, 2005).

The USU Luminescence Lab follows the latest single-aliquot regenerative-dose (SAR) procedures for dating quartz sand (Murray and Wintle, 2000, 2003; Wintle and Murray, 2006). The SAR protocol includes tests for sensitivity correction and brackets the equivalent dose (De) the sample received during burial by irradiating the sample at five different doses (below, at, and above the De, plus a zero dose and a repeated dose to check for recuperation of the signal and sensitivity correction). The resultant data are fit with a saturating exponential curve from which the De is calculated on the mean, Central Age Model (CAM) or the Minimum Age Model (MAM) of Galbraith et al. (1999) or Juyal et al. (2006), depending on the distribution of De results and evidence for partial bleaching*. In cases where the samples have significant positive skew, ages are calculated based on a MAM. OSL age is reported at 1σ or 2σ standard error* and is calculated by dividing the De (in grays, gy) by the environmental dose rate (gy/ka) that the sample has been exposed to during burial.

Dose-rate calculations were determined by chemical analysis of the U, Th, K and Rb content using ICP-MS and ICP-AES techniques by ALS Chemex, Elko NV and conversion factors from Guerin et al. (2011). The contribution of cosmic radiation to the dose rate was calculated using sample depth, elevation, and latitude/longitude following Prescott and Hutton (1994). Dose rates are calculated based on water content, sediment chemistry, and cosmic contribution (Aitken, 1998).

Under the collaborative agreement to analyze samples at the USU Luminescence Lab, please consider including Dr. Rittenour as a co-author on resultant publications. Contact me for additional information and help with describing the OSL technique when you plan your publication.

Dr Tammy Rittenour

Director
USU Luminescence Lab
1770 N Research parkway, suite 123
North Logan, UT 84341

Assistant Professor
Department of Geology, Utah State University
4505 Old Main Hill
Logan, UT 84322-4505

tammy.rittenour@usu.edu
ph (435) 213-5756, fax (435) 797-1588
http://www.usu.edu/geo/luminlab/

* these parameters are sample dependant, see first page of report for specific sample information

References cited:

Aitken, M.J. 1998: An Introduction to Optical Dating: The dating of Quaternary sediments by the use of photon-stimulated luminescence. New York, Oxford University Press, 267 p.

Bailey, R.M. and Arnold, L.J., 2006. Statistical modeling of single grain quartz De distributions and an assessment of procedures for estimating burial dose. Quaternary Science Reviews 25, 2475-2502.

Galbraith, R.F., Roberts, R.G., Laslett, G.M., Yoshida, H., Oleey, J.M., 1999. Optical dating of single and multiple grains of quartz from Jinmium Rock Shelter, northern Australia: Part I, experimental design and statistical models. Archaeometry 41, 339-364.

Goble, R.J. and Rittenour, T.M., 2006, A linear modulation OSL study of the unstable ultrafast component in samples from glacial lake Hitchcock, Massachusetts, USA: Ancient TL 24, 37-46.

Guerin, G., Mercier, N., Adamiec, G., 2011. Dose-rate conversion factors: update: Ancient TL 29, 5-8.

Juyal, N., Chamyal, L.S., Bhandari, S., Bhushan, R., Singhvi, A.K., 2006. Continental record of the southwest monsoon during the last 130 ka: evidence from the southern margin of the Thar Desert, India. Quaternary Science Reviews 25, 2632-2650.

Prescott, J. R., Hutton, J.T., 1994. Cosmic ray contributions to dose rates for luminescence and ESR dating: Radiation Measurements 23, 497-500.

Murray, A.S., Wintle, A.G., 2000. Luminescence dating of quartz using an improved single aliquot regenerative-dose protocol. Radiation Measurements 32, 57-73.

Murray, A.S., Wintle, A.G., 2003. The single aliquot regenerative dose protocol: potential for improvements in reliability. Radiation Measurements 37, 377-381.

Olley, J.M., Pietsch, T., Roberts, R.G., 2004. Optical dating of Holocene sediments from a variety of geomorphic settings using single grains of quartz: Geomorphology 60, 337-358.

Rittenour, T.M., Goble, R.J., Blum, M.D., 2003, An Optical Age Chronology of Fluvial Deposits in the Northern Lower Mississippi Valley: Quaternary Science Reviews, v. 22, p. 1105-1110.

Rittenour, T.M., Goble, R.J., Blum, M.D., 2005, Development of an OSL chronology for late Pleistocene channel belts in the lower Mississippi valley: Quaternary Science Reviews, v.24, p.2539-2554.

Rittenour, T.M. 2008. Luminescence dating of fluvial deposits: applications to geomorphic, palaeoseismic and archaeological research. Boreas, 37, 613-635.

Wintle, A.G. Murray, A.S., 2006, A review of quartz optically stimulated luminescence characteristics and their relevance in single-aliquot regenerative protocols: Radiation Measurements, v. 41, p. 369-391.

APPENDIX C

Western GeoArch Research Ages – Trench T-5

Western GeoArch Research Ages - Trench T-5

Big Horn Designation	Beta/USU Report No.	Geologic Unit	Feature	T-5 Station Number	AGE		
					Conventional ^{14}C age (RCYBP) [1] or OSL Age	2 Sigma Calibrated Conventional[1] ^{4}C age[2]	Calendar Calibrated years before present (Cal yr BP)[3]
FS06 (C^{14})	278065	0.5 ft. above base of UNIT 4	charcoal staining in the middle excavation block on the south side of the trench	0+74	5150 ±40	5895	5855
FS09 (C^{14})	278066	0.5 ft. above base of UNIT 4	charcoal staining in the middle excavation block on the south side of the trench	0+56.5	4980 ±40	5707	5767
FS19 (C^{14})	278067	0.5 ft. above base of UNIT 4	general charcoal staining in the middle excavation block on the south side of the trench	0+58	5400 ±40	6211	6273
FS29 (C^{14})	278068	UNIT 10	hearth in Bighorn western-most excavation block in the north trench profile	1+40	1900 ±40	1825	1885
FS31 (C^{14})	278069	UNIT 10	hearth in Bighorn western-most excavation block in the north trench profile	1+43	2030 ±40	2005	2065
FS34(C^{14})	278070	base of UNIT 4	hearth on the east end of the trench in the north profile	0+17	4640±40	5382	5442
FS113(C^{14})	278638	base of UNIT 4	hearth on the south edge of Bighorn larger middle excavation block (feature 11).	0+50.5	5730 ±40	6525	6585
FS115 (C^{14})	278639	1.2 ft. above base of UNIT 4	hearth in the southeast corner of Bighorn larger middle excavation block (feature 10).	0+57.5	5360 ±40	6140	6200
OSL A*	UIC 2769	UNIT 4**	Qaf sediments	0+56	9,940±1,030	na	9940
OSL C*	UIC 2770	UNIT 4**	Qaf sediments	0+57	12,910±1,415	na	12,910
OSL E	UIC 2768	UNIT 10	Qaf sediments	1+43	4,830±430	na	4,830

*location of OSL A is 3.75± ft. above location of OSL C **Unit 4 is stratigraphically below Unit 10

[1] The Conventional Radiocarbon Age (^{14}C) represents the Measured Radiocarbon Age corrected for isotopic fractionation, calculated using the delta 13C. The Conventional Radiocarbon Age is not calendar calibrated.

[2] Weighted average of multiple intercepts calculated using OxCal (http://c14.arch.ox.ac.uk). 2 Sigma Calibrated ^{14}C RCYBP.

[3] For 14C ages, "present" = AD 1950 plus 60 years.

PLATES

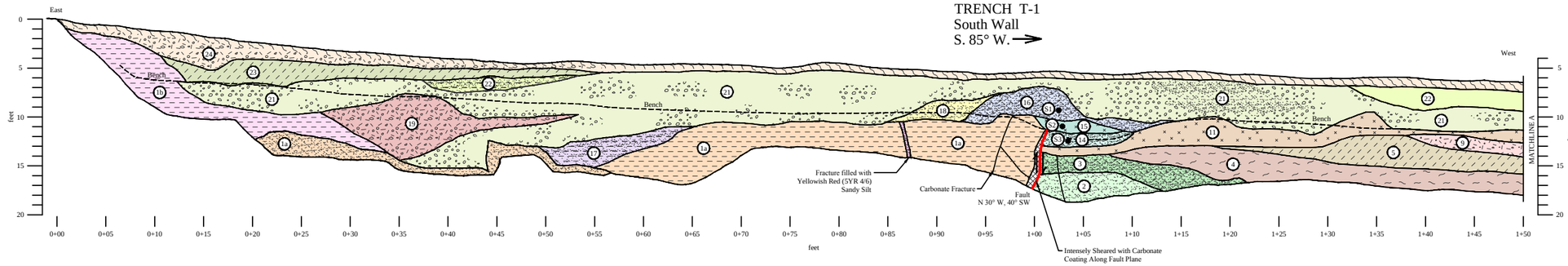

TRENCH 1

1 Bedrock (upper red member of the Moenkopi Formation)

1a sandstone, thinly to moderately bedded, fractured, bedding N. 65° W., 15° SW.

1b mudstone, thinly bedded, fractured, bedding N. 75° W., 10° SW.

2 Alluvium: Sand (SP) with some silt, very fine grained, yellowish red (5YR 5/6).

3 Loess: Silty Sand (SM), very fine grained, massive, reddish yellow (5YR 7/6).

4 Loess: Silt (ML) with some very fine grained sand and pinkish white (5YR 8/2) carbonate modules ≤0.5 inches long, massive, red (2.5YR 4/6).

5 Loess: Silt (ML) with very fine grained sand and some clay, massive, pin-hole voids, and carbonate filaments and nodules ≤0.2 inches long, massive, reddish brown (2.5YR 4/4) to red (2.5YR 4/6).

6 Alluvium: Gravelly Sand (SP) to Sandy Gravel (GP), 30-50% angular to subangular clasts ≤18 inches long , average size ≤6 inches long, in a fine to medium grained matrix, weak sub-horizontal bedding, with discontinuous lenses of sandy gravel, pebbly sand and very coarse grained sand, reddish yellow (5YR 6/6).

7 Loess: Silt (ML), with <1% angular clasts ≤0.3 inches long, average size ≤0.2 inches long, carbonate filaments, thin (≤1-inch thick) discontinuous very fine grained carbonaceous sand lenses, massive, reddish yellow (5YR 6/6).

8 Alluvium: Sand (SP), medium to coarse grained, weak horizontal, bedding with 5% angular clasts ≤ 2 inches long, average size ≤ 1-inch long, discontinuous sandy gravel, pebbly sand lenses, yellowish red (5YR 4/6).

9 Alluvium: Sandy Silt (ML) to Silt (ML), with some sand, and discontinuous pebbly sand lenses, carbonate filaments, and 1-2% angular clasts ≤0.5 inches long, light brown (7.5YR 6/4).

10 Alluvium: Gravelly Sand (SP), medium to coarse grained, with angular clasts ≤6 inches long, average size ≤4 inches long, discontinuous coarse grained sand, pebbly sand, and sandy gravel lenses, weak horizontal bedding, yellowish red (5YR 4/6).

11 Loess: Silt (ML), with ≤ 5% carbonate filaments ≤ 0.1-inch long, massive, reddish yellow (5YR 6/6).

12 Alluvium: Silty Fine Sand (SM) to Sandy Silt (ML), with discontinuous gravelly sand and sandy gravel lenses, reddish yellow (5YR 6/6).

13 Alluvium: Sandy Gravel (GP) to Gravelly Sand (SP), 50% angular clasts <12 inches long, average size ≤4 inches long, in a fine to medium grained silty sand matrix, yellowish red (5YR 4/6).

14 Fault Derived Colluvium: Silt (ML) with some very fine sand, yellowish red (5YR 4/6).

15 Fault Derived Colluvium: Silt (ML), light brown (7.5YR 6/4).

16 Alluvium: Sandy Silt (ML) with 2±% angular to subangular clasts ≤1-inch long, average size ≤0.2-inches, reddish yellowish (7.5YR 6/6) (paleo-sand dune or levee).

17 Loess: Silt (ML), gypsiferous, with carbonate filaments and nodules (< 0.1-inch long), massive, yellowish red (5YR 5/6).

18 Alluvium: Sand (SP) fine to coarse grained, weak horizontal bedding, with thin (4 inches thick) discontinuous lenses of silt with 3±% angular clasts ≤1-inch long, average size ≤0.5 inches long, strong brown (7.5YR 5/6).

19 Alluvium: Gravelly Silt (ML) with some very fine sand and 3-5% subangular to angular clasts ≤4-inches long, average size ≤2 inches long, and discontinuous very fine sand and sandy silt lenses, reddish yellow (5YR 6/6).

20 Loess: Silt (ML) with some fine grained sand, massive, pinkish gray (7.5YR 6/2).

21 Alluvium: Gravelly Sand (SP), medium to coarse grained, weak horizontal bedding, 30-40% angular to subangular clasts ≤12 inches long, average size ≤3 inches long, strong brown (7.5YR 5/6).

22 Loess: Silt (ML) with some fine grained sand, massive, pinkish gray (7.5YR 6/2).

23 Loess: Sandy Silt (ML), medium dense with some gypsum and carbonate clasts (≤ 0.01 inch long), massive, reddish yellow (5YR 6/6)

24 Alluvium: Silty Sand (SM), very fine grained, with 5% angular clasts ≤12 inches long, average size ≤4 inches long, red (2.5YR 4/6), with modern organic (A) horizon.

● Sample location for age dating.

Fault arrows showing the direction of movement.

T-1 Radiocarbon Ages			
Sample No.	Unit	Age (2σ)	
		^{14}C yr B.P.	cal yr B.P.
T1-S1	16	2140 ± 15	2160 - 2060
T1-S2	15	205 ± 15	300-260 (25.6%) 190-140 (47.1%) 20-(-11) (22.7%)
T1-S3	14	465 ± 15	530 - 500

T-1 OSL Ages (ka)		
Sample No.	Unit	Age (2σ)
T1-S2	15	6.76 ± 1.94
T1-S3	14	8.27 ± 1.21

Logged by: DBS/JRH/DRB

TRENCH PROFILE T-1

SOUTHERN CORRIDOR PHASE 3
WASHINGTON COUNTY, UTAH

ROSENBERG ASSOCIATES

PROJECT # 5507-P3

PLATE # 1

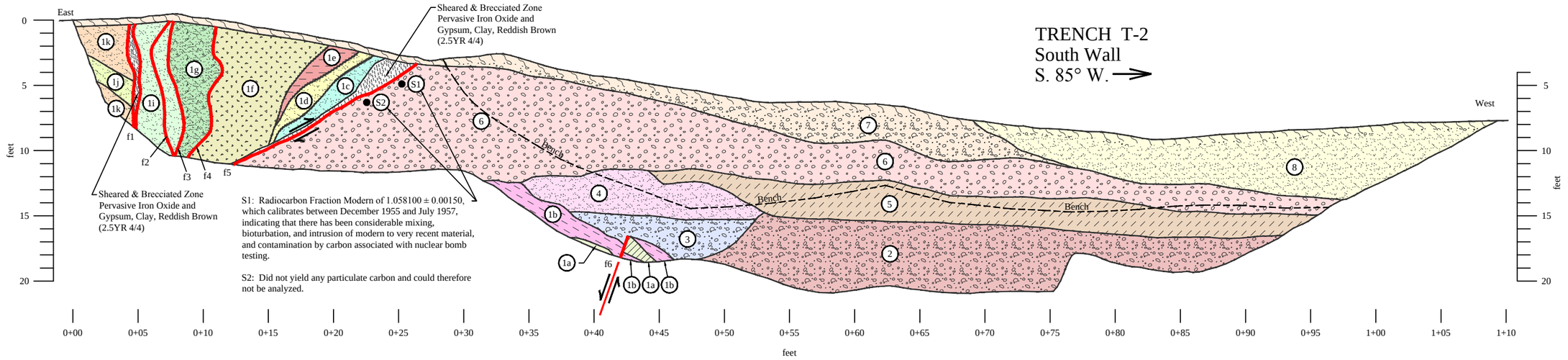

TRENCH 2

1 Bedrock: Sheared, brecciated, and faulted “slivers” of Petrified Forest (gray and purple mudstone) and Shinarump Conglomerate Members (yellow and yellowish brown sandstone) of the Chinle Formation, and upper red member of the Moenkopi Formation (deep red and dusky red mudstone).

1a Claystone, sheared, brecciated, dusky red (10R 3/3).

1b Sandstone, light reddish brown (2.5YR 7/3), with thin (≤0.25 inches thick) interbeds of red (2.5YR 4/6), siltstone.

1c Claystone, sheared, brecciated, with iron oxide staining, white (10YR 8/1).
1d Sandstone, sheared, brecciated, light gray (7.5YR 7/1).
1e Claystone, sheared, brecciated, gypsiferous, yellow (10YR 8/6).

1f Claystone, red (2.5YR 5/6), with ≤8 inch long clasts of reddish gray (2.5yr 1/6) to pale red (2.5YR 6/2) sandstone.

1g Sandstone, silty, very fine grained, brecciated, yellow (10YR 7/6).

1h Brecciated Sandstone Fragment within unit 1i, red (2.5YR 4/6).

1i Sandstone, silty, fine grained, massive, some iron oxide staining, very pale brown (10YR 8/4).

1j Sandstone, fractured, light reddish brown (2.5YR 7/3).

1k Sandstone, fine to medium grained, with some iron oxide nodules (≤0.25 inches long) and iron oxide staining, white (5YR 8/1).

2 Alluvium: Sandy Silt (ML), massive, dense, with 10% angular sandstone clasts ≤18 inches long, average size ≤12 inches long, yellowish red (5YR 5/6).

3 Alluvium: Silty Sand (SM), very fine grained, massive, with 5% sandstone clasts ≤10 inches long, average size ≤6 inches long, dense reddish yellow (5YR 7/6).

4 Loess: Silty Sand (SM) very fine grained, dense, massive, with 2% angular clasts ≤1-inch long, pink (7.5YR 7/4).

5 Loess: Sandy Silt (ML), gypsiferous, yellowish red (5YR 4/6).

6 Alluvium: Sandy Silt (ML), very fine grained, red (2.5YR 5/6) with 3 to 5% angular pale red (2.5YR 7/2) sandstone clasts ≤12 inches long, average size ≤4 inches long, with calcium carbonate nodules and filaments.

7 Alluvium: Silty Sand (SM), very fine grained with 20% angular clasts ≤12 inches long, average size ≤6 inches long, and discontinuous gravel and coarse grained sand lenses, reddish brown (5YR 5/4), with modern organic A-horizon.

8 Alluvium: Sand (SP) with silt, very fine grained, pin-hole voids, with 2% clasts ≤1-inch long, some gypsum, yellowish red (5YR 4/6), with modern organic A-horizon.

● Sample location for age dating.

Fault arrows showing the direction of movement.

Fault	Strike	Dip	Displacement	Comments
f1	N. 20° W.	vertical	unknown	0.2 inch (0.5 cm) to 12 inch (30 cm) wide clay gouge zone with gypsum, yellow (5YR 6/6).
f2	N. 20° W.	vertical	unknown	0.2 inch (0.5 cm) wide clay gouge zone with gypsum, red (2.55YR 4/6) and light reddish gray (2.5YR 7/1).
f3	N. 20° W.	vertical	unknown	0.2 inch (0.5 cm) wide clay gouge zone with gypsum, light reddish gray (2.5YR 7/1).
f4	N. 20° W.	vertical	unknown	0.15 inch (0.5 cm) wide clay gouge zone, light reddish gray (2.5YR 7/1).
f5	N. 20° W.	65° E.	≥ 9 ft. (2.7 m.)	0.2 inch (0.5 cm) to 12 inch (30 cm) wide sheared and brecciated clay gouge zone, dark gray (10YR 4/1).
f6	N. 20° W.	88° E.	0.7 ft. (0.2 m.)	--

Logged by: DBS/JRH/DRB

TRENCH PROFILE T-2

SOUTHERN CORRIDOR PHASE 3
WASHINGTON COUNTY, UTAH

ROSENBERG ASSOCIATES
CIVIL ENGINEERS - LAND SURVEYORS

PROJECT # 5507-P3

PLATE # 2

TRENCH T-3
South Wall
S. 87° W. →

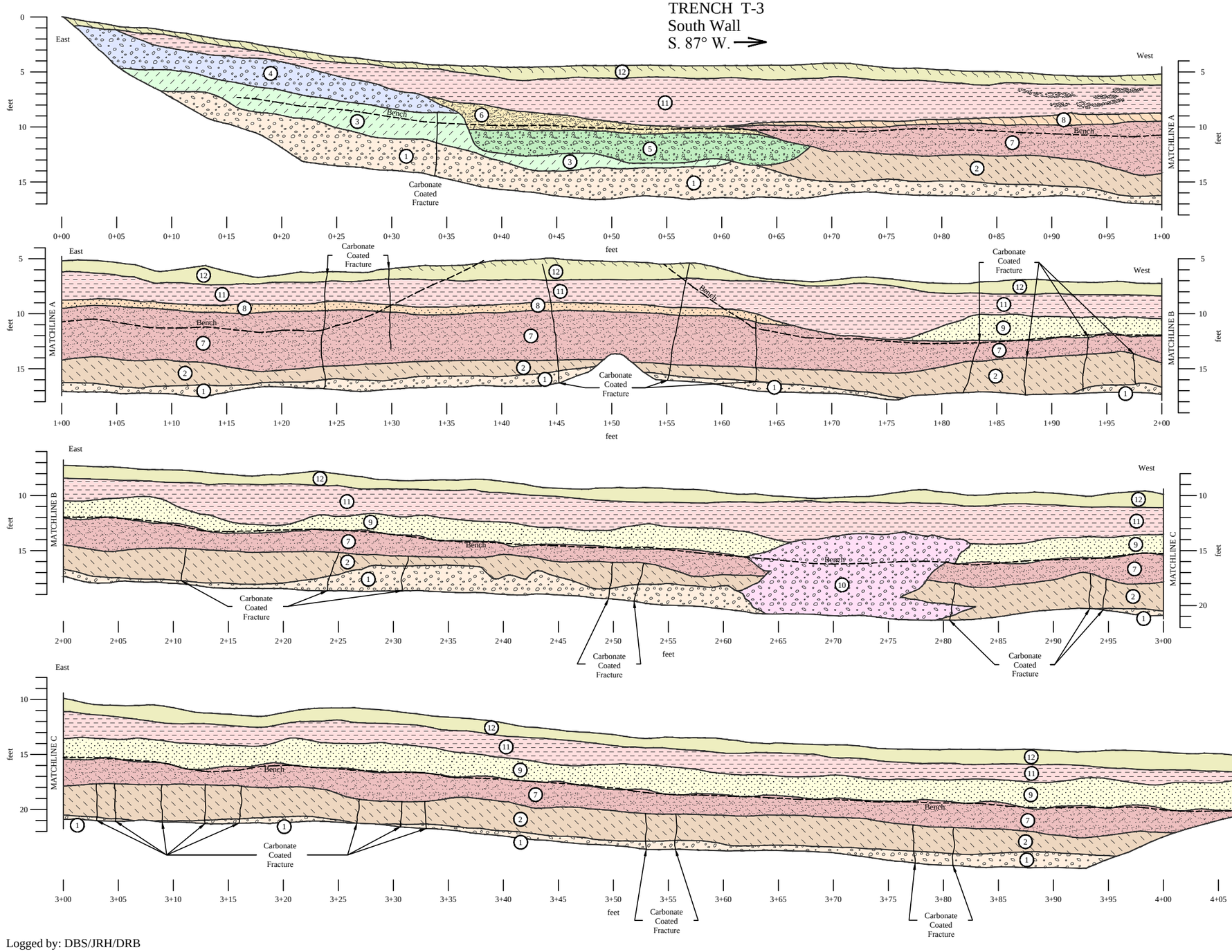

TRENCH 3

1 Alluvium (older): Sandy Silt (ML), massive, dense, with 10% angular sandstone clasts ≤18 inches long, average size ≤12 inches long, yellowish red (5YR 5/6).

2 Alluvium (older): Sandy Silt (ML), massive, dense, gypsiferous, yellowish red (5YR 5/6).

3 Alluvium (older): Sandy Silt (ML), gypsiferous, with 5% subangular clasts at east end of trench, yellowish red (5YR 4/6).

4 Alluvium (older): Sandy Silt (ML), with 15% angular clasts ≤24 inches long, average size 12 inches long, larger clasts concentrated along top of unit, yellowish red (5YR 4/6).

5 Alluvium (older): Gravelly Sand (SP), fine to medium grained with 20% subangular clasts ≤ 8 inches long, average size ≤0.5 inches long, gypsiferous, light brown (7.5YR 6/4).

6 Alluvium (older): Sandy Silt (ML) with 5% subangular to angular clasts ≤1 inch long, average size ≤0.5 inches long, yellowish red (5YR 5/6).

7 Alluvium (older): Silty Sand (SM) very fine grained, massive, gypsiferous, with 1% angular clasts ≤10 inches long, average size ≤2 inches long, reddish yellow (5YR 6/6).

8 Alluvium (older): Sand (SP), fine to medium grained, gypsiferous, with 5% angular clasts (primarily sandstone) ≤4 inches long, dark red (2.5YR 3/6).

9 Alluvium (older): Sand (SP), fine to medium grained with some silt and 5% angular clasts ≤6 inches long, average size ≤3 inches long, gypsum, red (2.5YR 4/6).

10 Alluvium (older): Sand (SP), fine grained, dense, massive with 20% angular clasts ≤3 inches long, gypsiferous, light reddish brown (5YR 6/4).

11 Alluvium (older): Sandy Silt (ML), massive, dense, with some gravel lenses and pin-hole voids, yellowish red (5YR 5/6).

12 Alluvium (older): Silty Sand (SM), very fine grained, with gravel lenses, and modern organic A-horizon, reddish brown (5YR 5/4) to yellowish red (5YR 5/6).

Logged by: DBS/JRH/DRB

TRENCH PROFILE T-3

SOUTHERN CORRIDOR PHASE 3
WASHINGTON COUNTY, UTAH

ROSENBERG ASSOCIATES CIVIL ENGINEERS – LAND SURVEYORS

PROJECT #	PLATE #
5507-P3	3

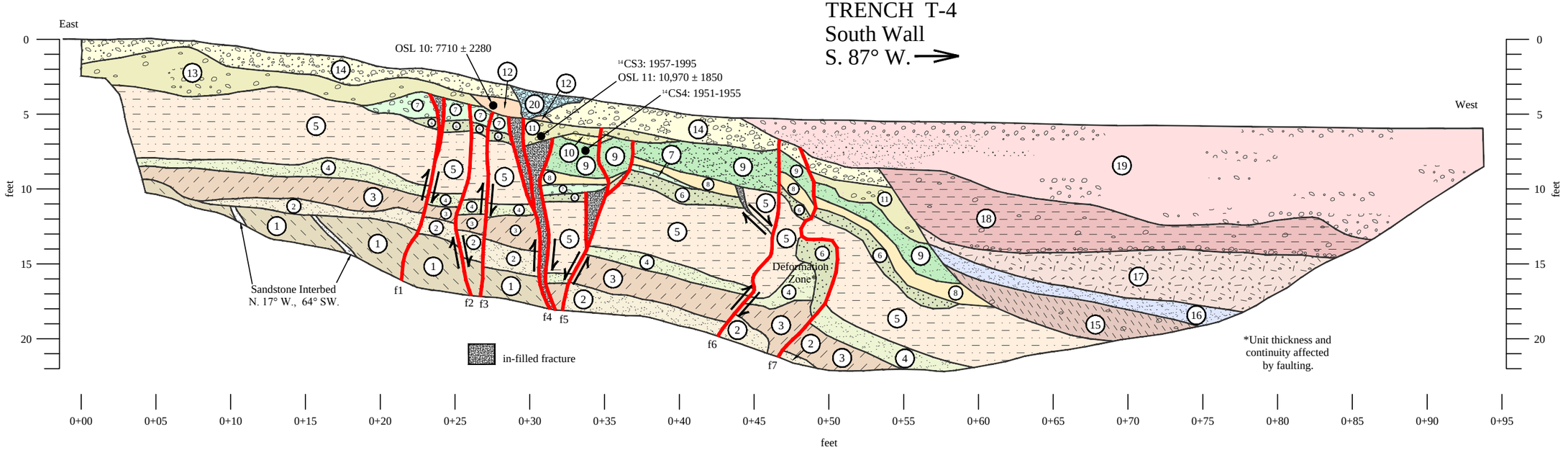

TRENCH 4

1 Bedrock - Shinarump Conglomerate Member of the Chinle Formation: shale, reddish brown (2.5YR 4/4), with thin (≤12 inches thick) interbeds of white (2.5YR 8/1) sandstone.

2 Alluvium: Silty Sand (SM), fine grained with coarse grained sand and pebbles (≤0.1-inch long), light reddish brown (5YR 6/4) to reddish yellow (5YR 6/6).

3 Alluvium: Sandy Silt (ML), massive, dense, with ≤3% angular sandstone clasts ≤0.3 inches long, yellowish red (5YR 4/6).

4 Eolian: Silty Sand (SM) fine grained, yellowish red (5YR 4/6)

5 Alluvium: Sandy Silt (ML), massive, very dense, gypsiferous, with coarse grained sand and pebbles (≤0.1 inch long), and angular sandstone clasts ≤2 inches long, yellowish red (5YR 4/6).

6 Eolian: Sand (SP) fine grained, very thin horizontal bedding (≤0.2 inch thick), some weak cross-bedding, reddish yellow (5YR 6/8).

7 Alluvium: Silty Sand (SP), fine to medium grained with 20% subangular clasts ≤2 inches long, average size ≤0.5 inches long, reddish yellow (5YR 6/6).

8 Alluvium: Silty Sand (SM), very fine grained, yellowish red (5YR 5/6).

9 Alluvium: Silt Sand (SP), very fine to fine grained, very dense, gypsiferous, reddish yellow (5YR 6/6) to yellowish red (5YR 5/6).

10 Alluvium: Sandy Silt (ML), reddish yellow (5YR 6/6).

11 Fault Derived Colluvium: Sandy Silt (ML), gypsiferous, with angular clasts of sandstone and shale ≤6 inches long, average size ≤1-inch long, yellowish red (5YR 5/6).

12 Alluvium: Sandy Silt (ML), fine grained, yellowish red (5YR 5/6).

13 Alluvium: Sandy Silt (ML), massive, with 5% subangular clasts ≤0.5 inches, yellowish red (5YR 5/6) with a pedogenic B-horizon, yellowish red (5YR 4/6).

14 Alluvium: Gravelly Sand (SP), fine grained, massive, with 30% angular to subangular clasts ≤8 inches long, average size ≤4 inches, yellowish red (5YR 5/6).

15 Fluvial: Sandy Silt (ML), clayey, with 20% angular clasts ≤3 inches long, reddish brown (5YR 4/4).

16 Fluvial: Silty Sand (SM), fine grained with 2% angular clasts ≤0.25 inches long, yellowish red (5YR 5/6).

17 Fluvial: Silty Sand (SM), fine grained, some pin-hole voids yellowish red (5YR 4/6).

18 Fluvial: Sandy Silt (ML), gypsiferous with 10% angular clasts ≤3 inches long, well developed stone-line along base of unit, reddish yellowish (5YR 4/4)

19 Fluvial: thin to moderately bedded (≤0.3 inches to 12 inches thick) sandy gravel, sandy silt, and coarse grained sand, bedding horizontal, some x-bedding, reddish brown (5YR 4/3).

20 Fluvial: Gravelly Sand (SP), fine to medium grained with about 30% angular clasts 6 to 12 inches long, yellowish red (5YR 5/6).

● Sample location for age dating.

Fault arrows showing the direction of movement.

Logged by: DBS/JRH/DRB

TRENCH PROFILE T-4

SOUTHERN CORRIDOR PHASE 3
WASHINGTON COUNTY, UTAH

ROSENBERG ASSOCIATES
CIVIL ENGINEERS ~ LAND SURVEYORS

PROJECT #	PLATE #
5507-P3	4

TRENCH 5

1 Bedrock: Schnabkaib Member of the Moenkopi Formation

1a Siltstone with very fine sand and some clay, yellow (10YR 7/6).

1b Sandy Siltstone with clay, brownish yellow (10YR 6/6).

1c Sandstone, fine grained, some lithic fragments, moderately to thinly bedded, moderate to intensely sheared, brownish yellow (10YR 6/6).

2 Loess: Silt (ML) with some very fine grained sand, massive, yellow (10YR 7/6).

3 Loess: Sandy Silt (ML), some gypsum, massive, yellow (10YR 7/6) to brownish yellow (10YR 6/6).

4 Alluvium: Gravelly Sand (SP), fine to medium grained with about 20 percent angular clasts ≤1-inch long, red (2.5YR 4/8).

5 Alluvium: Sand (SP) with silt, fine grained, red (2.5YR 4/8).

6 Loess: Silt (ML) with very fine grained sand, massive, reddish yellow (7.5YR 6/6).

7 Loess: Silty Sand (SM) very fine grained, massive, yellowish red (5YR 5/6).

8 Loess: Silt (ML) with some very fine grained sand, massive, yellow (10YR 7/6).

9 Loess: Sandy Silt (ML), some pin hole voids, massive, reddish yellow (7.5YR 6/6).

10 Alluvium: Sandy Silt (ML), with some discontinuous sandy gravel lenses, massive, reddish yellow (5YR 7/6).

11 Loess: Sandy Silt (ML) massive, yellowish red (5YR 5/6).

12 Alluvium: Sandy Gravel (GP), 40 percent angular gravels, ≤3 inches long, average size ≤0.3 inches long, in a silty fine grained sand matrix, with very thin (≤0.3 inches thick) discontinuous silty sand layers, light red (2.5YR 6/8).

13 Alluvium: Silty Sand (SM), very fine grained, weakly developed horizontal bedding, yellowish red (5YR 5/6).

14 Alluvium: thinly interbedded (≤12 inches thick) very fine grained Silty Sand (SM) and Sandy Silt (ML), some cross-bedding, red (2.5YR 5/8).

15 Alluvium: Sandy Gravel (GP), 75 percent angular clasts ≤12 inches long, average size ≤0.5 inch long, in a silty fine grained sand matrix, some clast supported, yellowish red (5YR 5/6 to 5/8).

16 Loess: Sandy Silt (ML), some gypsum, massive, reddish yellow (7.5YR 7/6).

17 Loess: Sandy Silt (ML), massive, reddish yellow (7.5YR 7/6 to 7.5YR 6/6).

18 Alluvium: Sand (SP), fine grained, thin bedded (≤0.2 feet thick), some cross-bedding and sandy gravel lenses, reddish yellow (5YR 5/6).

● Sample location for age dating.

Sample	Geologic Unit	Station	Feature	Age	
				Conventional ^{14}C age (RCYBP)	Average Calendar Calibrated Years Before Present (cal yr. BP)
FSO6	Unit 8	0+73.8	cultural charcoal	5150 ± 40	5875 ± 115
FSO9	Unit 8	0+56.0	cultural charcoal	4980 ± 40	5745 ± 135
FS19	Unit 8	0+58.7	cultural general charcoal	5400 ± 40	6205 ± 85
FS29	Unit 10	1+40.0	cultural hearth	1900 ± 40	1830 ± 100
FS31	Unit 13	1+43.0	disseminated cultural charcoal layer	2030 ± 40	2000 ± 110
FS34	Unit 8	0+18.0	cultural charcoal stained sediment	4640 ± 40	5380 ± 60
FS113	Unit 8	0+50.5	cultural charcoal stain/hearth	5730 ± 40	6530 ± 110
FS115	Unit 8	0+56.7	cultural charcoal stain/hearth	5360 ± 40	6140 ± 140

Sample	Geologic Unit	Station	Feature	OSL Age
OSL A	Unit 8	0+55.5	upper bracket of a typical charcoal staining	9940 ± 1030
OSL C	Unit 8	0+56.5	lower bracket of a typical charcoal staining	12,910 ± 1415
OSL E	Unit 10	1+43.2	cultural staining immediately below a cobble-size manuport	4830 ± 430

Logged by: DBS/JRH/DRB

TRENCH PROFILE T-5

SOUTHERN CORRIDOR PHASE 3
WASHINGTON COUNTY, UTAH

ROSENBERG ASSOCIATES

PROJECT # 5507-P3 | PLATE # 5

TRENCH T-6 South Wall

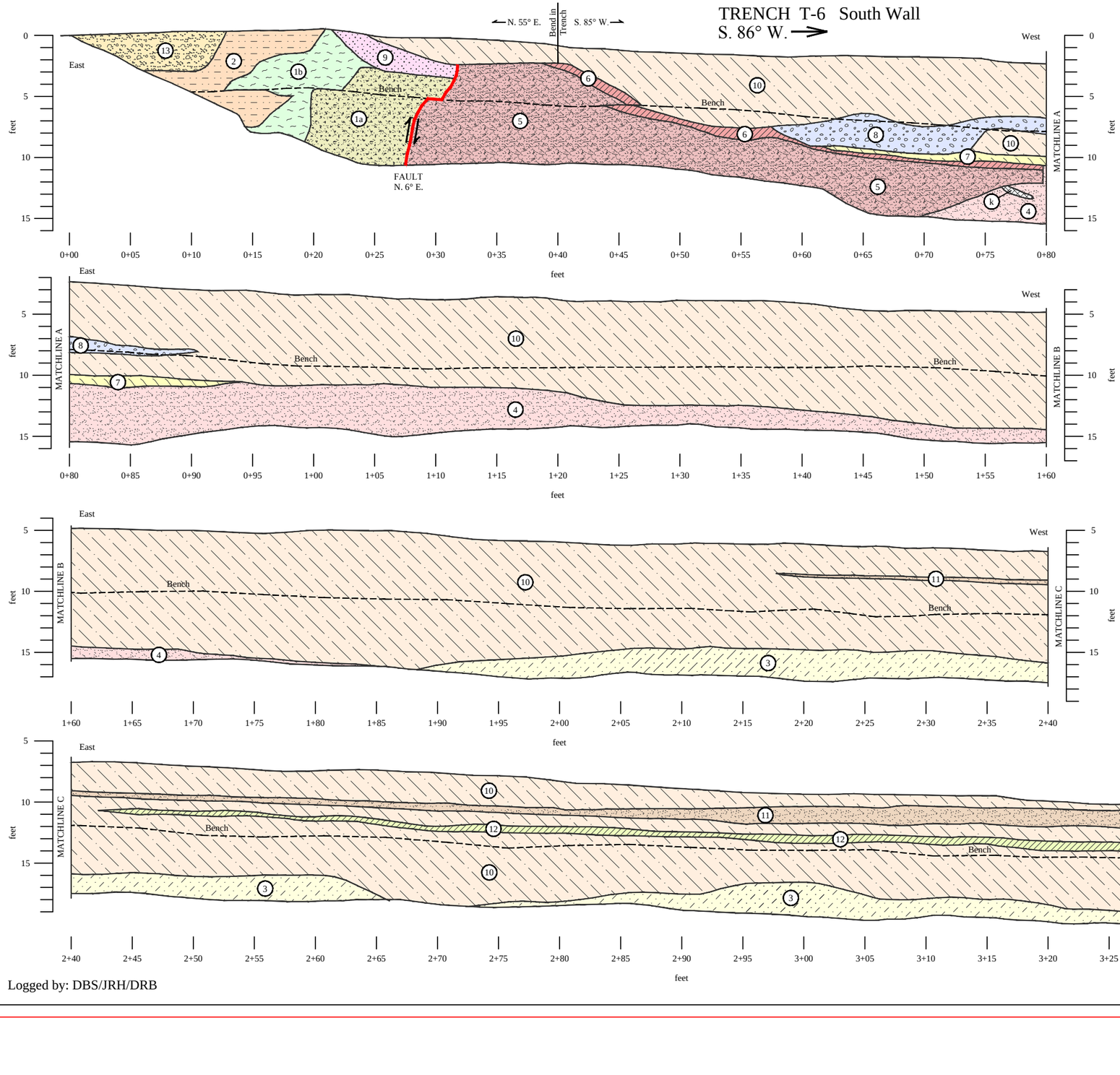

TRENCH 6

1 Bedrock: Shnabkaib Member of the Moenkopi Formation

1a Shale, very thinly bedded (≤0.2 inch thick), reddish brown (5YR 5/3) with very thin (≤0.2 inches), white (10YR 8/1) shale layers, bedding N. 65° W., 15° SW.

1b Shale, very thin to thinly bedded (0.2 to 6 inches thick), moderately fractured, light gray (5YR 7/1), gypsiferous, with "honey-comb" structure.

2 Loess: Sandy Silt (ML) massive, mottled pink (7.5YR 7/4) to pink (7.5YR 8/3).

3 Loess: Sandy Silt (ML) some coarse grained sand, massive, contact with overlying unit gradational.

4 Alluvium: Silty Sand (SM), fine grained, with 3% angular clasts ≤0.5 feet long, "honey-comb" structure, gypsiferous, reddish yellow (7.5YR 6/6).

5 Loess: Sandy Silt (ML), some pin-hole voids, massive, pink (7.5YR 8/3).

6 Loess: Silt (ML), pervasive carbonate staining, white (2.5YR 8/1) to pale yellow (2.5YR 8/2).

7 Loess: Sandy Silt (ML), massive, reddish yellow (5YR 6/6).

8 Alluvium: Gravelly Sand (SP), fine to medium grained with 20% angular clasts ≤6 inches long, average size ≤2 inches long, some weakly developed horizontal bedding, pinkish gray (7.5YR 7/2).

9 Alluvium: Sand (SP) medium grained, massive, gypsiferous, very pale brown (10YR 8/3), some "honey-comb" blocks.

10 Alluvium: Sand (SP), fine to medium grained, pink (7.5YR 8/3), with 10% angular clasts ≤6 inches long, average size ≤3 inches long with discontinuous pinkish white (7.5YR 8/2) silty fine grained sand layers.

11 Alluvium: Thinly interbedded (0.2 to 0.5 inches thick) Silty Sand (SM), coarse grained Sand (SP), and pebbly Sand (SP), red (2.5YR 5/6).

12 Loess: Silt (ML), massive reddish yellow (5YR 6/6).

13 Alluvium: Sand (SP) fine to coarse grained with thin (≤6 inches thick) horizontal layers of gravelly sand , pinkish white (7.5YR 8/2).

k Krotovina

Fault arrows showing the direction of movement.

Logged by: DBS/JRH/DRB

TRENCH PROFILE T-6

SOUTHERN CORRIDOR PHASE 3
WASHINGTON COUNTY, UTAH

ROSENBERG ASSOCIATES
CIVIL ENGINEERING – LAND SURVEYING

PROJECT #	PLATE #
5507-P3	6

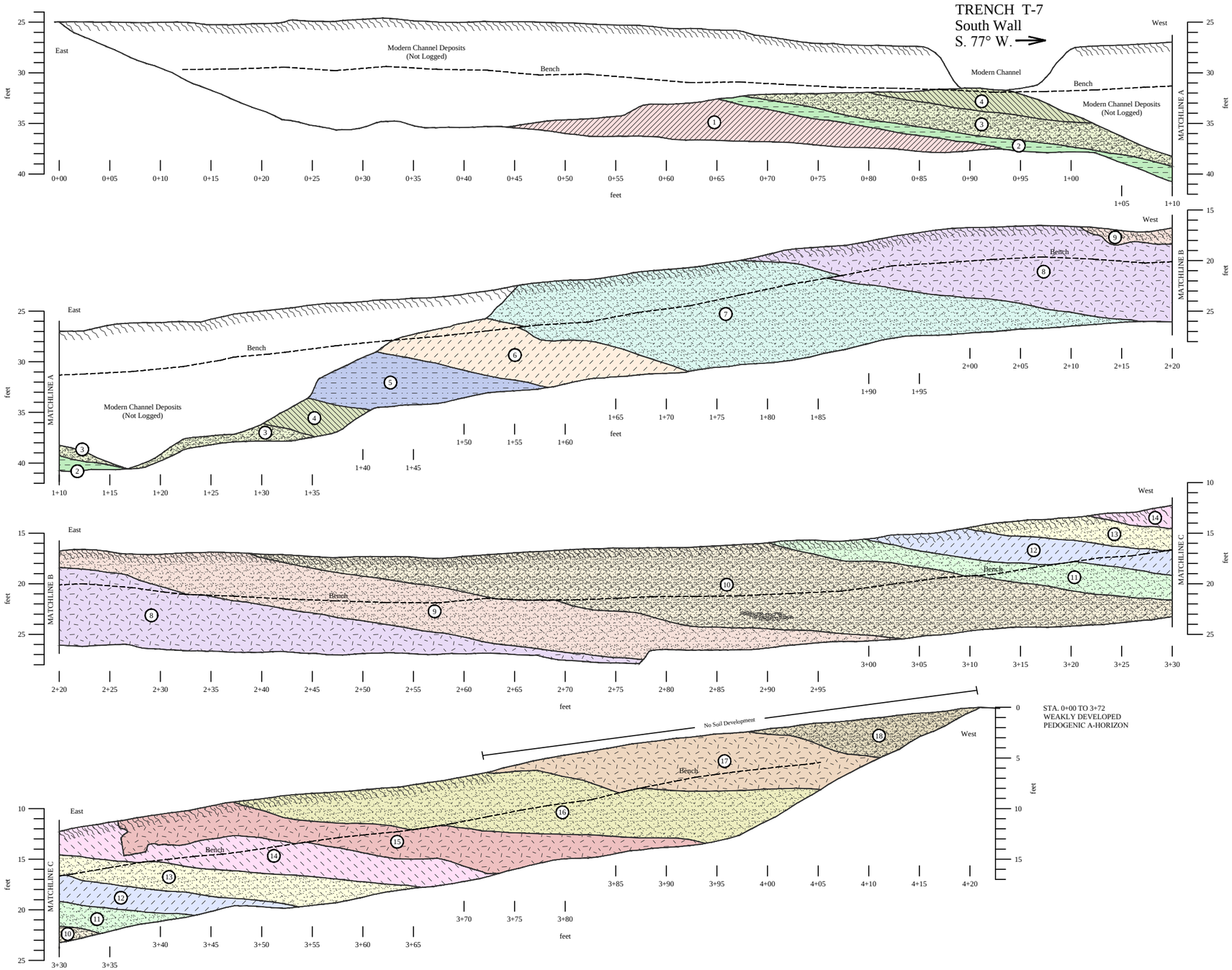

TRENCH 7

1 Alluvium: Sandy Silt (ML), well indurated, hard, massive, with 10 percent angular to rounded clasts (≤0.5 inches long) of gray sandstone, light red (2.5YR 6/8) to red (2.5YR 5/8).

2 Alluvium: Sandy Silt (ML), well indurated, hard, massive, with 5 percent rounded gray sandstone clasts (≤0.1 inch long), light red (2.5YR 6/6).

3 Loess: Sandy Silt (ML), well indurated, massive, hard, red (2.5YR 5/6).

4 Loess: Silt (ML), well indurated, hard, light red (2.5YR 6/6).

5 Alluvium: Sandy Silt (ML), with thin (≤6 inches thick), very fine grained discontinuous sand lenses, massive, light red (2.5YR 7/6).

6 Loess: Sandy Silt (ML), massive, light red (2.5YR 6/6) to red (2.5YR 5/6).

7 Alluvium: Silty Sand (SM), very fine to fine grained, massive, reddish yellow (5YR 6/8), with weakly developed pedogenic A-horizon.

8 Alluvium: Sandy Silt (ML), pin hole voids, some gypsum and discontinuous fine grained sand and pebble lenses, moderate carbonate cementation, resistant layer, red (2.5YR 5/6), with weakly developed pedogenic A-horizon.

9 Alluvium: Sand (SP), very fine to fine grained, massive, reddish yellow (5YR 6/8), with weakly developed pedogenic A-horizon.

10 Alluvium: Silty Sand (SM), fine grained, massive, light red (2.5YR 6/6) to red (2.5YR 5/6, with weakly developed pedogenic A-horizon).

11 Alluvium: Sand (SP), very fine to fine grained, massive, light red (2.5YR 6/8) to red (2.5YR 5/8), with weakly developed pedogenic A-horizon.

12 Loess: Sandy Silt (ML) to Silty Sand (SM), massive, red (2.5YR 5/6), with weakly developed pedogenic A-horizon.

13 Alluvium: Sand (SP) with silt, very fine grained, massive, light red (2.5YR 6/8), with weakly developed pedogenic A-horizon.

14 Loess: Sandy Silt (ML), massive, red (2.5YR 5/8), with weakly developed pedogenic A-horizon.

15 Loess: Silt (ML) with some fine grained sand, massive, moderate carbonate cementation, resistant layer, light red (2.5YR 6/6), with weakly developed pedogenic A-horizon.

16 Alluvium: Sand (SP), very fine grained, some silt, massive, reddish yellow (5YR 6/8), with weakly developed pedogenic A-horizon.

17 Loess: Silt (ML) with some fine grained sand, massive, cementation, resistant layer, light reddish brown (5YR 6/4).

18 Alluvium: Sandy Silt (ML), moderate carbonate cementation, massive, resistant layer, light red (2.5YR 6/6).

Logged by: DBS/JRH/DRB

TRENCH PROFILE T-7

SOUTHERN CORRIDOR PHASE 3
WASHINGTON COUNTY, UTAH

ROSENBERG ASSOCIATES CIVIL ENGINEERS • LAND SURVEYORS

PROJECT #	PLATE #
5507-P3	7

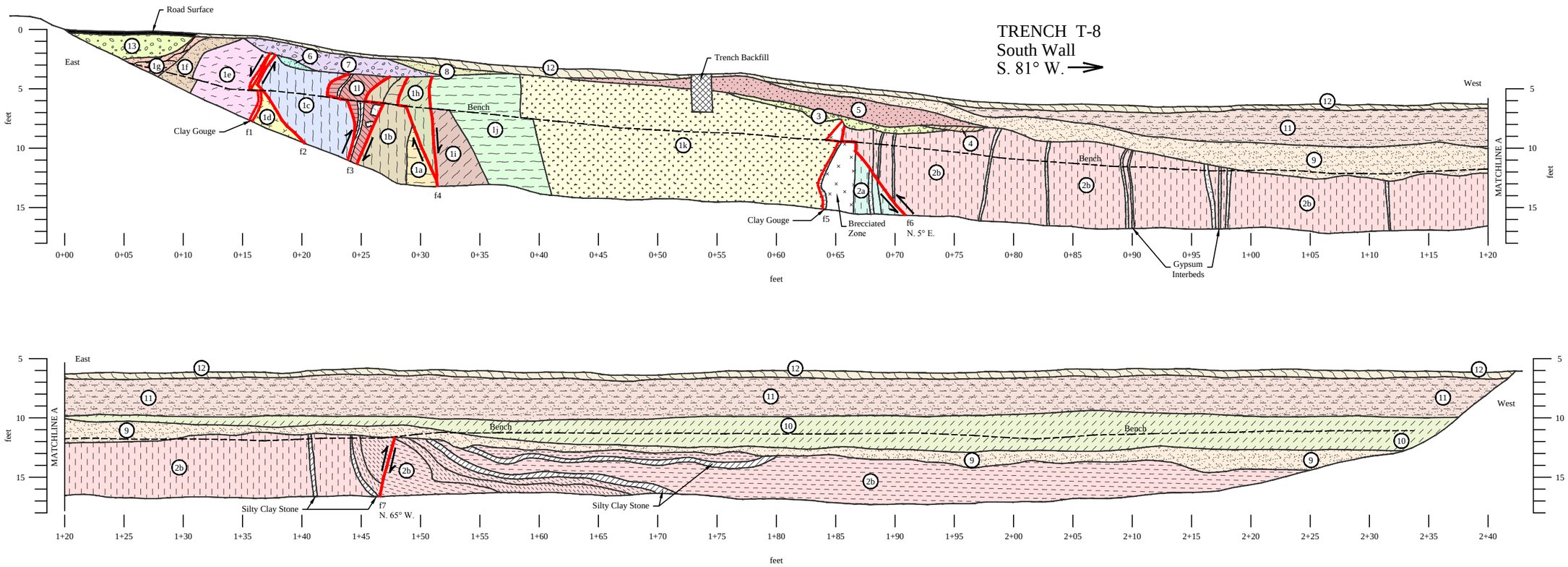

TRENCH 8

1 Petrified Forest Member of the Chinle Formation

1a Claystone, gypsiferous, sheared, weak red (10R 4/2).

1b Claystone, reddish brown (2.5YR 4/4).

1c Claystone, reddish brown (2.5YR 4/4), with fragments and discontinuous interbeds of white (2.5Y 8/1) claystone.

1d Claystone, dark reddish brown (2.5YR 3/3).

1e Claystone, thinly bedded, highly fractured, dark reddish brown (5YR 3/4).

1f Thinly interbedded light gray (10YR 7/1) clayey sandstone and dark reddish brown (5YR 3/3) Claystone.

1g Sandstone, deeply weathered with pervasive carbonate filled fractures and veins, pinkish white (5YR 8/2)

1h Claystone, silty, sheared, weak red (10R 4/4).

1i Claystone, sheared, weak red (10R 5/3 to 4/3).

1j Claystone, gypsiferous, sheared, weak red (10YR 5/3) with fragments and discontinuous interbeds of white (2.5Y 8/1) claystone which gives the unit a mottled appearance.

1k Claystone, massive, gypsiferous, moderately weathered, sheared, weak red (10R 4/2).

1l Fault zone alternating near vertical layers of light gray (7.5YR 7/1), dark reddish brown (2.5YR 3/4), dark reddish gray (2.5YR N4/1), and reddish brown (2.5YR 5/3) Claystone with fragments (≤12 inches long) of pale red (2.5YR 6/2) silty Sandstone with some shearing along interbeds.

2 Dinosaur Canyon Member of the Moenave Formation

2a Claystone, red (2.5YR 5/6), with pinkish gray (7.5YR 7/2) Claystone interbeds (≤12 inches thick).

2b Silty Claystone, red (2.5YR 4/6), gypsiferous, with thin (≤12 inches thick) white (10YR 8/1) silty claystone interbeds, moderately weathered.

3 Alluvium: Sand (SP) with silt, reddish brown (5YR 5/4) with 5 percent sub-angular clasts ≤10 long, average size ≤3 inches long.

4 Loess: Silt (ML) with some very fine grained sand, reddish yellow (5YR 6/6).

5 Alluvium: Sandy Silt (ML) to Silty Sand (SM), very fine grained, yellowish red (5YR 4/6) with 20 percent pinkish white (5YR 8/2) gypsum fragments which gives the unit a mottled appearance, sheared.

6 Alluvium: Sand (SP) with silt, very fine grained, reddish brown (5YR 5/4).

7 Alluvium: Sand (SP) with silt, very fine to fine grained, yellowish red (5YR 4/6) with pervasive pinkish white (5YR 8/2) gypsum fragments which gives the unit a mottled appearance.

8 Loess: Sandy Silt (ML), gypsiferous, pin-hole voids, mottled yellowish red (5YR 5/6) to weak red (10R 4/2).

9 Alluvium: Silty Sand (SM) to Sandy Silt (ML), very fine grained, pin-hole voids, yellowish brown (5YR 5/8).

10 Loess: Sandy Silt (ML) some gypsum and pin-hole voids, yellowish red (5YR 5/6).

11 Alluvium: Silty Sand (SM), very fine grained, red (2.5 YR 5/6 to 4/6) with thin (≤6 inches thick), reddish yellow (5YR 6/6) Silty Sand (SM) (interbeds give the unit a striped appearance).

12 Alluvium: Silty Sand (SM), very fine to fine grained, light reddish brown (5YR 6/4) with an organic-rich pedogenic A-horizon about 6 inches thick.

13 Road Fill: Silty Sand (SM), very fine grained with ≤10 percent angular clasts ≤12 inches long, average size ≤4 inches, yellowish red (5YR 5/6).

Fault arrows showing the direction of movement.

Logged by: DBS/JRH/DRB

TRENCH PROFILE T-8

SOUTHERN CORRIDOR PHASE 3
WASHINGTON COUNTY, UTAH

ROSENBERG ASSOCIATES
CIVIL ENGINEERS – LAND SURVEYORS

PROJECT #	PLATE #
5507-P3	8

TRENCH T-9
South Wall
N. 89° W. →

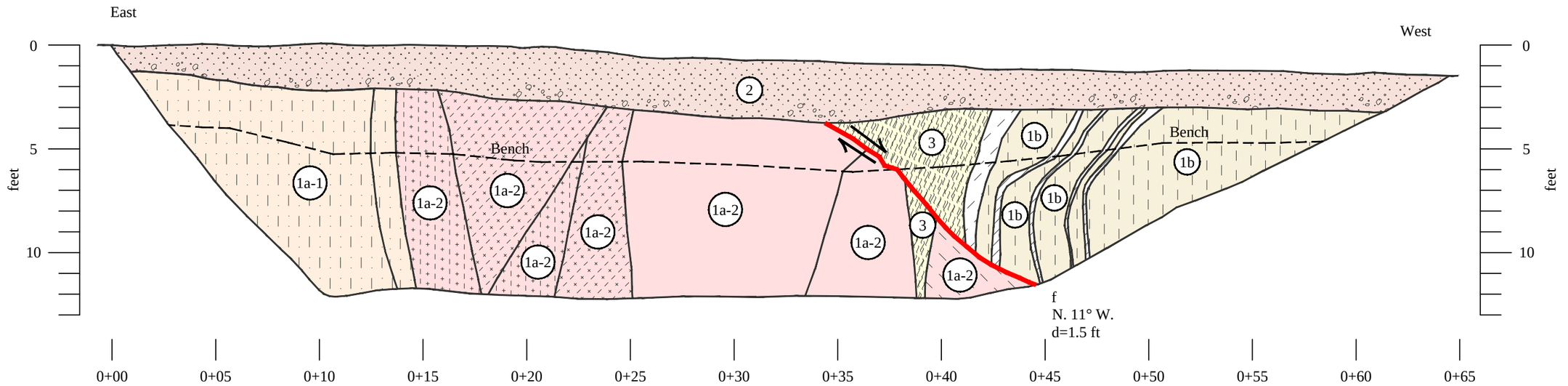

TRENCH 9

1 Bedrock

1a Petrified Forest Member of the Chinle Formation

1a-1 Claystone, gypsiferous, near vertical bedding, intensely sheared, weak red (10R 4/3).

1a-2 Claystone, gypsiferous, near vertical bedding, intensely sheared, weak red (10R 4/2).

1b Dinosaur Canyon Member of the Moenave Formation: Silty Claystone, gypsiferous, red (2.5YR 4/6), moderately weathered, with thin (≤12 inches thick) interbeds of white (10YR 8/1) Claystone.

2 Alluvium: Sandy Silt (ML), with 3±% angular clasts ≤ 3 inches long, weak stone line, reddish yellow (5YR 6/6).

3 Breccia Zone: Intensely sheared and fragmented claystone (primarily units 1a-1 and 1a-2).

Fault arrows showing the direction of movement.

Logged by: DBS/JRH/DRB

TRENCH PROFILE T-9

SOUTHERN CORRIDOR PHASE 3
WASHINGTON COUNTY, UTAH

ROSENBERG ASSOCIATES CIVIL ENGINEERS • LAND SURVEYORS

PROJECT #	PLATE #
5507-P3	9

TRENCH T-10
South Wall
S. 79° W. →

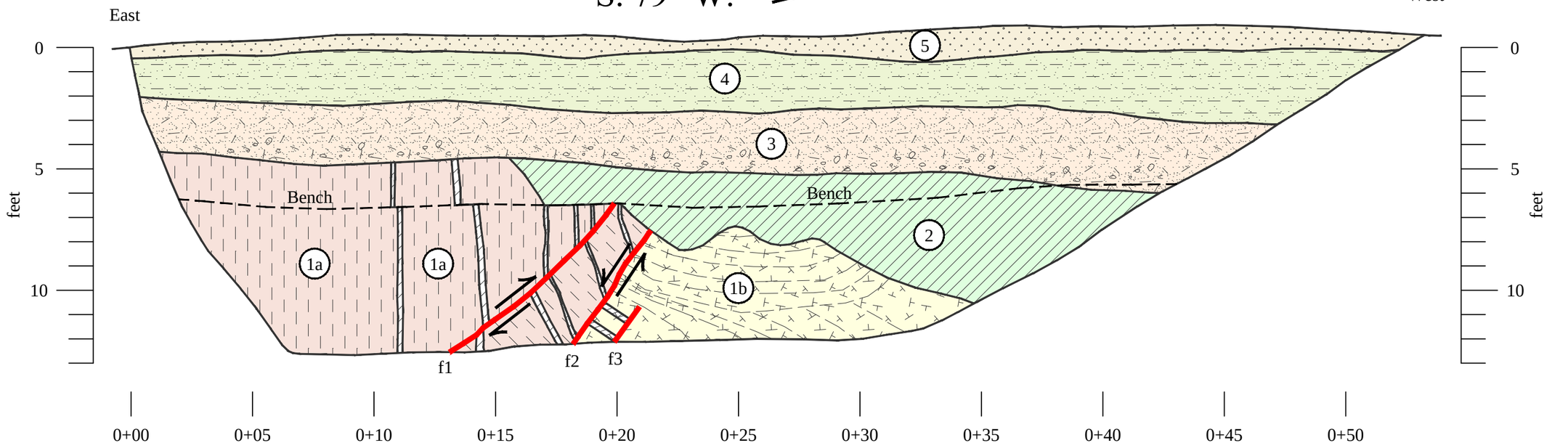

TRENCH 10

1 Bedrock: Dinosaur Canyon Member of the Moenave Formation

1a Silty Claystone, gypsiferous, red (2.5YR 4/6), with thin (≤12 inches thick) interbeds of Silty Claystone, moderately weathered, white (10YR 8/1).

1b Sandy Siltstone (ML), gypsiferous, thin to moderately bedded (1 to 12 inches thick), red (2.5YR 5/6).

2 Loess: Silt (ML), gypsiferous, with 5% angular clasts ≤0.2 inches long, light red (2.5YR 6/8).

3 Loess: Silt (ML) with some fine grained sand, pink (5YR 7/4).

4 Alluvium: Silty Sand (SM), very fine grained, red (2.5YR 5/6 to 4/6) with thin (≤6 inches thick) interbeds of reddish yellow (5YR 6/6) Silty Sand (SM) (interbeds give the unit a “striped" appearance).

5 Alluvium: Sandy Silt (ML), with ±3% angular clasts ≤3 inches long, weak stone line, reddish yellow (5YR 6/6).

Fault arrows showing the direction of movement.

Sample	Strike	Dip	Displacement
f1	N. 20° W.	40° E.	12 inches (0.3 m)
f2	N. 23° W.	57° E.	unknown
f3	N. 18° W.	59° E.	unknown

Logged by: DBS/JRH/DRB

TRENCH PROFILE T-10

SOUTHERN CORRIDOR PHASE 3
WASHINGTON COUNTY, UTAH

ROSENBERG ASSOCIATES
CIVIL ENGINEERS • LAND SURVEYORS

PROJECT # 5507-P3

PLATE # 10

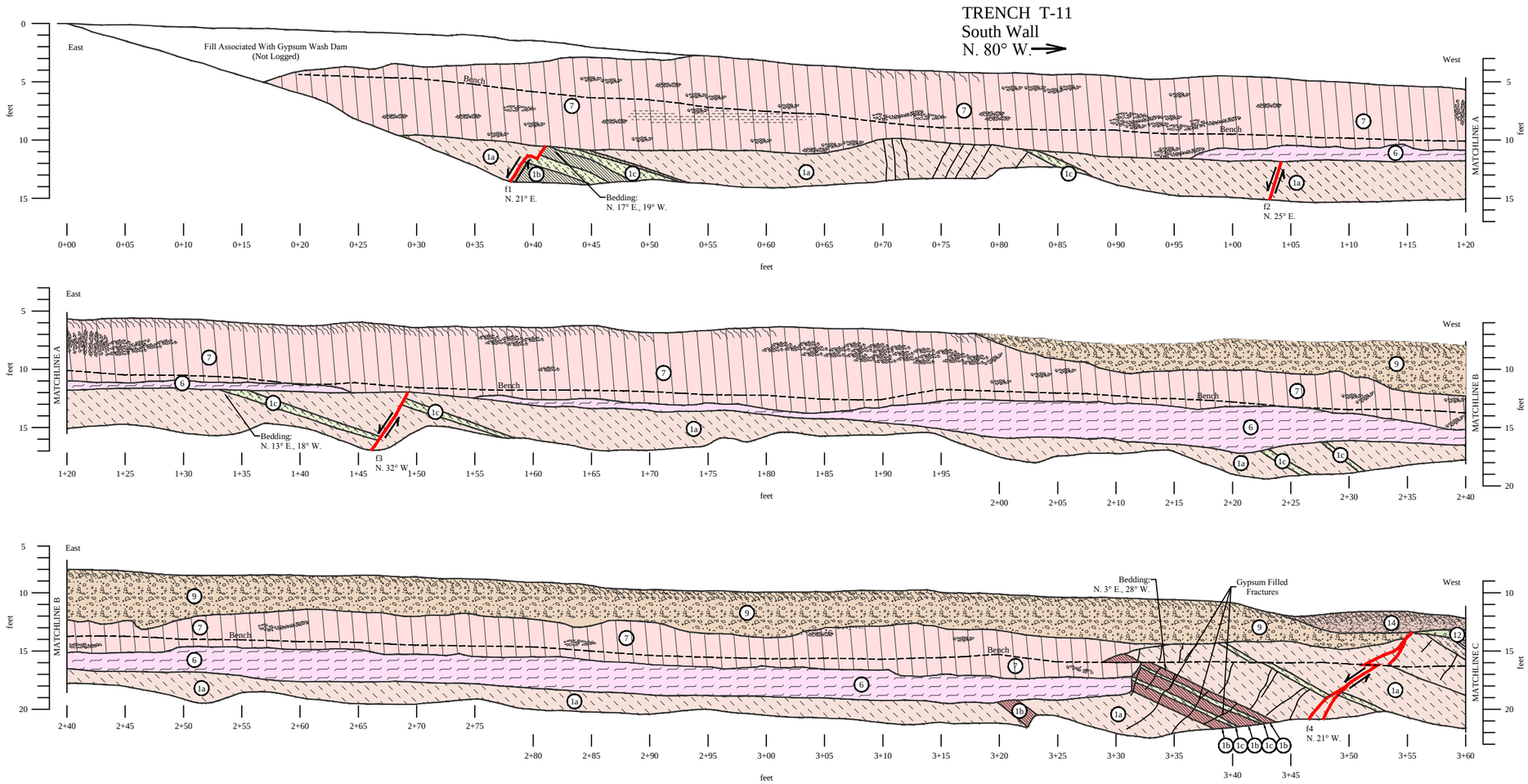

TRENCH 11

1 Bedrock: middle red member of the Moenkopi Formation

1a Silty Claystone (primary unit in trench), thin to moderately bedded (6 to 24 inches thick), gypsiferous, friable, intensely fractured and "broken", west dipping, reddish brown (2.5YR 4/3), with numerous, east dipping to vertical gypsum filled fractures, generally ≥0.2 inches wide.

1b Clayey Siltstone interbeds, well indurated, very hard, gypsiferous, reddish yellow (5YR 6/6)

1c Claystone interbeds, light greenish gray (5GY 7/1 - GLEY)

2 Alluvium: Silty Sand (SM), fine grained, with 15% angular clasts ≤6 inches long, average size ≤2 inches long, reddish yellow (5YR 6/6) to yellowish red (5YR 5/6).

3 Loess: Sandy Silt (ML), massive, reddish yellow (7.5YR 7/6).

4 Loess: Silt (ML), some very fine grained sand, reddish yellow (5YR 6/6).

5 Alluvium: Sand (SP), fine to medium grained with 20± percent angular clasts ≤4 inches long, average size ≤2 inches long, reddish brown (5YR 5/4).

6 Alluvium: Gravelly Sand (GP), fine to coarse grained, with 15 to 30 percent sub-angular to angular clasts ≤12 inches long, average size ≤4 inches long, brown (7.5YR 4/3).

7 Alluvium: Sand (SP), fine to medium grained, dark reddish brown (5YR 3/4) with thin (≤0.5 inches thick) horizontal interbeds of reddish yellow (5YR 6/6) Silt (ML), with a weakly developed pedogenic A-horizon.

8 Fault Derived Colluvium: Sand (SP) fine to medium grained, some silt and angular clasts (≤0.5 inches long) of adjacent middle red member of the Moenkopi Formation claystone, yellowish red (5YR 5/6).

9 Alluvium: Sand (SP), fine to medium grained with 5 percent angular clasts ≤0.3 inches long, reddish brown (5YR 5/4), with a weakly developed pedogenic A-horizon.

10 Loess: Silt (ML) with some fine grained sand , massive, reddish yellow (5YR 7/6 to 6/6).

11 Alluvium: Gravely Sand (SP), fine to medium grained, weak horizontal bedding with 25% angular clasts ≤8 inches long, average size ≤4 inches long, light reddish brown (5YR 6/4).

12 Alluvium: Sand (SP), medium grained with 15 percent angular clasts ≤0.6 inches long, reddish yellow (5YR 6/6).

13 Loess: Clayey Silt (ML) with very fine grained sand, reddish brown (5YR 5/4), with weakly developed pedogenic A-horizon.

14 Loess: Silty Sand (SM), fine grained, yellowish red (5YR 5/6), with a weakly developed pedogenic A-horizon.

Fault arrows showing the direction of movement.

Fault	Strike	Dip	Displacement	
			ft.	m.
f1	N. 21° E.	58° E.	unknown	unknown
f2	N. 25° E.	25° E.	unknown	unknown
f3	N. 25° E.	57° E.	2.8	9.2
f4	N. 32° W.	43° E.	0.5	1.6
f5	N. 12° W.	75° E.	5	16.4
f6	N. 15° W.	73° W.	≥7	≥2.1

Logged by: DBS/JRH/DRB

TRENCH PROFILE T-11

SOUTHERN CORRIDOR PHASE 3
WASHINGTON COUNTY, UTAH

ROSENBERG ASSOCIATES

PROJECT #	PLATE #
5507-P3	11

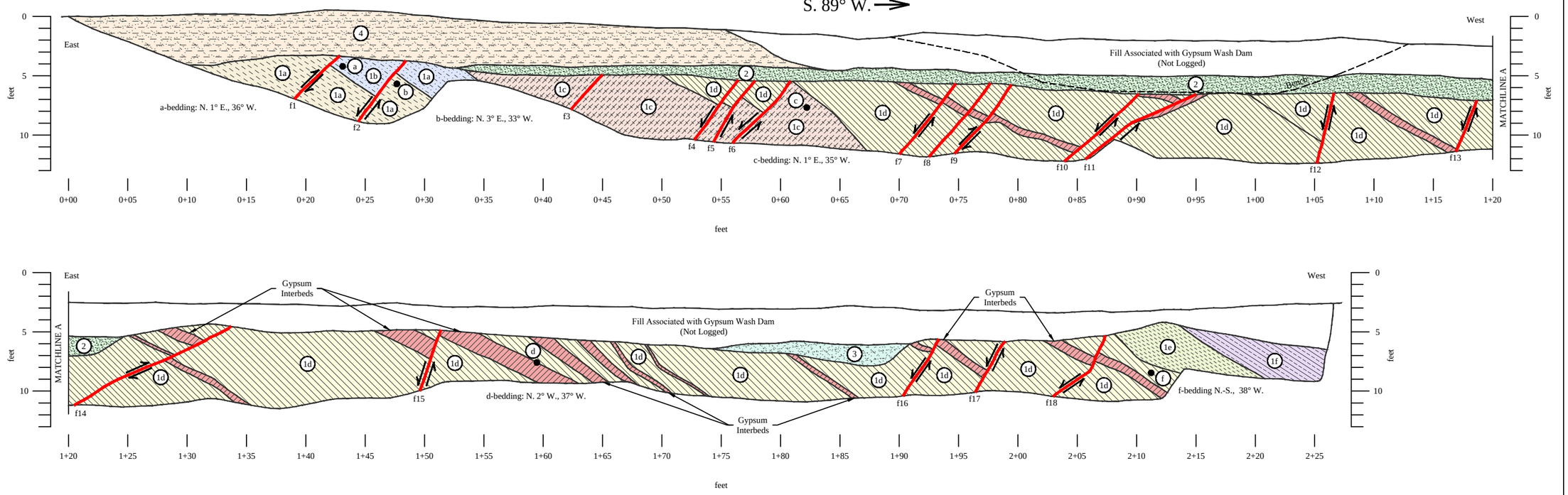

TRENCH 12

1 Bedrock: Middle red member of the Moenkopi Formation

1a Siltstone, thinly bedded (≤2 inches thick), light greenish gray (GLEY 5GY 7/1).

1b Sandstone, fine grained, moderately bedded (≤12 inches thick), well cemented, some lithic clasts (≤0.1 inch long) and secondary gypsum, pale yellow (2.5Y 8/4).

1c Siltstone, thinly bedded (≤2 inches thick), gray (7.5YR 6/1)

1d Clayey Siltstone, thinly bedded (≤1 inch thick), brown (7.5YR 4/3) with interbeds of Silty Claystone, light greenish gray (GLEY 5GY 7/1).

1e Sandstone, fine grained, very hard, well cemented with gypsum, light gray (10YR 7/1).

1f Siltstone, pervasive gypsum seams, light gray (10YR 7/1).

2 Alluvium: Sand (SP), fine to medium grained, massive, gypsiferous, dark reddish brown (2.5YR 3/3).

3 Alluvium: Sandy Silt (ML), massive, pink (5YR 7/3).

4 Alluvium: Sand (SP), fine to coarse grained, thinly bedded (≤1 inch thick), reddish brown (5YR 4/4), with weakly developed pedogenic A- horizon.

● Sample location for age dating.

Fault arrows showing the direction of movement.

Fault	Strike	Dip	Displacement - ft. (m)
f1	N. 22° E.	44° E.	unknown
f2	N. 25° E.	52° E.	4.2 (1.4)
f3	N. 23° E.	48° E.	unknown
f4	N. 0° E.	55° E.	0.2 (0.07)
f5	N. 0° E.	55° E.	0.3 (0.09)
f6	N. 33° E.	50° E.	5.6 (1.7)
f7	N. 5° W.	51° E.	0.5 (0.15)
f8	N. 28° E.	49° E.	0.5 (0.15)
f9	N. 16° W.	49° E.	0.5 (0.15)

Fault	Strike	Dip	Displacement - ft. (m)
f10	N. 20° E.	41° E.	4.3 (1.3)
f11	N. 10° W.	29° E.	unknown
f12	N. 10° W.	77° E.	>2.0 (>0.6)
f13	N. 0° E.	68° E.	6.5 (2.0)
f14	N. 43° W.	37° E.	1.5 (0.5)
f15	N. 38° E.	71° E.	2.0 (0.6)
f16	N. 15° W.	58° E.	0.6 (0.18)
f17	N. 30° E.	60° E.	6.0 (0.18)
f18	N. 10° W.	50° E.	unknown

Logged by: DBS/JRH/DRB

TRENCH PROFILE T-12

SOUTHERN CORRIDOR PHASE 3
WASHINGTON COUNTY, UTAH

ROSENBERG ASSOCIATES
CIVIL ENGINEERS - LAND SURVEYORS

PROJECT #	PLATE #
5507-P3	12

TRENCH T-13
South Wall
N. 90° W.

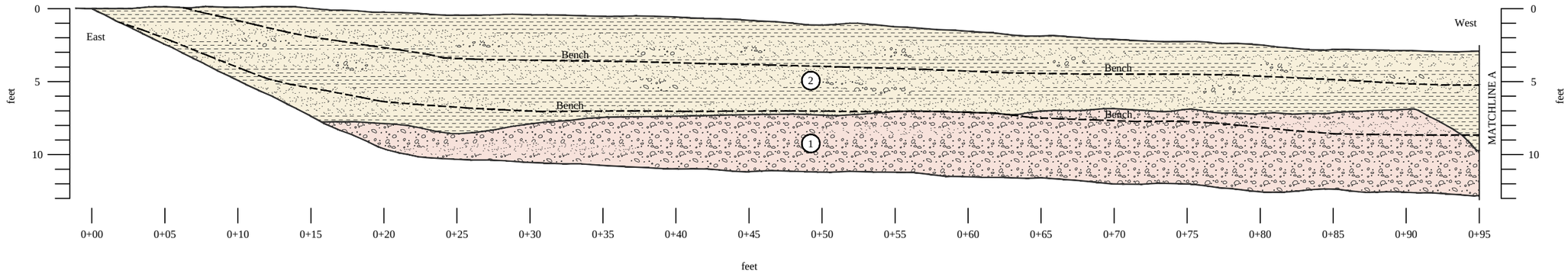

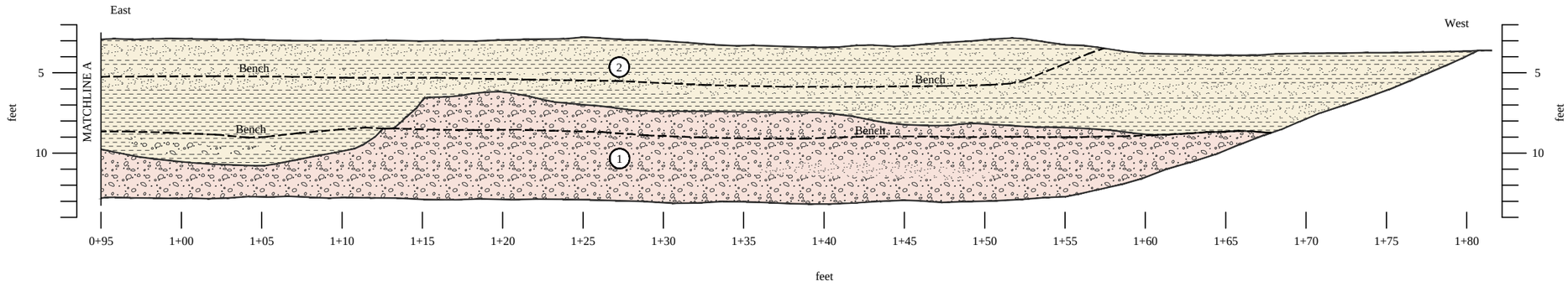

TRENCH 13

1 Alluvium: Gravelly Sand (GP) to Sandy Gravel (SP), fine to coarse grained with sub-angular to angular clasts ≤12 inched long, average size ≤3 inched long, and with discontinuous fine to medium grained sand lenses, yellowish brown (5YR 5/8).

2 Alluvium: Silty Sand (SM) fine to medium grained, light red (2.5 YR 6/8) with thin to moderate (6 to 12 inches thick) interbeds of light reddish brown (5YR 6/4) sandy silt (ML) which give the unit a "striped" appearance. Unit also contains discontinuous fine to medium grained sand lenses, yellowish brown (5YR 5/8).

Logged by: DBS/JRH/DRB

TRENCH PROFILE T-13

SOUTHERN CORRIDOR PHASE 3
WASHINGTON COUNTY, UTAH

ROSENBERG ASSOCIATES CIVIL ENGINEERS – LAND SURVEYORS

PROJECT #	PLATE #
5507-P3	13

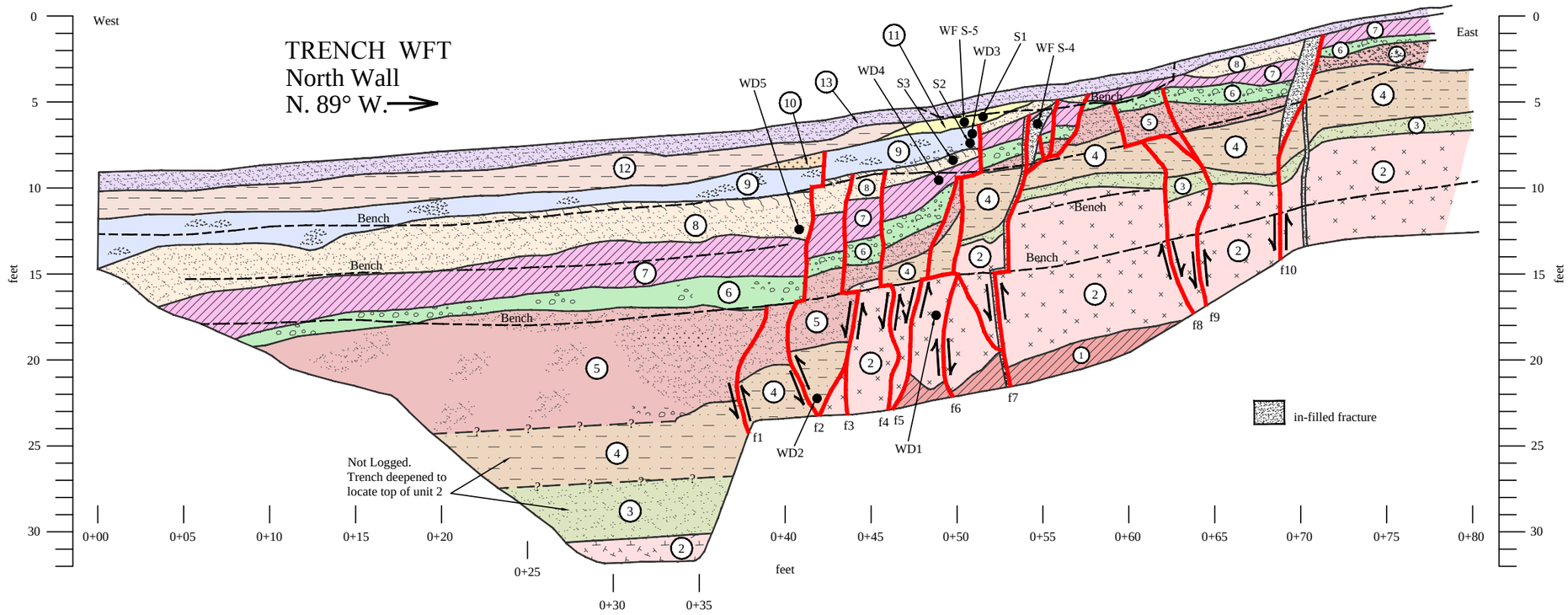

WF T-1 NORTH

1 Alluvium: Sand (SP) with silt, very fine grained, massive, yellow (10YR 7/6).

2 Alluvium: Sandy Silt (ML), massive, gypsiferous, with 5% angular clasts ≤0.25 inches, pin hole voids, light brown (7.5YR 6/4).

3 Alluvium: Sand (SP) with some silt, fine grained, massive, some carbonate and gypsum nodules, yellowish red (5YR 5/6).

4 Alluvium: Sandy Silt (ML), massive, with 10% angular gypsum clasts ≤0.5 inches, reddish yellow (5YR 6/6) to yellowish red (5YR 5/6).

5 Alluvium: Silty Sand (SM), very fine grained, massive, yellowish red (5YR 4/6).

6 Alluvium: Sandy Gravel (GP), 60% angular clasts ≤2 inches, average size ≤1 inch, matrix silty fine grained sand, some carbonate staining, reddish yellow (5YR 7/6).

7 Alluvium: Sandy Silt (ML), very fine grained, massive, reddish yellow (5YR 7/6).

8 Alluvium: Silty Sand (SM), very fine grained, massive, reddish yellow (5YR 6/8), with a weakly developed pedogenic horizon (Bk).

9 Alluvium: Sand (SP), with some silt, very fine to fine grained, massive, yellowish red (5YR 5/8).

10 Alluvium: Silty Sand (SM) very fine grained, yellowish red (5YR 5/6).

11 Colluvial wedge: Sandy Silt (ML) with 3% angular clasts ≤2 inches, average size ≤1 inch, yellowish red (5YR 5/6).

12 Alluvium: Silty Sand (SM), massive, reddish yellow (5YR 6/6).

13 Loess: Sand (SP), fine to medium grained, loose (modern, actively accumulating eolian sand), yellowish red (5YR 4/6).

In-filled fractures: Silty Sand (SM), very fine to fine grained with 5% angular carbonate coated clasts ≤0.25 inches, reddish yellow (5YR 6/6)

Fault	Strike	Dip	Displacement feet (m)
f1	N. 5° E.	85° W. to vertical	1 (0.3)
f2	N. 8° E.	85° W. to vertical	1.6 (0.5)
f3	N. 2° E.	85° W. to vertical	3.3 (1)
f4	N. 5° W.	85° W. to vertical	1.6 (0.5)
f5	N.-S.	80° W. to vertical	5 (1.5)
f6	N. 10° W.	85° W. to vertical	2 (0.6)
f7	N. 15° W.	85° W. to 85° E.	3.3 (1)
f8	N. 5° E.	85° E. to vertical	1 (0.3)
f9	N. 5° W.	85° W. to 85° E.	0.7 (0.2)
f10	N. 2° W.	85° W. to vertical	3 (0.9)

OSL Ages			
Sample	Geologic Unit		OSL Age
WF S-5[a]	11	colluvial wedge	4170 ± 1360
WF S-4[a]	8	fracture in-filling	7020 ± 1480
WD 3[b]	9	alluvium	18,590 ± 1160
WD 5[b]	8	alluvium	30,810 ± 2110
WD 4[b]	7	alluvium	30,590 ± 2100
WD 1[b]	2	fracture in-filling	67,750 ± 4560
WD 2[b]	4	alluvium	75,570 ± 5130

[a] Sample obtained during this study.

[b] Sample obtained by the UGS (Lund and others, 2008).

Radiocarbon Ages				
Sample	Geologic Unit		Age	
			RCYBP[1]	cal yr B.P.[2]
S-1	11	colluvial wedge	645 ± 15	670-640 (38.8%) 600 -550 (56.6%)
S-2	9	alluvium	530 ± 15	560 - 510
S-3	8	alluvium	925 ± 15	920 - 790

[1] RCYBP = radiocarbon years before present (AD 1950)

[2] cal yr B.P. = calibrated years before present (2σ)

● Sample location for age dating.

Fault arrows showing the direction of movement.

Logged by: DBS/JRH/DRB

TRENCH PROFILE WFT

SOUTHERN CORRIDOR PHASE 3
WASHINGTON COUNTY, UTAH

ROSENBERG ASSOCIATES
CIVIL ENGINEERS – LAND SURVEYORS

PROJECT #	PLATE #
5507-P3	14

UTAH GEOLOGICAL SURVEY
a division of
Utah Department of Natural Resources

Plate 1
Utah Geological Survey Miscellaneous Publication 15-6
Paleoseismic Investigation of the Fort Pearce and Washington Hollow Sections of the Washington Fault Zone

NORTH TRENCH

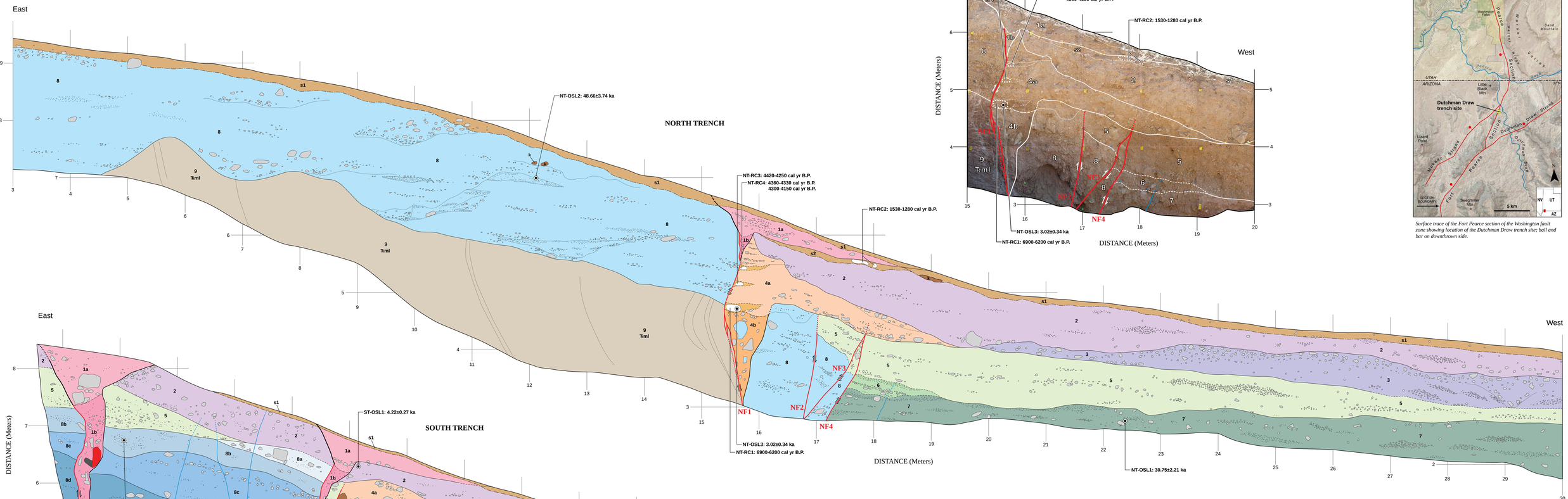

SOUTH TRENCH

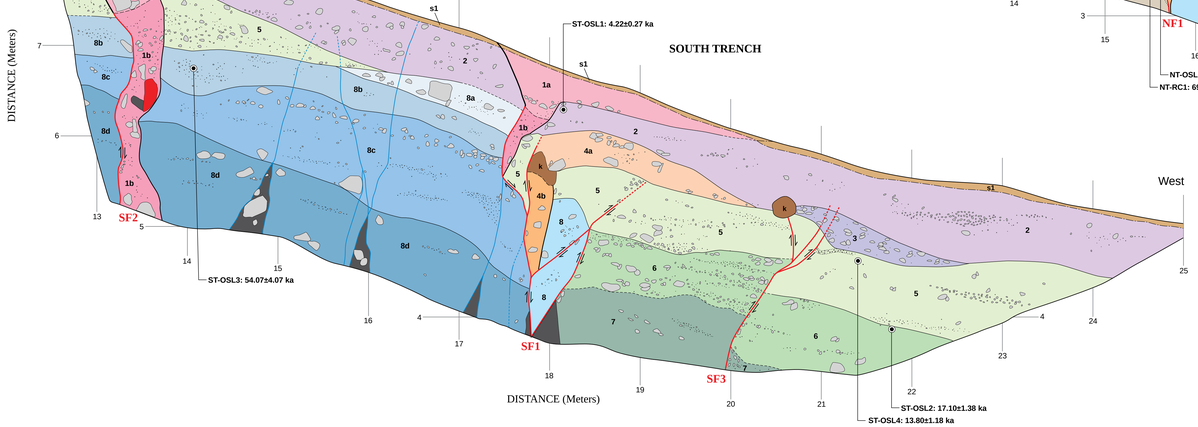

PHOTOMOSAIC OF THE WASHINGTON FAULT ZONE IN THE SOUTH WALL OF THE NORTH TRENCH

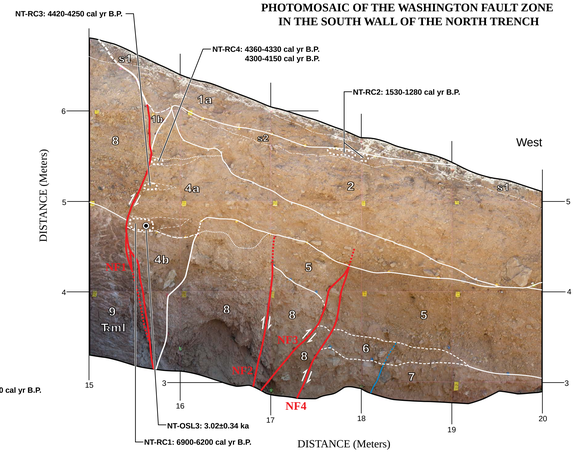

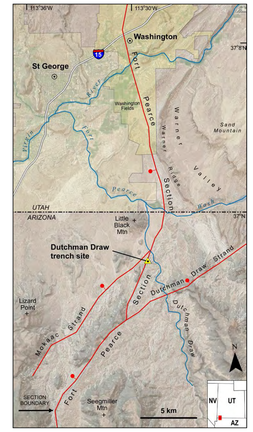

Surface trace of the Fort Pearce section of the Washington fault zone showing location of the Dutchman Draw trench site; ball and bar on downthrown side.

PHOTOMOSAIC OF THE WASHINGTON FAULT ZONE IN THE SOUTH WALL OF THE SOUTH TRENCH

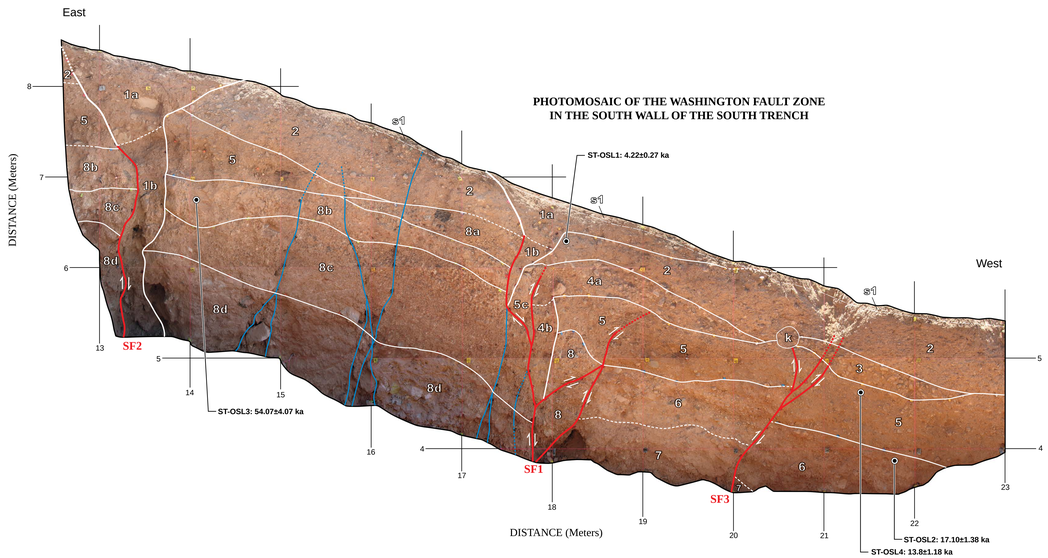

EXPLANATION

- s1 — Soil horizon; s1=modern soil, s2=buried soil horizon
- Weakly organic sediment in unit 4
- k — Infilled burrow (krotovina)
- Block in colluvial unit
- Block of unit 8 in colluvial unit
- Open void
- Bulk sample for radiocarbon analysis
- Sample for OSL dating
- Gravel
- Sand and silt

- Contact; well located, dashed where indistinct
- Contact above scarp-colluvial crack fill
- Intra-unit bedding
- Base of modern or buried soil organic material
- Fault; arrows indicate direction of relative movement; dashed where indistinct
- Eroded fault-scarp free face; dashed where indistinct
- Fissure wall
- Fracture

- 1a / 1b — Scarp colluvium (paleoearthquake P1) (1a) colluvium (1b) crack fill
- 2 — Debris-flow and debris-flood deposits
- 3 — Debris-flow deposit
- 4a / 4b — Scarp colluvium (paleoearthquake P2) (4a) colluvium (4b) crack fill
- 5 — Debris-flow deposit

- 6 — Debris-flow deposit
- 7 — Debris-flow deposit
- 8 — 8a, 8b, 8c, 8d: Strongly indurated (chiefly gypsum-cemented) debris-flow and stream deposits
- 9 (Tkml) — Mudstone and siltstone of the lower red member of the Triassic Moenkopi Formation

NOTES

Stratigraphic units and soils are described in appendix A.

Bulk-soil samples (e.g., NT-RC1) and radiocarbon ages (e.g., 6900-6200 cal yr B.P.) are summarized in appendix B.

Optically stimulated luminescence samples (e.g., NT-OSL1) and ages (e.g., 30.75±2.21 ka) are summarized in appendix C.

Although this product represents the work of professional scientists, the Utah Department of Natural Resources, Utah Geological Survey, makes no warranty, expressed or implied, regarding its suitability for a particular use. The Utah Department of Natural Resources, Utah Geological Survey, shall not be liable under any circumstances for any direct, indirect, special, incidental, or consequential damages with respect to claims by users of this product.

STRATIGRAPHIC AND STRUCTURAL RELATIONS EXPOSED IN TRENCHES AT THE DUTCHMAN DRAW TRENCH SITE, FORT PEARCE SECTION, WASHINGTON FAULT ZONE, ARIZONA

by William R. Lund, Tyler R. Knudsen, Christopher B. DuRoss, and Greg N. McDonald

UTAH GEOLOGICAL SURVEY
a division of
Utah Department of Natural Resources

Plate 1
Utah Geological Survey Miscellaneous Publication 15-6
Geologic Map of the Northern Part of the Fort Pearce Section and the Washington Hollow Section of the Washington Fault Zone

MAP A

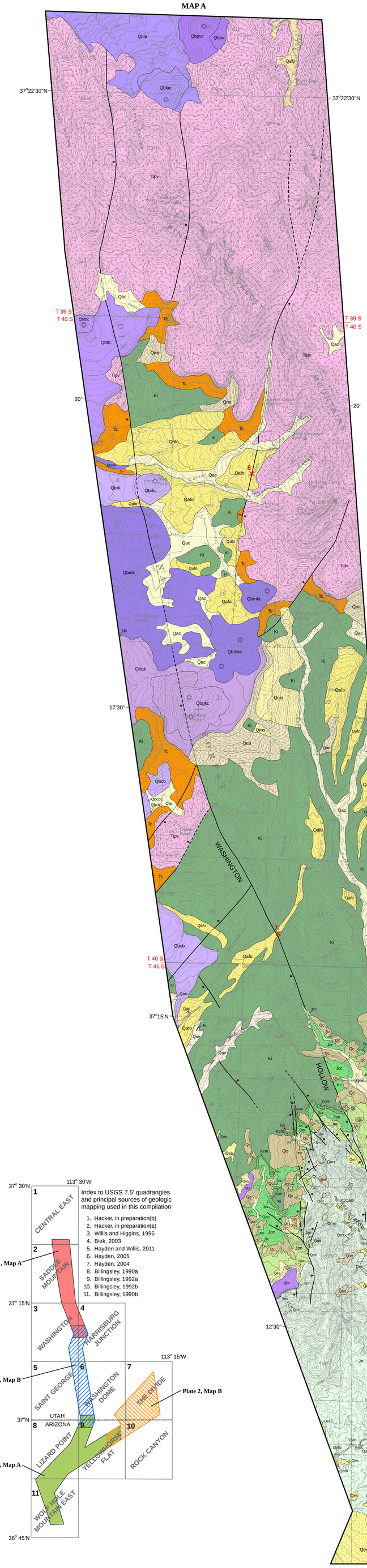

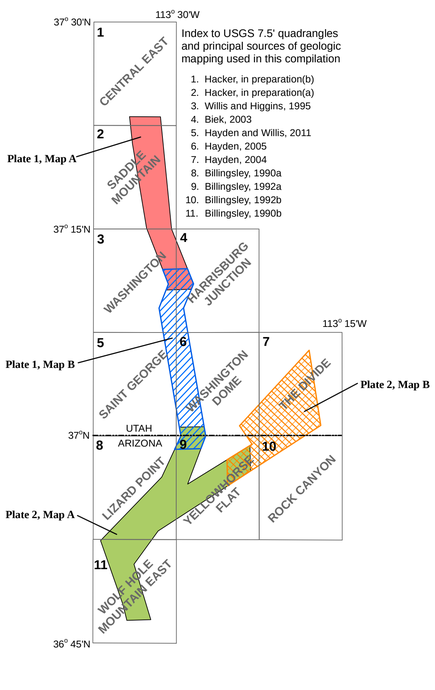

MAP B

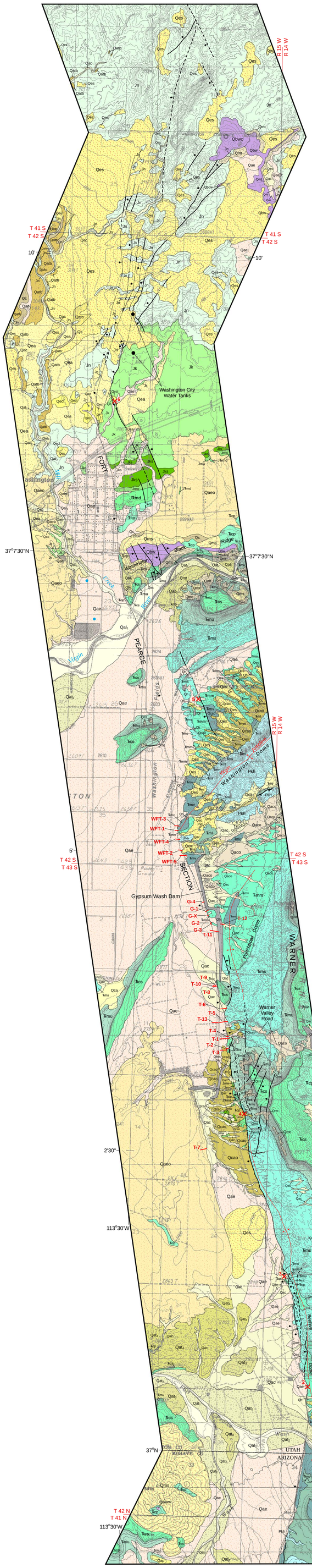

DESCRIPTION OF MAP UNITS
(See appendix A for detailed descriptions)

QUATERNARY

Human-derived deposits

- Qh — Artificial fill (Historical)

Alluvial deposits

- Qal$_1$ — Stream deposits (Holocene)
- Qal$_2$, Qal$_3$, Qal$_4$, Qal$_{5\text{-}6}$ — Stream-terrace deposits (Holocene to middle Pleistocene)
- Qatb — Boulder-terrace deposits (upper to middle Pleistocene)
- Qato — Older alluvial-terrace deposits (upper to middle Pleistocene)
- Qap — Pediment alluvium (Holocene to middle Pleistocene)
- Qaf$_1$ — Level-1 fan alluvium (Holocene)
- Qaf$_2$ — Level-2 fan alluvium (Holocene to upper Pleistocene)
- Qaf$_3$ — Level-3 fan alluvium (upper Pleistocene)
- Qafy — Younger fan alluvium (Holocene to upper Pleistocene)
- Qafo — Older fan alluvium (Pleistocene)

Colluvial deposits

- Qc — Colluvium (Holocene to upper Pleistocene)

Eolian deposits

- Qes — Eolian sand (Holocene to upper Pleistocene)
- Qecl — Eolian calcic soils and sand (upper to middle Pleistocene)

Mass-movement deposits

- Qmt — Talus (Holocene to upper Pleistocene)
- Qms — Landslides (Holocene to middle [?] Pleistocene)

Mixed-environment deposits

- Qac — Alluvium and colluvium (Holocene)
- Qaco — Older alluvium and colluvium (Holocene to upper Pleistocene)
- Qea — Eolian sand and alluvium (Holocene to upper Pleistocene)
- Qae — Alluvium and eolian sand (Holocene)
- Qaeo — Older Alluvium and eolian sand (Holocene to upper Pleistocene)
- Qca — Colluvium and alluvium (Holocene)
- Qcao — Older colluvium and alluvium (Holocene to upper Pleistocene)

Basaltic lava flows

- Qbd — Divide lava flow (middle Pleistocene)
- Qbla, Qblac — Lark Canyon lava flow and cinder cone (middle Pleistocene)
- Qbmk, Qbmkc — Mahogany Knoll lava flow and cinder cone (middle [?] Pleistocene)
- Qbrk, Qbrkc — Red Knoll lava flow and cinder cone (middle [?] Pleistocene)
- Qbtb, Qbtbc — Truman Bench lava flow and cinder cone (middle [?] Pleistocene)
- Qbpv, Qbpvc — Pine Valley lava flow and cinder cone (middle Pleistocene)
- Qbgk, Qbgkc — Grass Knoll lava flow and cinder cone (middle to lower Pleistocene)
- Qbw, Qbwc — Washington lava flow and cinder cone (lower Pleistocene)
- Qbgv, Qbgvc — Grass Valley lava flow and cinder cone (lower Pleistocene)
- Qbr — Remnants lava flow (lower Pleistocene)
- Qbcb, Qbcbc — Cedar Bench lava flow and cinder cones (lower Pleistocene)
- Qbe — East Mesa lava flow (lower Pleistocene)
- Qbdd$_1$ — Dutchman Draw-1 lava flow (lower Pleistocene?)
- Qb — Unnamed lava flow (lower Pleistocene?)
- Qblbm — Little Black Mountain lava flow (lower Pleistocene)
- Qbs — Seegmiller Mountain lava flow (lower Pleistocene)
- Qbdd$_2$ — Dutchman Draw-2 lava flow (lower Pleistocene?)
- Qbt — Twin Peaks lava flow (lower Pleistocene)

TERTIARY

- Tbqd$_1$, Tbqdc$_1$ — Quail Draw-1 lava flow and cinder cone (Pliocene)
- Tbw — Wolf Hole Mountain lava flow (Pliocene)
- Tbqd$_2$ — Quail Draw-2 lava flow (Pliocene?)
- Tipv — Pine Valley laccolith (lower Miocene)
- Tc — Claron Formation (Paleocene to Eocene)

unconformity

CRETACEOUS

- Ki — Iron Springs Formation (Upper Cretaceous)
- Kcm — Cedar Mountain Formation (Cretaceous)

unconformity

JURASSIC

- Jcx — Crystal Creek Member of the Carmel Formation (Middle Jurassic)
- Jcc — Co-op Creek Member of the Carmel Formation (Middle Jurassic)
- Jtm — Manganese Wash Member of the Temple Cap Formation (Middle to Lower Jurassic)

unconformity

- Jn — Navajo Sandstone (Lower Jurassic)
- Jk — Kayenta Formation (Lower Jurassic)
- Jks — Springdale Sandstone Member of the Kayenta Formation (Lower Jurassic)

unconformity

- Jmw — Whitmore Point Member of the Moenave Formation (Lower Jurassic)
- JTrmd — Dinosaur Canyon Member of the Moenave Formation (Lower Jurassic to Upper Triassic)

unconformity

TRIASSIC

- Trcp — Petrified Forest Member of the Chinle Formation (Upper Triassic)
- Trcs — Shinarump Conglomerate Member of the Chinle Formation (Upper Triassic)

unconformity

- Trmu — Upper red member of the Moenkopi Formation (Lower Triassic)
- Trms — Shnabkaib Member of the Moenkopi Formation (Lower Triassic)
- Trmm — Middle red member of the Moenkopi Formation (Lower Triassic)
- Trmv — Virgin Limestone Member of the Moenkopi Formation (Lower Triassic)
- Trml — Lower red member of the Moenkopi Formation (Lower Triassic)
- Trmt — Timpoweap Member of the Moenkopi Formation (Lower Triassic)
- Trmr — Rock Canyon Conglomerate Member of the Moenkopi Formation (Lower Triassic)
- Trn — Moenkopi Formation, undivided (Lower Triassic)
- Trmtr — Timpoweap and Rock Canyon Conglomerate Members, undivided (Lower Triassic)

unconformity

PERMIAN

- Pkh — Harrisburg Member of the Kaibab Formation (Lower Permian)
- Pkf — Fossil Mountain Member of the Kaibab Formation (Lower Permian)

unconformity

- Ptw — Woods Ranch Member of the Toroweap Formation (Lower Permian)
- Ptb — Brady Canyon Member of the Toroweap Formation (Lower Permian)
- Pts — Seligman Member of the Toroweap Formation (Lower Permian)

unconformity

- Pq — Queantoweap Sandstone (Lower Permian)

MAP SYMBOLS

- Contact
- Normal fault - dashed where approximate, dotted where concealed; bar and ball on downthrown side
- Thrust fault - dotted where concealed; teeth on upper plate
- Anticline - dotted where concealed
- Volcanic vent
- EM — Sample location and name
- 8 — Station location and number discussed in text
- Approximate location of water well near Mill Creek
- T-1 — Approximate trench location and name; T=Simon Bymaster Inc. trench (Simon and others, this volume); WFT=AGEC trenches at Washington Fields; G=Earth Sciences Associates trench (ESA, 1982)

This geologic map was supported by the Utah Geological Survey and the U.S. Geological Survey (USGS), Department of the Interior, under USGS National Earthquake Hazards Reduction Program award number G11AP20061. The views and conclusions contained in this document are those of the author and should not be interpreted as necessarily representing the official policies, either expressed or implied, of the U.S. Government.

Although this product represents the work of professional scientists, the Utah Department of Natural Resources, Utah Geological Survey, makes no warranty, expressed or implied, regarding its suitability for a particular use. The Utah Department of Natural Resources, Utah Geological Survey, shall not be liable under any circumstances for any direct, indirect, special, incidental, or consequential damages with respect to claims by users of this product.

For use at 1:24,000 scale only.

MAP LOCATION

APPROXIMATE MEAN DECLINATION, 2015

GEOLOGIC MAP OF THE NORTHERN PART OF THE FORT PEARCE SECTION AND THE WASHINGTON HOLLOW SECTION OF THE WASHINGTON FAULT ZONE, WASHINGTON COUNTY, UTAH, AND MOHAVE COUNTY, ARIZONA

by
Tyler R. Knudsen

2015

SCALE 1:24,000

1 0.5 0 1 MILE
1000 0 1000 2000 3000 4000 5000 6000 7000 FEET
1 0.5 0 1 KILOMETER
CONTOUR INTERVAL 20 FEET

Base from USGS Central East, Saddle Mountain, Washington, Harrisburg Junction, Saint George, Washington Dome, Lizard Point, and Yellowhorse Flat 7.5' quadrangles
Projection: UTM Zone 12
Datum: NAD 1927
Spheroid: Clarke 1866

GIS: Tyler R. Knudsen
Cartography: Tyler R. Knudsen, Corey D. Unger, and Jay Hill

Utah Geological Survey
1594 West North Temple, Suite 3110
P.O. Box 146100, Salt Lake City, UT 84114-6100
(801) 537-3300
geology.utah.gov

UTAH GEOLOGICAL SURVEY
a division of
Utah Department of Natural Resources

Plate 2
Utah Geological Survey Miscellaneous Publication 15-6
Geologic Map of the Southern Part of the Fort Pearce Section of the Washington Fault Zone

CORRELATION OF MAP UNITS

Index to USGS 7.5' quadrangles and principal sources of geologic mapping used in this compilation

1. Hacker, in preparation(b)
2. Hacker, in preparation(a)
3. Willis and Higgins, 1995
4. Biek, 2003
5. Hayden and Willis, 2011
6. Hayden, 2005
7. Hayden, 2004
8. Billingsley, 1990a
9. Billingsley, 1992a
10. Billingsley, 1992b
11. Billingsley, 1990b

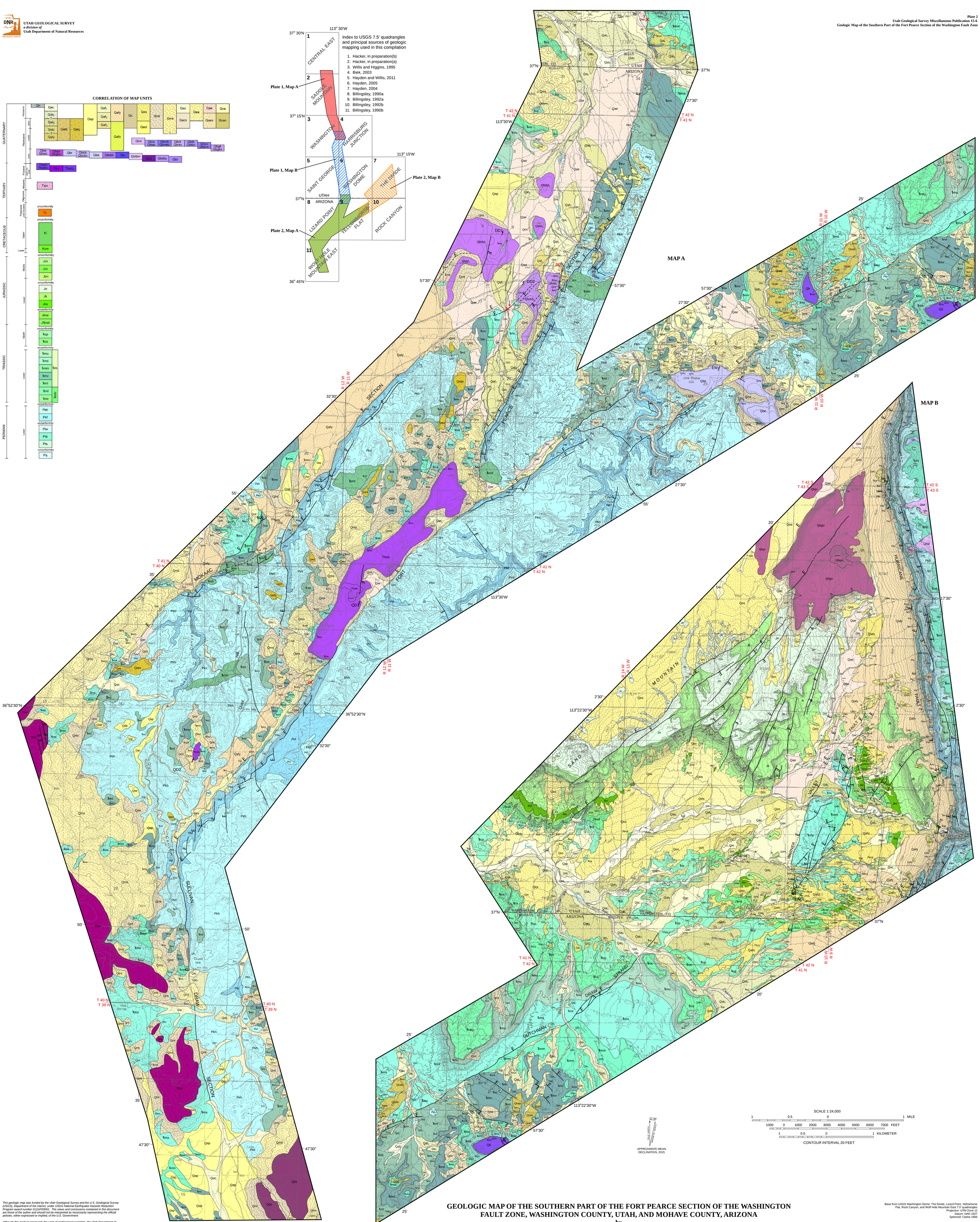

SCALE 1:24,000
1 0.5 0 1 MILE
1000 0 1000 2000 3000 4000 5000 6000 7000 FEET
1 0.5 0 1 KILOMETER
CONTOUR INTERVAL 20 FEET

APPROXIMATE MEAN DECLINATION, 2015

This geologic map was funded by the Utah Geological Survey and the U.S. Geological Survey (USGS), Department of the Interior, under USGS National Earthquake Hazards Reduction Program award number G11AP20061. The views and conclusions contained in this document are those of the author and should not be interpreted as necessarily representing the official policies, either expressed or implied, of the U.S. Government.

Although this product represents the work of professional scientists, the Utah Department of Natural Resources, Utah Geological Survey, makes no warranty, expressed or implied, regarding its suitability for a particular use. The Utah Department of Natural Resources, Utah Geological Survey, shall not be liable under any circumstances for any direct, indirect, special, incidental, or consequential damages with respect to claims by users of this product.

For use at 1:24,000 scale only.

GEOLOGIC MAP OF THE SOUTHERN PART OF THE FORT PEARCE SECTION OF THE WASHINGTON FAULT ZONE, WASHINGTON COUNTY, UTAH, AND MOHAVE COUNTY, ARIZONA

by
Tyler R. Knudsen

2015

Base from USGS Washington Dome, The Divide, Lizard Point, Yellowhorse Flat, Rock Canyon, and Wolf Hole Mountain East 7.5' quadrangles
Projection: UTM Zone 12
Datum: NAD 1927
Spheroid: Clarke 1866

GIS: Tyler R. Knudsen
Cartography: Tyler R. Knudsen, Corey D. Unger, and Jay Hill

Utah Geological Survey
1594 West North Temple, Suite 3110
P.O. Box 146100, Salt Lake City, UT 84114-6100
(801) 537-3300
geology.utah.gov